# Workshop on Martian Phyllosilicates: Recorders of Aqueous Processes?

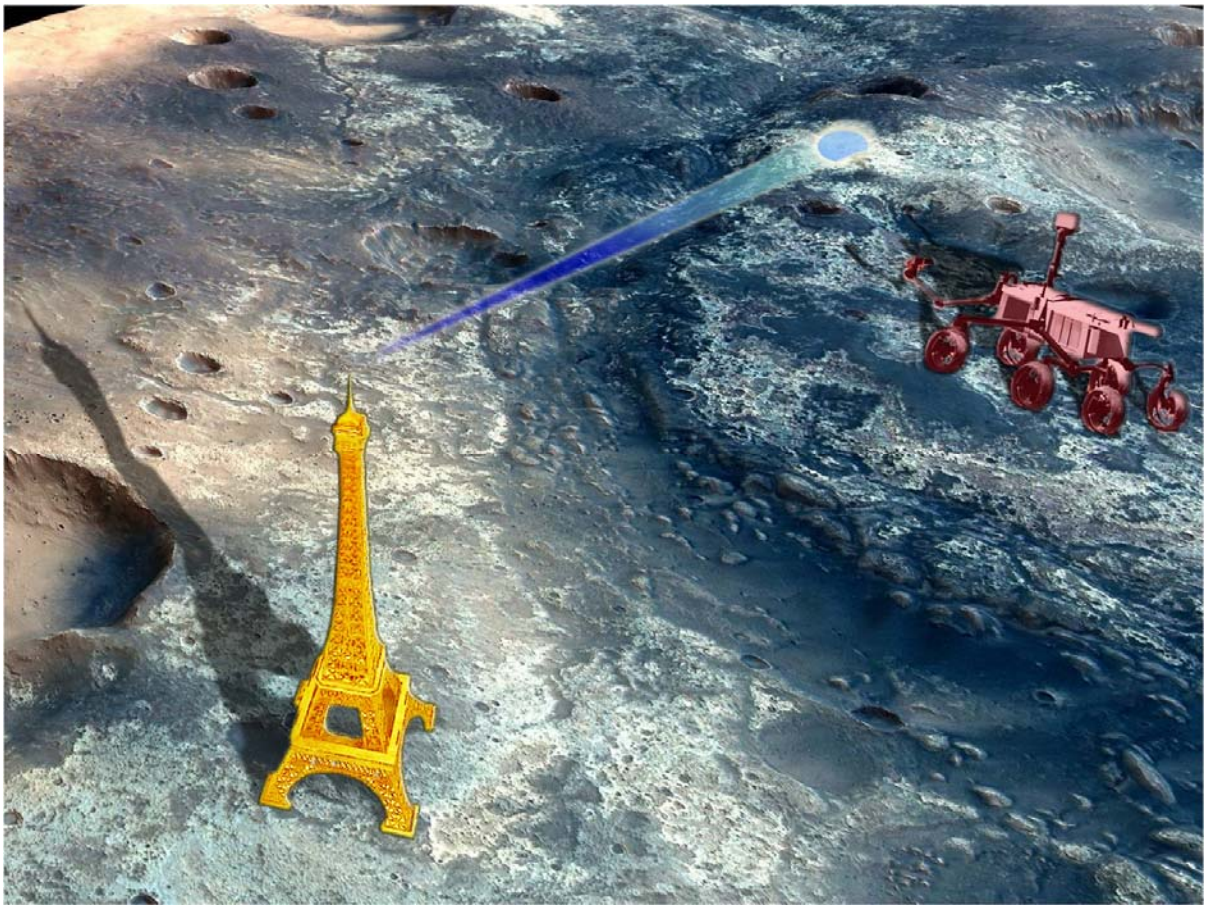

**October 21–23, 2008**

**Paris, France**

# PROGRAM AND ABSTRACTS

LUNAR AND PLANETARY INSTITUTE

LPI Contribution No. 1441

# Workshop on Martian Phyllosilicates: Recorders of Aqueous Processes?

**October 21–23, 2008 • Paris, France**

## Sponsors

European Space Agency
Centre National d'Etudes Spatiales
Lunar and Planetary Institute
National Aeronautics and Space Administration
Institut d'Astrophysique Spatiale

## Scientific Organizing Committee

Jean-Pierre Bibring
David Bish
Janice Bishop
Eldar Noe Dobrea
Jack Mustard
Francois Poulet
Sabine Petit
David Beaty

Lunar and Planetary Institute 3600 Bay Area Boulevard Houston TX 77058-1113

LPI Contribution No. 1441

Compiled in 2008 by
LUNAR AND PLANETARY INSTITUTE

The Lunar and Planetary Institute is operated by the Universities Space Research Association under a cooperative agreement with the Science Mission Directorate of the National Aeronautics and Space Administration.



Abstracts in this volume may be cited as

Author A. B. (2008) Title of abstract. In *Workshop on Martian Phyllosilicates: Recorders of Aqueous Processes?*, p. XX. LPI Contribution No. 1441, Lunar and Planetary Institute, Houston.

This volume is distributed by

ORDER DEPARTMENT
Lunar and Planetary Institute
3600 Bay Area Boulevard
Houston TX 77058-1113, USA
Phone: 281-486-2172
Fax: 281-486-2186
E-mail: order@lpi.usra.edu

*A limited number of copies are available for the cost of shipping and handling.*
*Visit the LPI Online Store at https://www.lpi.usra.edu/store/products.cfm.*

ISSN No. 0161-5297

# Preface

This volume contains abstracts that have been accepted for presentation at the Workshop on Martian Phyllosilicates:  Recorders of Aqueous Processes?, October 21–23, 2008, Paris, France.

Administration and publications support for this meeting were provided by the staff of the Publications and Program Services Department at the Lunar and Planetary Institute.

# Guide to Technical Sessions

## Workshop on Martian Phyllosilicates: Recorders of Aqueous Processes?

### October 21–23, 2008

### Tuesday, October 21, 2008

| | |
|---|---|
| 9:00 a.m. | Introduction |
| 10:10 a.m. | Mineralogy and Geology of Phyllosilicate Deposits |
| 2:00 p.m. | Characteristics of Hydrated Mineral Deposits and Detection Limits |
| 5:00 p.m. | Discussion and Summary of Identification of Phyllosilicates and Hydrated Materials and the Geologic Setting |

### Wednesday, October 22, 2008

| | |
|---|---|
| 9:00 a.m. | Capabilities of Current and Future Instruments and Missions to Constrain Phyllosilicates and Habitability on Mars |
| 12:20 p.m. | Discussion and Summary of Current and Future Instruments and Missions |
| 2:30 p.m. | Formation Conditions of Phyllosilicates on Mars |
| 5:10 p.m. | Discussion and Summary of Physical, Chemical, and Environmental Constraints on Formation Conditions of Phyllosilicates on Mars |

### Thursday, October 23, 2008

| | |
|---|---|
| 9:00 a.m. | Analog Sites for Formation of Phyllosilicates on Mars |
| 11:20 a.m. | Discussion and Summary of Analog Sites for Formation of Phyllosilicates on Mars |
| 12:20 a.m. | Discussion and Summary of Studies |

# Contents

# Program

**Tuesday, October 21, 2008**
**INTRODUCTION**
**9:00 a.m.**

9:00 a.m. Bibring J.-P. *
*Welcome and Introduction*

9:10 a.m. Bibring J.-P. *
*Themes and Goals of the Workshop*

9:30 a.m. Bish D. L. * Vaniman D. T.
*What Can Clay Mineralogy Tell Us About Alteration Environments on Mars?* **[#7025]**

9:50 a.m. Velbel M. A. *
*Interpreting Martian Phyllosilicates: Transferability of an Inferential Framework from Terrestrial Experience to Mars* **[#7008]**

**Tuesday, October 21, 2008**
**MINERALOGY AND GEOLOGY OF PHYLLOSILICATE DEPOSITS**
**10:10 a.m.**

**Chairs:** **Francois Poulet**
**Eldar Noe Dobrea**

10:10 a.m. Poulet F. * Bibring J.-P. Carter J. Langevin Y. Mangold N. Mustard J. Loizeau D. Gondet B.
*Identification, Mapping and Mineralogy of Phyllosilicates on Mars as seen by MEx/OMEGA* **[#7023]**

10:30 a.m. Mangold N. * Poulet F. Loizeau D. Bouley S. Ansan V. Bibring J.-P. Langevin Y. Gondet B. Masson P.
*Geological Relationships Between Phyllosilicates and Fluvial Landforms in Three Regions of Mars* **[#7024]**

10:50 a.m. Loizeau D. * Mangold N. Poulet F. Ansan V. Hauber E. Bibring J.-P. Langevin Y. Gondet B. Masson P. Neukum G.
*Stratigraphy of the Mawrth Vallis Region Through Omega, HRSC Color Imagery and DTM* **[#7041]**

11:10 a.m. BREAK

11:30 a.m. Noe Dobrea E. Z. * Bishop J. L. McKeown N. K. Fu R. Rossi C. Swayze G. Michalski J. R. Poulet F. Bibring J.-P. Mustard J. F. Arvidson R. Morris R. V. Murchie S. McEwen A. S. Malret E. Hash C.
*Clay-bearing Units in Western Arabia Terra: Stratigraphy, Extent, and Possible Regional Alteration Fronts* **[#7040]**

11:50 a.m. Ehlmann B. L. * Mustard J. F. Swayze G. A. Wray J. J. Barnouin-Jha O. S. Bishop J. L. Des Marais D. J. Poulet F. Roach L. H. Milliken R. E. Clark R. N. Murchie S. L. MRO CRISM Team
*Phyllosilicates, Zeolites, and Carbonate near Nili Fossae, Mars: Evidence for Distinct Environments of Aqueous Alteration* **[#7019]**

12:10 p.m. Buczkowski D. L. * Murchie S. Clark R. Seelos F. Malaret E. Hash C. CRISM Science Team
*Phyllosilicates in the Argyre Basin, Mars* **[#7031]**

12:30 p.m. Mustard J. F. * Murchie S. L. Ehlmann B. L. Milliken R. E. Bibring J.-P. Poulet F. Bishop J. Noe Dobrea E. Roach L.
*Geologic Environments of Phyllosilicate Deposits from Orbit* **[#7026]**

12:50 p.m. LUNCH

**Tuesday, October 21, 2008**
**CHARACTERISTICS OF HYDRATED MINERAL DEPOSITS AND DETECTION LIMITS**
**2:00 p.m.**

**Chairs:** **John Mustard**
**Nancy McKeown**

2:00 p.m. Roach L. H. * Mustard J. F. Murchie S. Milliken R. E. Litchenberg K. Ehlmann B. L. Bishop J. Arvidson R. E. CRISM Team
*New Hydrated Spectral Phase and Stratigraphy of Smectite Clays, Sulfates and Other Hydrated Minerals in Ius Chasma, Valles Marineris* **[#7017]**

2:20 p.m. Wiseman S. M. * Avidson R. E. Poulet F. Morris R. V. Murchie S. Seelos F. P. Andrews-Hanna J. C. CRISM Science Team
*Stratigraphic Context of Phyllosilicate Deposits in Sinus Meridiani, Mars* **[#7035]**

2:40 p.m. Massé M. * Bourgeois O. Le Mouélic S. Le Deit L. Verpoorter C. Combe J.-Ph. Sotin C. Bibring J.-P. Gondet B. Langevin Y. OMEGA Team
*Sulfates, Ferric Oxides and Al-OH Bearing Minerals in Aram Chaos: Comparison of OMEGA and CRISM Data* **[#7002]**

3:00 p.m. Viviano C. E. * Moersch J. E. Piatek J. L.
*A THEMIS Spectral Index for Detection of Phyllosilicates on Mars* **[#7032]**

3:20 p.m. BREAK

3:40 p.m. Le Deit L. * Le Mouélic S. Bourgeois O. Mège D. Massé M. Quantin-Nataf C. Sotin C. Bibring J.-P. Gondet B. Langevin Y.
*Composition and Morphology of Hydrated Layered Deposits on the Plains Around Valles Marineris (Mars)* **[#7016]**

4:00 p.m. Wray J. J. * Seelos F. P. Murchie S. L. Squyres S. W.
*Hydrated Mineral Exposures in the Southern Highlands* **[#7018]**

4:20 p.m. McKeown N. K. * Bishop J. L. Cuadros J. Amador E. Silver E.
*Characterization of Phyllosilicate Units at Mawrth Vallis: Comparison of CRISM Observations and Intimate Phyllosilicate Mixtures* **[#7033]**

4:40 p.m. Parente M. * Bishop J. L. Cuadros J.
*Lab Experiments to Simulate Coatings on Phyllosilicate Rocks and Comparison with CRISM Data of Mars* **[#7039]**

5:00 p.m. Ruff S. W. *
*Emerging Connections Between TIR and VNIR Observations of Martian Phyllosilicates* **[#7044]**

**Tuesday, October 21, 2008**
**DISCUSSION AND SUMMARY**
**IDENTIFICATION OF PHYLLOSILICATES AND HYDRATED MATERIALS**
**AND THE GEOLOGIC SETTING**
**5:20 p.m.**

**Chair: Dave Beaty**

**Wednesday, October 22, 2008**
**CAPABILITIES OF CURRENT AND FUTURE INSTRUMENTS AND MISSIONS TO CONSTRAIN PHYLLOSILICATES AND HABITABILITY ON MARS**
**9:00 a.m.**

**Chairs:** **Jean-Pierre Bibring**
**Darby Dyar**

9:00 a.m. Tomkinson T. * Wolters S. D. Hagermann A. Bohman A. F. Sund A. T. Hagene J. K. Grady M. M.
*Insights into the Past Mineralogy and Fluvial Activity of Mars with WatSen* **[#7005]**

9:20 a.m. Blake D. F. * Bish D. L. Chipera S. J. Vaniman D. T. Sarrazin P. Gailhanou M.
*In Situ Analysis of Martian Phyllosilicates Using the CheMin Mineralogical Instrument on Mars Science Laboratory* **[#7006]**

9:40 a.m. Ollila A. M. * Lanza N. L. Clegg S. M. Barefield J. E. Newsom H. King P. L. Crossey L. J. Wiens R. C. Vaniman D.
*Determination of Hydration States in Smectites Using LIBS* **[#7022]**

10:00 a.m. Tucker J. M. * Dyar M. D. Clegg S. M. Wiens R. C. Barefield J. E. II Schaefer M. W. Bishop J. L.
*Quantitative Chemistry of Phyllosilicate Minerals Using Laser-induced Breakdown Spectroscopy* **[#7028]**

10:20 a.m. BREAK

10:40 a.m. Murad E. *
*$^{57}$Fe Mössbauer Spectroscopy: A Tool for the Remote Characterization of Phyllosilicates?* **[#7020]**

11:00 a.m. Dyar M. D. * Schaefer M. W.
*Discriminating Among Layer Silicates Using Remote Mössbauer Spectroscopy* **[#7034]**

11:20 a.m. Maturilli A. * Helbert J.
*Emissivity Spectra of Some Phyllosilicates in the [3, 50] µm Spectral Range from the Berlin Emissivity Database (BED)* **[#7004]**

11:40 a.m. Zalewska N. * Wolkenberg P.
*Mineralogical Composition of the Martian Surface on the Basis on Infrared Spectroscopy* **[#7010]**

12:00 p.m. Bibring J.-P. * MicrOmega Team
*The MicrOmega/ExoMars Investigation* **[#7043]**

**Wednesday, October 22, 2008**
**DISCUSSION AND SUMMARY**
**CURRENT AND FUTURE INSTRUMENTS AND MISSIONS**
**12:20 p.m.**

**Chair: Dave Beaty**

1:00 p.m. LUNCH

**Wednesday, October 22, 2008**
**FORMATION CONDITIONS OF PHYLLOSILICATES ON MARS**
**2:30 p.m.**

**Chairs:** **David Bish**
**Sabine Petit**

2:30 p.m. Murchie S. * Mustard J. Ehlmann B. Milliken R. Bishop J. Seelos F. CRISM Team
*An Overview of Classes of Martian Phyllosilicate Deposits from Orbital Remote Sensing* **[#7029]**

2:50 p.m. Milliken R. E. *
*Which Clays are Really Present on Mars and How Did They Form?* **[#7009]**

3:10 p.m. Bishop J. L. * McKeown N. K. Noe Dobrea E. Z. Murchie S. L. Mustard J. F.
*Aqueous Processes and Active Chemistry Inferred from Phyllosilicate Record at Mawrth Vallis, Mars* **[#7038]**

3:30 p.m. Chevrier V. F. *
*Early Martian Surface Conditions from Thermodynamics of Phyllosilicates* **[#7011]**

3:51 p.m. BREAK

4:10 p.m. Cuadros J. * Dekov V. Aldega L. Fiore S.
*Chemical Controls on Phyllosilicate Composition at the Early Formation Stage* **[#7027]**

4:30 p.m. Tosca N. J. * Milliken R. E. Michel F. M.
*Smectite Formation on Early Mars: Experimental Constraints* **[#7030]**

4:50 p.m. Andrieux P. * Petit S. Decarreau A.
*Synthesis of Clay Minerals and the Relationship with Formation Processes and Crystal Chemistry* **[#7042]**

5:10 p.m. Altheide T. S. * Chevrier V. F. Gavin P.
*Acidic Weathering of Martian Relevant Phyllosilicates* **[#7007]**

**Wednesday, October 22, 2008**
**DISCUSSION AND SUMMARY**
**PHYSICAL, CHEMICAL, AND ENVIRONMENTAL CONSTRAINTS ON FORMATION CONDITIONS OF PHYLLOSILICATES ON MARS**
**5:10 p.m.**

**Chair: Dave Beaty**

**Thursday, October 23, 2008**
**ANALOG SITES FOR FORMATION OF PHYLLOSILICATES ON MARS**
**9:00 a.m.**

**Chairs:** **Janice Bishop**
**Alain Meunier**

9:00 a.m. Bristow T. F. * Kennedy M. J.
*Mechanisms and Conditions of Saponite Production in the Precambrian Doushantuo Formation* **[#7036]**

9:20 a.m. Morris R. V. * Hamilton V. E. Gruener J. E. Ming D. W. Mertzman S.
*Visible and Near-IR Spectra for Aqueous Alteration Products (Palagonite, Phyllosilicates, Sulfates) of Basaltic Tephra on Mauna Kea Volcano, Hawaii* **[#7037]**

9:40 a.m. Schwenzer S. P. * Kring D. A.
*Phyllosilicates Produced by Impact-generated Hydrothermal Systems on Mars* **[#7014]**

10:00 a.m. Gavin P. * Chevrier V. Ninagawa K.
*Effects of Impact and Heating on the Spectral Properties of Clays on Mars* **[#7012]**

10:20 a.m. Fairén A. G. Davila A. F. * Marzo G. A. Roush T. L. McKay C. P.
*Post-Noachian Water Activity on Mars Inferred from Shock Decomposition Analysis of Phyllosilicates Within Impact Craters* **[#7021]**

10:40 a.m. Meunier A. * Mas A. Beaufort D. Patrier P. Dudoignon P.
*Do Magmatic Clays Exist? The Importance of Terrestrial Analogues* **[#7003]**

11:00 a.m. BREAK

**Thursday, October 23, 2008**
**DISCUSSION AND SUMMARY**
**ANALOG SITES FOR FORMATION OF PHYLLOSILICATES ON MARS**
**11:20 p.m.**

**Chair: Dave Beaty**

**Thursday, October 23, 2008**
**DISCUSSION AND SUMMARY OF STUDIES**
**12:20 p.m.**

**Moderators:**
**Dave Beaty, Jean-Pierre Bibring,**
**David Bish, Janice Bishop, John Mustard**

12:20 p.m. *Summary of Discussion Points from Session*

12:40 p.m. *Identification of top 10 unresolved questions related to observations, experimental studies, and theoretical models. Identification of what is needed to better constrain types of phyllosilicates present on Mars and their likely formation conditions.*

**ACIDIC WEATHERING OF MARTIAN RELEVANT PHYLLOSILICATES.** T. S. Altheide[1], V. F. Chevrier[1], and P. Gavin[1], [1]W. M. Keck Laboratory of Space Simulation, Arkansas Center for Space and Planetary Sciences, MUSE 202, University of Arkansas, Fayetteville, AR, 72701, talthei@uark.edu.

**Introduction:** The OMEGA reflectance spectrometer onboard Mars Express and CRISM onboard the Mars Reconnaissance Orbiter have identified large phyllosilicate deposits on heavily impacted Noachian aged terrains, some associated with fluvial and deltaic deposits . This contrasts with the sulfate deposits which are mainly present in Hesperian aged terrains . This difference of age has led to a new model of the evolution of the martian surface: formation of phyllosilicates (pH of ~ 7 to 10), then sulfates (pH < 5), and finally poorly crystalline iron oxides . Therefore, phyllosilicates and sulfates define two different and apparently incompatible environments .

Recent studies have shown that this model may be more complicated. Phyllosilicates have been identified in younger regions such as Meridiani Planum and Gusev Crater , eventually in association with sulfates. Such observations raise questions about the spatial, temporal, and chemical relationships between various types of phyllosilicates (chlorite vs. smectite, composition variations), and between phyllosilicate and sulfate deposits.

To investigate the stability of phyllosilicates and their relationship with sulfates, we have designed experiments to test the stability of martian relevant phyllosilicates exposed to acidic solutions of varying pH.

**Methods and Materials:** Various phyllosilicates (Table 1) were weathered with sulfuric acid ($H_2SO_4$) solutions at varying pH. Two grams of each phyllosilicate were placed in tubes containing 30 mL of $H_2SO_4$ initially at pH 0, 2 and 4 (Table 2). Tubes were stored at temperatures of 30 and 60 °C to increase the kinetics of the reactions. Each mineral, at each pH level, was setup in quadruplicate in order to study the kinetics of the weathering process. Samples will be removed every 30 days, with the last set of samples removed after 120 days of exposure to the acidic solution.

The first set of phyllosilicates was removed from the acidic solution after 30 days. The solid phase was separated by centrifugation and subsequently freeze dried. The pH of the acidic solutions was measured (Table 2), then each solid phase was analyzed using XRD and FT-IR reflectance spectroscopy. NIR spectra were obtained using a Nicolet 6700 Smart Diffuse spectrometer with $N_2$ purge gas. Our configuration consisted of a quartz-halogen source, a $CaF_2$ beam splitter, and a DTGS detector.

X-ray diffraction patterns of each weathered phyllosilicate were obtained for absolute mineral identification, including for the possible presence of new mineral phases. XRD spectra were acquired between 2θ = 5 and 80° with steps of 0.02° and 13 seconds of counting for each step, resulting in an acquisition time of 13 hr 45 min. This allows for sufficiently high resolution to separate and identify individual components in complex mixtures, especially since some of them may be nanophase and/or poorly crystalline.

**Table 1.** Phyllosilicate minerals used in acidic weathering experiments. Samples were cleaned and sieved to below 63 μm prior to acidic weathering.

| Phyllosilicate | Formula |
|---|---|
| Chlorite | $(Mg,Fe)_3(Si,Al)_4O_{10}(OH)_2$ |
| Serpentine | $(Mg,Fe)_3Si_2O_5(OH)_4$ |
| Kaolinite | $Al_2Si_2O_5(OH)_4$ |
| Montmorillonite | $(Na,Ca)_{0.33}(Al,Mg)_2Si_4O_{10}(OH)_2{\cdot}nH_2O$ |
| Nontronite | $Na_{0.3}Fe_2(Si,Al)_4O_{10}(OH)_2{\cdot}nH_2O$ |

**Table 2.** pH of acidic solutions before and after 30 days of phyllosilicate weathering.

| Phyllosilicate | pH before | pH after |
|---|---|---|
| Chlorite | 0 | 0.8 |
| | 2 | 2.9 |
| | 4 | 5.2 |
| Serpentine | 0 | 1.0 |
| | 2 | 6.5 |
| | 4 | 6.9 |
| Kaolinite | 0 | 0.2 |
| | 2 | 2.4 |
| | 4 | 4.0 |
| Montmorillonite | 0 | 0.9 |
| | 2 | 4.5 |
| | 4 | — |
| Nontronite | 0 | 1.2 |
| | 2 | 3.0 |
| | 4 | 6.6 |

**Results:** pH of solutions increases systematically for each phase (Table 2), indicating strong leaching of the phyllosilicates. Final pHs indicate equilibrium has been reached, unless the amount of phyllosilicate was not enough to reach such equilibrium, as is systematically the case for initial pH = 0. Kaolinite also shows such an increase but to a much lesser extent. Kaolinite appears more resistant to the acidic weathering process, being stable at pH ~ 2. A thin crust was observed, after drying, for some of the phyllosilicate minerals, depending on the pH of the solution used to weather the samples (Fig. 1).

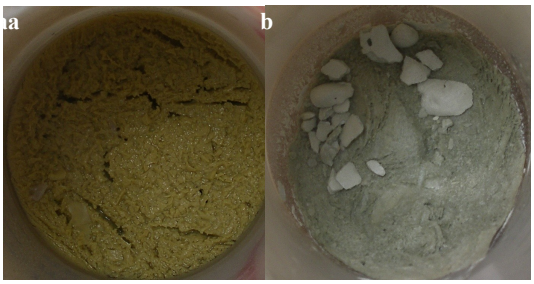


**Figure 1.** Crust layers formed after drying under 7 mbar of atmospheric pressure. **(a)** nontronite (pH 2) and **(b)** chlorite (pH 4).

NIR reflectance spectra of nontronite (Fig. 2a) and chlorite (Fig. 2b) samples indicate significant alteration at lower pH levels. Most absorption bands progressively disappear. Nontronite spectra a pH = 0 appears nearly featureless. Similarly, the spectra of chlorite strongly changes with intensity of weathering, in particular with the appearance of a strong 1.9 µm band suggesting hydrated phases, possibly sulfates.

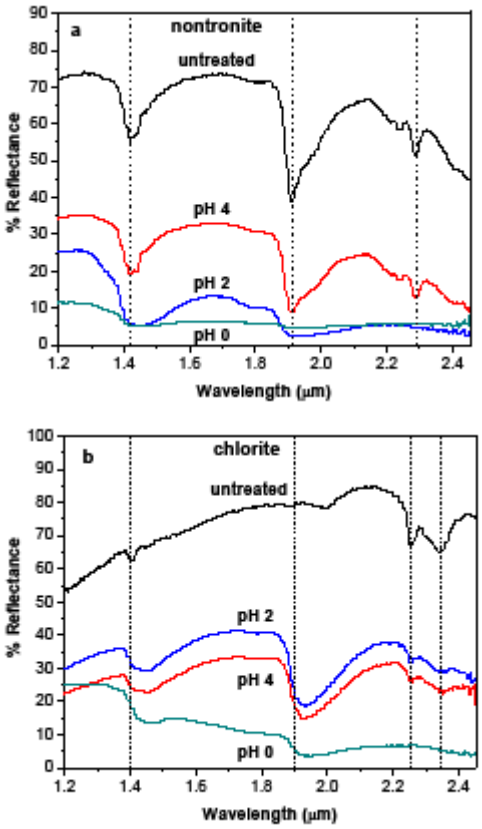


**Figure 2.** NIR reflectance spectra of **(a)** nontronite and **(b)** chlorite crust layers. Spectra of experimental samples show features suggestive of hydrated minerals formed from leached minerals of the primary phyllosilicate. In addition, samples weathered at pH=0 demonstrate significant loss of phyllosilicate features.

For nontronite, XRD analysis of sample weathered at pH 0 (Fig. 3) indicates no pattern of initial nontronite. Instead, we observe a pattern similar to amorphous silica with a double peak feature at 2θ = 20 and 25º, and some additional small peaks related to rhomboclase ($HFe(SO_4)_2.4H_2O$), which is a usual ferric sulfate formed in strongly acidic environments

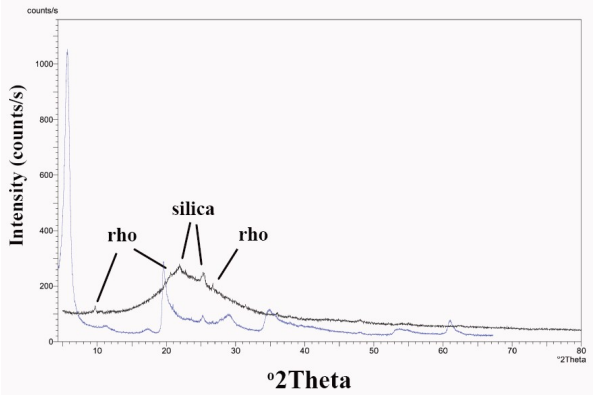


**Figure 3.** XRD patterns of nontronite untreated (blue) and acid weathered for 30 days (black; pH 0). Rho = rhomboclase.

**Discussion:** Initial results of $H_2SO_4$ weathered phyllosilicates suggest significant alterations of the primary mineralogy, seen in both reflectance and XRD spectra. This includes the formation of hydrated phases from mineral leaching after 30 days of weathering at pHs of 4 and 2. At pH 0, weathered samples of both nontronite and chlorite demonstrate alteration of primary mineralogy to amorphous phases (silica) and ferric sulfates.

**Conclusions:** The chemical stability of phyllosilicates has important implications for the spatial and temporal relationship between hydrated silicates and sulfates, especially in the Meridiani Planum region. Our results suggest that acidic weathering of phyllosilicates may be locally constrained, and may have led to secondary mineral phases which have been detected on Mars, including silica and $Fe^{3+}$ sulfates (rhomboclase).

**References:** [1] Bibring, J.-P., *et al.*, (2005) *Science* 307, 1576-1581. [2] Poulet, F., *et al.*, (2005) *Nature* 481, 623-627. [3] Ehlmann, B. L., *et al.*, (2008) *Nature Geoscience* 1, 355-358. [4] Grant, J. A., *et al.*, (2008) *Geology* 36, 195-198. [5] Gendrin, A., *et al.*, (2005) *Science* 307, 1587-1591. [6] Bibring, J. P., *et al.*, (2006) *Science* 312, 400-404. [7] Chevrier, V., *et al.*, (2007) *Nature* 448, 60-63. [8] Poulet, F., *et al.*, (2007) *Icarus* 195, 106-130. [9] Wang, A., *et al.*, (2006) *Journal of Geophysical Research* 111 . [10] Clark, B. C., *et al.*, (2007) *Journal of Geophysical Research* 112 .

**SYNTHESIS OF CLAY MINERALS AND THE RELATIONSHIP WITH FORMATION PROCESSES AND CRYSTAL CHEMISTRY.** P. Andrieux[1] , S. Petit[1], and A. Decarreau[1], [1]HydrASA, Université de Poitiers, 40 avenue du Recteur Pineau, 86022 Poitiers Cedex, pauline.andrieux@etu.univ-poitiers.fr, sabine.petit@univ-poitiers.fr

Different approaches have been used for the determination of the mineralogy at the Mars surface.

The direct measurements with spacecraft, the study of Martian meteorites, and the laboratory measurements on analogue materials have permitted to determine the Martian soil composition. Thanks to theses different approaches, clays and clay minerals have been discovered on Mars surface [1].

Several smectites have been identified. The main phyllosilicates on Mars are the iron-rich clays as nontronite. But Mg- and Al-rich members are also present and have been detected on Mars' surface for example as Saponite and Montmorillonite. Clay minerals on Mars can compare to Earth's analogues which could permit to understand the condition of formation and crystal chemistry [2].

Three processes are important in the origin of clay minerals. Under the condition of the earth's surface, the alteration of other silicate minerals could lead to the formation of clay minerals. At pressures or temperatures higher than those of the earth's surface, clay minerals are the result of recrystallisation processes. And, precipitation from solution is the third process. For theses different processes, aqueous solution plays a major role in the formation of clays in natural and synthetic system [3].

Clay minerals synthesis is useful to the understanding of formation processes in nature on Earth and Mars. Synthesis at low temperatures can permit to understand the formation processes in surface.

The clay minerals which were already evidenced on Mars could be possibly synthesized in laboratory.

The conditions of formation of clay minerals in synthetic systems depend on pH, temperature, pressure, starting materials and element concentrations.

For example, regarding nontronites, their synthesis have been realized in the past by Caillère and al. (1953, 1955) mixing dilute solution of silica, iron (II) or (III) chlorides, and salts of Mg and Al at low temperature (100°C) and adjusting pH between 8,5 and 9,5. They obtained very diluted suspensions of nontronites. Hamilton and Furtwängler (1951) obtained also very diluted suspensions of nontronite using sodium metasilicate and iron (III) chloride at high temperature. Decarreau and Bonnin (1986) or Decarreau and al. (1987) synthesized ferric smectite under partially reducing or oxidizing conditions using coprecipitated gels of silica and $FeSO_4$ at low temperature below 150°C. But they obtained "defect nontronite". Several authors described the synthesis of nontronites but obtained poorly crystalline nontonites or in very diluted solutions [4, 5, 6, 7, 8].

Recently, we obtained synthetic nontronites using coprecipitated gels containing Si, Al and Fe. Iron-rich nontronites with different rates of aluminium are obtained.

Using Clay minerals synthesis, we can better determine the condition of formation of equivalent natural clays knowing their physical and chemical conditions of synthesis.

Furthermore, synthetic clays can be used as reference samples for spectroscopic interpretations. Analogue Martian clay minerals synthesized in laboratory could lead very important research on the formation of this clays and their crystallochemistry.

**References:**

[1] Chevrier V. and Mathe P. E. (2006) Planetary and Space Science, *55*, 289–314. [2] Poulet F. and al. (2005) Nature, *438*, 623–627. [3] Velde B. (1992), 198p. [4] Kloprogge J. T. et al. (1999) Clays and Clay minerals, *47*, 529–554. [5] Caillère et al. (1953) Comptes rendus de l'Academie Sciences (Paris), *237*, 1724–1726. [6] Caillère et al. (1955) Bulletin de la Societe Francaise de Mineralogie et Crystallographie, *78*, 227–241. [7] Decarreau and Bonnin (1986) Clay minerals, *21*, 861–877. [8] Decarreau et al. (1987) Clays and clay minerals, *22*, 207–223.

**THE MICROMEGA/EXOMARS INVESTIGATION**

J-P. Bibring and the MicrOmega Team

MicrOmega is a set of highly miniaturized microscopes designed to analyze the samples collected on board the ESA/ExoMars Rover, to be launched in 2013. It is constituted of : 1) an optical microscope, that will produce colour and polarized images of the drilled samples with a spatial sampling of 4 μm; 2) a VIS/NIR imaging spectrometer, acquiring (x,y,λ) image cubes of the processed samples within the Analytical Laboratory. It will provide the hyperspectral near infrared spectrum within each pixel 20 μm in size, enabling to derive the composition at a grain scale, through diagnostic signatures of a variety of silicates, oxides, salts and hydrated phases. We will present the goals, the specifications, the performances and the development status of this instrument, in the frame of the global ExoMars objectives.

**WHAT CAN CLAY MINERALOGY TELL US ABOUT ALTERATION ENVIRONMENTS ON MARS?** D. L. Bish[1] and D. T. Vaniman[2], [1]Dept. of Geological Sciences, Indiana University, 1001 E. 10th St., Bloomington, IN 47405; bish@indiana.edu, [2]Los Alamos National Lab, MS D462, Los Alamos, NM 87545; vaniman@lanl.gov

**Introduction:** Recent missions to Mars have provided considerable new data supporting the widespread occurrence of hydrous alteration products on the martian surface, and these observations focus new attention on hydrous environments and the minerals formed therein. In order to understand the evolution of Mars, it is useful to sample or orbitally evaluate assemblages that can provide information on the evolution of the martian atmosphere, the nature of martian surface processes, and the thermal-magmatic evolution of the martian mantle and crust. Orbital and surface-derived data have greatly expanded our understanding of Mars' surface and have shown that hydrous minerals are far more common than previously imagined. Recently, orbital data (e.g., CRISM) have begun to show in more detail not only the areal distribution of clay minerals on the surface but also the vertical distribution. By taking advantage of regions excavated by impacts, it is possible to formulate a picture of the effects of burial/depth on mineralogy, adding the valuable third dimension to our knowledge of the mineralogy of the martian surface.

Mars' surface mineralogy holds clues to its hydrologic and geochemical histories, and we can use mineralogy to constrain past processes, including weathering, metamorphism, and hydrothermal effects, just as we do on Earth. Based on early remote IR analyses [1] and Viking XRF results [2], Fe-rich smectites or their degradation products were proposed as major constituents of martian surface soils and dusts. Gooding [3] used thermodynamic data for kaolinite and estimations for a variety of smectites to conclude that smectites were unstable relative to kaolinite. However, he also concluded that metastable formation and/or preservation could make smectites important constituents of martian dusts and soils. The inference of Fe-rich clay minerals at the martian surface has persisted and clay minerals remain a major component of many surface mineralogic models in the assessment of newer data, *e.g.*, [4] and [5]. There is also abundant evidence for hydrous minerals in the martian regolith, supported by Viking thermal analyses and indirectly by Mars Odyssey results showing up to 10% $H_2O$-equivalent H in the upper meter of the surface in equatorial regions. However, the Viking and Odyssey data provide few constraints on the identity of these hydrous minerals.

More definitive data on the mineralogy of Mars [*e.g.*, 5 & 6] show that rock compositions are basaltic to andesitic and contain glass and/or phyllosilicate components. Recent OMEGA and CRISM spectral data suggest the presence of phyllosilicates in several Noachian deposits with a range of Fe, Al, and Mg bonded to structural OH [*e.g.*, 7, 8, 9, 10]. As discussed by [11], TES fits produce different results for the type-2 martian surface depending on which phyllosilicate and glass spectra are included in the end-member library. In many places, the chemistry of the martian fines is consistent with the presence of altered volcanic material including phyllosilicates, silica, and glass, and recent work [12, 13, & 14] suggested the presence of silica-rich deposits (e.g., opal).

**Clay Mineralogy and Alteration Processes on Mars:** Mineral alteration and formation on Mars can occur via many paths, including aqueous and vapor [*e.g.*, 15, 16, 17, 18, 19], and interpreting past alteration processes is complex. However, alteration conditions on Mars can be elucidated by an understanding of alteration mineralogy. Depending on conditions, volcanic glass can alter to a variety of mineral assemblages, including zeolites, smectites, kaolin minerals, hydrated volcanic glass, and opaline silica. For example, [18] suggested that amorphous silica, goethite, and kaolinite would form early under acid alteration conditions, whereas zeolites and carbonates would form later under more alkaline conditions. Yen et al. [14] suggested that recently observed silica deposits could have formed from hydrothermal alteration or from acidic vapors with small amounts of liquid water. Stability diagrams can shed light on alteration conditions, and Figure 1 shows the sequence from amorphous silica through progressively less siliceous phases as silica activity decreases. The discovery of amorphous silica thus greatly constrains formation conditions.

Smectites or zeolites can form from volcanic glass, depending on conditions, with smectite formation occurring in circum- or below-neutral pH conditions and zeolites forming under alkaline conditions. We cannot assume that basaltic volcanic ash will always alter to phyllosilicates. Detection of secondary zeolites would strongly imply the occurrence of alkaline conditions but detection of both smectites and zeolites would indicate a much more persistent and evolved hydrogeologic system. Formation of kaolin minerals would imply a reasonably distinct set of formation conditions. For example, Millot [20] emphasized that kaolin minerals form on Earth most commonly in tropical climates, usually under more-acidic conditions and with high water:rock ratios (well drained), although a

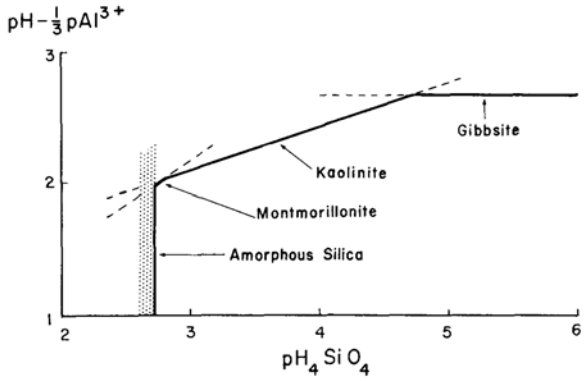


**Figure 1. Stability diagram for minerals in the $Al_2O_3$-$SiO_2$-$H_2O$ system at 25°C and 1 atm. Solutions are supersaturated with the respective phase to the left of or above the solid line (from [19]). The "p" in both axis labels refers to –log[].**

hydrothermal association is also common. Kaolinite, nacrite, and dickite all also commonly form under hydrothermal conditions, and kaolinite is known to transform with depth under diagenetic conditions to dickite in sandstone reservoirs. The kaolin minerals may also be accompanied by amorphous silica when formed hydrothermally, often at the expense of pre-existing volcanic rocks. In addition, they are often accompanied by $TiO_2$ minerals such as anatase and by other hydroxides, such as gibbsite and/or boehmite, if hydrothermal leaching is more severe. On Mars, a Ti-Si association has been considered to support acid vapor alteration [14]. The generally observed relationships between intensity of weathering and resultant mineralogy show relic micas and chlorites in the least weathered/altered assemblages, smectites and kaolinite as intermediates, and oxides/hydroxides (hematite, gibbsite) as end stages. Additional information on formation conditions can be obtained from experiments. For example, nontronite has been often suggested to occur on Mars; [21] showed that nontronite can form at low temperatures only under *reducing* conditions, where Fe is soluble. If this conclusion remains sound, the occurrence of nontronite on Mars obviously has important implications for redox conditions when the clay minerals formed.

We also have the potential to learn considerable new information concerning clay mineral stability from Mars' surface mineralogy. More poorly ordered clay minerals such as smectites and illite/smectites do not occur in old rocks on Earth, and it has often been assumed that these minerals gradually transform to more stable, higher-temperature phases such as illite, micas, and chlorites. This concept is illustrated in Figure 2, which implies that mixed-layer illite/smectites are not stable over long times even at low temperatures. The discovery of smectites in Noachian terrains [7, 8] has important implications for the long-term stability of clay minerals and suggests a possible alternative hypothesis, namely that tectonic activity on Earth eventually results in the progressive alteration of low-temperature minerals to higher-temperature assemblages. If the existence of smectites on Mars in rocks older than 3 By is verified, these results will rewrite our understanding of clay mineral stability and suggest that, in the absence of (plate) tectonic activity and burial, "metastable" clay minerals may be "stable" for times on the order of the age of our planet.

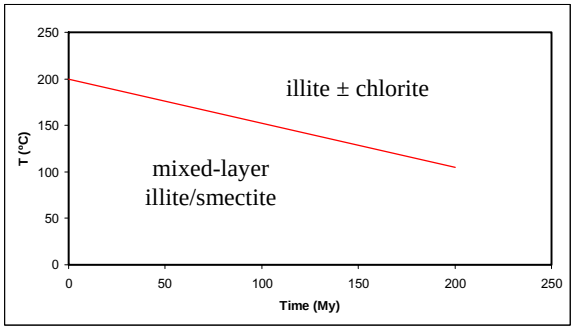


**Figure 2. Time-temperature limits on clay minerals (modified from [22]).**

**References:** [1] Hunt G. R. and Salisbury J. W. (1973) *Icarus*, 18, 459-469. [2] Toulmin P. et al. (1977) *JGR*, *82*, 4625-4634. [3] Gooding, J. L. (1978) *Icarus 33*, 483-513. [4] Calvin W. M. (1998) *LPS XXIX*, Abstract #1162. [5] Michalski J. R. et al. (2006) *JGR*, *111*, E03004. [6] Christensen P. R. et al. (2001) *JGR*, *106*, 23823-23871. [7] Bibring J-P. et al. (2006) *Science*, *312*, 400-404. [8] Poulet F. et al. (2005) Nature, 438, 623-627. [9] Milliken R. E. (2007) *EOS Trans AGU*, *88*, Abstract #P12A-02. [10] Bishop J. L. et al. (2007) *EOS Trans AGU*, *88*, Abstract #P13D-1559. [11] McSween H. Y. J. et al. (2003) *JGR*, *108*, 5135. [12] Michalski J. R. et al. (2005) Icarus, 174, 161-177. [13] Ruff S. W. et al. (2007) *EOS Trans AGU*, *88*, Abstract #P23A-1097. [14] Yen A. et al. (2007) *EOS Trans AGU*, *88*, Abstract #P23A-1095. [15] Gooding J. L. et al. (1992) in *Mars*, 626-651. [16] Banin A. et al. (1997) *JGR*, *102*, 13341-13356. [17] Hurowitz J. A. and McLennan S. M. (2007) *EPSL*, *260*, 432-443. [18] Zolotov M. Y. and Mironenko M. V. (2007) *JGR-Planets*, *112*, E07006. [19] Kittrick J. A. (1969) *Clays & Clay Min*, *17*, 157-167. [20] Millot G. (1970) Geology of Clays, Springer-Verlag. [21] Harder H. (1978) *Clays & Clay Min*, *26*, 65-72. [22] Velde B. (1992) Intro. to Clay Minerals, Chapman & Hall.

**AQUEOUS PROCESSES AND ACTIVE CHEMISTRY INFERRED FROM PHYLLOSILICATE RECORD AT MAWRTH VALLIS, MARS.** J. L. Bishop[1], N. K. McKeown[2], E. Z. Noe Dobrea[3], S. L. Murchie[4] and J. F. Mustard[5], [1]SETI Institute/ NASA-ARC, Mountain View, CA, 94043 (jbishop@seti.org), [2]Earth and Planetary Sciences, University of Calif. Santa Cruz, Santa Cruz, CA, 95064, [3]JPL/CalTech, Pasadena, CA 91109, [4]JHU/Applied Physics Laboratory, Laurel, MD 20723, [5]Dept. of Geological Sciences, Brown University, Providence, RI 02912.

**Introduction:** Phyllosilicate observations in the Mawrth Vallis region of Mars indicate thick, widespread and uniform deposits [1]. Light-toned outcrops imaged by CRISM show abundant phyllosilicates. Fe/Mg-smectite bearing rocks are covered by an $Fe^{2+}$-rich phase that may be a ferrous mica. This unit is overlain by rocks rich in hydrated silica and Al-phyllosilicates. Montmorillonite and kaolinite appear to be present primarily in mixtures with the hydrated silica. This builds on previous identifications of phyllosilicates in the Mawrth Vallis region [2, 3]. Here we discuss potential formation scenarios for the observed clay species at Mawrth Vallis.

The breadth of the phyllosilicate deposit at Mawrth Vallis implies abundant water in Mars' geologic past. A high density of phyllosilicates is observed along the main channel and nearby craters, however, phyllosilicates are observed in smaller outcrops across hundreds of km (Fig. 1). The extent of hydrated components including phyllosilicates is discussed in detail by [4].

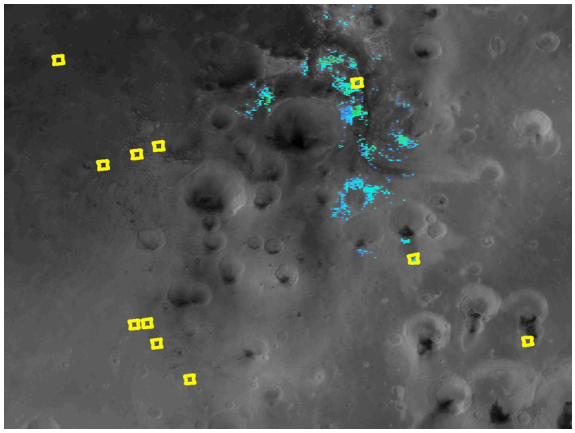

Fig. 1 Phyllosilicate identifications at Mawrth Vallis: Fe/Mg-smectite in OMEGA data (blue), Al-phyllosilicate in OMEGA data (green) and phyllosilicates in CRISM data (yellow squares). Image is 800 km across, modified from [4].

**Stratigraphy of Phyllosilicates:** The phyllosilicate units at Mawrth Vallis appear to share the same general stratigraphy in CRISM observations throughout the region (Figs. 2 and 3). Small differences are observed in spectral character and the nature of the outcrops; for example, in some cases we see kaolinite bordering the hydrated silica unit, while in other cases we see kaolinite bordering a montmorillonite unit on top of the hydrated silica. However, similar trends are observed in all images. This uniform stratigraphy at Mawrth Vallis is different from other regions on Mars, such as Nilli Fossae, where distinct provinces of clays and associated minerals have been identified [5, 6].

Analyses of spectra collected at Mawrth Vallis in relation to MOLA topography reveal that the Fe/Mg-smectite-rich rocks are typically 200-300 m lower in elevation than neighboring Al-phyllosilicate-rich and hydrated silica-rich layers [1]. The Fe/Mg-smectite exposures appear to be thicker and more resistant to erosion and in most areas they are the lowest unit visible. Differing textures and layering are also observed in HiRISE images for these distinct clay units [7, 8].

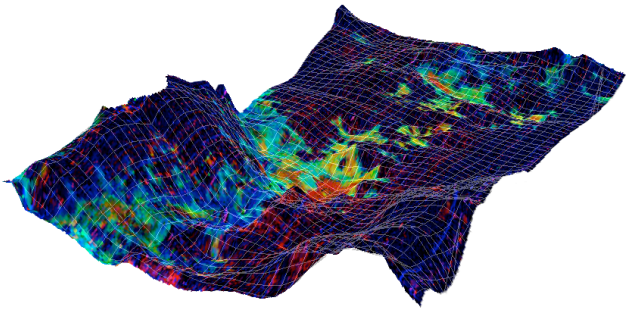

Fig. 2 CRISM image HRL43EC is draped over MOLA terrain and enhanced 20X vertically. Fe/Mg phyllosilicates are shown in orange/red, a ferrous phase in yellow, hydrated silica in green, and Al-phyllosilicates in blue.

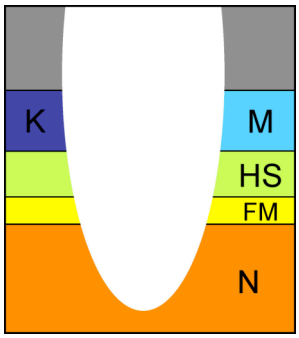


Fig. 3 Stratigraphy of phyllosilicates observed at Mawrth Vallis, where N is Fe/Mg-smectite (e.g. Mg-nontronite) in the lowest unit, FM is ferrous mica or other ferrous species bordering the nontronite, HS is hydrated silica, M is montmorillonite and K is kaolinite.

**Possible Formation Scenarios:** The nature of the phyllosilicate deposits in the Mawrth Vallis region provide insights into the possible formation processes that took place and enable determination of constraints on the early aqueous activity in the region. Smectites are commonly formed by chemical weathering in marine, lacustrine and hydrothermal environments on Earth and the species of smectite observed can provide information about the geochemical formation environment [9, 10]. Alteration of basaltic rocks typically produces Al- and Fe-bearing dioctahedral smectite, in

some cases via formation of serpentine, and metastable Mg-smectite as intermediate phases [11, 12].

The initial Fe/Mg-smectite observed at Mawrth Vallis likely formed via aqueous alteration of basalt, the dominant lithology of the Martian highlands [e.g. 13]. This smectite unit appears to drape the topography and exhibits layered textures suggesting that volcanic ash was the basaltic precursor [1]. Alternative sources include water-lain basaltic sediments and impact ejecta. The stratigraphy of the clay units is complex indicating that multiple depositional events occurred over a prolonged period of time [14].

A number of possible formation processes exist for the additional clay minerals and stratigraphy of these units. Cold and dry climates, such as those found at the Arctic, Antarctic, and high elevations on Earth, as well as on Mars today, have limited liquid water and are dominated by physical weathering [9, 10, 12, 15]. Cool and humid conditions may alter precursor rocks to form free silica and highly degraded rock-derived phyllosilicates, while warm-subarid climates favor formation of iron-bearing smectites, especially in environments with seasonal variations in humidity.

*Acid-leaching.* Alkaline conditions favor smectites under normal temperatures and pressures on Earth in the presence of Ca and favor mica in the presence of K, whereas acidic conditions support formation of kaolinite and hydrated silica [9, 10]. Assuming the presence of basaltic ash that at least partially altered to Fe/Mg-smectite, subsequent aqueous alteration and acid leaching of Fe and Mg could have produced hydrated silica, montmorillonite, mica, and kaolinite. Dissolution rates are similar for most phyllosilicates in near neutral environments and increase under lower and higher pH conditions [15]. Sedimentary micas (e.g. glauconite, illite) form from smectite under more highly altered conditions [e.g. 9]. Active hydrolysis and ion leaching in soils often results in formation of kaolinite, goethite, opal and gibbsite [e.g. 10]. Acid-leaching studies on smectites in the lab have shown the gradual formation of hydrated silica [16].

*Hydrthermal alteration.* Lab studies of hydrothermal alteration of volcanic glass have shown formation of increasing amounts of smectite and illite-smectite with reaction time [e.g. 17]. Hydrothermal alteration at Mawrth Vallis via warm standing water could have enabled formation of the multiple clay units observed due to changes in aqueous chemistry. Under long-term exposure to aqueous conditions smectites can convert to ferrous mica (e.g. glauconite) in a reducing environment, if wet/dry cycling occurs, or in the presence of abundant iron or high salinity [9, 15].

Another scenario could be hydrothermal alteration created by a large melt sheet that quickly covered a large region of basaltic ash mixed with $H_2O$ (permafrost of aquifer). The trapped $H_2O$ would have been heated and could have provided a mechanism for smectite formation from the basaltic ash. Perhaps an alteration front expanded downwards from the hot surface, thus forming the most highly altered and leached clay units (hydrated silica and Al-phyllosilicates) above the Fe/Mg-smectites.

A possible scenario for formation of the ferrous material could be an initial widespread aqueous event that produced Fe/Mg-smectite that then hardened, followed by subsequent melt sheet activity. Perhaps this could have created a layer of $Fe^{2+}$ that was leached quickly from the ash as the hydrated silica, montmorillonite and kaolinite were formed, but then was trapped at the border with the Fe/Mg-smectite and then formed $Fe^{2+}$ clays. Without contact with the surface and an oxidizing environment, this $Fe^{2+}$ could have remained in its reduced form.

**Summary:** Mawrth Vallis appears to have experienced at least one large-scale aqueous event that produced roughly uniform strata 100s of km across. Understanding the processes that formed Mawrth Vallis may enable a better picture of the early epoch of Mars.

**References:** [1] Bishop J. L. et al. (2008) *Science, 321,* DOI: 10.1126/science.1159699, pp. 830-833. [2] Poulet F. et al. (2005) *Nature, 438,* 632-627. [3] Loizeau D. et al. (2007) *JGR, 112,* doi:10.1029/2006JE002877. [4] Noe Dobrea E. Z. et al. (2008) *LPSC XXXIX*, #1077; Noe Dobrea E. Z. et al. (2008) this workshop. [5] Mustard J. F. et al. (2008) *Nature, 454,* doi: 10.1038/nature07097, 305-309. [6] Ehlmann B. L. et al. (2008) *LPSC XXXIX*, #2326. [7] Wray J. J. et al. (2008) *GRL, 35,* doi:10.1029/2008GL034385. [8] Bishop J. L. et al. (2008) *LPSC XXXIX*, #2124. [9] Chamley H. 1989), *Clay Sedimentology,* Springer-Verlag, NY. [10] Jackson M. L. (1959) *Clays Clay Miner., 6,* 133-143. [11] Caillaud J., D. Proust, & D. Right (2006) *Clays Clay Miner., 54,* 87-100. [12] Velde B. (1995), *Origin and Mineralogy of Clays*, Clays and the Environment, Springer-Verlag, Berlin. [13] Bandfield J. L., V. E. Hamilton, P. R. Christensen (2000) *Science, 287,* 1626-1630. [14] Michalski J. R. & E. Z. Noe Dobrea (2007) *Geology, 35,* 951-954. [15] Nagy K. L. (1995) in *Chemical Weathering Rates of Silicate Minerals* A. F. White, S. L. Brantley, Eds. (MSA, Wash. D.C.), vol. 31, pp. 173-233. [16] Madejova J., M. Pentrak, H. Palkova, & P. Komadel (2008) *Vibrational Spectroscopy,* in press. [17] de la Fuente S., J. Cuadros, & J. Linares (2000) *Clays Clay Miner., 48,* 299-303.

**Acknowledgements:** This work was supported by MRO, MFR, MDAP and the NAI. The CRISM Team enabled collection and processing of the data used for these analyses.

**IN SITU ANALYSIS OF MARTIAN PHYLLOSILICATES USING THE CHEMIN MINERALOGICAL INSTRUMENT ON MARS SCIENCE LABORATORY.** D. F. Blake[1], D. L. Bish[2], S. J. Chipera[3], D. T. Vaniman[4], P. Sarrazin[5] and M. Gailhanou[6] [1]MS 239-4, NASA Ames Research Center, Moffett Field, CA 94035 dblake@mail.arc.nasa.gov; [2]Dept. of Geological Sciences, Indiana University, 1001 East Tenth St., Bloomington, IN 47405; [3]Chesapeake Energy Corporation, 6100 N. Western Ave., Oklahoma City, OK 73118; [4]EES-6, MS D462, Los Alamos National Laboratory, Los Alamos, NM 86545; [5]inXitu, Inc., 2551 Casey Ave., Suite A, Mountain View, CA 94043; [6]IM2NP, UMR 6242 CNRS, Universite Paul Cezanne, Aix-marseille III, Marseille, France.

**Introduction:** The CheMin mineralogical instrument on Mars Science Laboratory (MSL '09) [1] will return quantitative X-ray diffraction data (XRD) and qualitative X-ray fluorescence data (XRF; 14<Z<92) from scooped soil samples and drilled rock powders collected from the Mars surface. Samples of 45-65 $mm^3$ from material sieved to <150 µm will be delivered through a funnel to one of 27 reusable sample cells (five additional cells on the sample wheel contain diffraction or fluorescence standards). Sample cells are 8-mm diameter discs with 7-µm thick Mylar or Kapton windows spaced 170 µm apart. Within this volume, the sample is shaken by piezoelectric vibration at sonic frequencies, causing the powder to flow past a narrow, collimated X-ray beam in random orientations over the course of an analysis. In this way, diffraction patterns exhibiting little to no preferred orientation can be obtained even from minerals exhibiting strong preferred orientation such as phyllosilicates. Figure 1 shows the geometry of the source, sample, and detector.

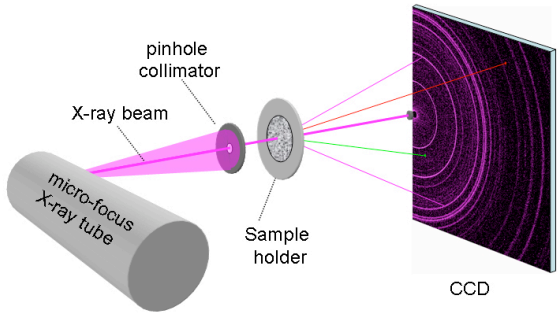


***Fig. 1.*** *Geometry of CheMin instrument. A 50-µm diameter collimated Co X-ray beam is directed through a powder sample held between X-ray transparent windows.*

Individual analyses will require several hours over one or more Mars sols. For typical well-ordered minerals, CheMin has a Minimum Detection Limit (MDL) of <3% by mass, an accuracy of better than 15% and a precision of better than 10% for phases present in concentrations >4X MDL (12%). CheMin utilizes a Co X-ray tube which minimizes absorption in iron-rich samples. The resolution of the diffraction patterns is 0.30° 2θ, and the angular measurement range is 4-55° 2θ.

**Terrestrial Versions of CheMin:** Several terrestrial prototype CheMin instruments have been developed to evaluate the capability of the instrument for qualitative and quantitative analysis of single minerals and complex mixtures. Patterns are of sufficient quality that commercial search-match programs can readily identify the major mineralogy of a sample and quantitative analysis via Rietveld refinement or full-pattern fitting can be performed with 1-4 hours of data or less, depending on sample complexity. Successful Rietveld analyses have been performed using data collected for only 5-10 minutes using the field-deployable Terra instrument, a commercial version of CheMin [2].

**Phyllosilicates on Mars:** The OMEGA imaging spectrometer aboard Mars Express [3,4] has revealed a rich diversity of mineralogy on the surface of Mars, including the hydrated clay mineral nontronite in older cratered terrains [5], along with montmorillonite and other clay minerals [6]. Recent observations of hydrated silicate minerals by the CRISM instrument on Mars Reconnaissance Orbiter have validated these observations and provided an even more detailed picture of the distribution of hydrous phyllosilicates on the martian surface [7,8]. OMEGA and CRISM data also suggest the presence of diverse clay minerals, including kaolins, chlorites, and serpentine minerals, along with a variety of hydrous sulfate minerals.

**Clay mineral analysis with CheMin:** Although orbiters and rovers have provided tantalizing clues regarding alteration mineralogy on the martian surface, the traditional method for analyzing mineralogy, particularly clay mineralogy, is X-ray diffraction (XRD). Discriminating between the variety of possible silicate clay minerals is traditionally done by taking advantage of the existence of distinct large repeat distances perpendicular to the phyllosilicate layers. As clay mineral discrimination is based primarily on these repeat distances in their structures, it is therefore crucial that a martian XRD instrument be capable of detecting low-angle (large d-spacing) diffraction peaks. Figures 2, 3 and Table 1 show CheMin results obtained from a synthetic mixture of phyllosilicate and evaporite minerals. In figure 2, the ~15Å d-spacing from nontronite (7º 2θ) is seen as the first spatially distinct bright ring of intensity around the undiffracted beam (silhouette of beam stop is seen at the center of the lower edge of the image). Figure 3 shows the conventional 1-D diffracto-

gram that results from summing the 2-D pattern circumferentially around the central undiffracted beam. Table 1 shows a quantitative analysis of this sample using the program FULLPAT [9].

With this performance, CheMin can identify and distinguish a number of clay minerals. For example, discrimination between 1:1 phyllosilicates (such as the kaolin minerals), with repeat distances of ~7Å, and smectites (e.g., montmorillonite, nontronite, saponite), with repeat distances from 10-15Å, is straightforward. However, it is important to note that the variety of treatments used in terrestrial laboratories to aid in discrimination of clay minerals will not be accessible on Mars (e.g., saturation with ethylene glycol vapor, heat treatments). Although these treatments will not be available on Mars, dehydration within the CheMin instrument could be used to advantage in discriminating between phyllosilicate minerals that exhibit different dehydration behavior, such as chlorite vs. smectite. In addition, it should be possible to identify the hydrated kaolin mineral, halloysite. The lowest-angle diffraction peak from 10.1Å hydrated halloysite occurs at ~10.2º 2θ with Co radiation and is easily detectable; the mineral may readily dehydrate to ~7Å, making its identification possible based on this transition.

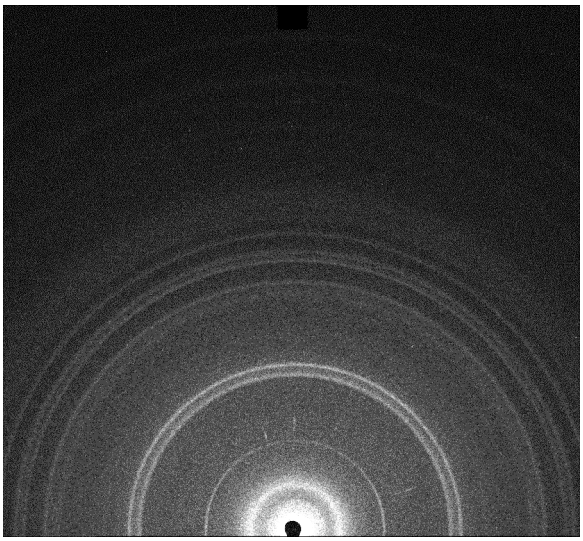

***Fig 2.*** *2-D image of diffraction pattern from a synthetic clay-bearing evaporite sample. The direct beam is at the lower center of the image; 2θ increases radially with distance from this point.*

**Clay Minerals and MSL landing sites:** Study of clay mineralogy *in situ* on Mars will begin with the arrival of CheMin on MSL in 2010. Potential landing sites include the Nili Fossae Trough, Mawrth Vallis, Southern Meridiani, Holden Crater, Miyamoto Crater, Eberswalde Crater, and Gale Crater. All sites have evidence of sedimentary processes along with spectral signatures of smectites and, in many cases, kaolinite. Wherever MSL lands, clay mineralogy will be a critical component of determining hydrogeologic history and habitability.

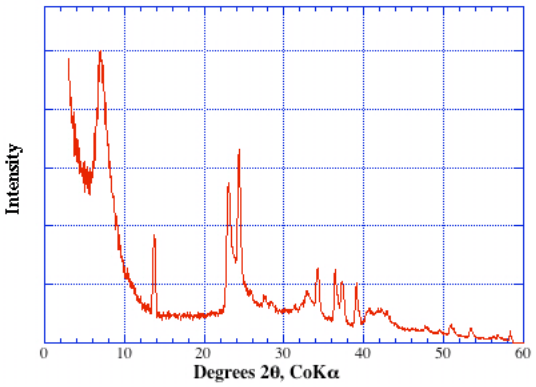


***Fig 3.*** *1-D 2θ diffractogram of the 2-D image in Fig. 2. The low angle detection capabilities of CheMin allow detection of the basal spacing of all natural phyllosilicates.*

***Table 1.*** *Quantitative XRD analysis of a synthetic clay-bearing evaporite.*

| Phase | Measured (wt%) | Known (wt%) | Known vs. measured (diff., %) | Comment |
|---|---|---|---|---|
| Nontronite | 69 | 61 | 13.1 | Within 15% |
| Gypsum | 22.6 | 25 | -9.6 | Within 15% |
| Halite | 2.8 | 8.7 | -67.8 | <4x MDL |
| Hematite | 5.7 | 5.3 | 7.5 | Within 15% |

**References:** [1] P. Sarrazin et al., (2005). *Powder Diffraction* **20**, 128-133.
[2] http://www.inxitu.com/index_analytical.html. [3] J-P Bibring et al., (2004). Eur. Space Agency Spec. Pub. **1240**, 37. [4] A. Chicarro, et al., (2004). Eur. Space Agency Spec. Pub. **1240**, 3. [5] J-P Bibring et al., (2005). *Science* **307**, 1576-1581. [6] F. Poulet et al., (2005). *Nature* **431**, 623-627. [7] J.F. Mustard et al., (2008). *Nature* **454**, 305-309. [8] J.L. Bishop et al., (2008). *Science* in press. [9] Chipera, S.J., and Bish, D.L. (2002). *J. Applied Crystallography*, **35**, 744-749.

**MECHANISMS AND CONDITIONS OF SAPONITE PRODUCTION IN THE PRECAMBRIAN DOUSHANTUO FORMATION.** T. F. Bristow and M. J. Kennedy, Department of Earth Sciences, University of California – Riverside, 900 University Ave, Riverside, CA 92521. tbris001@student.ucr.edu

**Introduction:** In the Yangtze Gorges region of South China, exposures of Doushantuo Formation record sedimentation in an intrashelf basin on the Yangtze Block between 635 and 551 Ma [1]. The Doushantuo Formation is probably best known because it hosts exquisitely preserved spherical multicellular fossils, widely thought to represent embryos of some of the oldest animals fossils [2]. However, sections in the Yangtze Gorges area also contain some of the oldest sedimentary saponite deposits on Earth [3]. This paper documents the clay mineralogy of the Doushantuo Formation, focusing on the mechanisms and conditions in which saponite formed, as well as diagenetic reactions that affected clays during burial. The discussion of formation processes on early Earth may give new insights into the origins of extensive magnesium-smectite deposits found on Mars.

**Methods:** Clay mineralogy was investigated using X-ray diffraction of powdered whole rock samples and clay extracts of representative samples, as well as SEM observations of broken chips.

**Background:** Stratigraphic sections of the Doushantuo Formation are between 100-200m thick in the Yangtze Gorges area, and are typically divided into four members (fig.1). Member 1 is the 3-5m thick 'cap carbonate,' that consists of vuggy, carbonate and silica cemented dolomicrites passing upward into partially disrupted, thinly bedded micritic carbonates. The cap marks the transition from intense icehouse conditions that characterize the middle Neoproterozoic (reviewed by [4]), and in S. China sharply overlies glacially derived diamictites of the underlying Nantuo Formation. The cap is conformably overlain by ~80m of calcareous mudstones and marls with interbedded muddy dolomites and limestones. A predominance of mm-scale, parallel laminations indicate deposition below storm wave-base. In member 3 (~60m thick) cross-bedding and scouring observed in silty dolomites with thin mudstone partings, indicate deposition in shallower water depths. There is a sharp lithological change to organic-rich, silty mudstones of member 4, that are ~10m thick

**Distribution of Clays:** *Lower Doushantuo Fm.* Saponite and its diagenetic products, corrensite and chlorite dominate the clay mineral assemblage and make up to 30% of the bulk rock in samples from the lower 80m of the Doushantuo Formation. Corrensite and chlorite are more abundant in the cap carbonate and the lower part of member 2, with an upward transition to pure saponite. However, the stratigraphic position and extent of the transition varies between sections.

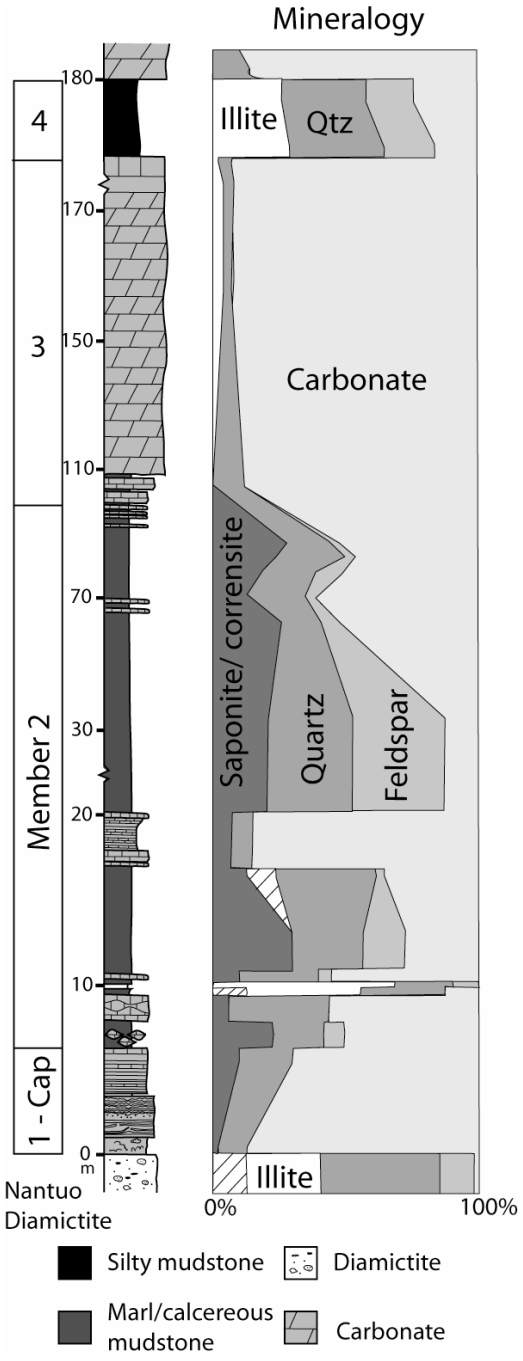


*Figure 1.* Simplified stratigraphy and mineralogical distribution of the Doushantuo Formation in the Yangtze Gorges.

*Upper Doushantuo Fm and ash beds.* In contrast, Mg-smectites are absent in the upper part of the formation. Silty mudstones of member 4 contain illite-rich, mixed layer, dioctahedral, illite/smectite (I/S). The clay fraction of thin (<5cm) ash beds occurring within the cap carbonate and at the top of member 4 also consists of illite-rich I/S.

**Origin of saponite:** A secondary mechanism for the formation of saponite, such as hydrothermal alteration of basaltic detritus [5], or diagenetic reaction between dolomite and Al-phyllosilicates [6] is ruled out because: a) SEM observations show random clay fabrics, which are interpreted as having a detrital origin [7], rather than secondary fabrics such as pore-filling cements or mineral overgrowths, b) the absence of basaltic material in the Doushantuo Formation, and in underlying lithological units in this part of the Yangtze Platform, and c) the purity of saponites in many samples (the reaction between dolomite and Al- phyllosilicates produces corrensite [6]), and absence of saponite in calcareous mudstones of member 3 despite evidence that the entire formation experienced the same thermal history.

The reworking of an older deposit, or erosion of a saponite generating soil as a source of clays is also unlikely given that the monomineraliac nature of the clay mineral assemblage through the lower 80m of the formation requires an exclusively saponitic clay source to be maintained and eroded for millions of years – based on current estimates of depositional rates in the Doushantuo Formation [8].

Instead, compositional and textural evidence indicate that saponite formed by neogenesis of original detrital clays. The conversion of Al to Mg-rich phyllosilicates occurs in sedimentary systems under high pH (greater than ~9) or high Mg concentrations. During the Phanerozoic, favorable conditions are found in alkaline lakes or evaporative sabkahs [9, 10, 11]. The absence of evaporites in the Doushantuo Formation leads to two possible interpretations for the presence of saponite: a) deposition in an isolated basin under alkaline conditions, or b) anomalous Precambrian ocean chemistry that was favorable for the process of neogenesis.

Based on this interpretation, the switch to an Al-phyllosilicate assemblage indicates a change in paleoenvironmental conditions during member 3.

**Diagenetic pathways of Al and Mg-smectites:** Comparisons of clays in different parts of the Doushantuo Formation also give indications of the relative resistance of Mg and Al-smectites to diagenetic change under the same thermal conditions. Ash beds at the top and bottom of the formation were presumably devitrified and converted to Al-smectites soon after deposition, but were largely illitized during burial. Member 4 mudstones probably originally contained Al-smectite or smectite-rich I/S and followed the same diagenetic pathway. In comparison, many saponite-rich samples from member 2 have not been chloritized. The difference in degree of diagenesis can be attributed to greater thermal stability of saponite [12] and differences in the alteration pathways of trioctahedral and dioctahedral smectites (chloritization vs. illitization) [13]. The host lithology is also an important factor in controlling the degree of chloritization of saponite because Mg or Fe is required for the reaction [6, 14].

**References:** [1] Condon, D. et al. (2005) *Science, 308,* 95-98. [2] Xiao, S. et al. (1998) *Nature, 391,* 553-558. [3] Bristow, T. F. *GSA Abstracts, 36,* no. 5, 377. [4] Fairchild, I. J. and Kennedy, M. J. (2007) *J. Geol. Soc., 164,* 895-921. [5] Setti, M. et al. (2004) *Clay Miner., 39,* 405-421. [6] Hillier, S. (1993) *Clays Clay Miner., 41,* 240-259. [7] O'Brien, N. R. and Slatt, R. M. (1990) *Argillaceous rock atlas*, New York, Springer-Verlag, 141 p. [8] Zhou, C. et al. (2007) *Geol. J., 42*, 229-262. [9] Jones, B. F. (1986) *USGS Bull.,* 1578, 291-300. [10] Banfield, J. F. (1991) *GCA, 55,* 2795-2810. [11] Hover, V. C. et al. (1999) *Clays Clay Miner., 47,* 252-268. [12] Velde, B. (1977) *Clays and clay minerals in natural and synthetic systems,* Amsterdam, Elsevier, 218 p. [13] Meunier, A. (2005) *Clays,* Berlin, Springer, 472 p. [14] Sandler, A. (2001) *Clay Miner., 36,* 29-47.

**PHYLLOSILICATES IN THE ARGYRE BASIN, MARS.** D. L. Buczkowski[1], S. Murchie[1], R. Clark[2], F. Seelos[1], E. Malaret[3], C. Hash[3] and the CRISM Science Team, [1]Johns Hopkins University Applied Physics Lab (Laurel, MD 20723, Debra.Buczkowski@jhuapl.edu), [2]USGS (Denver, CO 25046), [3]Applied Coherent Technology (Herndon, VA 20170).

**Introduction:** The Argyre basin is a >1500 km, well preserved impact basin in the southern highlands of Mars. The geologic units associated with the basin (Fig. 1) are mostly Noachian in age [1]. Thus, Argyre is an ideal location to characterize ancient highland rocks.

**Methods:** We analyzed 72-channel CRISM multispectral data that had been map projected to 256 pixels per degree. The data were corrected for illumination by dividing by the cosine of the solar incidence angle and a multiplicative correction for atmospheric gas absorption [2] was applied. Spectrally distinct regions were identified by calculating summary parameters [3]; spectra of key areas were then examined in detail. Based on our evaluation of these data, areas of interest were identified and higher resolution targeted observations covering them were aquired. Phyllosilicates have been detected in eight 20 m/pixel resolution targeted observations of the basin interior (Fig. 2).

**Observations:** We use tetracorder to interpret CRISM full resolution data. Tetracorder is a software tool which utilizes an expert system decision methodology to analyze spectra to identify components in the spectrum [4].

In northwest Argyre is a scarp roughly associated with a contact between the $Hpl_3$ (interpreted as Hesperian aged lava flows and eolian deposits) and $Npl_1$ (interpreted as a Noachian mixture of lava flows, pyroclastic material and impact breccia) units. Phyllosilicates have been identified extending laterally along the scarp, related to the fluvially dissected impact breccias of unit Npld (same origin as unit $Npl_1$ but is more eroded by fluvial processes). Below the phyllosilicates are found deposits of high-Ca pyroxene in unit Npld, similarly hugging scarps. High-Ca pyroxene is also identified in the undissected impact breccias of unit $Npl_1$, perhaps at the same stratigraphic level of the Npld pyroxenes.

Phyllosilicates have also been observed on the north-central Argyre rim and around Hale crater, which impacts the north-central Argyre rim. Interestingly, other CRISM images of the northern rim of Hale do not indicate phyllosilicates, only those CRISM images at or inside the Argyre rim line. This may indicate that these phyllosilicates did not form during the Hale impact event, but rather are sampling pre-existing phyllosilicates exposed by the Argyre event.

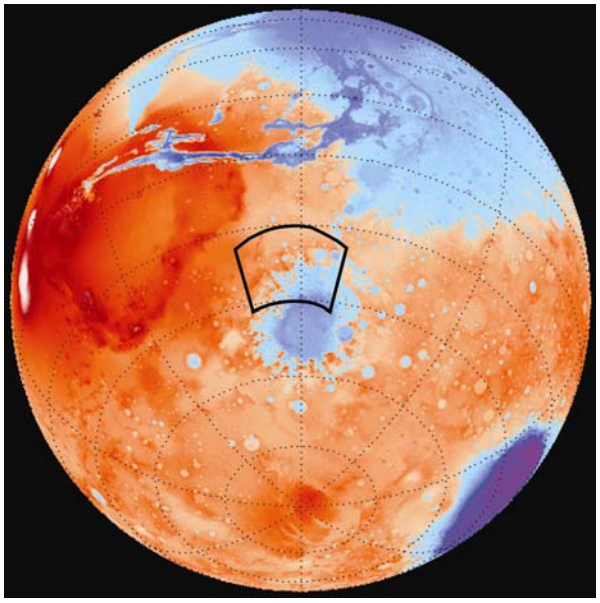

Figure 1. MOLA topography of Mars centered at 45°S, 45°W showing the location of the Argyre basin. Inset box shows location of figure 2.

Also, at least two high-standing knobs in the $Npl_1$ unit have a strong phyllosilicate signature. A targeted observation of one of the knobs indicates that the phyllosilicate might be prehnite (Fig. 3). However, other Arygre images indicate the presence of chlorite.

**Conclusions**: We suggest that these deposits, along with other minerals identified in the CRISM data, reveal the stratigraphy of the Noachian crust in this region (Fig. 4). At the bottom of the stratigraphic column are olivine and low-Ca pyroxene associated with uplifted ancient volcanic rocks (unit Nplh). Above these deposits are high-Ca pyroxenes associated with lavas and impact-formed materials (unit $Npl_1$ and Npld). The phyllosilicates we've observed appear within the same units as the high-Ca pyroxene, but stratigraphically above it, preserved both in freestanding knobs and along scarp walls. At the top of the stratigraphic column in northwest Argyre is olivine associated with the early Hesperian $Hpl_3$ unit.

**References:** [1] Scott and Tanaka (1986) Inv. Series Map I-1802-A. [2] Bibring et al. (2005) Science 307(5715):1576-81. [3] Pelkey et al. (2007) JGR, 112, E08S14, doi:10.1029/2006JE002831. [4] Clark et al. (2003) JGR, doi: 10.1029/2002JE001847.

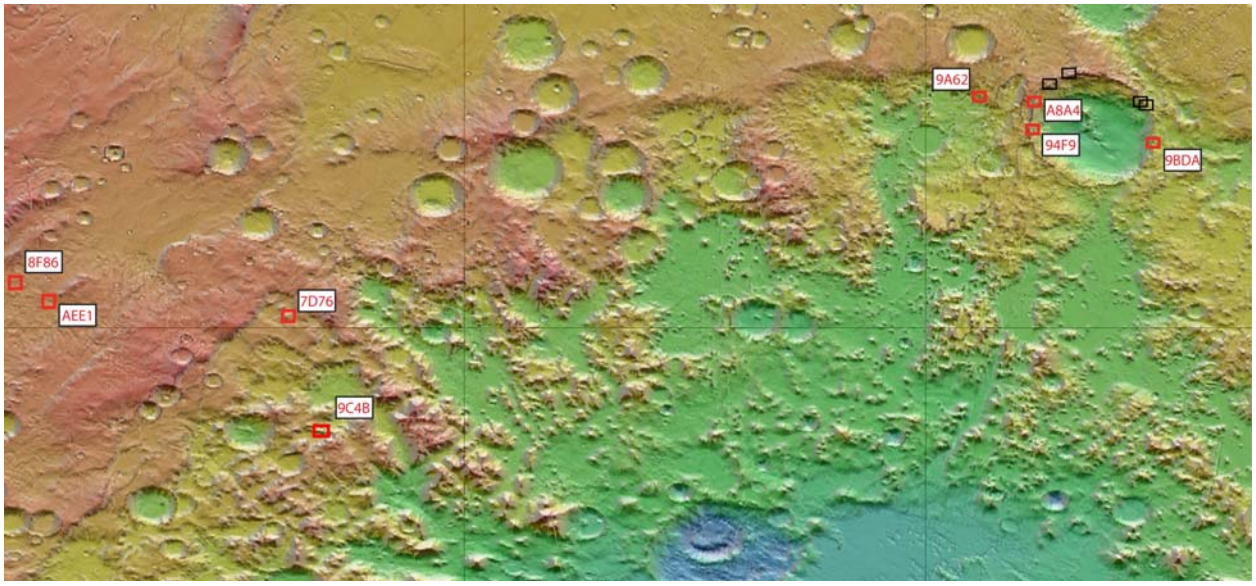


Figure 2. Colorized MOLA topography draped over THEMIS daytime infrared mosaic of north-western Argyre. Red boxes show the location of CRISM targeted observations that show phyllosilicates. Black boxes indicate CRISM targeted observations of the Hale crater rim that do not show phyllosilicates.

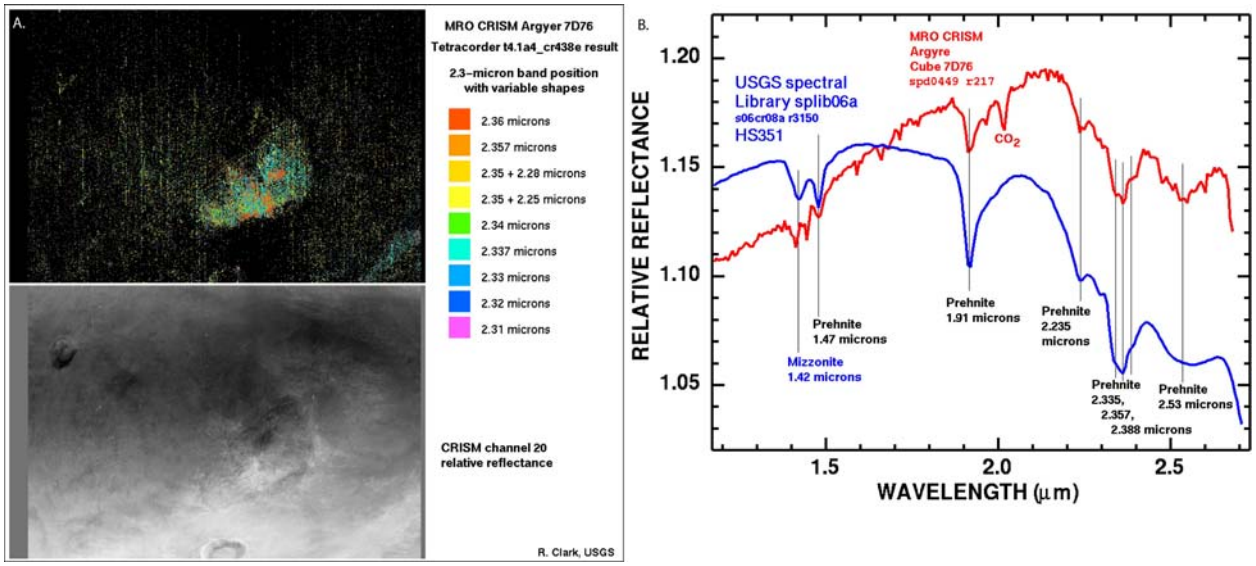


Figure 3. a) Tetracorder analysis of CRISM FRT 7D76 shows range of 2.3 micron absorptions in image. b) Comparison of spectra from 7D76 to USGS spectral library indicates that this phyllosilicates knob is primarily prehnite.

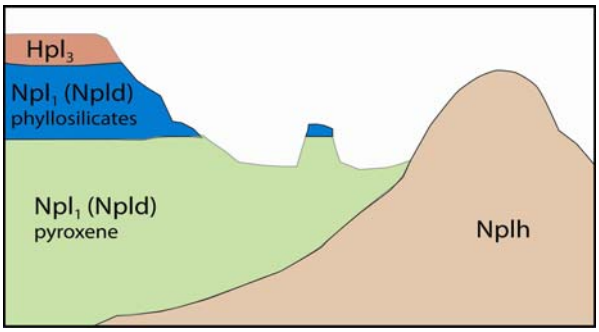


Figure 4. Proposed Argyre stratigraphic cross-section.

**EARLY MARTIAN SURFACE CONDITIONS FROM THERMODYNAMICS OF PHYLLOSILICATES.**
V.F. Chevrier[1], [1]W.M. Keck Laboratory for Space Simulations, Arkansas Center for Space and Planetary Sciences, 202 Old Museum Building, University of Arkansas, Fayetteville, AR 72701, USA. <vchevrie@uark.edu>.

**Introduction:** The Mars Express OMEGA and Mars Reconnaissance Orbiter CRISM imaging spectrometers have identified phyllosilicates (Fe, Mg, Ca-smectites, kaolinite and chlorite) in Noachian aged terrains [1,2], often associated with lacustrine or fluvial deposits [3,4]. Clay minerals usually result from long term weathering of primary minerals by liquid water at neutral to alkaline pH [5], suggesting an early environment completely different from the acidic conditions responsible for the formation of sulfate outcrops widely observed on Mars [6,7]. This also suggests a global evolution of the martian surface environment, through loss of water from the surface [5,8].

Starting from the hypothesis that phyllosilicates are formed by liquid water induced weathering of the primary basaltic outcrops, thermodynamic models are used to study the conditions on the surface during the Noachian. Focus was placed on the effect of acidic conditions and temperature using solution equilibria and thermodynamic models.

**Methods:** The water composition data presented in Table 1 was used as input of the models. This composition reflects possible primary solutions on Mars [9]. $Al^{3+}$ and $SiO_2$ have been set up at typical terrestrial values, being generally driven by their low solubility. The Geochemical Workbench software package was used to model thermodynamic equilibria, with the *thermo_phrqpitz* database, which is especially designed for solution equilibrium at ionic strength using the Pitzer model. This database was updated by including the Pitzer parameters for $Fe^{2+}$ and $Fe^{3+}$ as well as ferric and ferrous aqueous species [10,11]. Also included are approximately 350 silicates taken from the *thermo.com.v8.r6+* database.

**Table 1**. Primary concentrations and activities of dissolved species taken from [9] except for $Al^{3+}$ and $H_4SiO_4$ which are estimated for the present work.

| Specie | Log (Activity, $10^{-3}$ mol $l^{-1}$) | Concentration (mg $L^{-1}$) |
|---|---|---|
| $SiO_2$ | -4.5 | 60.1 |
| $Al^{3+}$ | -5 | 0.3 |
| $Fe^{2+/3+}$ | -3.1 | 44.7 |
| $Mg^{2+}$ | -3.0 | 24.3 |
| $Ca^{2+}$ | -3.3 | 20 |
| $K^+$ | -4.2 | 2.7 |
| Na+ | -3.1 | 18.4 |
| $SO_4^{2-}$ | -3.7 | 17.3 |
| $Cl^-$ | -3.2 | 23 |

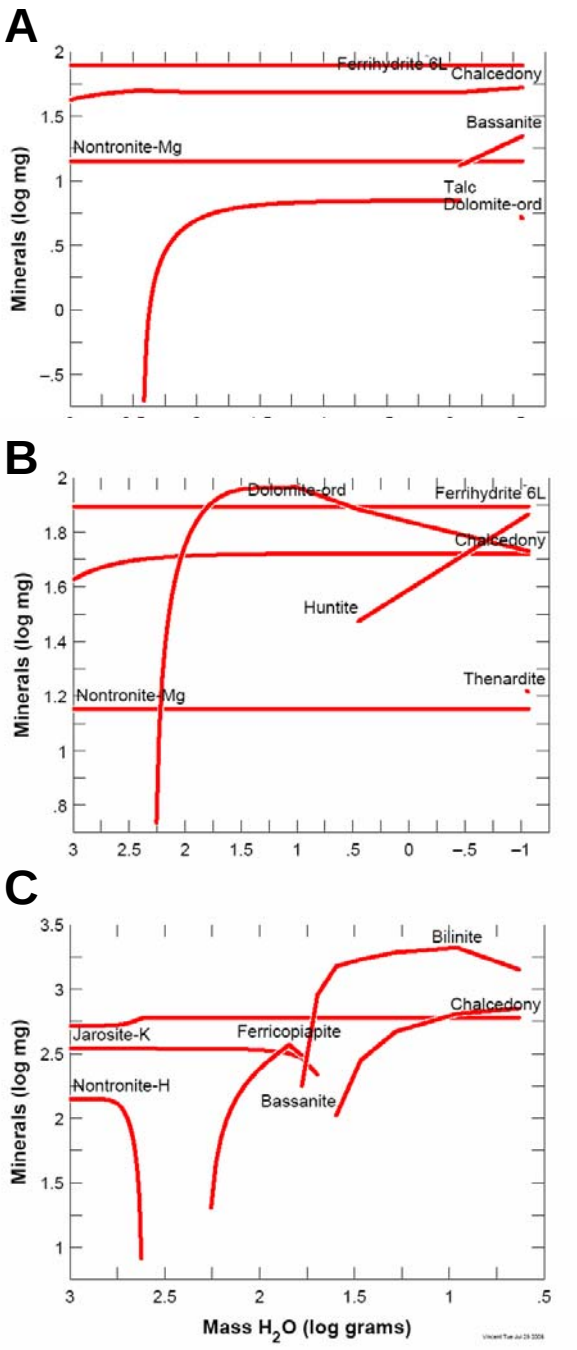


**Figure 1**: Three simulations of evaporation processes at 25ºC using initial compositions presented in Table 1 with pe = 13.05 (high oxidation level). **(A)** $p_{CO2}$ = 0.001 bar, pH = 7. **(B)** $p_{CO2}$ = 1 bar, pH = 7, $[Cl^-]$ = 120 mg $L^{-1}$. **(C)** $p_{CO2}$ = 0.006 bar, pH = 3, $SO_4^{2-}$ = 5000 mg $L^{-1}$, all concentrations are multiplicated by 10 to simulate an advance state of evaporation.

**Evaporation simulations:** In all simulations, the evaporation paragenesis is largely dominated by ferric phases. In such a Fe-rich geochemical system, the early paragenesis (high water content) includes mostly nontronite, ferrrihydrite and chalcedony (Fig. 1A&B). All these phases precipitate from the very beginning of the simulation, indicating that the early solution is supersaturated at neutral pH and high pe. The amount of precipitated phyllosilicate is largely dependent on availability of $Al^{3+}$.

In low $p_{CO2}$, nontronite dominates along with silica (chalcedony) and ferrihydrite (Fig. 1A). If the $CO_2$ pressure becomes high, then carbonates become prdominant (Fig. 1B). However, siderite does not appear because the conditions are too oxidizing.

Finally, in the presence of sulfur (in this case $SO_4^{2-}$, resulting from sulfides or $SO_2$), the evaporite assemblage is dominated by ferric sulfates (jarosite, ferricopiapite and bilinite). This case shows the lowest stability of nontronite, which dissolves very early in the evaporation sequence as a result of conditions becoming strongly acidic. In most simulations, smectites did not last in acidic conditions, with the exception of kaolinite which can precipitate down to pH ~ 2.

**Temperature effect**: Two different scenarios were investigated for the effect of temperature on the precipitating parageneses. In the first one, the conditions are oxidizing (pe = 13.05) which can simulate the effect of increasing the temperature on the surface, for example by volcanic activity. In this case, nontronite appears remarkably stable, destabilizing only at temperature above 190ºC.

In the second scenario, conditions are strongly reducing (pe = -5). This corresponds to typical terrestrial subsurface hydrothermal systems. In this case the mineralogical paragenesis appears very complex, with several assemblages of $Fe^{2+}$ and $Fe^{3+}$ phyllosilicates evolving with the temperature. Globally, carbonates and nontronite are stable up to ~50ºC. Other iron silicates are present up to 75ºC, including minnesotaite and cronstedtite. At higher temperature, iron phyllosilicates are not stable any more and are replaced by magnetite + saponite. At temperatures higher than ~140ºC, chlorite (clinochlore) becomes stable.

**Conclusions**: These simulations confirm previous results concerning low-$CO_2$ pressure during the Noachian [5]. Nevertheless, while some specific conditions could lead to clays-carbonates associations (high pH, low pe, low temperature), these minerals appear mutually excusive with sulfate deposits.

Thermal results indicate that chlorite identified by CRISM [2] formed in localized reducing conditions. However, the genral abundance of Fe,Mg-smectites still suggests an overall oxidizing environment.

Further study will focus on the variability of smectite silicates (Fe, Mg, Al) to constrain primary solutions and the relationship with bedrock and atmosphere.

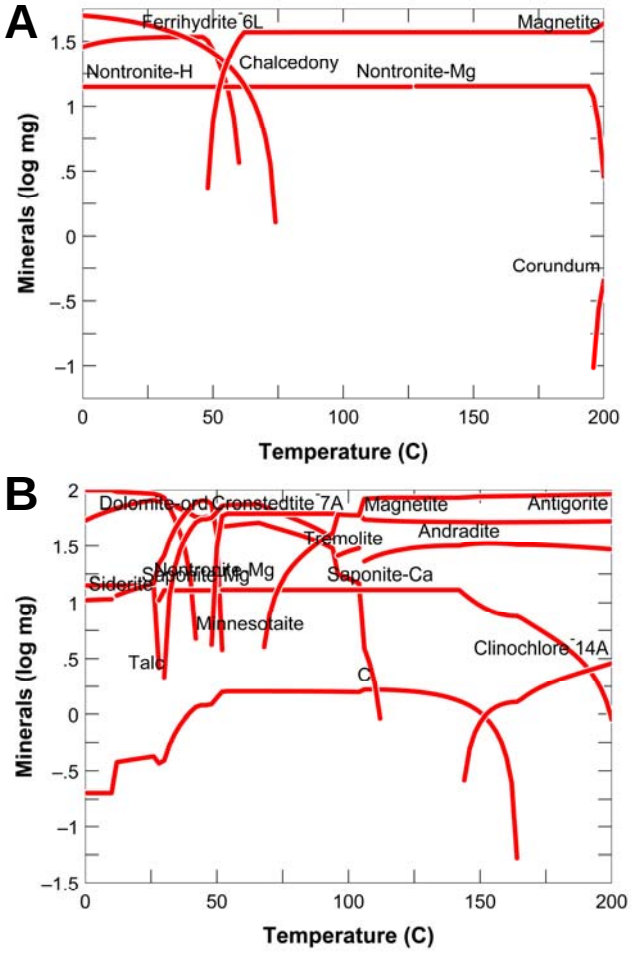


**Figure 3**: Evolution of the secondary paragenesis as a function of the temperature of the system. **(A)** pH = 7 and pe = 13.05. **(B)** more reducing conditions with pH = 7 but pe = -5. Nontronite is much more stable at high pe, but the conditions need to be reducing for chlorite to precipitate.

**References:** [1] Poulet F. et al. (2005) *Nature* 481, 623-627. [2] Mustard J. F. et al. (2008) *Nature* 454, 305-309. [3] Ehlmann B. L. et al. (2008) *Nature Geosci.* 1, 355-358. [4] Grant J. A. et al. (2008) *Geology* 36, 195-198. [5] Chevrier V. et al. (2007) *Nature* 448, 60-63. [6] Gendrin A. et al. (2005) *LPSC* XXXVI. [7] Squyres S. W. et al. (2004) *Science* 306, 1709-1714. [8] Bibring J. P. et al. (2006) *Science* 312, 400-404. [9] Catling D. C. (1999) *J. Geophys. Res.* 104, 16453-16469. [10] Marion G. M. et al. (2008) *Geochim. Cosmochim. Acta* 72, 242-266. [11] Tosca N. J. et al. (2007) *Geochim. Cosmochim. Acta* 71, 2680-2698.

**CHEMICAL CONTROLS ON PHYLLOSILICATE COMPOSITION AT THE EARLY FORMATION STAGE.** J. Cuadros[1], V. Dekov[2], L. Aldega[3], S. Fiore[4], [1]Natural History Museum, (Department of Mineralogy, Cromwell Road, London SW7 5BD, UK, j.cuadros@nhm.ac.uk), [2]University of Sofia (Department of Geology and Palaeontology, 15 Tzar Osvoboditel Blvd., 1000 Sofia, Bulgaria), [3]Universitá di Roma Tre (Department of Geology, L.go San L. Murialdo 1, 00146 Rome, Italy), [4]Istituto di Metodologie per l'Analisi Ambientale, CNR (Tito Scalo [PZ], Italy).

**Introduction:** The average rock on Mars surface is of magmatic type with a felsic composition in the northern hemisphere and a mafic composition in the southern hemisphere. The chemistry of the original rock should be one of the controls on the type of clay minerals that formed (and are still forming?) on Mars surface. However, the interplay between rock chemistry and that of the altering fluids to produce clay minerals can be rather complicated. The present contribution presents some studies of clay formation, mainly at the early stage, where several factors affecting chemical control are illustrated. They can be used to analyse what type of clay minerals can be expected to form in the several environments on Mars surface.

**Rock control on clay formation:** The first study reported is a hydrothermal alteration of rhyolitic glass in a wide range of temperature and water chemistry conditions (5 g of glass in 25 ml of water; NaCl/KCl molar ratio 0.01-100; total chloride concentration 0.01-1 M; other experiments used deionized water; 60-180 ºC; 60-360 days). The aim was to investigate the formation of illite-smectite of different illite content. Surprisingly, the products were consitently illite-smectite with approximately 25% illite layers [1]. SEM and TEM studies with microanalysis showed that the major mechanism for illite-smectite formation was a direct transformation of the glass, with evidence of minor precipitation from solution [2]. Analysis of the aqueous activity diagrams showed that some were consistent and some inconsistent with illite-smectite formation. These results were interpreted to indicate a complete control of the glass chemistry on the composition of the neoformed clay.

In a second study (in progress) we investigated the alteration of phlogopite crystals in a matrix of phonolitic glass, from a (seemingly) pyroclastic deposit (although one author describes it as a dyke), in a karstic environment (Grotta del Cervo, Pietrasecca, Italy). Fine phlogopite crystals show alteration to mica-smectite with 1-4% smectite. SEM-EDS observation of large phlogopite crystals shows progressive in-situ alteration of mica layers towards beidellite (dioctahedral, Al-rich smectite). In this case, the almost complete loss of octahedral Mg from the phlogopite precursor and large increase in Al and Si contents indicates that water chemistry controlled the composition of the neoformed phase, even though the alteration mechanism appears to be a solid-state transformation, as in the case of the rhyolitic glass. Seemingly, the local environments where the transformation reaction takes place in the glass and the mica have different characteristics. Glass alteration starts by penetration of protons (with cation exchange) and water within the glass, which may result on the transformation process taking place within the glass grains (very near the surface) and thus, controlled mainly by glass chemistry. Alteration of the phlogopite crystals probably takes place from the outer surface (edges of the layers, primarily) and water chemistry controls the coposition of the resulting phase.

**Mg-rich phyllosilicates:** Trioctahedral Mg-rich phyllosilicates of the 2:1 type (2 tetrahedral sheets, 1 octahedral sheet) can be easily synthesized hydrothermally. The yields are large in periods as short as several hours, depending on the method. The synthesis of Al-rich (dioctahedral) counterparts is much slower, with reactions taking months. However, Al-rich phyllosilicates are a much more common product of silicate alteration in natural environments. This is probably a reflection of the fact that Mg is less abundant than Al in silicates and of the mechanism of the alteration process, both favouring rock control. The formation of Mg-rich phyllosilicates needs high Mg contents in the rock and/or a high Mg activity in the altering fluids. Recently, a study of the early stage of amphibole weathering in a soil environment showed that Mg-rich smectite formed on some crystallographic faces and Al-rich smectite on others [3].

Our recent study of clay minerals from several submarine hydrothermal fields [4] showed talc formation on the surface of the marine sediment and in open cracks in contact with seawater, where the Si-rich hydrothermal fluids mixed with the seawater and the Mg supply from the latter is unrestricted. On the contrary, we observed the formation of talc-smectite with increasing Al content in the interior of chimney structures. In this secluded environment, the Mg supply is restricted as seawater has to penetrate through the chimney walls and the resulting phase contains more Al. Accordingly with these considerations, Mg-rich phyllosilicates are probably restricted to the southern Martian hemisphere.

**Fe-rich phyllosilicates:** Iron is abundant on Mars surface. A recent study, still in progress, of metalliferous deposits from the East Pacific Rise, off the Chilean coast, has shown a mechanism of phyllosilicate (smectite-type) formation that may be relevant to Mars.

The hydrothermal fluids in the studied region are rich in Si and Fe. At the contant between these fluids and seawater, Fe is oxidized and precipitated as very fine-grained, low crystallinitiy Fe oxide. Our samples from the east Pacific Rise have large amounts of biogenic calcite and lower amounts of a non-crystalline Fe-rich phase. Calcite was removed by reaction with dilute HCl. X-ray diffraction does not detect crystalline clay phases. However, SEM-EDS observation reveals numerous μm-size grains of smectite-like composition. Many of these have a high Fe content (nontronite-like) whereas others are Al-rich (montmorillonite-like). Our interpretation is that these grains correspond to "proto-clays", particles with smectitic or near-smectitic composition in the process of maturation to acquire a crystalline structure. Reaction of amorphous Fe oxyhydroxide with dissolved silica is one of the proposed mechanisms for the formation of nontronite in submarine hydrothermal fields [5].

**References:** [1] de la Fuente S. et al. (2002) *Clays Clay Miner., 50,* 578-590. [2] de la Fuente S. et al. (2000) *Clays Clay Miner., 48,* 339-350. [3] Proust D. et al. (2006) *Clays Clay Miner., 54,* 351-362. [4] Dekov V. et al. (2008) *Chem. Geol., 247,* 171-194. [5] Severmann S. et al. (2004) *Geochim. Cosmochim. Acta, 68,* 73-88.

**Acknowledgements:** Sandra de la Fuente, now working for Industry, and Jose Linares, now retired, also contributed as authors to some of the studies in this contribution, at the Departamento de Ciencias de la Tierra y Quimica Ambiental, Estacion Experimental del Zaidin, CSIC, Granada, Spain.

**DISCRIMINATING AMONG LAYER SILICATES USING REMOTE MÖSSBAUER SPECTROSCOPY.** M. D. Dyar[1] and M. W. Schaefer[2]. [1]Department of Astronomy, Mount Holyoke College, 50 College St., South Hadley, MA 01075, mdyar@mtholyoke.edu. [2]Department of Geology and Geophysics, E235 Howe-Russell, Louisiana State University, Baton Rouge, LA 70803, mws@lsu.edu.

**Table 1 Classification of Layer Silicates [1]**

| Layer Type | Layer Charge | Interlayer | Group | Sub-group | Examples of species |
|---|---|---|---|---|---|
| 1:1 | 0 | none or $H_2O$ only | kaolin-serpentine | serpentine | chrysotile |
| | | | | kaolinite | kaolinite |
| 2:1 | <0.2 | none | talc-pyrophyllite | talc | talc |
| | | | | pyrophyllite | pyrophyllite |
| | 0.2-0.6 | hydrated exchangable cations | smectite | saponite | saponite |
| | | | | montmorillonite | nontronite |
| | 0.6-0.9 | hydrated exchangable cations | vermiculite | trioctahedral vermiculite | vermiculite |
| | | | | dioctahedral vermiculite | vermiculite |
| | 0.6-1.0* | non-hydrated cations | true micas | trioctahedral micas | phlogopite |
| | | | | dioctahedral micas | muscovite |
| | ≈ 2.0 | non-hydrated cations | brittle micas | trioctahedral brittle micas | clintonite |
| | | | | dioctahedral brittle micas | margarite |
| | Variable | hydroxide sheet | chlorite | trioctahedral chlorites | clinochlore |
| | | | | dioctahedral chlorites | donbasseite |
| | | | | di-, trioctahedral chlorites | cookeite |

* The charge on the layer for a true mica is 0.85 to 1.0 for dioctahedral micas. Trioctahedral micas may have a layer charge of near 0.6, with the possible exception of wonesite (layer charge of 0.5). Any layer charge of 0.6 to 0.85 represents an "interlayer-cation-deficient mica".

**Introduction:** The ExoMars mission payload includes a Miniaturized Mössbauer Spectrometer (MIMOS-II) that is an upgraded version of the successful Mössbauer spectrometers from the MER mission. Given the interest in phyllosilicates as recorders of aqueous processes on Mars, it is posssible that the landing site chosen for ExoMars might be rich in hydrous phases. This abstract addresses the question of how MIMOS-II might distinguish among varous phyllosilicate minerals that might be encountered.

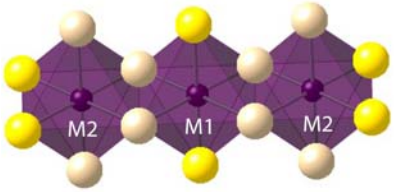


**Figure 1**. Schematic of 6-coordinated polyahedra in the octahedral sheet of layer silicates. In trioctahedral minerals, all three sites are occupied, while in dioctahedral species, the M1 site is vacant.

**Structures:** $^{57}$Fe Mössbauer spectra give information about the geometry of the coordination polyhedra occupied by Fe, and the valence state of the iron. In layer silicates (**Table 1**), both $Fe^{2+}$ and $Fe^{3+}$ occupy 6-coordinated sites (in rare Si-deficient cases, there may also be tetrahedral $Fe^{3+}$). In layer silicates there are a total of three M sites per formula unit in the octahedral sheet: one slightly larger M1 site, with OH's positioned on adjacent (*cis*) sides of the octahedra, and two slightly smaller M2's, with OH's on opposite sides (*trans*) of the octahedra (**Figure 1**). Because of the difference in size, trivalent cations generally prefer to occupy the M2 sites, while divalent cations can enter either site. In *di*octahedral species, *two* of the three M sites are filled, leaving the M1 site vacant. In *tri*octahedral minerals, all *three* M sites are occupied. If the polyhedral distortion around the Fe atom varies among species, then the Mössbauer parameters, especially quadrupole splitting (QS), are affected.

**Previous Work:** The literature on Mössbauer spectroscopy of layer silicates is voluminous [see reviews in 2,3]. There are two key issues: the proper line shape to be used to model the spectra, and the ability of the technique to discriminate between $Fe^{2+}$ in M1 and M2 [4]. Recent work applying several different line shapes to a range of layer silicates [5] suggests that use of Lorentzian, pseudo-Voigt, and quadrupole splitting distributions as line shapes gives similar results for areas of the two octahedral $Fe^{2+}$ doublets (in some cases, a third $Fe^{2+}$ distribution is also reported). However, the resultant areas are very difficult to interpret. Most workers generally accept that fact that Mössbauer spectra of 2:1 layer silicates cannot resolve the octahedral $Fe^{2+}$ *cis* (M2) and *trans* (M1) sites. Rather, the areas of the various prominent $Fe^{2+}$ doublets in layer silicates are interpreted to represent different populations of next nearest neighbor cations. These may or may not be characteristic of different layer silicate species.

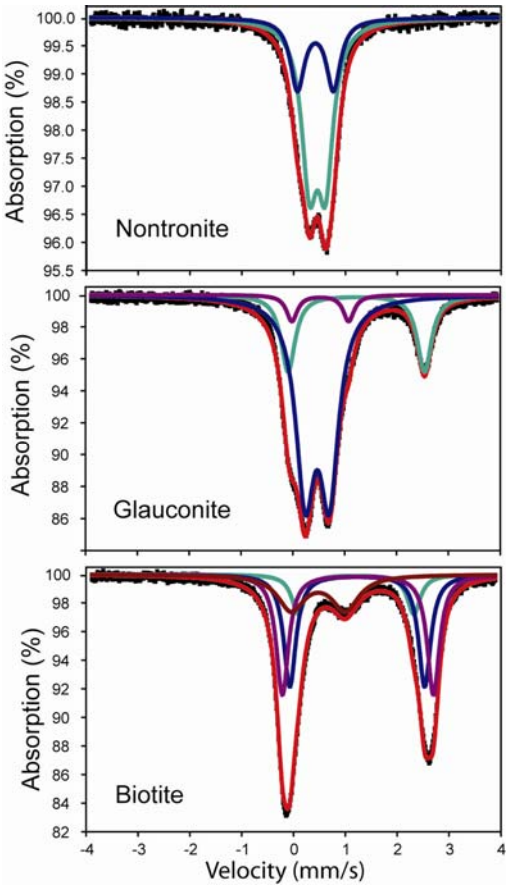


Figure 2. Typical Mössbauer spectra of layer silicates. Only $Fe^{3+}$ is present in nontronite; this spectrum is typical of all the $Fe^{3+}$ layer silicates. Glauconite and biotite show examples of mixed valence secies, and are typical of the micas and chlorite group minerals.

**Results:** Typical Mössbauer parameters for layer-silicate mineral species are given in **Table 2**, and spectra shown in **Figure 2**. The $Fe^{2+}$ species generally have 2-3 distributions, all with similar isomer shifts (IS ~ 1.13 mm/s) but different QS (~2.75, 2.20, and rarely 1.7 mm/s). The pure $Fe^{3+}$ species may contain one or two closely-overlapped doublets/distributions representing 6-coordination, again with similar IS (~0.35-0.45 mm/s) and variable QS (0.46-1.0 mm/s). Tetrahedral $Fe^{3+}$ has the best-constrained parameters, with IS ~ 0.20 mm/s and QS ~ 0.50 mm/s. Because all these minerals have very similar structures, the Mössbauer parameters are consistent, and depend more on the nearest-neighbor chemistry in an individual sample than on the steric constraints of any particular species. Furthermore, the $Fe^{3+}/Fe^{2+}$ range of layer silicates (particularly micas and chlorites) is large, and depends on the oxidation state of the mineral assemblage rather than on any particular crystal structure. Thus, distinguishing among different species of layer silicates using Mössbauer alone would be difficult. Of course, the combination of this technique with other types of spectroscopy on ExoMars should be effective in determining not only mineralogy, but also redox equilibria should layer silicates be studied.

**Acknowledgments:** Work supported by NASA grant NNG06G130G and NSF grant EAR-0439161.

**References:** [1] Bailey, S.W. (1988) *Revs. Mineral.*, 19, 9-27. [2] Dyar, M.D. (2002) *Revs. Mineral.*, 46, 313-349. [3] Pollack H. and Stevens J.G. (1986) *Hyper. Interact.*, 29, 1153-1156. [4] Rancourt, D.G. (1994) *Phys. Chem. Minerals.*, 21, 250-257. [5] Dyar, M.D. et al. (2007) *Clay Mins.*, 43, 3-33.

**Table 2. Typical Mössbauer Parameters of Layer Silicates***

| Group | Sub-group | Example Species | $Fe^{2+}$ | | $Fe^{2+}$ | | $Fe^{3+}$ | | $Fe^{3+}$ | |
|---|---|---|---|---|---|---|---|---|---|---|
| | | | IS | QS | IS | QS | IS | QS | IS | QS |
| kaolin-serpentine | serpentine | chrysotile | 1.13 | 2.75 | | | 0.31 | 0.86 | 0.18 | 0.33 |
| | kaolinite | kaolinite | 1.11 | 2.53 | | | 0.41 | 0.46 | | |
| talc-pyrophyllite | talc | talc | 1.13 | 2.57 | 1.12 | 2.15 | | | | |
| | pyrophyllite | pyrophyllite | 1.12 | 2.65 | 1.14 | | | | | |
| smectite | saponite | saponite | 1.18 | 2.70 | 1.20 | 2.40 | | | | |
| | montmorillonite | nontronite | 1.12 | 2.61 | | | 0.36 | 0.61 | | |
| vermiculite | trioctahedral vermiculite | vermiculite | 1.15 | 2.90 | 1.12 | 2.53 | 0.40 | 0.94 | | |
| | dioctahedral vermiculite | vermiculite | 1.11 | 2.41 | | | 0.34 | 0.88 | | |
| true micas | trioctahedral micas | phlogopite | 1.13 | 2.57 | 1.12 | 2.15 | 0.40 | 0.87 | 0.20 | 0.75 |
| | dioctahedral micas | muscovite | 1.15 | 2.93 | 1.14 | 2.13 | 0.37 | 0.84 | | |
| brittle micas | trioctahedral brittle micas | clintonite | 1.16 | 2.48 | 1.15 | 1.72 | 0.47 | 0.51 | 0.24 | 0.68 |
| | dioctahedral brittle micas | margarite | 1.10 | 2.37 | | | 0.40 | 0.63 | | |
| chlorite | trioctahedral chlorites | clinochlore† | 1.14 | 2.66 | 1.11 | 2.33 | 0.35 | 0.65 | 0.12 | 0.39 |

*Parameters given in mm/s relative to the midpoint of Fe metal; the range of reported values for eaxh species is at least ±0.05 mm/s for isomer shift (IS) and ±0.15 mm/s for quadrupole splitting (QS). Data from [2] and [3] and unpublished work by this group. †Some workers resolve three octahedral doublets representing the Fe sites in the "brucite sheet" in the interlayer of the chlorite structure; two $Fe^{3+}$ doublets may also be observed with QS = 0.40 and 0.65 mm/s.

**PHYLLOSILICATES, ZEOLITES, AND CARBONATE NEAR NILI FOSSAE, MARS: EVIDENCE FOR DISTINCT ENVIRONMENTS OF AQUEOUS ALTERATION.** B.L. Ehlmann[1], J.F. Mustard[1], G.A. Swayze[2], J.J. Wray[3], O.S. Barnouin-Jha[4], J.L. Bishop[5], D.J. Des Marais[6], F. Poulet[7], L.H. Roach[1], R.E. Milliken[8], R.N. Clark[2], S.L. Murchie[4], and the MRO CRISM Team. [1]Dept. of Geological Sciences, Brown University, [2]U.S. Geological Survey, Denver, [3]Cornell University, [4]JHU-Applied Physics Laboratory [5]SETI Institute [6]NASA Ames [7]IAS, Université Paris-Sud, [8]JPL-Caltech (bethany_ehlmann@brown.edu)

**Introduction:** The region west of the Isidis basin, near Nili Fossae, hosts the greatest mineral diversity mapped from orbit: olivine [1, 2], low- and high- calcium pyroxene [3], and iron-magnesium smectite [4-6]. High resolution targeted observations (18-36 m/pixel) from the Compact Reconnaissance Imaging Spectrometer for Mars (CRISM) [7] reveal diverse alteration minerals generated by aqueous processes, including nontronite, saponite, kaolinite, chlorite, illite or muscovite, carbonate, analcime and another zeolite, and a hydrated Si-OH bearing phase whose spectra are consistent with altered basaltic glass or opaline silica [4-6, 8-11]. The spatial distribution of these minerals (Fig. 1), suggests distinct mineralogic provinces which may indicate different environments for aqueous alteration or different starting materials. Both near surface and subsurface—possibly hydrothermal—settings of neutral to alkaline pH are implicated by the mineralogy and geomorphology of the provinces discussed below.

**"Provinces" of alteration:** Three distinct provinces of alteration mineral assemblages are tentatively identified:

(1) *Western*: Near the Antoniadi basin, multiple generations of impact craters are superposed on one another. Fe/Mg smectite, chlorite and hydrated Si-OH bearing phases are found, usually associated with crater central peaks and walls. The zeolite analcime is detected in the central peaks of two craters (e.g. Fig. 2A; [10]) that also exhibit "quartzofeldspathic" (QF) material [12]. Chlorite, smectite, and zeolite occur in small knobs within the central peak, while the Si-OH phase is associated with aeolian deposits at the base of the peak which also hosts the QF material.

(2) *Central*: West of Nili Fossae near a 50 km crater, chlorite is the dominant phyllosilicate with Fe/Mg smectite and a mica, illite or muscovite, as minor phases [9]. The strongest mineral signatures are associated with small craters and topographic highs. At the base of some of these highs, areas polygonally fractured at meter-scale contain chlorite (Fig. 2B). Elevation around the crater is asymmetric with the chlorite/mica-rich eastern side lower by several hundred meters. This may reflect pre-impact topography or may indicate chlorite and illite are exposed by erosion from the lower portion of the ejecta blanket or underlying crust.

(3) *Eastern*: This region encompasses the concentric grabens of Nili Fossae which formed between the inner and outer rings of the basin during structural readjustment following the Isidis impact ~3.9 Ga [13]. West and south of Isidis in Nili Fossae and Libya Montes, a consistent stratigraphy is observed with a basement of Fe/Mg smectites and low-calcium pyroxene overlain unconformably by olivine and a mafic cap rock [5].

While the regional Fe/Mg smectite-bearing rocks are cut by the fossae, placing their age as early Noachian [4, 6, 13], there is geomorphic evidence for the continued presence of water into the Hesperian from valleys and channels which dissect both the Noachian cratered terrains and the Hesperian Syrtis Major lavas. Filled craters, alluvial fans, and a 15,000 km$^2$ valley system feeding Jezero crater lake provide evidence for extensive sedimentary transport [6, 14-15].

Kaolinite is found in 11 locations and typically occurs as the topmost layer of phyllosilicate, found in a tens of meters thick layer above Fe/Mg smectite (Fig. 2C). It is sometimes the uppermost unit and sometimes exposed from beneath apparently unaltered mafic cap rock. Eastern Nili Fossae also hosts a phase most likely to be carbonate, specifically magnesite [8]. With the exception of carbonate associated with transported sediments within Jezero crater, the carbonate is in a rock unit above and draped over

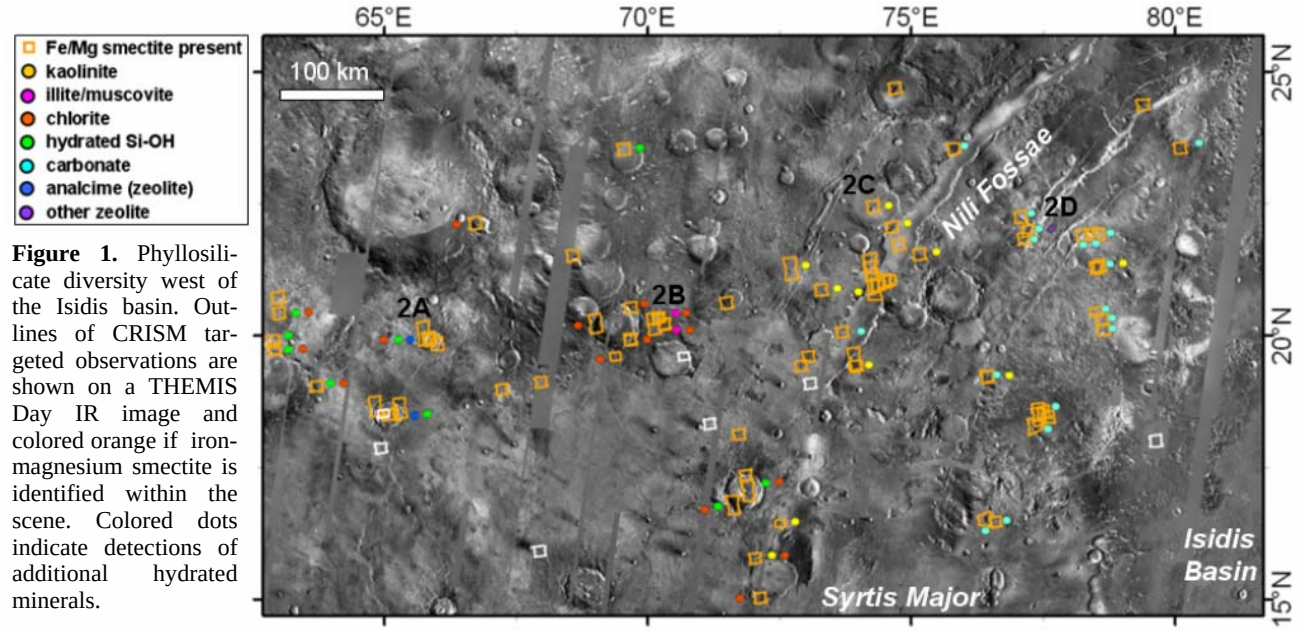


**Figure 1.** Phyllosilicate diversity west of the Isidis basin. Outlines of CRISM targeted observations are shown on a THEMIS Day IR image and colored orange if iron-magnesium smectite is identified within the scene. Colored dots indicate detections of additional hydrated minerals.

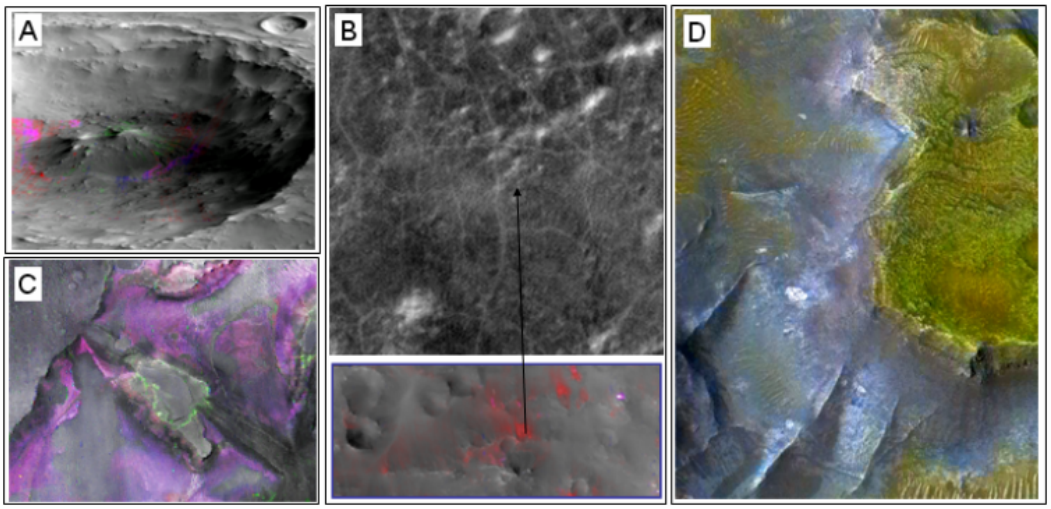


**Figure 2.** (A) Fe/Mg smectite and chlorite (green) along with zeolite (red) in the ~4 km wide crater central peak, which is surrounded by hydrated silica-bearing aeolian sediments (magenta-blue) (B) fractured chlorite-bearing terrain (polygons are ~10-20m). Chrolite (red) and illite (magneta) are associated with topographic highs near 500m craters (C) a kaolinite layer (green), exposed in a 2 km wide mesa, caps a thick Fe/Mg smectite basement (magneta) (D) Olivine (yellow) and carbonate (green) overlie Fe/Mg smectite (blue). Image is 1km across.

Fe/Mg smectites and beneath a mafic cap rock, in a similar stratgraphic position to olivine (Fig. 2D). The carbonate is light toned and layered with extensive polygonal fracture patterns. It and the mafic cap are both cut by valleys, indicating formation was likely subsequent or coincident with valley formation (no later than Hesperian).

**Implications**: Distinct assemblages of minerals suggest that the nature of aqueous activity varied in space and time across the region west of the Isidis basin. Fe/Mg smectites are exposed as the lowermost unit in images sampling over 100,000 km$^2$. The great spatial extent of this unit seems to exclude lacustrine or volcanic hydrothermal processes as the primary mechanism for regional smectite formation and instead favors pervasive near surface alteration or hydrothermal/metamorphic alteration in the crust [16]. However, existence of multiple secondary minerals suggests locally more intensive or distinct processes for alteration.

Eastern Nili Fossae crustal materials apparently experienced multiple episodes of aqueous activity. The first was early Noachian alteration, which formed a Fe/Mg smectite-rich basement. Later episode(s) are indicated by fluvial geomorphology and by mineralogic evidence, namely kaolinite and carbonate. A plausible formation mechanism for a capping kaolinite layer on smectite deposits is top down leaching of pre-existing phyllosilicates, leading to loss of Ca, Mg, and Fe ions from smectite and its transformation to kaolinite.

Carbonate formation conditions are more ambiguous and may have taken place in the surface or subsurface. The carbonate may have formed in the same episode as the kaolinite, by alteration of olivine by water at the surface and subsequent emplacement of mafic cap rock. An alternative is carbonate formation at depth by a initiation of metasomatic alteration along a contact between hot olivine bearing rocks and underlying hydrous Fe/Mg smectite. A key control on carbonate distribution appears to be existence of precursor ultramafic rock, since carbonate is not observed moving west as olivine abundance decreases. In any case, the persistence of carbonate to the present indicates waters interacting with this unit were not acidic.

Greater mineral diversity in the Central and Western provinces may have been generated in local hydrothermal systems related to impact events. The mineralogy associated with impact craters in the Central and Western provinces is remarkably similar to the Fe/Mg-rich smectites or chlorites with accessory zeolite, silica, quartz, and K-feldspar which result from hydrothermal alteration in terrestrial craters [17]. Such an assemblage suggests the QF material [12] may be hydrothermal rather than igneous. The low TES-modeled abundances of quartz and K-spar and association with hydrated Si-OH bearing phases (e.g. altered impact glass [11]) are consistent with such a formation process. Experimental data show smectite-zeolite assemblages result from glasses and or basalt powders and are stable at temperatures <150°C [18] while illite-chlorite assemblages are stable at T>200°C [17]. Hence, variation in the temperature of the hydrothermal system may result in the distinctive Central and Western assemblages.

An alternative hypothesis is that alteration materials associated with craters reflect changes in underlying crustal materials westward of the Isidis basin and that aqueous alteration pre-dated formation of the impact structures in which these minerals are mapped. Smectite transforms to illite upon burial at T>50-80°C [19]. Illite and chlorite altered at depth may have been excavated by impact.

Collectively, the data indicate multiple episodes of aqueous activity, perhaps resulting from multiple processes, and suggest that the region west of the Isidis basin was over early Mars history persistently and unusually water-rich.

**Acknowledgements:** Thanks to the ongoing efforts of the MRO operations team, and the HiRISE and CTX teams for coordinating with CRISM, enabling high resolution studies combining geomorphology and mineralogy.

**References:** [1] Hoefen, T.M. et al. (2003) *Science*, 302, 627-630 [2] Hamilton, V.E., Christensen P.R. (2005) *Geology, 33*, 433-436 [3] Mustard J.F. et al. (2005) *Science, 307*, 1594-1597 [4] Poulet F. et al. (2005) *Nature, 438*, 623-627 [5] Mustard, J.F. et al. (2008) *Nature 454, 305-309* [6] Mangold, N. et al., *JGR* 112, E08S04 [7] Murchie, S.L. et al. (2007) *JGR* 112, E05S03.[8] Ehlmann, B.L. et al., submitted, *Science.* [9] Ehlmann, B.L. et al. 2007, *7th Mars Conf*., Abs. #3270 [10] Ehlmann, B.L et al., (2008) *LPSC 39*, Abs. #2326. [11] Swayze, G.A. et al., 2007, *7th Mars Conf.* Abs. #3384 [12] Bandfield, J.L. (2006) *GRL* 33, L06203. [13] Mustard, J.F. et al., (2007) *JGR* 112, E08S03 [14] Ehlmann, B.L. et al. (2008) *Nature Geosci.* 1, 355-358 [15] Fassett, C.I. and Head, J.W. (2005) *GRL* 32, L14201. [16] Parmentier, E.M. (2008) LPSC 39, Abs. # 1544 [17] Allen, C.C. et al. (1982) *JGR* 87, 10,083-10,101. [18] Robert, C. and Goffe, B. (1993), *Geochim. Cosmochim. Acta* 57, 3597-3612. [19] Hower, J. (1981) *Clays & Resource Geol.* Min. Assoc. Can., 60-80.

**POST-NOACHIAN WATER ACTIVITY ON MARS INFERRED FROM SHOCK DECOMPOSITION ANALYSIS OF PHYLLOSILICATES WITHIN IMPACT CRATERS.**

A.G. Fairén, A.F. Davila, G.A. Marzo, T.L. Roush, C.P. McKay. NASA Ames Research Center, Space Science and Astrobiology Division, Moffett Field, CA 94035, USA.

**Introduction:** Multiple phyllosilicate deposits on Mars appear associated with impact craters and distributed throughout the rims, ejecta and central peaks [1-4]. It has been suggested that these deposits derived from pre-existing phyllosilicate-rich materials that were excavated in the process of crater formation [3,5], and are therefore indicative of aqueous activity early in the history of the planet. We have analyzed if the distribution of phyllosilicates within impact craters is consistent with their stability against shock and thermal decomposition, to test the hypothesis that these deposits represent vestiges of early Mars aqueous activity.

**Thermal and Shock stability:** Hydrated silicate minerals are characterized by a low thermal stability due to the presence of OH-groups in their lattice, and many mixed-layer phyllosilicates become unstable at temperatures of ~370 K, resulting in phase transformation and loss of volatile components (mainly $H_2O$ or OH) contained in the crystal lattice [6]. Nontronite is completely decomposed at temperatures as low as 625 K [7], the iron-enriched smectites dehydroxylate at 725 K [8], and kaolinite starts undergoing dehydroxylation at 775 K [9]. In general, 920 K can be considered the upper average decomposition temperature for phyllosilicates, as it is the decomposition temperature of serpentine to glass and anhydrous silicates [10]. The large shock pressures resulting from a meteor impact can also induce the dehydration of silicate minerals. Theoretical estimates and shock recovery experiments show incipient to complete water loss from 200 to 600 kbar respectively, with an average 40% water loss at 300 kbar shock pressures [11]. Up to 2/3 of the interlayer water of nontronite samples is lost at shock pressures of 300 kbar [12], and phyllosilicates shocked above 260 kbar can be changed to an almost amorphous state [13].

We adapted the model derived by Kieffer and Simonds [14] to compute the shock-induced pressure and the residual temperature of an impact event on Mars. The top panel of Figure 1shows the radii of the areas heated up to 370 K and 920 K and shocked at 300 kbars around the impact point. The radius of the area experiencing temperatures and pressures leading to complete phyllosilicate decomposition, the total decomposition zone (TDZ), is ~1/5 of the crater radius at the surface level. Subsurface clay-bearing horizons located in the central peak and surrounding areas, would not survive the impact process. However, peripheral deposits outside these regions could survive the impact forces, due to shock pressure and temperature dissipation.

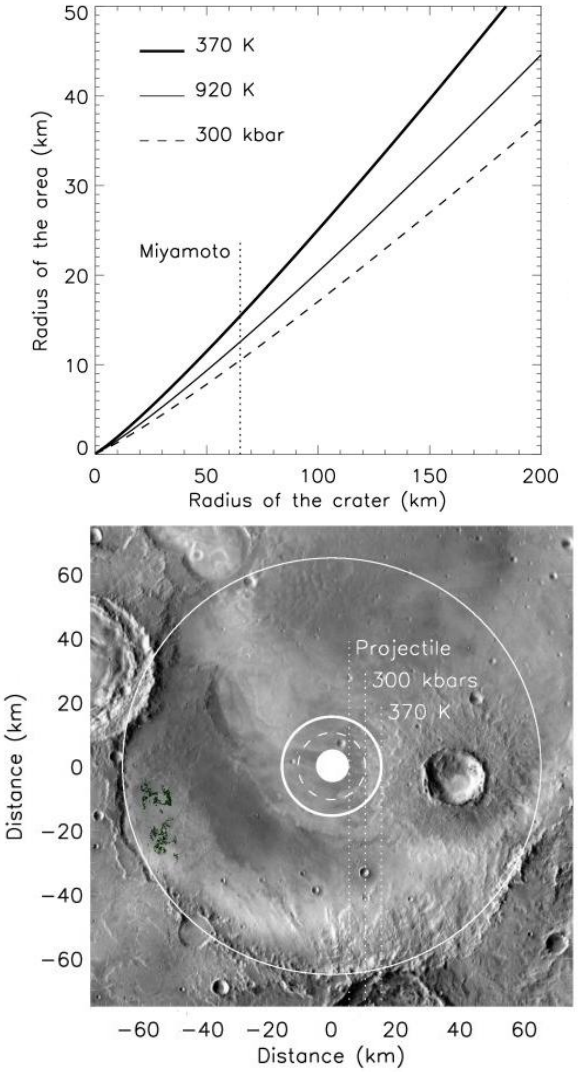


**Figure 1.** (Top) Radius of non-stability areas for phyllosilicates, as function of the crater diameter, due to a shock-induced pressure (300 kbars) and two different temperatures (370 and 920 K). (Bottom) Simulation for Miyamoto crater. The phyllosiclicates (green) lie outside the TDZ.

In the bottom panel of Figure 1 we simulate the case of Miyamoto crater in Meridiani Planum. The green deposits, in the southwest portion of the crater,

exhibit spectral features indicative of Fe/Mg-smectite clays [15], and are located in the periphery of the crater floor, outside the TDZ. Therefore their presence is compatible with excavation models of crustal phyllosilicate-rich deposits formed prior to the impact.

**Late stage phyllosilicates:** We have analyzed several examples of impact craters with phyllosilicate deposits that fall within the TDZ.

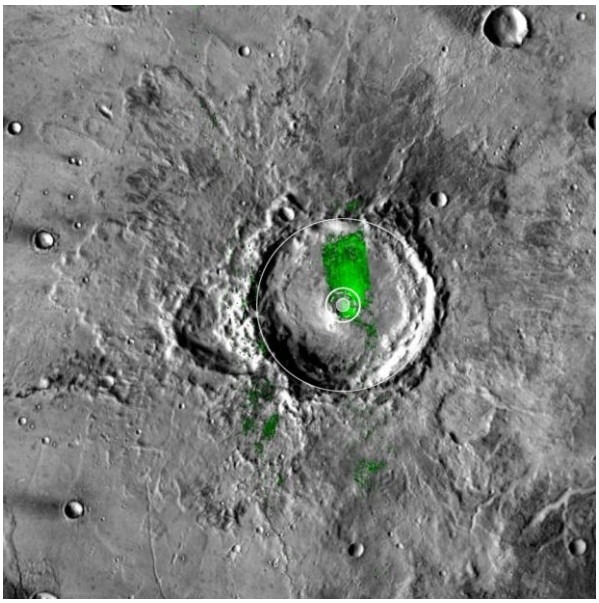

**Figure 2.** Crater in the Syrtis Major region (71.8E, 17.0N). Areas indicated in green have spectral signatures of phyllosilicates; some of which occur within the TDZ (circles in center of crater).

The crater shown in Figure 2 is 40 km in diameter and 2 km depth, and is located close to the northern edge of the Syrtis Major Volcanic Plains (SMVP). It is deep, bowl-shaped with maximum slopes of 25º, and has a well developed central peak with a central pit, fresh ejecta blankets, megabreccia on the crater floor, terraced walls, and a well-defined and complete rim. These features are all diagnostic of a fresh impact [16]. The formation age of the SMVP has been constrained to the Hesperian [17], and this places an upper limit for the age of the impact crater. The crater is located in the Late Hesperian units and there are only meter-scale superposed impacts on the crater floor, and two larger impacts [~2 km diameter] on the area covered by the ejecta. This suggests that the crater formed towards the end, or after the volcanic activity that resulted in the formation of the SMVP. Hydrated silicate deposits, mainly composed of Fe/Mg smectites and chlorites appear inside the TDZ. At high resolution, the deposits have the appearance of bright outcrops, partially covered with sand dunes. Current models suggest that these deposits are Noachian in age and were excavated after the impact [3,5]. But phyllosilicate outcrops appear on the rim of the central peak, where our model predicts a TDZ, and Mg/Fe smectites would dehydroxylate and decompose completely [8,11,12]. Our model also predicts that any preexisting phyllosilicate deposits would be completely decomposed down to a depth of ~2 km beneath the TDZ.

We favor the hypothesis that phyllosilicates in this crater formed through hydrothermal activity associated with the impact itself, as is documented on Earth [18]. Impact-induced hydrothermal activity is initiated by an impact event into water-rich or ice-rich crustal material. The resulting release of heat provides a thermal driver for the circulation of water and volatiles [19, 20]. Numerical models of groundwater flow within freshly formed martian impact craters indicate that hydrothermal systems will develop if sufficient water is present [21]. Impact triggered hydrothermal activity can last over $10^5$ yrs for a crater the size of that analyzed here [20]. Based on this cumulative information, we favor the hypothesis that the presence of phyllosilicates within the TDZ of this fresh impact crater is indicative of hydrothermal activity on Mars after the Noachian.

**References:** [1] F. Poulet, et al., Nature 438, 623-627 (2005). [2] J. P. Bibring, et al., Science 312, 400-404 (2006). [3] J. F. Mustard, et al., Nature 454, 305-309 (2008). [4] J. L. Bishop, et al., Science 321, 830-833 (2008). [5] S. M. Pelkey, et al., J. Geophys. Res. 112, E08S14, doi: 10.1029/2006JE002831 (2007). [6] K. Byrappa, M. Yoshimura, Handbook of hydrothermal technology (William Andrew Inc., 2001), 870 pages. [7] P. Gavin, et al., LPSC 2007. [8] R. L. Frost, et al., Thermochim. Acta 346, 63-72 (2000). [9] H. He, et al., J. Am. Ceramic Soc. 88, 1017-1019 (2005). [10] G. W. Brindley, J. Lemaitre, in Chemistry of clays and clay minerals (ed. A. C. D. Newman); Mineral. Soc. Monogr. 6, pp. 319-370, Longman (1987). [11] M. A. Lange, et al., Geochim. Cosmochim. Acta 49, 1715-1726 (1985). [12] M. B. Boslough, et al., LPSC 1980. [13] J. Akai, T. Sekine, Proc. NIPR Symp. Antarct. Meteorites 7, 101-109 (1994). [14] S. W. Kieffer, C. H. Simonds, Rev. Geophys. Space Phys. 18, 143-181 (1980). [15] S. M. Wiseman, et al., LPSC 2008. [16] R. E. Arvidson, Icarus 22, 264-271 (1974). [17] H. Hiesinger and J. W. Head III, J. Geophys. Res. 109, doi:10.1029/2003JE002143 (2004). [18] M. V. Naumov, Geofluids 5, 165 – 184 (2005). [19] H. E. Newsom, Icarus 44, 207-216 (1980). [20] O. Abramov, D.A. King, J. Geophys. Res. 110, doi:10.1029/2005JE002453 (2005). [21] J. A. Rathbun, S.W. Squyres, Icarus 157, 362-372 (2002).

**EFFECT OF IMPACT AND HEATING ON THE SPECTRAL PROPERTIES OF CLAYS ON MARS.** P. Gavin[1], V. Chevrier[1], K. Ninagawa[2] [1]W. M. Keck Laboratory for Space Simulations, Arkansas Center for Space and Planetary Sciences, 202 Old Museum Building, University of Arkansas, Fayetteville, AR 72701, [2]Department of Applied Physics, Okayama University of Science, Okayama, Japan.

**Introduction:**

Clay minerals have been found in some of the oldest terrains on Mars. Because of their Noachian age, clays hold clues to the earlier history of the surface of Mars [1, 2]. CRISM/MRO data have confirmed OMEGA data of clays' existence in outcrops surrounded by lava flows and in small impact crater ejecta [3, 4]. It has been suggested that clays may have formed due to hydrothermal processes induced by impacts [5] and later underwent thermal and/or impact alteration. Studies have suggested that heated/impacted clays may be responsible for the physical and magnetic properties of the red dust on Mars [6, 7]. In this study, we investigate the effects of heat and impact on the spectral properties of clays and their relation to the martian surface.

**Experimental and Analytical Methods:**

One-gram samples of nontronite ($Fe^{3+}$, Mg) and montmorillonite (Al, Ca) were heated in a Lindberg tube furnace to temperatures ranging from 350°C to 1150°C for 4 to 24 hours. Samples were heated in air as well as under a steady flow of $CO_2$ to more closely replicate early martian conditions. Each sample was allowed to cool overnight and weighed after heating. Samples were also impacted with an SUS projectile using a two-stage light gas gun. Projectile speeds ranged from 2-3.3 km/s resulting in shock pressures from ~10-60GPa.

The samples' extreme color change after heating was precisely characterized using Munsell soil color charts. Samples were analyzed using X-ray diffraction and reflectance spectroscopy.

**Results and Discussion:**

*Heating Experiments:*

Each heated sample of nontronite and montmorillonite showed significant color change. Nontronite samples changed from yellow-green to shades of reddish brown. Montmorillonite samples transitioned from gray to shades of orange.

Weighing the heated samples showed there was an average of about 25% mass loss, most likely due to the loss of interlayer water, as is has been shown to be lost at lower temperatures than structural water is [6].

XRD spectra taken of nontronite samples heated to low temperatures (T < 750°C) showed significant variation from the untreated sample. The 001 peak disappeared, consistent with the loss of interlayer water, but all other peaks were still intact. There was also very little difference in the spectra of sample heated in air and those heated in $CO_2$, indicating the $CO_2$ atmosphere had little, if any, effect on the transformation process.

The XRD spectra of samples heated to intermediate temperatures (800°C < T < 1000°C) showed low intensity, broad peaks. These are evidence of a complex mixture of secondary nanocrystalline phases.

The sharp, well-defined peaks in the XRD spectra of samples heated to high temperatures (T > 1100°C) indicate the sample has melted and recrystallized into new phases (Figure 1). We identified hematite, cristobalite and sillimanite as these new phases.

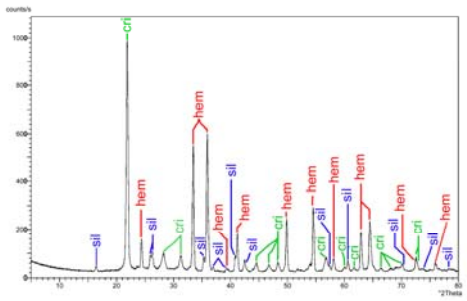


**Figure 1:** *XRD of a sample heated to 1130°C. The identifying peaks of the new phases that formed have been marked (hem: hematite, sil: sillimanite, and cri: crystoballite).*

Near infrared (NIR) reflectance spectra were taken of each sample. Figure 2 shows the NIR reflectance spectra of an untreated sample of nontronite compared to several heated samples. At T = 475°C and 630°C, the 1.4μm band corresponding to the structural hydroxyl in the clay has disappeared. This correlates with the fact that structural $OH^-$ is lost at temperatures above ~300°C [8]. However, the 1.9μm hydration band is still visible. This is most likely the result of the nontronite being destroyed locally so that interlayer water can still be present [6]. The 2.3μm band has not completely disappeared, but instead has flattened into a plateau rather than a distinct peak. After temperatures have reached ~800°C, the spectra become featureless in this range indicating the structure of nontronite has been completely destroyed.

Figure 3 shows the NIR spectra of several heated samples of montmorillonite. The same trends can be seen: the hydration band is still intact at low temperatures and the spectra are featureless after ~800°C, and the 2.2μm band has also flattened into a plateau shape.

*Impacted Samples:*

An XRD spectrum taken of a sample of nontronite impacted with a projectile speed of 2.5 km/s showed very little difference from the XRD of an untreated sample. The 001 peak was still intact as well as the other signature peaks of nontronite. This suggests that

the shock pressure from the impact did not have any significant effect on the clay's overall structure, although amorphous phases may have been formed indicated by the decrease in peak intensity.

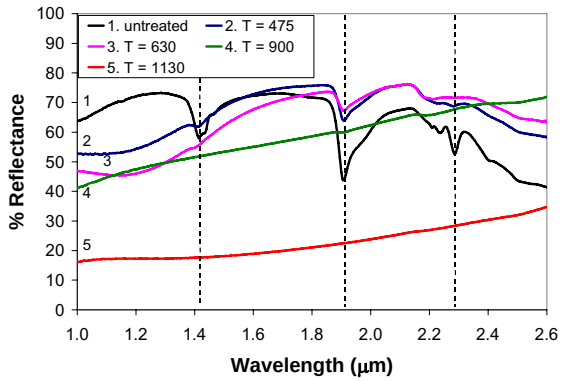


**Figure 2:** *NIR spectra of samples of nontronite heated to various temperatures (shown in °C).*

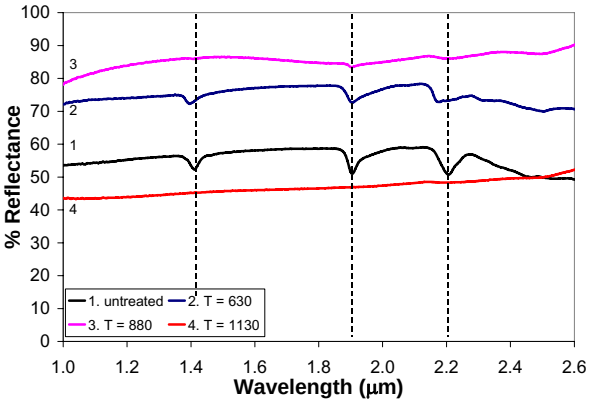


**Figure 3:** *NIR spectra of samples of montmorillonite heated to various temperatures (shown in °C).*

NIR reflectance spectra of several impacted samples (Figure 4) confirm the XRD data. All three signature bands of nontronite are still clearly visible. There are three trends that can be seen in the impacted samples' spectra that correspond to higher projectile speeds: (1) a decrease in band depth, (2) a slight shift in the 1.4μm band to higher wavelengths and (3) a decrease in overall reflectance. These are most likely a result of the heat being generated by the impact that has begun transforming the clays and the possible formation of impact glass.

**Implications for Mars:**

Our experiments have confirmed that the clays that have been detected in ejecta of small craters were pre-existing and were simply excavated by the impact. If impact-induced hydrothermal processes formed the clays seen in crater ejecta, their spectral signature would be identical to that of untreated clays. This is not the case. Their spectra are more similar to that of the heated and impacted clays indicating they were pre-existing and altered by the heat and shock pressure of the impact.

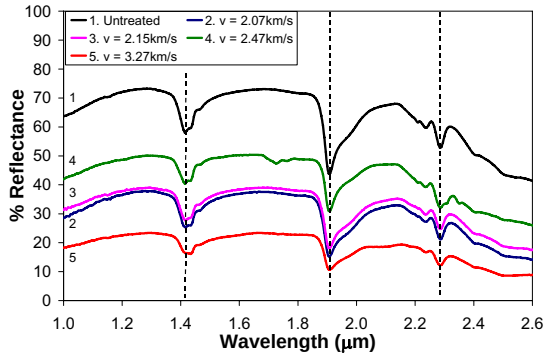


**Figure 4:** *NIR reflectance spectra of impacted samples of nontronite.*

**Conclusions:**

Two major conclusions can be drawn from our experiments: (1) Impact alone does not cause major transformations in clays and (2) heat in the substantial factor in transforming clays. Clays are affected even at low temperatures (~350°C) by the loss of interlayer water and color change. Clays (especially nontronite) transform into secondary phases, such as hematite, sillimanite, and cristoballite, at temperatures above ~1100°C. The temperatures needed for such transformations cannot be reached by small impacts, but rather by contact with lava flows. The clays seen in crater ejecta on Mars could not have been formed by impact-induced hydrothermal systems but existed pre-impact because their spectra are not identical to that of untreated clays rather they are more similar to that of altered clays.

**Future work:**

Further analysis of the heated and impacted samples included Raman spectroscopy to detect any amorphous phases that may have been formed at low temperatures. We intend to calculate the post-shock temperature of our impacted samples and compare them to the temperatures reached by the impacts on Mars.

**References:**

[1] Chevrier, V., (2006) *Lunar Planet. Sci.* XXXVII. [2] Gavin, P., *et al.*, (2008) LPSC XXXIX, #2033. [3] Poulet, F., *et al.*, (2005) *Nature* 481, 623-627. [4] Mangold, N., *et al.*, (2007) *J. Geophys. Res.* 112. [5] Naumov, M., (2005) *Geofluids* 5, 165 - 184. [6] Weldon, R. J., *et al.*, (1982) *J. Geophys. Res.* 97, 10102-10114. [7] Boslough, M. B., *et al.*, (1986) *J. Geophys. Res.* 91, E207-E214. [8] MacKenzie, K. J. B. and D. E. Rogers, (1977) *Thermochemica Acta* 18, 177-196.

**COMPOSITION AND MORPHOLOGY OF HYDRATED LAYERED DEPOSITS ON THE PLAINS AROUND VALLES MARINERIS (MARS).** L. Le Deit[1], S. Le Mouélic[1], O. Bourgeois[1], D. Mège[1], M. Massé[1], C. Quantin-Nataf[2], C. Sotin[3], J.-P. Bibring[4], B. Gondet[4], Y. Langevin[4], [1]Laboratoire de Planétologie et Géodynamique UMR 6112, CNRS, Université de Nantes, Faculté des Sciences et Techniques, 2 chemin de la Houssinière BP 92208, 44322 Nantes Cedex 3, France (Laetitia.Ledeit@univ-nantes.fr), [2]Laboratoire des Sciences de la Terre, Université Claude Bernard, 2 rue Raphaël Dubois, 69622 Villeurbanne, Lyon, France, [3]Jet Propulsion Laboratory and California Institute of Technology, Pasadena, CA, 91011, U.S.A, [4]Institut d'Astrophysique Spatiale, Université Paris 11, Bâtiment 121, 91405 Orsay Campus, France.

**Introduction:** An extensive light-toned formation tops the plains around Valles Marineris near Juventae, Melas, Ius, Candor, Tithonium and Ganges Chasma (***Figure 1***). Near Juventae Chasma, these layered deposits (LDs) have been interpreted to have a possible lacustrine, volcanic or eolian/glacial origin due to their light tone, apparent friability and flat-lying shape [1]. Mineralogical studies based on the analysis of CRISM data show that some parts of the LDs are hydrated near Juventae, Melas, Ius and Candor Chasma [2, 3]. Typical spectra of these areas display absorption bands at ~1.4 µm (OH overtone), at ~1.9 µm ($H_20$ band) and at ~2.2 µm (OH vibration band). These properties may correspond to hydrated silicates such as phyllosilicates (e.g. montmorrillonite, palygorskite), amorphous or finely crystalized silica, or weathered basaltic glass [2, 3, 4].

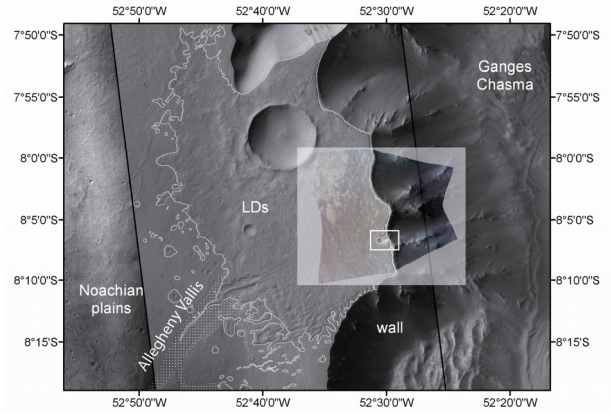


***Figure 1*** *Layered Deposits (LDs) resting on the Noachian plains west of Ganges Chasma (CRISM cube FRT 8949 superimposed on a mosaic of CTX images). The location of Figure 2 is indicated by a white box.*

We describe here the morphology of the LDs and report on the identification, based on the analysis of OMEGA [5] and CRISM [6] data, of hydrated minerals occurring in LDs that cover the plateau near Ganges Chasma. We compare their spectral characteristics with those of LDs around Juventae and Melas Chasma and discuss their mineralogical composition.

**Morphology:** The LDs near Ganges Chasma are stratigraphically above the Noachian plains and are younger than the Hesperian [7] Allegheny Vallis out flow channel (***Figure 1***). Like in the other regions, the light-toned layers are subparallel and do not exceed a hundred of meters in thickness. They are apparently interbedded with darker beds; this can be due to variations in mineralogical composition, topographic slope, roughness, grain size or state of erosion of the different layers, or to partial covering of certain layers by a dark mantle.

**Spectral properties and location of hydrated layers near Ganges Chasma (*Figure 2*):** The analysis of CRISM cube FRT 8949 shows the presence of spectra with a small absorption band at ~1.4 µm, ~1.94 µm and a large band between ~2.2 and ~2.27 µm. This is confirmed by the analysis of the OMEGA data (orbit 0394_2). One pixel of OMEGA orbit 0394_2, located on the LDs, shows similar spectral properties, which reinforces the confidence in the detection.

The comparison of CRISM data with HiRISE image PSP_005939_1720 shows that the hydrated minerals correspond to the basal layer of the LDs (arrows on ***Figure 2a)***, which has been exposed after erosion of the upper part of the LDs. No hydrated signature has been detected on the LDs topographic surface so far. This must be due to the dusty material mantling the LDs.

**Comparison with spectral properties of LDs in other regions (*Figure 3*):** We analysed CRISM cubes FRT 5814 and HRL 44ac near Juventae and Melas Chasma. The ratio spectra are consistent with previous analysis of the same cubes [2,3]. Band positions and global shapes of ratio spectra of LDs near Melas Chasma are similar to those near Ganges Chasma, which suggest that they constitute the same compositional unit. Several minerals are consistent with the observed spectral characteristics. The band centered at ~2.20 µm may be due to Al-OH bonds and/or Si-OH bonds. The large width of the band between ~2.20 µm and ~2.27 µm suggest that Si-rich phases such as opal and chalcedony are good candidates. On the other hand, the band at ~2.2 µm is generally narrower for Al-rich phyllosilicates such as montmorillonite and palygorskite. Linear mixing of a spectrum of montmorillonite with a spectrum of an iron-rich sulfate (e.g. jarosite) produces a spectrum with a large band

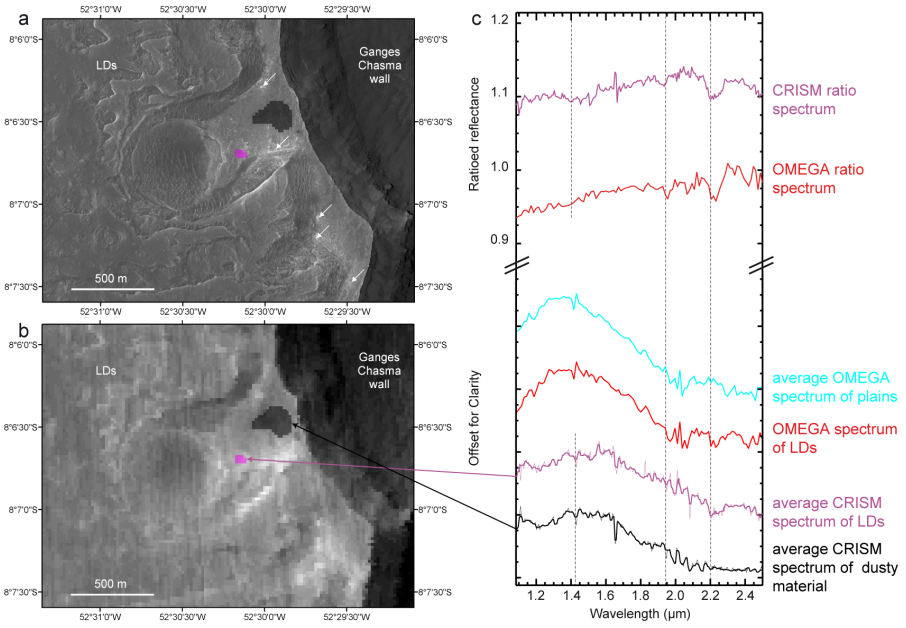


***Figure 2*** *Spectral properties and location of hydrated layers near Ganges Chasma. (a) Subset of HiRISE image PSP_005939_1720. Bright outcrops with hydrated signatures are shown (white arrows). (b) Subset of CRISM image FRT 8949 of the LDs. Colored pixels correspond to the location of averaged spectra shown in (c). (c) Spectrum, average spectra overlain by smoothed spectra for CRISM spectra (colored areas) and ratio spectra (division by an average spectrum of spectrally featureless surfaces) of the LDs.*

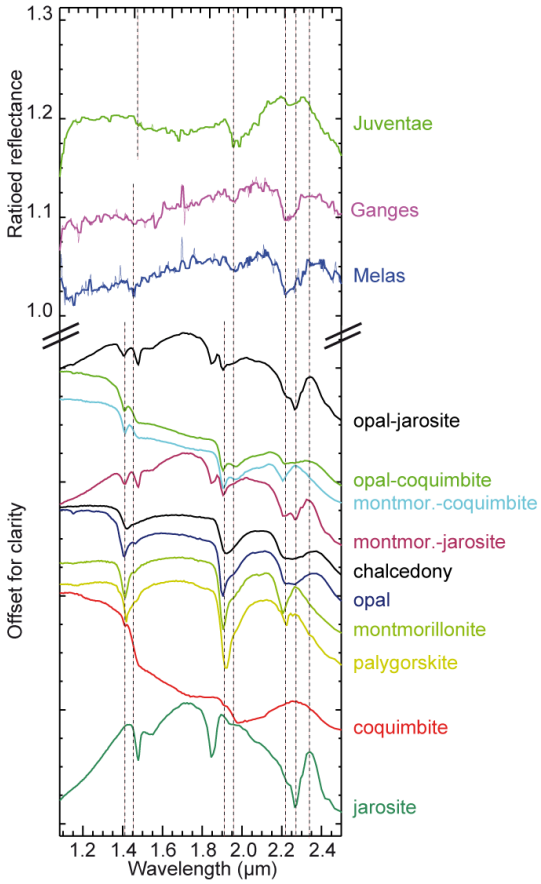


***Figure 3*** *Comparison of ratio spectra of LDs with library spectra. Top: CRISM ratio spectra of LDs near Juventae (FRT 5814), Ganges (Figure 2) and Melas Chasma (HRL 44ac) (overlain by smoothed ratios). Bottom: USGS library spectra [7] and linear mixtures of these spectra (50% each).*

between ~2.20 μm and ~2.26 μm. This synthetic spectrum fits the band observed on CRISM spectra of the LDs. Similarly, linear mixing of a spectrum of opal with a spectrum of jarosite produces a spectrum with a band between ~2.20 μm and ~2.26 μm as large as the one of a spectrum of pure opal. Consequently, a linear mixture of Al-rich phyllosilicates and/or hydrated silica with a mineral that has Fe-OH bonds may explain the observed spectra. The detection of jarosite by [2] near Melas and Ius Chasma reinforces the possibility of the occurrence of this kind of mixture in LDs.

Ratio spectra of LDs near Juventae Chasma show bands at positions similar to those of Ganges and Melas Chasma but the band at ~1.9 μm is deeper and larger near Juventa Chasma, and the band between ~2.20 μm and ~2.26 μm is shallower. This may be due to the relative abundance of the Al/Si-rich material and also to a mixing with other minerals such as iron-rich sulfates like coquimbite, which do not display aborption band between ~2.20 μm and ~2.26 μm (no Fe-OH bond).

**Conclusion:** The LDs on the plains around Valles Marineris display hydrated layers revealed from the analysis of CRISM and OMEGA data. Some layers near Ganges Chasma display spectral characteristics similar to other LDs that have been previously reported [2, 3]. They may correspond to hydrated silica and/or Al-OH phyllosilicates possibly mixed with other phases.

**References:** [1] Lucchitta B. K. (2005) LPSC XXXVI, Abstract #1500. [2] Milliken R. E. et al. (2008) LPSC XXXIX, Abstract #2025. [3] Bishop J. L. et al. (2008) LPSC XXXIX, Abstract #2334. [4] Mustard J. F. et al. (2008) Nature, 454, 305-309. [5] Bibring J.-P. et al. (2004) *ESA-SP 1240*. [6] Murchie S. et al. (2007) JGR, 112, E05S03, doi:10.1029/2006JE002682. [7] Coleman N. M. (2007) Icarus, 189, 344-361. [8] Clark R. N. et al. (2007) USGS splib06a: U.S. Geological Survey, Digital Data Series 231.

**STRATIGRAPHY OF THE MAWRTH VALLIS REGION THROUGH OMEGA, HRSC COLOR IMAGERY AND DTM.** D. Loizeau[1], N. Mangold[1], F. Poulet[2], V. Ansan[1], E. Hauber[3], J.-P. Bibring[2], Y. Langevin[2], B. Gondet[2], P. Masson[1], G. Neukum[4]. [1]IDES, Bat. 509, Universite Paris XI, 91405 Orsay cedex, France, [2]Institut d'Astrophysique Spatiale, Bat. 121, Universite Paris XI, 91405 Orsay cedex, France, [3]Institute for Planetary Exploration, German Aerospace Center (DLR), 12489 Berlin, Germany, [4]Institut für Geologische Wissenschaften, Freie Universitaet Berlin, Germany. damien.loizeau@u-psud.fr.

**Introduction:** OMEGA/Mars Express has discovered large outcrops rich in phyllosilicates in the region of the outflow channel Mawrth Vallis, Mars, around 20°W, 25°N [1], through the detection of absorption bands at 1.4 and 1.9 µm, and at 2.2 or 2.3 µm. Comparison with laboratory spectra reveals similarities with clay minerals such as Al-OH smectites (with the presence of 2.2 µm band) and Mg- or Fe-OH smectites (with the 2.3 µm band) [2]. Moreover the abundances of clay minerals in the Mawrth Vallis region are the highest detected on Mars, reaching more than 65% in volume in some outcrops [3].

Those hydrated minerals are located exclusively on strongly eroded bright outcrops, exhumed from the Noachian plateaus, and cut by the outflow channel Mawrth Vallis, as seen on HRSC/MEx and MOC/MGS narrow angle images. Several MOC and HiRISE/MRO images also reveal that those bright Noachian terrains display meter-scale layers, over more than 150 meter depth as seen on some crater walls. The horizontal extension of more than 300 km x 400 km of this thick phyllosilicate-rich unit implies an important volume of altered rocks, formed during the "phyllosian era" [2,4].

The use of HRSC color imagery and the computation of HRSC Digital Terrain Models (DTM) provides helpful information to understand the geometry and stratigraphy of the phyllosilicate-rich unit. In the context of landing sites selection for the future rover mission, it is highly important to elect the most scientificaly relevant sites through the diversity of the exhumed terrains [5].

**Correlation between OMEGA, HRSC color imagery and stratigraphy:** The red, green and blue channels of the HRSC camera (High Resolution Stereo Camera) have been used to compose RGB images. No calibration has been applied, the aim is to detect easily different terrains by their different colors.

When looking at the bright exhumed outcrops of the phyllosilicate-rich unit on HRSC color imagery and comparing it to OMEGA detection of the 1.93 µm band, and the 2.20 or 2.30 µm absorption bands, it appears that, as in figure 1:

1. Al-bearing smectite-rich outcrops (2.2 µm band) always appear as white, grey or bluish outcrops;

2. Fe-bearing smectite-rich outcrops (2.3 µm band) display a yellow, red, pink or brown color.

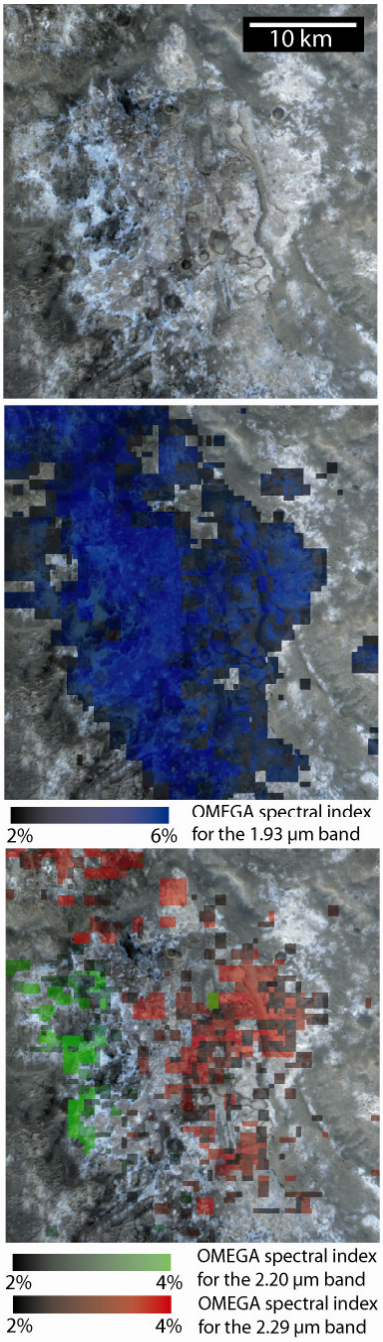


*Fig. 1: Part of HRSC color image on Mawrth Vallis floor and OMEGA detection of Al-phyllosilicates (green) and Fe-/Mg-phyllosilicates (red)..*

Moreover, when looking at very high resolution datasets (HiRISE or MOC narrow angle images), and relating them to HRSC or HiRISE color imagery, we see that the different colors correspond locally to different groups of layers deposited on top of each other, thus contructing different color sub-units indicating different compositions.

Hence, we used the color properties in the visible to map at high resolution the different smectites over the whole Mawrth Vallis region. This is complementary to the use of the CRISM dataset [5,6].

**The stratigraphy of the phyllosilicate-rich unit:** We apply the color mapping in addition to the use of the HRSC high resolution DTM to map constrained cross-sections of the phyllosilicate-rich outcrops across the plateau and the Mawth Vallis channel (example Fig. 2). When the same color sub-unit crops out at different levels along the cross-section, by linking the limits between the different sub-units, it is possible to retrieve a value of the apparent dip of the sub-unit –and hence of the layers– in the direction of the cross-section, with an error <0.5°. It was possible to count up to five color sub-units on top of each other in the region, but other sub-units may be present. The mapping method applied to other large outcrops of the region reveals generally sub-horizontal sub-units, or with < 3° dips.

Layers cannot be tracked from the top to the bottom of the Mawrth Vallis channel due to local mantling, but layered terrains can be seen in some outcrops on the sides and floor of the channel, implying that the phyllosilicate-rich unit extend down to below Mawrth Vallis floor. This possibility is even reinforced by the presence of large deposits of clay minerals in other parts of the channel floor.

We also identified in numerous locations, outcrops of a paleo-surface. This surface is also phyllosilicate-rich, and appears brown in HRSC and HiRISE color images.

**Implications for the formation**: We observed a paleo-surface on top of which the layered unit was deposited and later impacted and eroded, enabling today to see large sections of the unit.

The link between the deposition and alteration of the rocks is still a fundamental issue: 1) the alteration could have happened during the accumulation of the material, building different sub-units depending of changing conditions of formation; 2) the alteration could have happened by groundwater/pedogenic processes after depositionof a thick layered unit..

Moreover, the presence of layers outcropping at the dichotomy boundary in the western part of the region (Fig. 2), and in the sides of Mawrth Vallis channel, imply a deposition prior to the Mawrth Vallis present channel and the dichotomy boundary erosion, for at least part of the sediments.

**References:** [1] Poulet F. et al. (2005), *Nature, 438*, 623-627. [2] Loizeau D. et al. (2007), *JGR, 112*. [3] Poulet et al., submitted to *Science*. [4] Michalski J. R. and E. Z. Noe Dobrea (2007), *Geology 35*, 951-954. [5] Mustard et al. (2008), *Nature 454,* 305-309. [6] Wray et al. (2008), *GeoRL 35*.

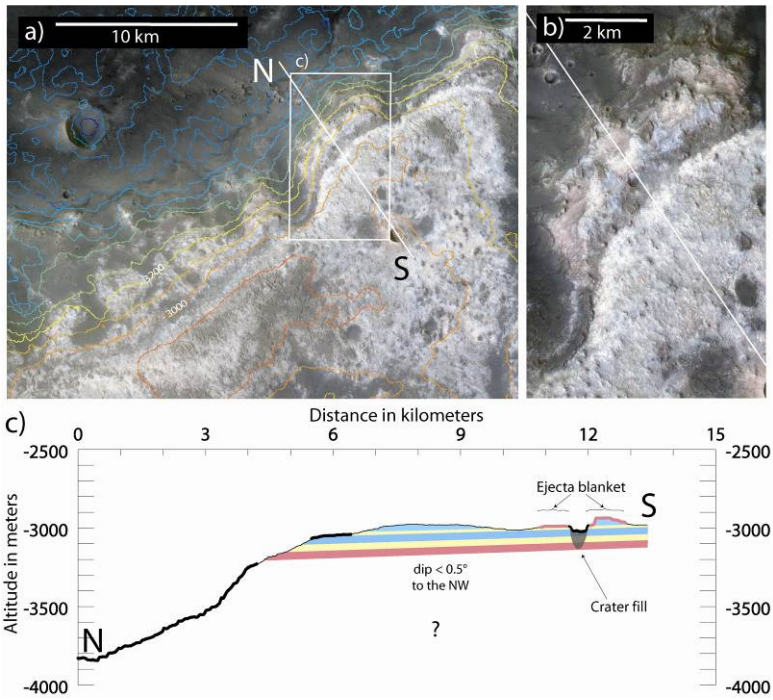


*Fig. 2: a) Close-up on a scarp at the dichotomy boundary. CTX images, and HRSC color images are displayed. HRSC DTM height contours are displayed with an interval of 100 m.*
*b) Close-up on the cross-section of the scarp presented in (c).*
*c) Constrained cross-section of the upper-figure derived from the HRSC DTM and the color imagery.*

**GEOLOGICAL RELATIONSHIPS BETWEEN PHYLLOSILICATES AND FLUVIAL LANDFORMS IN THREE REGIONS OF MARS.** N. Mangold[1], F. Poulet[2], D. Loizeau[1], S. Bouley[1], V. Ansan[1], J.-P. Bibring[2], Y. Langevin[2], B. Gondet[2], P. Masson[1]. [1]IDES, Bat. 509, Université Paris XI, 91405 Orsay cedex, France, [2]Institut d'Astrophysique Spatiale, Bat. 121, Universite Paris XI, 91405 Orsay cedex, France, nicolas.mangold-psud.fr

**Introduction:** Surface weathering by running water can form phyllosilicate if the action of water is long enough [e.g., 1]. However, hydrothermal circulation can lead to phyllosilicates too, without that liquid water would have to be present at the surface [2]. This questions the origin of phyllosilicates and their relevance to understand the past climate of Mars. Two approaches can improve this question. First, new minerals found with spectral data can provide a better view of the type of alteration, and its surficial characteristics, i.e. kaolinite now found extensively in two regions might be the signature of more extended surface alteration [e.g. 3]. Second, the association of phyllosilicates with geologic units formed at the surface such as fluvial landforms is another potential signature of surface processes. Here, we use this second approach, by showing several chronological and stratigraphical relationships between fluvial landforms and phyllosilicates detected in three regions, Nili Fossae, Mawrth Vallis, and Thyrrena Terra.

**Mawrth Vallis region**: This region displays extensive clay-rich outcrops distributed in many layers of both Al-rich phyllosilicates and Fe/Mg-rich smectites [2, 4] with proportion of smectites often reaching 50% [5]. Layers were deposited on top of the crust with thickness reaching >300 m extending over a broad area of 300 by 300 km [4, 6, 7]. This region displays different fluvial landforms. The Mawrth Vallis outflow channel is known to be a snapshot episode of aqueous flow as most outflow channels, therefore it is not expected to play a major role in the alteration process. In contrast, small branching valleys exist throughout the region, which appear to erode inside the layered unit. Of interest is an inverted valley located on the eastern side of Mawrth Vallis. This valley appears to be more and more inverted to the west were the erosion exhumes the clay-rich unit deeper. This shows that these valleys formed inside the clay-rich unit which was later eroded enough to invert the alluvial deposit of these valleys. These alluvial deposits likely behaves stronger against erosion than the clay-rich unit composed of fine grained material easy to erode. These examples show that these branching fluvial patterns formed after the layered deposits and dissected them, but there seems to be no genetic relationships between them.

**Nili Fossae:** In this region phyllosilicates exist as Fe-rich smectites mainly into the outcrops of the exhumed bedrock and associated to olivine rich unit [2,8]. The Nili Fossae floor and the whole Syrtis Major unit, a volcanic early Hesperian unit, is devoid of any alteration which limits the period of activity of this alteration to earlier geologic phases in the Noachian period (crust formation and olivine-rich unit formation). Two main types of fluvial landforms are observed in the Nili Fossae region. First, ancient valleys cross the Noachian highlands. These display sinuous shapes typical of meanders of fluvial origin, having a depth that reaches locally 300 m and extend up to 180 km in length. The valley floor exhibits a large channel with braided patterns typical of high-energy flows. A discharge of 500–900 $m^3/s$ was estimated for the EW oriented valley [9]. The poorly branching geometry of these valleys is different from the usual dendritic valley systems observed on Earth for valleys formed by precipitation. Their width and the presence of large channels suggest better flash floods, subsurface discharge or glacial surges. These valleys are superimposed on the olivine-rich unit that compose many outcrops of the eastern part of the region. This olivine-rich unit is only partially altered compared to the underlying bedrock which displays more extensive alteration. For this reason, the fluvial valleys observed might have participated into the local alteration of the olivine-rich unit, but their participation to the extensive alteration of the bedrock is unlikely, because this early phase of alteration was likely finished at the time of formation of the olivine-rich unit which is not massively altered.

Second, deep but poorly organized valleys emerge on the rim of the Nili Fossae trough system and some other landforms. Their short length, theater-shaped head and constant width are typical of sapping canyons, i.e., valleys formed by headward erosion due to subsurface flows. Several debris fans are associated with their termination in the Nili Fossae trough. These deposits are likely not deltas but alluvial fans (deposited subaerially). Additionally, another unusual fan is observed on high-resolution MOC images in a 80 km large crater. The ejecta of this crater are superimposed on the Nili Fossae floor, therefore involving an age younger than the alteration sequences for these alluvial fans, which formation was finished at the time of the Nili Fossae floor formation. One of this fan shows little alteration in a secondary trough of Nili Fossae [8, Fig. 13]. As the surrounding bedrock displays stronger signature of alteration than the fan, we interpret this fan to present clays mainly due to the transport and

deposition of these outcrops rather than any *in situ* formation. In general, to understand if clay deposits in fans, such as in Jezero crater, are due to *in situ* alteration or transport of upward material of the crust is a critical question for the origin of clays. It requires to study outcrops surrounding the fan deposits to understand if the lacustrine system was enough long to permit to the bedrock to be altered or not.

In summary, these fluvial landforms and their depositional products formed late in this region: all of them formed after the emplacement of the Noachian units that are rich in LCP, olivine or phyllosilicates, with some of them (sapping valleys especially) being clearly active during the Hesperian period. It is thus not surprising that most of the observed fluvial landforms are poorly correlated with hydrated regions: they cannot account for the epoch in which the largest outcrops of phyllosilicates formed, but some of them could be correlated to small outcrops altered late.

**Thyrrena region:** In this region, most outcrops of phyllosilicates are observed on craters walls or ejecta which does not allow an easy correlation with fluvial landforms [2, 10]. Nevertheless, a small plain displays hydrated minerals (single 1.93 micron signature with poor 2.3 micron peak locally). This plain is at the foot of hilly outcrops of Noachian bedrock dissected by few fluvial valleys. The study of this region is under progress to evaluate the relationships between these valleys and the observed signatures.

**Conclusion:** The timing of formation of most fluvial landforms observed in the vicinity of phyllosilicates indicate that these minerals formed mainly earlier than the fluvial systems still observed at the surface. Transport and deposition might explain many secondary deposits such as clays in alluvial fans. However, late alteration related to river streams is possible in several locations such as Nili Fossae and Thyrrena. Moreover, most of the fluvial landforms observed are the last episodes of aqueous deposition in the early Mars period, so they can not inform on the aqueous episodes that occurred earlier and might have been eroded or buried.

**References:** [1] Velde, Clays, 1995. [2] Poulet F. et al. (2005), *Nature, 438*, 623-627. [3] Bishop et al. (2008), *Science*. [4] Loizeau D. et al. (2007), *JGR, 112*. [5] Poulet et al., Astronomy Astrophysics., 2008 [6] Loizeau et al., submitted to Icarus [7] Wray et al. (2008), *GeoRL 35*. [8] Mangold et al., JGR, 2007. [9] Fasset and Head, GRL, 2005. [10] Costard et al., LPSC, 2006.

**SULFATES, FERRIC OXIDES AND Al-OH BEARING MINERALS IN ARAM CHAOS: COMPARISON OF OMEGA AND CRISM DATA.** M. Massé[1], O. Bourgeois[1], S. Le Mouélic[1], L. Le Deit[1], C. Verpoorter[1], J.-Ph. Combe[2], C. Sotin[1,3], J.-P. Bibring[4], B. Gondet[4],Y. Langevin[4] and the OMEGA Team. [1]Laboratoire de Planétologie et Géodynamique, UMR 6112, CNRS, Université de Nantes, 2 chemin de la Houssinière, BP 92208, 44322 Nantes Cedex 3, France (marion.masse@univ-nantes.fr), [2] Bear Fight Center, Box 667, Winthrop WA 98862, USA, [3]Jet Propulsion Laboratory, M/S 183-303, 4800 Oak Grove Drive, Pasadena, CA 91109, USA, [4]Institut d'Astrophysique Spatiale, Bâtiment 121, 91405 Orsay Campus, France.

**Introduction:** Aram Chaos is a 280 km wide Martian crater centered at 2.5°N, 338.5°E. This depression is connected to the Ares Vallis outflow channel by a gorge 15 km wide and 2.5 km deep, which cuts across the eastern wall of the crater. Previous studies have shown that this crater is filled by chaotic terrains, overlain by a presently dome-shaped, layered, 900 m thick formation (*Figure 1*), displaying spectral signatures of ferric oxides and sulfates on TES and OMEGA data [1,2,3,4,5]. In a previous study [6,11], we described the mineralogical composition, the structure and the morphology of this crater fill using various kinds of data: OMEGA, MOLA, MOC, TES, THEMIS, CTX and HiRISE. The aim of the present work is to refine these results and to compare them with newly acquired, high resolution, hyperspectral data from the Mars Reconnaissance Orbiter Compact Reconnaissance Imaging Spectrometer for Mars (CRISM).

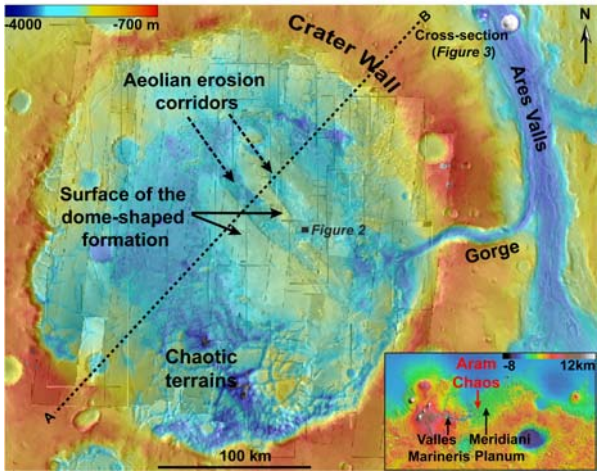


*Figure 1: Morphological map of Aram Chaos (superimposition of a MOLA DTM on a mosaic of visible THEMIS images). The box indicates the location of Aram Chaos on a MOLA topographic map of Mars.*

**Methodology:** The mineralogical composition of Aram Chaos was investigated from data acquired by the OMEGA imaging spectrometer, which collects 352 spectral channels from 0.38 to 5.2 µm at a spatial resolution ranging from 300 m to 4 km [7]. These data are compared with data from the CRISM imaging spectrometer, which collects 544 wavelengths from 0.36 to 3.9 µm at a spatial resolution ranging from 15 to 19 m/pixel [8]. We computed maps of various spectral parameters, which we integrated into a Geographic Information System (GIS) containing also high-resolution images from different instruments such as MOLA, MOC, THEMIS, CTX and HiRISE.

**Sulfates and ferric oxides detected by OMEGA:** Our previous study, based on OMEGA data, revealed that the floor of Aram Chaos is made of chaotic terrains, the composition of which remains unclear because they are covered by dust. A sulfate-rich formation, presently dome-shaped and layered, seems to have been emplaced unconformably on these chaotic terrains (*Figures 1 and 3*). The surface of this formation is partially covered by dust and displays wind erosion landforms (*Figure 3*). After its emplacement, this formation has been grooved down to various depths by large aeolian erosion corridors (*Figures 1 and 3*). On the floor of these corridors, strong spectral signatures of ferric oxides (possibly hematite and/or goethite and ferrihydrite and/or schwertmannite) are identified and correspond to large sheets of dark dunes. These dunes cover some outcrops of a bright, layered, cohesive material, which displays, in addition to ferric oxides, a monohydrated sulfate signature (kieserite or szomolnokite). The borders of the corridors are steep linear cliffs where the bright, layered, sulfate-rich material crops out (*Figure 3*). These cliffs are also partially covered by dark debris fans, which originate from the bright formation itself, and feed the dark sand sheets (*Figure 3*). We therefore infer that the dark ferric oxide sand sheets and debris fans are erosional products of the bright formation. However, due to the relatively low spatial resolution of OMEGA, it is not possible to analyse the exact composition of these cliffs.

**Sulfates and ferric oxides confirmed by CRISM:** New CRISM data on the dome-shaped formation are consistent with the results of our previous study. On the corridor floors, CRISM images display also a strong ferric oxide signature on the dark dunes, and a monohydrated sulfate signature that correlates well with the bright outcrops. According to the shape of the 2.4 µm band, CRISM data favour kieserite and therefore, enable us to discriminate between the two mono-

hydrated sulfates suggested by OMEGA. Moreover, with the better resolution of CRISM images, it is possible to observe this mineralogy with both ferric oxides and sulfates, on the bright corridor cliffs.

**Al-OH minerals (phyllosilicates?):** On two CRISM cubes (FRT 7FA4 and HRL 646A), an additional absorption band centered at 2.23 µm is detected on some very localized areas of the corridor floors (*Figure 2*), in association with sulfate and ferric oxide signatures. Carefull re-examination of OMEGA data on these areas shows that this band is also present, but with a detection level very close to the noise level (*Figure 2c*). The detection of this feature on several OMEGA and CRISM cubes, exactly at the same locations (*Figure 2a and b*), confirms that this band is not an artifact but a real mineralogical signature. The comparison with high-resolution images shows that this spectral feature is always found at the base of the dome-shaped formation, at the boundary with the underlying chaotic terrains. Systematic investigation of this feature on OMEGA data, which have a wider spatial extent, confirms this stratigraphic position, on the whole Aram Chaos area *(Figure 3)*.

The absorption band centered at 2.23 µm can be attributed to the presence of Al-OH or SiO [9]. However, the absorption band near 2.2 µm, due to the presence of SiO, is commonly wider than the 2.2 µm Aram Chaos absorption band. This new signature is therefore most probably correlated to Al-OH minerals. The accurate mineralogical identification is still in progress but this signature could be attributed, for exemple, to an Al-OH phyllosilicate such as montmorillonite, as was suggested on Mawth Vallis [10].

**Conclusion:** CRISM data confirm the conclusions made with OMEGA data. The dome-shaped formation is composed of a bright, layered material, which contains both sulfates (kieserite) and ferric oxides. The erosion of these rocks induces ferric oxides accumulations in the form of dark dunes on topographic lows.

CRISM data allowed the detection of a new layer at the bottom of this dome-shaped formation (*Figure 3*). This layer contains an Al-OH mineral, which can possibly belong to the phyllosilicate family.

**References:** [1] Christensen P. R. et al. (2001) *JGR, 106,* 873-885. [2] Catling D. C. and Moore J. M. (2003) *Icarus, 144,* 21-26. [3] Glotch T. D. and Christensen P. R. (2005) *JGR, 110,* E09006. [4] Oosthoek et al. (2007) *LPSC XXXVIII,* Abstract #1577. [5] Noe Dobrea E.Z. et al. (2007) *Icarus, 193,* 516-534. [6] Massé M. et al. (2008) *LPSC XXXIX*, Abstract #1391. [7] Bibring J.-P. et al. (2004) *Eur. Space Agency Spec. Publ. 1240, 37.* [8] Murchie S. et al. (2007), *JGR, 112,* E05S03, doi:10.1029/2006JE002682. [9] Hunt G.R. and Salisbury J.W. (1973), *Modern Geology,* vol.4, p. 85-106. [10] Loizeau et al. (2007), *JGR, 112,* E08S08, doi :10.1029/2006JE002877. [11] Massé et al. (2008), *JGR*, accepted.

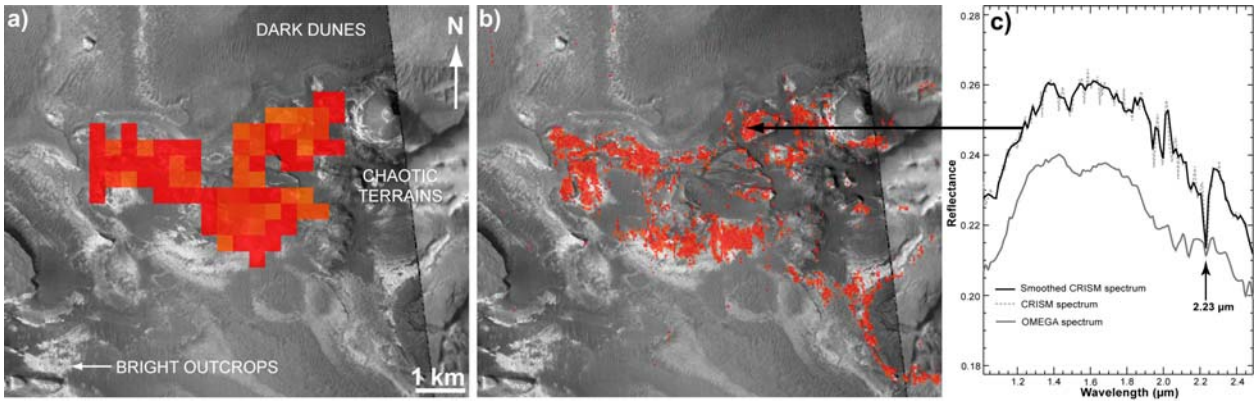


*Figure 2: Map of a spectral criterion (location on Figure 1) corresponding to the 2.23 µm band depth computed on a) OMEGA data and b) CRISM data. This map is superimposed on a CTX image c) Comparison between an OMEGA and a CRISM spectrum acquired at the same place.*

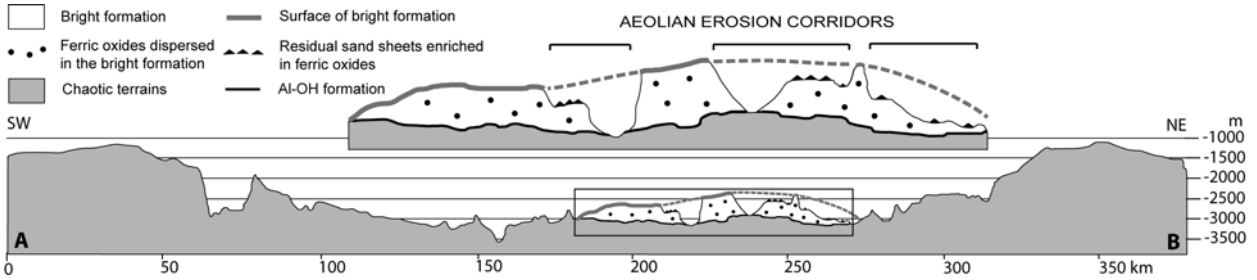


*Figure 3: Interpretative cross-section of Aram Chaos (location on Figure 1), vertical exaggeration: x12.5.*

**EMISSIVITY SPECTRA OF SOME PHYLLOSILICATES IN THE [3, 50] μm SPECTRAL RANGE FROM THE BERLIN EMISSIVITY DATABASE (BED).** A. Maturilli and J. Helbert, Institute for Planetary Research, DLR, Rutherfordstrasse 2, 12489, Berlin, Germany (alessandro.maturilli@dlr.de)

**Introduction:** Hydrous minerals as phyllosilicates class have been detected on Mars by the OMEGA instrument, onboard the ESA Mars Express mission [1, 2]. These minerals can keep the record of the interaction of martian pristine rocks with water. The OMEGA analysis found a limited range of mineralogy (Fe/Mg and Al smectite), located only in ancient terrains [3]. The very recent measurements of the CRISM instrument, onboard the NASA MRO mission, show that the phyllosilicate mineralogy on Mars is wider, giving evidence of kaolinite, chlorite, illite or muscovite, and hydrated silica. Furthermore, nontronite, saponite, and in less amount, chlorite are the most common smectites [3].

Actually, still another instrument is observing Mars from orbit: the PFS on Mars Express, measuring the emerging Mars radiation in the SWC from 1 to 5 μm and in the LWC from 5 to 45 μm.

For the interpretation of the remote sensing measured data an emissivity spectral library of planetary analogue materials is needed. The Berlin Emissivity Database (BED) presented here is focused on relatively fine-grained size separates, providing a realistic basis for interpretation of thermal emission spectra of planetary regoliths, and is therefore complimentary to existing thermal emission libraries.

**Spectral Library:** The Berlin Emissivity Database (BED) is a spectral library containing the emissivity measurements of several planetary analogues. It contains currently entries for plagioclase and potassium feldspars, low Ca and high Ca pyroxenes, olivines, elemental sulphur, common martian analogues (JSC Mars-1, Salten Skov, palagonites, montmorillonite, hematite, goethite), phyllosilicates (several kaolinites, chlorite, illite, some nontronites, saponite, talc, biotite), garnets, feldspathoids, and a lunar highland soil sample measured in the wavelength range from 3 to 50 μm as a function of particle size. For each sample, the spectra of four well defined particle size separates (<25 μm, 25-63 μm, 63-125 μm, 125-250 μm) are measured with a 4 $cm^{-1}$ spectral resolution. These size separates have been selected as typical representations for most of the planetary surfaces [4, 5].

**Laboratory set-up:** The instrumentation is located in the Planetary Emissivity Laboratory (PEL) at the Institute for Planetary Research (PF) of the German Aerospace Center (DLR) in Berlin, Germany. It consists of a spectrometer attached to an external emissivity device. The Bruker VERTEX 80v spectrometer, has a very high spectral resolution (better then 0.2 $cm^{-1}$), and a resolving power of better than 300,000:1, and can be operated under vacuum conditions. To cover the to 16 μm spectral range, a liquid nitrogen cooled MTC detector, a KBr beam-splitter, and a KBr entrance port are used. The 16 to 50 to μm spectral range is measured using a room temperature DTGS, a Multilayer beam-splitter, and a CsI entrance port.

The emissivity device is composed of the sample chamber, a double-walled box with three apertures: a 15 cm squared door used to insert the cup in the box, a 5 cm rounded opening through which the beam is directed to the spectrometer and a 5 cm opening facing the attached blackbody unit. A heater is placed in the chamber and is used to heat the cup with samples from the bottom. The thermal radiation emitted normal to the surface by the sample or the blackbody is collected by an Au-coated parabolic off-axis mirror and reflected to the entrance port of the spectrometer.

A pump circulates water at a constant temperature in the volume between the inner and outer walls of the chamber. The surfaces of the box are painted with black high emissivity paint. The chamber is purged with dry air to remove particulates, water vapour and $CO_2$. Further details can be found in [6, 7].

**Validation of the measurements:** An exhaustive suite of tests has been performed to study and characterize our experimental setup. Among these, the repeated measurement of the same target is a meaningful test for the investigation of the instrument stability. Eleven measurements of the same target, a cup containing the 125-250 μm grain size separate of quartz at 180° C, has been repeated, with a time interval of 5 minutes between each shot.

Figure 1 shows the calibrated emissivity for all the 11 measurements (each in a different colour), together with the average over all the calibrated data. The picture clearly prove the stability of our set-up, especially when considering that the whole 3 to 50 μm spectral range is covered operating the instrument with the two detectors, the beam-splitters and the entrance windows in two different days.

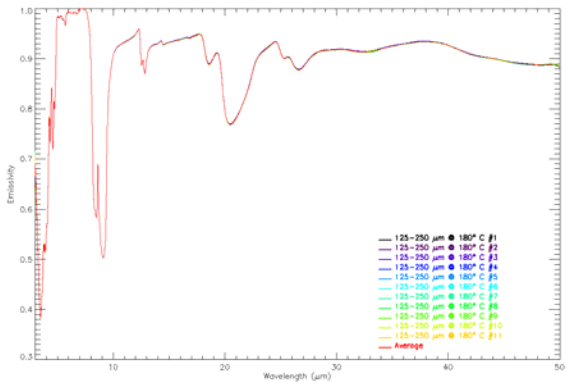


**Fig. 1** Repeated measurements of a 125-250 μm quartz sample at 180° C.

By means of such kind of repeated measurements, we can estimate the standard deviation of our calibrated data, as shown in Figure 2. It is evident from the picture how limited is the error on our measurements, always well below 0.1% across the whole spectral range, except for the region between 3 and 4 μm, where the noise level is higher, due to the blackbody radiation approaching the zero value, at the samples operational temperature (180° C).

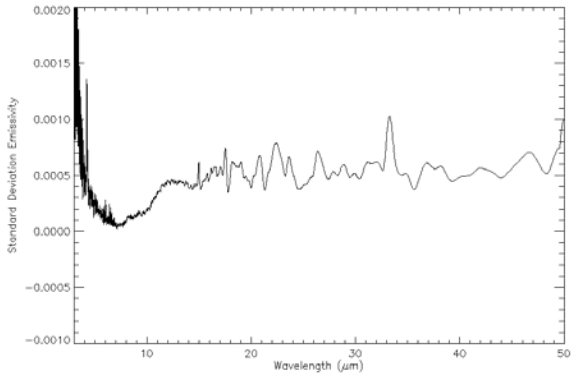


**Fig. 2** Standard deviation for the repeated measurements of a 125-250 μm quartz sample at 180° C.

Future measurements at 500° C will allow us to extend the spectral range to at least 1 μm, providing the scientific community a unique new set of data.

**Emissivity of phyllosilicates:** As an example of the numerous spectra of phyllosilicates present in the BED library, we discuss the emissivities of our 4 standard grain sizes of the Fe/Mg rich saponite endmember, shown in Figure 3. A serie of diagnostic maxima and minima in emissivity occur in the 3 to 30 μm spectral region, while the rest of the spectra is almost flat and featureless. The Cristiansen feature (a maximum in emissivity) is located at 8.04 μm, corresponding to 1244 $cm^{-1}$, in agreement with previous studies [8]. The bands depth strongly depends on the grain sizes, this is a well known already described phenomena. The large adsorption band around 10 μm (1000 cm-1) is due to Si-O stretching, while the $Mg_3OH$ bending vibration is observed at 15.15 μm (660 $cm^{-1}$). To note is the series of bands between 10 and 14 μm, in particular the change in shape, depending on the grain size, of the band at 11 μm and the shift in the band center position for the 12 μm feature. The 6.94 (1440 $cm^{-1}$) feature could be due to ammonium substitution in the mineral [9].

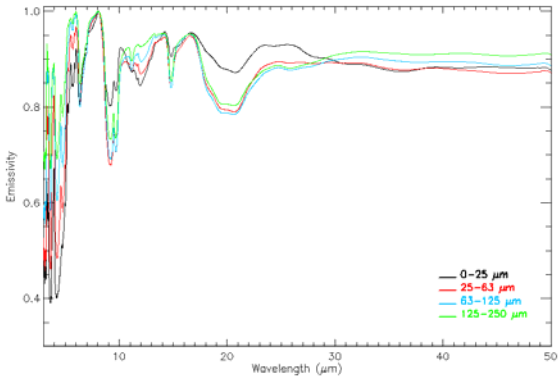


**Fig. 3** Emissivity spectra of saponite in the 4 BED grain sizes.

**Outlook:** The spectral library has been built to analyse the PFS measured spectra, especially for the LWC channel. The first step of this process is to search for confirmation of the OMEGA and CRISM results using the PFS data, and then use the large database of martian measurements for new investigations. However, the spectral range covered by the BED data could be of primary importance to understand the PFS SWC, OMEGA and CRISM measurements in the 3 to 5 μm spectral region.

The activity in the lab will be focused on understanding the spectral influence for different degrees of hydration in the martian analogue minerals.

**References:** [1] Bibring J. P. et al. (2005) *Science, 307*, 1576-1581. [2] Poulet F. et al. (2005) *Nature, 438*, 623-627. [3] Mustard J. F. et al. (2008) *Nature, doi:10.1038/nature07097*. [4] Hiesinger H., Helbert J., et al. (2008), *submitted to PSS*. [5] Helbert J. et al. (2007) *ASR, 40*, 272-279. [6] Maturilli A. et al. (2006) *PSS, 54*, 1057-1064. [7] Maturilli A. et al. (2008) *PSS, 56*, 420-425. [8] Koeppen W. C. and Hamilton V. E. (2005) *JGR, doi:10.1029/2005JE002474*. [9] Glotch T. D. et al. (2007) *Icarus, 192*, 605-622.

**CHARACTERIZATION OF PHYLLOSILICATE UNITS AT MAWRTH VALLIS: COMPARISON OF CRISM OBSERVATIONS AND INTIMATE PHYLLOSILICATE MIXTURES.** N. K. McKeown[1], J. L. Bishop[2], J. Cuadros[3], E. Amador[1], E. Silver[1], [1]University of California Santa Cruz (Earth and Planetary Sciences, 1156 High St., Santa Cruz, CA 95064, nmckeown@pmc.ucsc.edu), [2]SETI Institute/NASA-ARC (515 N. Whisman Rd., Mountain View, CA 94043), [3]Natural History Museum (Cromwell Rd., London, SW7 5BD, UK).

**Introduction:** Mawrth Vallis is one of the oldest outflow channels on Mars, cutting through Noachian-aged terrain on the border of the southern highlands and northern lowlands at ~25°N, -20°W [1, 2]. OMEGA detected large exposures of the phyllosilicates nontronite and montmorillonite in this region [3-6]. CRISM has refined these observations with the detection of an Fe/Mg-phyllosilicate such as Mg-nontronite, hydrated silica, and kaolinite in addition to nontronite and montmorillonite [7-10]. However, the montmorillonite and kaolinite spectra appear to be mixed with another material, possibly hydrated silica [7, 11]. We have prepared laboratory mixtures of a) montmorillonite and obsidian, b) kaolinite with montmorillonite, and c) kaolinite with altered ash from Kilauea dominated by opal-A in order to better characterize the CRISM spectra collected at Mawrth Vallis having a band near 2.2 µm.

**Methods:** Kaolinite (KGa) and montmorillonite (SWy) were sieved to <125 µm and then mixed at intervals of 25 wt%, from pure montmorillonite to pure kaolinite, with additional measurements at 15, 30, 40, and 60 wt% kaolinite. The mixtures were then sieved to <125 µm to homogenize the mixture and break up any clumps that may have formed. Kaolinite (KGa) and hydrated silica (SiOH) from Kilauea were sieved to <125 µm then mixed at 25 wt% intervals, with additional mixtures at 30 and 40 wt% kaolinite, and then sieved again. Montmorillonite and obsidian were sieved to <125 µm and mixtures prepared of 2, 5, 8, 10, 20, 50, and 80 wt% montmorillonite. The spectra were then measured in the lab relative to spectralon using a contact-probe ASD handheld spectrometer. The laboratory spectra were then compared to spectra previously collected from CRISM images [7, 8].

**Results of Mixture Studies:** We have focused here on the ~2.2 µm absorption feature due to a combination of the OH stretching and bending modes since the greatest change in spectral features is observed at this wavelength. In all cases, the 1.4 and 1.9 µm hydration features are reduced in strength as the amount of phyllosilicate decreases.

*Montmorillonite-obsidian.* Montmorillonite spectra have an absorption at 2.210 µm due to $Al_2OH$ and obsidian spectra have a broader absorption centered at 2.216 µm due to SiOH species; therefore, the band center of the mixtures does not shift greatly (fig. 1). However, since the obsidian feature is broader, the maximum inflection point on the longward side shifts to longer wavelengths with decreasing amounts of montmorillonite. At 50 wt% montmorillonite the inflection is still in the same position as for pure montmorillonite, but is not as sharp. At 20 wt% it is in an intermediate position, at 10 wt% it is slightly shorter than pure obsidian, and at 8 wt% it is in the same position as pure obsidian (fig. 1).

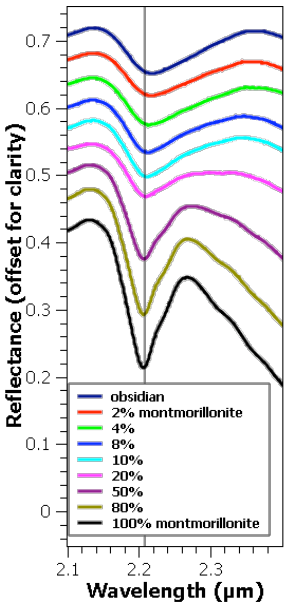


Fig.1 (left). Reflectance spectra from 2.1-2.4 µm of mixtures of montmorillonite and obsidian. Vertical line marks band center in pure montmorillonite at 2.21 µm.

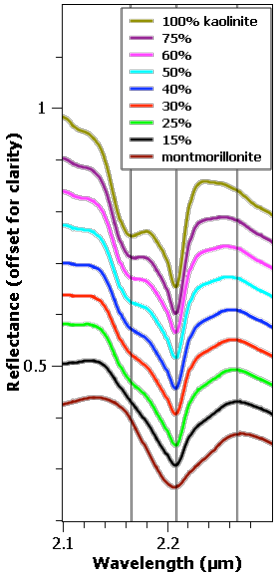


Fig. 2 (right). Reflectance spectra from 2.1-2.3 µm of mixtures of kaolinite and montmorillonite. Vertical lines from left to right show the position of the 2.17 and 2.21 µm doublet and the maximum inflection point of pure montmorillonite longwards of 2.21µm.

*Kaolinite-montmorillonite.* Kaolinite spectra have a doublet at 2.17 and 2.21 µm with very steep slopes. Montmorillonite spectra have a single absorption at 2.21 µm with an asymmetry to longer wavelengths. With decreasing kaolinite, the maximum inflection point on the longward side of this absorption shifts to longer wavelengths, more similar to montmorillonite (fig. 2). Additionally, the absorption at 2.17 µm is reduced. At 60 wt% kaolinite, this feature is a clear shoulder, while at 50 wt% it is a more gradual shoulder, and at 25 wt% it is barely detectable (fig. 2).

*Kaolinite-SiOH.* The Kilauea SiOH spectrum has an absorption at ~2.26 µm, slightly longer than that of

kaolinite. As a result, the depth of the kaolinite absorption with decreasing wt% kaolinite is greatly reduced on the longward side, but the maximum inflection point does not shift wavelengths (fig. 3). There is a clear 1.17 µm absorption observed at 75 wt% kaolinite, a clear shoulder down to 30 wt%, and a weak shoulder at 25 wt% (fig. 3).

**Analysis of CRISM Spectra**: Spectra from multiple images at Mawrth Vallis exhibiting a band near 2.2 µm were compared with the lab mixture spectra. The mixture with 20 wt% montmorillonite-80% obsidian appears to most closely match the majority of CRISM spectra collected from Mawrth Vallis on the longward side of the ~2.2 µm feature (fig.4). Most Mawrth Vallis spectra with a band near 2.2 µm exhibit a gradual slope on the shortward side of the ~2.2 µm absorption which is not observed in the mixtures. Therefore, more mixtures are needed to try and explain the shape of this feature.

The kaolinite-Kilauea SiOH mixtures do not match the CRISM observations as the 2.21 µm band is not broadened (fig. 5). Future mixture experiments with kaolinite and a pure opal or hydrated glass component are planned to test this further.

The 2.21 µm feature is broadened in spectra of the kaolinite-montmorillonite mixtures, but not to the extent observed in CRISM spectra (fig. 6). Additionally, the mixture spectra show a break in slope at ~2.24 µm which may be present in spectrum 43EC-b but is not resolved in the other CRISM observations (fig. 6).

In summary, CRISM spectra of the Mawrth Vallis region having a band near 2.2 µm appear to be most consistent with mixtures of hydrated glass with either montmorillonite or kaolinite. The kaolinite doublet is observable in mixtures down to ~25 wt% kaolinite.

**Acknowledgements:** This work was supported by MFR, NASA-Ames UARC, and the NPS at Monterey. Thank you to the CRISM Team for the collection and processing of the CRISM images.

**References:** [1]Scott, D. H., et al. (1986) *USGS MI*, I-1802-A. [2]Edgett, K. S., et al. (1997) *GRL*, *24*, 2897-2900. [3]Loizeau, D., et al. (2007) *JGR*, *112*, E08S08. [4]Bibring, J.-P., et al. (2007) *LPS XXXVIII* Abstract #2160. [5]Bibring, J.-P., et al. (2005) *Science*, *307*, 1576-1581. [6]Poulet, F., et al. (2005) *Nature*, *438*, 632-627. [7]Bishop, J. L., et al. (2008) *Science*, *321*, 830-833. [8]McKeown, N. K., et al. (2008) *LPS XXXIX* Abstract #1400. [9]Noe Dobrea, E. Z., et al. (2008) *LPS XXXIX* Abstract #1077. [10]Wray, J. J., et al. (2008) *GRL*, *35*, L12202. [11]Milliken, R. E., et al. (2008) *Geology*, *in press*.

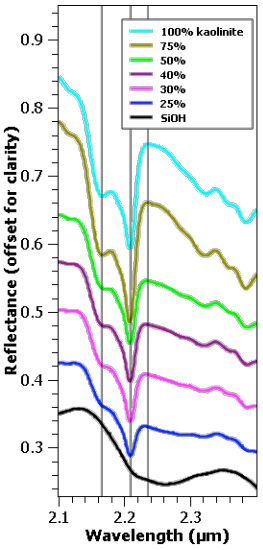


Fig. 3 (left). Spectral results of kaolinite-Kilauea SiOH mixtures. Vertical lines from left to right show the position of the 2.17 and 2.21 µm doublet and the maximum inflection point of pure kaolinite.

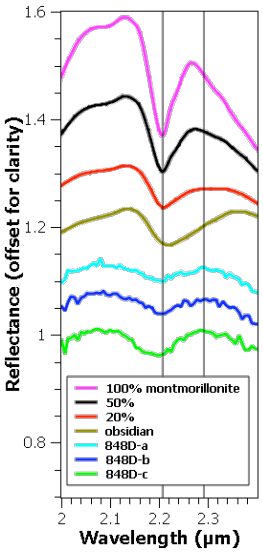


Fig. 4 (right). Comparison of montmorillonite-obsidian mixtures with CRISM observations from image FRT0000848D, labeled a-c. Vertical lines show the center of the 2.21 µm feature and the maximum inflection point in the CRISM observations. Note how well CRISM spectra a and b match the spectrum of 20% montmorillonite longwards of 2.21 µm.

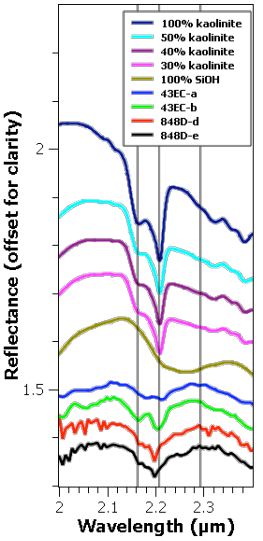


Fig. 5 (left). Comparison of kaolinite-SiOH mixtures with CRISM observations from images FRT0000848D, labeled d and e, and HRL000043EC, labeled a and b. Vertical lines from left to right show the position of the 2.17 and 2.21 µm doublet and the maximum inflection point of the CRISM observations. None of the mixtures match the CRISM observations.

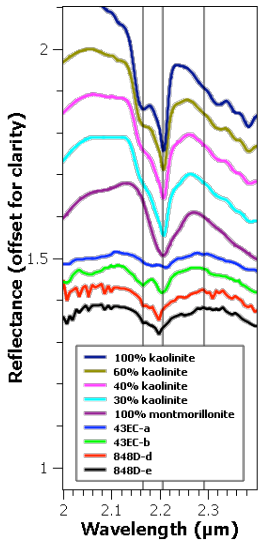


Fig. 6 (right). Comparison of kaolinite-montmorillonite mixtures with the same CRISM observations as in fig. 5. Vertical lines from left to right show the position of the 2.17 and 2.21 µm doublet and the maximum inflection point of the CRISM observations.

**DO MAGMATIC CLAYS EXIST? THE IMPORTANCE OF TERRESTRIAL ANALOGUES**. A. Meunier[1], A. Mas[1], D. Beaufort[1], P. Patrier[1] and P. Dudoignon[1]. University of Poitiers, HYDRASA INSU-CNRS, 40 avenue Recteur Pineau , 86022 Poitiers Cedex, France. *Alain.meunier@univ-poitiers.fr*

**Introduction:** Mars' crust in the southern hemisphere is mainly composed of basalt-like rocks. The discovery of nontronite in Syrtis Major, Nili Fossae and Mawrth Vallis regions [1] has been attributed to long-term contact of these rocks with liquid water. The conditions in which nontronite has been formed at the surface of Mars were discussed assuming a low-temperature alteration process [2]. However, the question is: do clay minerals in basaltic rocks form exclusively through alteration? To address this question we studied terrestrial analogues in order to compare the petrography, mineralogy and geochemistry of clay minerals formed in altered glassy chilled or brecciated margins with those composing the mesostasis in the massive inner crystallized parts of three basalt-hawaiite bodies from Mururoa atoll (French Polynesia).

**Analytical methods:** X-ray diffraction (XRD) has been performed from randomly oriented powders and oriented preparations using a Philips PW 1730 diffractometer (Cu Kα radiation, 40 kV, 40 mA), equipped with a stepping motor drive (SOCABIM DACO system) and a KEVEX solid state detector. A JEOL 6400 scanning electron microscope (SEM) equipped with a KEVEX energy dispersive X-ray fluorescence analysis system (Si-Li diode – EDS) was used. Observations were performed both in the secondary (SE) and back-scattered electron (BSE) modes on small slabs of rocks (several $mm^3$) and petrographical thin sections previously coated with carbon.

Electron microprobe analyses were performed using a CAMECA SX50 electron microprobe (CAMPARIS service, Paris VI) equipped with wavelength dispersive spectrometers (4 nA, 15 kV, spot size 4µm, counting time 10s per element. The quantitative analyses have been obtained by comparison with natural silicate standards using a CAMECA PAP matrix correction.

The chemical analyses of the bulk rocks and the clay fractions were performed from <5µm and <0.2 µm powders respectively at the Service d'Analyse des Roches et des Minéraux (SARM), Nancy France (*http://www.crpg.cnrs-nancy.fr/SARM/*). Major elements and Rare Earth Elements (REE) were analyzed using atomic absorption spectrometry (AA), ICP-AES and ICP-MS respectively. Stable and radiogenic isotopes (O, Sr, Rb) were analyzed using mass spectrometry. The loss on ignition (LOI) was measured using a Netzsch apparatus for simultaneous thermal analyses (STA 409 EP).

**Results:** The clay minerals form polyphased assemblages either in the veins crosscutting the glassy chilled margins or in the mesostasis. All assemblages are composed of di- and trioctahedral phases which are formed of expandable (nontronite, saponite types) and non expandable layers (chlorite, celadonite types) either in discrete phases or interstratified in mixed layered minerals. These assemblages are different from that formed in hydrothermal systems or low grade metamorphic conditions which are characterized by the saponite → randomly ordered chlorite/smectite mixed layered minerals → corrensite → chlorite sequence (no plagioclase albitisation; no corrensite). Nontronite is systematically present. It is high-charge in the massive inner crystallized part.

Clay minerals formed in the chilled margins and the massive crystallized inner parts of three basalt-hawaiite bodies of Mururoa atoll (French Polynesia) exhibit contrasted textures. Glass alteration textures are observed around fractures crosscutting the quenched margins: Fe-rich clays grow inward the glass (retreating surface on which Ti-oxides accumulate) while Mg-rich ones grow outward (Fig. 1).

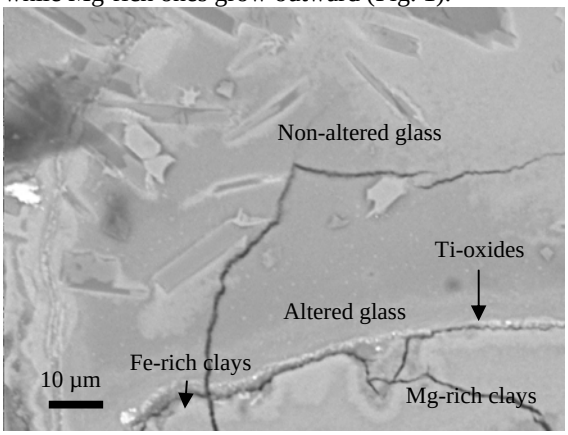


Figure 1: Submarine flow. BSE picture of the chilled margin.

The textures of clay deposits filling the diktytaxitic voids (mesostasis) in the massive inner parts of the three volcanic bodies are different: non-oriented clay matrix (submarine flow) embedding euhedral apatite and pyroxene microcrysts; palissadic clays (subaerial flow) coating the void walls and the crystal surfaces of apatite and K-feldspar microcrysts. In the

dyke, the central part of the void remain empty (Fig. 2A). Clay muffs (dyke) cover all the apatite needles (Fig. 2B),.

The non-oriented texture could result from the alteration of a glass precursor concomitantly to the olivine phenocrysts (clay pseudomorphs). The palissadic and muff textures form through heterogeneous nucleation on the solid surfaces and crystal growth from a saline solution. No glass precursor has existed before. The centre of the diktytaxitic voids in the dyke being empty, it is probable that the residual liquid was boiling.

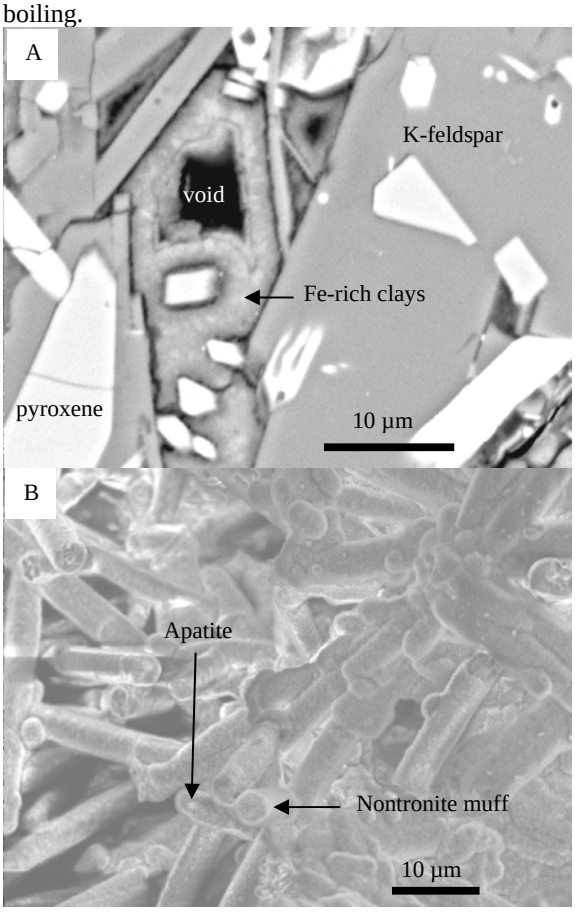


Figure 2: Dyke. A) BSE picture of small sized diktytaxitic voids. B) SE picture showing nontronite-like muffs coating apatite needles in a micro-geoda.

The amounts of LREE, Sr and the most incompatible elements are systematically higher in clays from diktytaxitic voids relatively to that formed in the altered glass of the chilled margins (Fig. 3). Thus, diktytaxitic clays formed from a residual liquid which gave either a glass or a saline solution after cooling (fractionation process). On the contrary, clays in quenched margins result from glass-solution interactions (alteration process). The $\delta^{18}O$ variation versus LOI indicates that sea water was involved either in rock alteration or magma contamination (Fig. 4). This is confirmed by the $^{87}Rb/^{86}Sr$ ratio of bulk rocks and clay fractions from the quenched and massive inner parts of the three volcanic bodies which do not fit with the 11.5 Ma isochron indicating that the Rb-Sr system was never closed during the magmatic history.

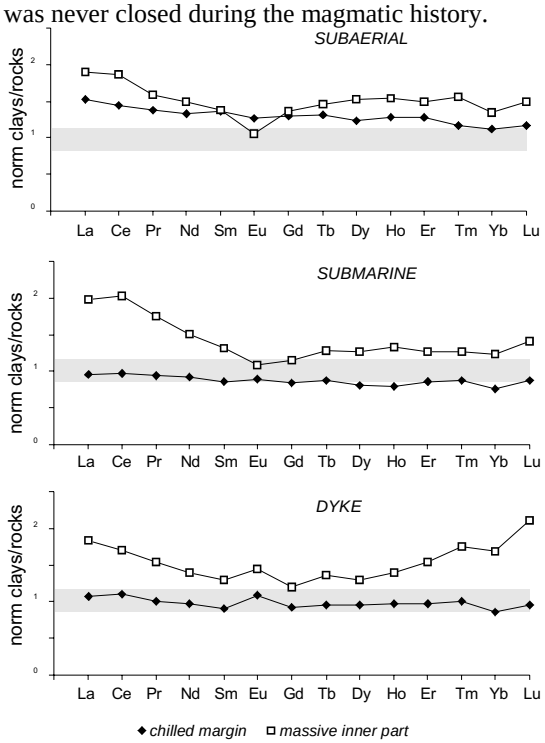


Figure 3: REE amounts normalized to the parent rock composition of the < 2µm fraction of the chilled margins (black diamonds) and the massive inner parts (square) of the three volcanic bodies. Grey zone: experimental error domain for the bulk rock composition.

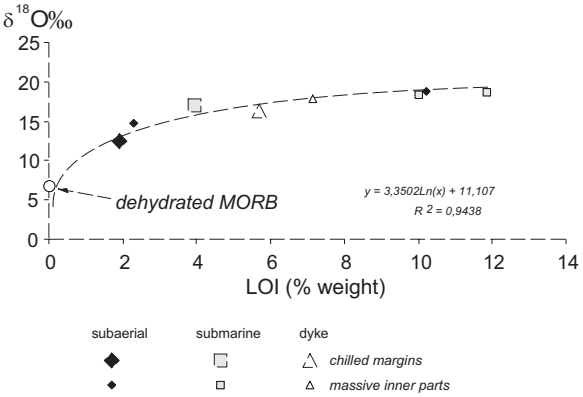


Figure 4: Relation between the loss on ignition (LOI) and $^{18}O/^{16}O$ isotopic ratio of the clay fractions .

**References:** [1] Poulet, F., Bibring, J.P, Mustard, J.F., Gendrin, A., Mangold, N., Langevin, Y., Arvidson, R.E., Gondet, B., Gomez, C. and the Omega Team (2005) *Nature*, **438**, 623-627. [2] Chevrier, V., Poulet, F. and Bibring, J.P. (2007) *Nature*, **448**, 60-63.

**WHICH CLAYS ARE REALLY PRESENT ON MARS AND HOW DID THEY FORM?** R. E. Milliken[1], Jet Propulsion Lab, Caltech, 4800 Oak Grove Dr. Pasadena, CA, 91109 ralph.milliken@jpl.nasa.gov

**Introduction:** The vast amount of spectral information regarding the composition of Mars returned by the OMEGA (Mars Express) and CRISM (MRO) visible-near infrared spectrometers has revolutionized our understanding of water-rock interactions on the red planet. The detection of regional phyllosilicate deposits [1] and numerous smaller phyllosilicate deposits scattered throughout the ancient crust [2] imply that water-rock interaction was spatially extensive during the early history of Mars. To date, researchers have identified deposits of smectites, kaolin group minerals, chlorites, and illite/mica [1, 2]. Though distinguishing between these major types of phyllosilicates is relatively straightforward, distinguishing between types within these groups can be more difficult. In addition, there are certain cases in which smectites or chlorites may be confused with other types of clay minerals. Finally, though many clay minerals can form in a variety of environments and are subject to aqueous and eolian transport, the accurate identification of certain types of clay minerals can be indicative of local geochemical conditions. These distinctions are crucial when interpreting the mineralogy of a given location to determine if it is suitable to address the science goals of future landers or rovers such as NASA's Mars Science Laboratory and ESA's ExoMars.

**Martian Spectra of Clays**: Phyllosilicates (clay minerals) have been identified on Mars primarily by the presence of metal-OH absorptions centered at wavelengths between ~2.2 – 2.4 µm, where the metal is usually Al, Fe, and/or Mg. Generally speaking, Al-OH features in smectites occur at shorter wavelengths (~2.2 µm), followed by Fe-OH bands at longer wavelengths (~2.28 µm), followed by Mg-OH (~2.31 µm). Cation substitution in smectites often give rise to multiple bands or shoulders in this region, though they are usually distinguishable from other clay mineral groups by the overall shape and width of these absorptions (Figure 1). Kaolin group minerals (e.g. kaolinite, halloysite) exhibit a clear doublet near ~2.2 µm and near ~1.4 µm that make them distinct from smectites. Similarly, chlorites exhibit bands that are wider and at longer wavelengths than smectites (~2.35 µm; Figure 1). Most serpentines exhibit diagnostic absorptions at ~1.4 µm and ~2.32 µm, though to date no serpentines have been unambiguously identified on Mars from orbit.

It is important to note that regions believed to have Fe/Mg smectites exhibit clear differences in their spectral properties, suggesting some may not be true smectites. As shown in Figure 2, spectra suggested to be indicative of smectites in Mawrth Vallis, Nili Fossae, and Gale Crater are quite variable. Specifically, the type spectrum for Nili Fossae exhibits a distinct asymmetry in the ~2.3 µm band that is not observed in true Fe/Mg-rich smectites such as nontronite or saponite and cannot be attributed to variations in albedo, particle size, or hydration level [3, 4]. An alternative explanation for this difference is that the Nili spectrum is indicative of hisingerite, and Fe-rich phyllosilicate with a halloysite-like (i.e. kaolin group) structure [5].

Another potential source of confusion is within the chlorite-serpentine groups. Though spectra of most serpentines exhibit a distinct sharp absorption near ~2.32 µm, some Fe-rich varieties such as greenalite exhibit a broader absorption [6] that may be confused with some chlorites at the signal to noise and spectral resolution of instruments such as OMEGA and CRISM (Figure 3). The presence of greenalite on Mars would be of interest because it can occur as an early diagenetic phase and is commonly formed under reducing conditions. Similarly, laboratory experiments have also shown that the formation of Fe-rich smectites and chlorites under low temperature conditions requires initially reducing conditions [7]. Therefore, the identification of Fe-rich clays formed under surface conditions on Mars would imply moderate pH levels and reducing conditions, factors that are favorable for life.

A third potential ambiguity in the identification of specific clay minerals is between saponite (Mg-rich smectite) and the fibrous clay sepiolite (also Mg-rich). The latter is commonly formed in saline lakes and, if found on Mars, could be diagnostic of clays precipitated *in situ* in standing bodies of water instead of clays transported as the suspended load to their current location. As an example, the detection of sepiolite in the Eberswalde or Jezero deltas would represent a mineral detection consistent with the morphology for standing bodies of water. Unfortunately, it may be quite difficult to distinguish between saponite and sepiolite with the resolution of OMEGA and CRISM, thus the identification of clays precipitated in saline lakes will likely continue to be speculative. In fact, spectra of clays in the Eberswalde delta exhibit similar asymmetric features

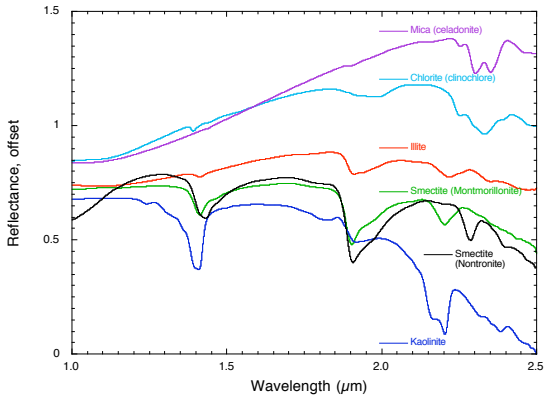


**Figure 1**. Lab spectra of representative clay groups.

as those in Nili, suggesting they may be detrital clays transported from the outcrops in the surrounding crater walls and rim.

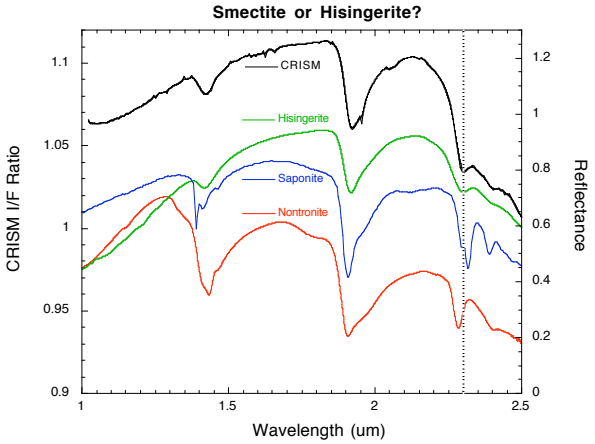


**Figure 2**. CRISM ratio from Nili Fossae. The asymmetry of the Fe/Mg-OH band at ~2.3 µm is more similar to hisingerite than similar bands in smectites.

**Formation Environments of Clays:** On Earth, the majority of clay minerals form as weathering products of the continental crust, which has a granitic bulk composition. Mars, on the other hand, is dominated by a basaltic crust and presumably decreasing levels of water-rock interaction through time. Plate tectonics, subsidence, and the presence of oceans result in large scale sedimentary sinks on Earth, whereas craters and large canyon systems (e.g. Valles Marineris) act as the primary sediment sinks on Mars. Most of the clay deposits on Mars are found within the ancient Noachian cratered terrain, suggesting they formed early in the history of Mars, though some are associated with Hesperian-aged sedimentary deposits. These younger clay deposits are often associated with fluvial systems and their spectra do not exhibit evidence of leaching by acidic fluids. This suggests that local geochemical conditions were quite variable during the Hesperian and that not all regions were altered by acidic fluids, even though it is known that large sulfate deposits were also formed during this period [8].

Though the martian surface exhibits clear geomorphic evidence of fluid flow (valley networks, channels, etc.), it is yet unclear if the clays formed primiarly on the surface (e.g. weathering) or in the subsurface (e.g. hydrothermal). Therefore, the primary mechanism of clay formation may be significantly different on Mars than Earth. The majority of clays discovered on Mars fall within the Fe/Mg-rich group, suggesting that chemical alteration and continuous leaching by fluids was not significant enough on a global scale to produce late stage Al-rich phases such as kaolinite and gibbsite. Extensive montmorillonite deposits in the Mawrth Vallis region are one of several exceptions and have been interpreted as altered volcanic ash deposits [9]. The presence of numerous Fe/Mg-rich chlorite deposits throughout the southern highlands suggest that physical, not chemical, weathering has dominated these regions since these clays were exposed.

The effects of subsidence, burial, and diagenesis on clay mineralogy have been studied extensively on Earth, but their Martian counterparts and implications for fluid chemistry have yet to be examined in detail for Mars. Burial and diagnesis of smectite commonly produces interlayered illite-smectite and ultimately illite. However, this requires substitution of K or an equivalent cation into the structure, and the relatively low abundance of K on Mars suggests that smectite may not readily convert to illite. Instead, the Fe/Mg-rich smectites may convert to inerlayered chlorite-smectite, possibly explaining the presence of Fe/Mg chlorite at depth in the sourthern highlands [2]. Alternatively, these chlorite deposits may have formed in the subsurface via hydrothermal processes.

**Conclusions:** In summary, though the detection of clay minerals on Mars appears to be unambiguous, the identification of specific clay minerals and their chemistry must be approached with caution. Clay minerals can form in a wide variety of environments and by a variety or processes, thus great care must be taken when interpreting a formation process based on a mineral identification. Local geology, morphology, zonation of minerals, and identifying mineral assemblages are important factors when attempting to distinguish whether or not individual clay deposits are detrital, formed *in situ*, or representative of diagnetic or hyrothermal processes. Constraining these possibilities will be critical for evaluating sites of potential habitability for future Mars missions.

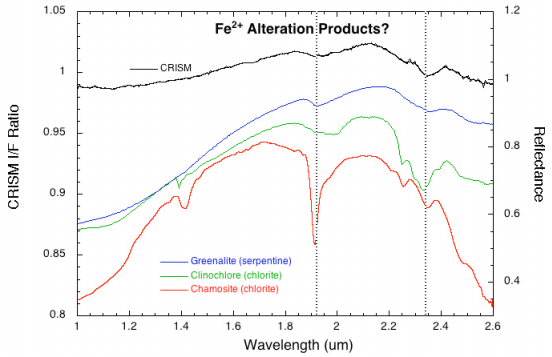


**Figure 3**. Example of a possible chlorite deposit in the walls of Juventae Chasma. Alternatively, this material could be the Fe-rich serpentine greenalite or a mixture of the two. Not all spectral features in the CRISM ratio match a single chlorite spectrum, such as the hydration feature at ~1.9 µm.

**References:** [1] Poulet, F. et al. (2005), *Nature*, 438; [2] Mustard, J. et al. (2008), *Nature*, 454 ; [3] Milliken, R. and J. Mustard, (2007a), *Icarus*, 189; [4] Milliken, R. and J. Mustard (2007b), *Icarus*, 189; [5] Eggleton, R. and D. Tilley (1998), *Clay Clay Min*., 46; [6] Calvin, W. and T. King (1997), *Met. Plan. Sci*., 32; [7] Harder, H. (1978), *Clay Clay Min*., 26; [8] Bibring et al. (2006), Science, 312; [9] Bishop et al. (2008*), Science, in press*.

**VISIBLE AND NEAR-IR SPECTRA FOR AQUEOUS ALTERATION PRODUCTS (PALAGONITE, PHYLLOSILICATES, SULFATES) OF BASALTIC TEPHRA ON MAUNA KEA VOLCANO, HAWAII.**

R. V. Morris[1], V. E. Hamilton[2], J. E. Gruener[1], D. W. Ming[1], and S. Mertzman[3]. [1]NASA Johnson Space Center, Houston, TX 77058 richard.v.morris@nasa.gov; [2]SRI, Boulder, CO 80302; [3]F & M College, Lancaster, PA 17604.

**Introduction:** Mauna Kea volcano is a basaltic volcano that has undergone a variety of aqueous alteration process that are also plausible for the Martian surface. The processes on Mauna Kea include low-temperature alteration (phyllosilicate-free palagonite alteration product) and hydrothermal alteration under near-neutral (phyllosilicate alteration products) and acid-sulfate conditions (jarosite, alunite, hematite spherules, and phyllosilicate alteration products) [e.g., 1,2,3]. Here, we summarize [3] and focus on the spectral region between 1.7 and 2.5 µm where spectral features resulting from $H_2O$ and M-OH occur in order to determine the strength of the spectral signatures of the alteration products and relate those signatures to specific alteration products.

**Discussion:** Reflectance spectra between 1.7 and 2.5 µm for unaltered tephra (513B), palagonitic tephra (600C and 530C), phyllosilicate-bearing tephra formed under hydrothermal conditions (911C, 741C, and 742C), and sulfate-bearing (jarosite or alunite) tephra formed under acid-sulfate, hydrothermal conditions are shown in Fig. 1 [after 3]. The spectral feature near 1.9 µm results from combination and overtone bands of the fundamental vibrations of the $H_2O$ molecule. The spectral features between ~2.0 and 2.5 µm result from OH stretch and (Al, Fe)-OH combination bands. All altered tephra samples have spectral features associated with $H_2O$ and (Al, Fe)-OH.

Palagonitic tephra (Fig. 1b) have a broad 1.9 µm band from adsorbed and/or trapped $H_2O$ and an asymmetric feature from (Al,Si,Fe,Mg)-OH. The band edge at 2.21 µm corresponds to the onset of absorption by Al-OH. The phyllosilicate bearing samples (Fig. 1c) have shaper (Al, Fe)-OH features, resulting from well-defined (relative to palagonite) cation sites. Sample 742C is dominated by Al-OH (2.21 µm), indicating montmorillionite. Samples 911C and 741C, with stronger bands near 2.24 and 2.30 µm from (Al, Fe)-OH, have aluminous nontronite. The spectral signatures of alunite (1.77 and 2.18 µm) and jarosite (1.85 and 2.27 µm) are clearly evident in 740C and 508C and in 515C, respectively (Fig. 1d).

These results show that aqueous process on Mauna Kea produce a variety of alteration products that depend on formation conditions and that can be identified in VNIR spectra. This information can be used to constrain formation processes of phases identified in Martian VNIR data obtained by CRISM and OMEGA.

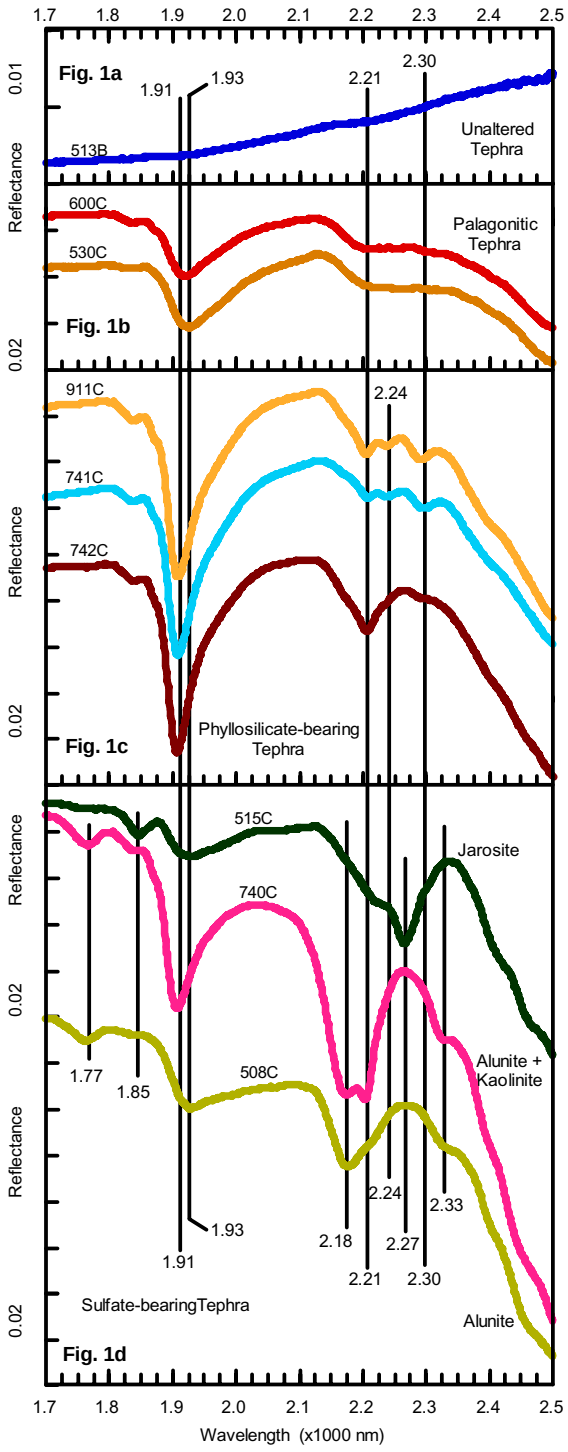


References: [1] Morris *et al.* (2000) *JGR, 105*, 1757. [2] Morris *et al.* (2001) *JGR, 106*, 5057. [3] Hamilton *et al.* (2008) *JGR*, accepted.

## $^{57}$Fe MÖSSBAUER SPECTROSCOPY: A TOOL FOR THE REMOTE CHARACTERIZATION OF PHYLLOSILICATES?

E. Murad, D-95615 Marktredwitz, Germany (emurad@yahoo.com)

**Introduction:** The earliest Mössbauer study of phyllosilicates dates back to 1962, when Pollak et al. [1] published Mössbauer data on several biotites. Some years later Malden and Meads [2] carried out a detailed Mössbauer study of a commercial kaolin. By removing associated mica, these authors arrived at a set of "true" parameters for the pure clay-sized phyllosilicate kaolinite. Since then a plethora of papers on phyllosilicates has been published. The Mössbauer Minerals Handbook [3] lists 111 papers that make reference to biotite, 26 papers that refer to muscovite and 11 references to kaolinite.

All phyllosilicates have the common structural features of continuous two-dimensional tetrahedral $(Si,Al)O_4$ sheets which are liked to $(Al,Mg)(O,OH)_6$ octahedral sheets. Different linkages of the sheets to layers give rise to an assortment of structures. Fig. 1 shows two common layers: a 1:1 layer that is, for example, observed in kaolinite, and a 2:1 layer that is developed in micas.

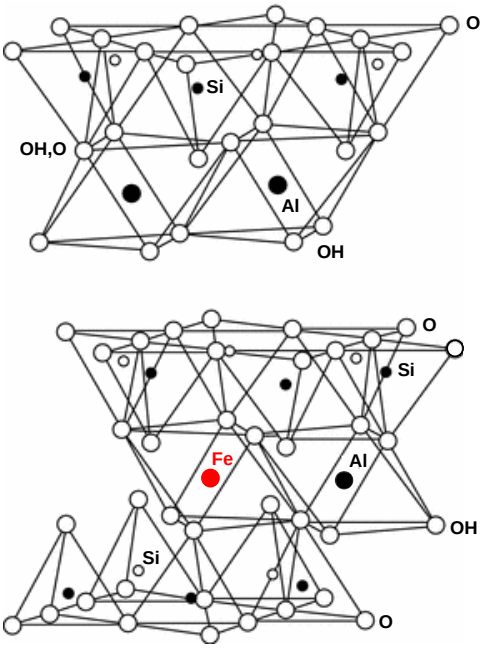


**Fig. 1.** Common phyllosilicate structures: 1:1 layer (top) and 2:1 layer (bottom).

Numerous other cations can replace Al and Mg in the octahedra, and Al often replaces part of the Si in the tetrahedra. Fe can enter into the octahedra both as $Fe^{2+}$ and $Fe^{3+}$ and to a lesser extent into the tetrahedra as $Fe^{3+}$.

**Problems**: The structural similarity of the phyllosilicates makes a distinction of individual species by Mössbauer spectroscopy difficult (and in many cases impossible), because the Fe atoms "sense" predominantly the immediate (tetrahedral or octahedral) environment. Mössbauer parameters of phyllosilicates therefore reflect the local Fe symmetry, and in general allow a distinction of $Fe^{2+}$ or $Fe^{3+}$ in more or less moderately distorted octahedral or tetrahedral environments.

The isomorphous substitution of cations in the octahedra and tetrahedra leads to variations in the environments of the resonant (Fe) atoms, causing the Mössbauer parameters of phyllosilicates to be often "smeared out". When studying specific clay-sized phyllosilicates ("clay minerals" *sensu stricto*), the problem of purity may also arise, because these minerals more often than not occur in close association with other minerals that can falsify both the bulk chemistry and physical properties. This problem is particularly serious when phyllosilicates are associated with paramagnetic or superparamagnetic $Fe^{3+}$ oxides, because these have Mössbauer parameters that resemble those of $Fe^{3+}$ in many phyllosilicates. The use of chemical treatments to remove such Fe oxides involves manipulations that will hardly be feasible on unmanned missions.

**Applications to clay minerals**: as indicated above, $^{57}$Fe Mössbauer parameters reflect the local Fe symmetry. This is straightforward in the case of octahedrally-coordinated $Fe^{3+}$, because in this case the quadrupole splitting ($\Delta$) is directly proportional to the site distortion. The $Fe^{3+}$ quadrupole splittings of clay minerals thus show some subtle variations: nontronite has a small average $\Delta$ of ~ 0.35 mm/s [4], kaolinite has an intermediate average $\Delta$ of ~ 0.51 mm/s [5], whereas illite has somewhat higher $\Delta$ values ranging from ~ 0.59 mm/s for Fe-rich (> 5 wt.-% Fe) illites to ~ 0.73 mm/s for Fe-poor (<1 – ~3 wt.-% Fe) samples [6], reflecting increasing octahedral flattening angles. Fig. 2 shows typical spectra of the mentioned minerals; these display an increasing separation of the doublet lines in the sequence nontronite → kaolinite → illite. These differences can, however, serve for diagnostic purposes only when studying pure, monomineralic samples, and seldom when untreated natural materials are studied (see comment above)

Sagging shoulders in the kaolinite spectrum in Fig. 2 point to a phenomenon which is common in Fe-poor samples (and is often mistaken for incipient magnetic ordering): slow paramagnetic relaxation.

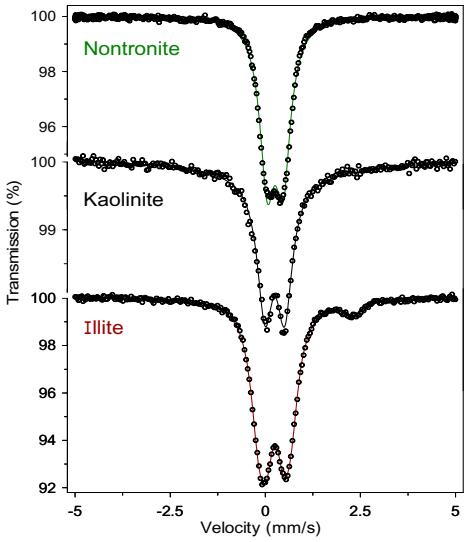


**Fig. 2.** Room-temperature Mössbauer spectra of nontronite (top), kaolinite (center) and illite (bottom).

A parameter which is readily revealed by Mössbauer spectroscopy is the $Fe^{2+}/Fe^{3+}$ ratio, which can provide important clues regarding the redox environment of a sample. The determination of this ratio by Mössbauer spectroscopy is relatively straightforward: thus Fig. 2 shows the illite to contain a minor proportion of $Fe^{2+}$, indicated by a resonant line at ~ 2.4 mm/s. Such a line is missing in the other two spectra, indicating Fe in these samples to be exclusively trivalent.

**Applications to natural clays of complex mineralogy on Earth and Mars**: a basic difference between clay minerals *s.s.* (clay-sized phyllosilicates) and Fe oxides is that almost all of the former are paramagnetic to ~ 10 K, whereas many Fe oxides are magnetically ordered at 300 K and all are magnetically ordered at ~ 20 K [7]. Natural clays (and sediments and soils) are usually more or less complex mixtures of clay minerals, Fe oxides, and other (Fe-bearing and Fe-free) minerals. Their room-temperature Mössbauer spectra thus generally comprise three sets of components: (1) $Fe^{3+}$ doublets from paramagnetic clay minerals and other silicates, and superparamagnetic Fe oxides and related minerals (e.g. schwertmannite), (2) $Fe^{2+}$ doublets that, if present, would in most cases originate from clay minerals, and (3) $Fe^{3+}$ sextets from magnetically ordered Fe oxides. These features have been used to characterize clays from a variety of environments using Mössbauer spectroscopy in combination with other techniques such as X-ray diffraction, visible, infrared and Raman spectroscopies, selective chemical extraction procedures, optical and electron microscopies, and thermal analysis [8,9,10]. As an example, Fig. 3 shows how the selective removal of Fe oxides affects the room-temperature Mössbauer spectrum of a bauxite. This treatment not only allows a better characterization of the paramagnetic components (residual minerals, some or all of which could contribute to the $Fe^{3+}$ doublet, have been identified by X ray diffraction as boehmite, kaolinite, anatase and crandallite), but also shows the residual hematite to be identical to that which has been extracted [11].

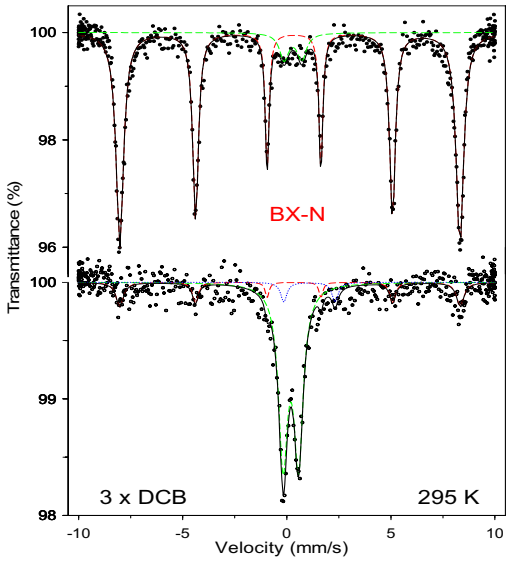


**Fig. 3.** Mössbauer spectra of a bauxite before (top) and after extraction with Na dithionite (bottom).

A constraint on remote work, e.g. on Mars, is that only minimal sample manipulation will be possible. Although Mössbauer work has been instrumental in identifying a variety of Fe oxides on Mars [12,13,14], a combination of various techniques including Mössbauer spectroscopy holds promise for a more comprehensive characterization of clay mineralogy than Mössbauer spectroscopy alone [15,16].

**References:** [1] Pollak et al (1962) *phys. stat. sol.*, 2, 1653, [2] Malden P.J. and Meads R.E. (1967) *Nature*, 215, 844, [3] Stevens J.G. et al. (1988) *Mössbauer Mineral Handbook*, MEDC, Asheville, N.C., [4] Cardile C.M. & Johnston J.H. (1985) *Clays Clay Min.*, 33, 295, [5] Murad E. & Wagner U. (1991) *N. Jb. Min. Abh.*, 162, 281, [6] Murad E. & Wagner U. (1994) *Clay Min.*, 29, 1, [7] Murad E. & Cashion J. (2004) *Mössbauer Spectroscopy of Environmental Materials*, Springer, [8] Murad E. & Wagner U. (1989) *Hyp. Int.*, 45, 161, [9] Murad E. and Rojík P. (2005) *Clay Min.*, 40, 427, [10] Bishop J.L. et al. (2007) *Clays Clay Min.*, 55, 1, [11] Murad E. (200x) *Min Eng.*, 18, 984, [12] Klingelhöfer G. et al. (2005) *Hyp. Int.*, 166, 549, [13], Morris R.V. et al. (2006) *JGR*, 111, E02S13, [14], Ming D.W. et al. (2006) *JGR*, 111, E02S12, [15] Bishop J.L. et al. (2004) *IJA*, 3, 275, [16] Lane M.D. et al. (2004) *GRL*, 31, L17902.

**An Overview of Classes of Martian Phyllosilicate Deposits from Orbital Remote Sensing.** S. Murchie[1], J. Mustard[2], B. Ehlmann[2], R. Milliken[3], J. Bishop[4], F. Seelos[1], and the CRISM Team. [1]Applied Physics Lab., Laurel, MD (scott.murchie@jhuapl.edu); [2]Brown U., Providence, RI; [3]JPL, Pasadena, CA; [4]NASA/Ames and SETI Institute, Mountain View, CA.

**Summary:** The occurrence, types, and geologic settings of aqueous minerals have been investigated by the Mars-orbital spectral mapping instruments TES, THEMIS, OMEGA, and CRISM using an increasingly expanded wavelength range and higher spatial resolution. Each has complemented previous investigations by re-imaging sites having spectral evidence for aqueous minerals, except using broader wavelength coverage and/or higher resolution. MRO's contribution is centered on the 20 m/pixel spatial resolution offered by CRISM, and 30 cm/pixel resolution of HiRISE images that typically are coordinated with CRISM observations. In conjunction with earlier data, these new measurements indicate at least five different classes of deposits containing phyllosilicates and related hydrated silica, each with a distinct combination of spectral signatures and morphological features. These deposits may represent depositional environments recording different phases of the history of water on Mars, and their future investigation promises significant new insights in Mars' hydrologic evolution.

**Layered Phyllosilicates.** The phyllosilicates detected by OMEGA at Nili Fossae and Mawrth Vallis [1], when observed at high spatial resolution, are resolved into layers having stratified compositions [2]. At Mawrth Vallis (Fig. 1) an erosion-resistant deposit typically overlies hydrated silica and Al-rich clays including kaolinite and montmorillonite, which in turn overly Fe/Mg-rich clays [3]. The layering is consistent over hundred of kilometers inplying regional processes, and remnants extend over a region 700x900 km suggesting a formerly more extensive deposit [4]. Stratigraphically it is younger than Mawrth Vallis indicating a lesser age than previously thought [5]. Comparable layered structure is observed in phyllosilicates occuring in eastern Nili Fossae, where Fe/Mg-rich clays are more predominant. There are only kilometer-scale, local occurrences of overlying Al-rich clay [6]. Proposed origins for the layered phyllosilicates include alteration of volcanic ash, subaerial weathering of basaltic regolith, subaqueous sedimentation of sorted, transported clays [7], and hydrothermal deposition [3].

**Massive Noachian Phyllosilicates:** These occur in ejecta, walls, and central peaks of several- to several-tens-of-kilometer diameter craters in the highland plateau (Fig. 2), in massifs of eroded highlands, and in the walls of Valles Marineris [2]. A variety of phyllosilicate mineral groups is indicated by their spectral signatures, with chlorite and saponite dominating in contrast to the smectite and kaolinite that dominate layered phollosilicates. Regional differences are observed in the relative abundance of these phases between Argyre, Tyrrhena Terra and western Nili Fossae, suggesting the occurrence of mineralogic "provinces" [8,9]. In general the mineralogy suggests a low level of alteration, but a few locations exhibiting kaolinite and muscovite may indicate locally higher temperatures or a more active hydrology to flush Fe and Mg from the rock (assuming basaltic parent rock). Based on CRISM global mapping at reduced (200 m/pixel) spatial resolution, we estimate that there are 5000-10,000 exposures exceeding 1 km in size, that occur throughout the Noachian highlands where tens-of-kilometers diameter craters and escarpments provide "windows" relatively free of eolian sediment through Hesperian and upper Noachian plains, to about 3-6 km depth. However larger basins such as Argyre that penetrate deeper expose massifs of relatively unaltered mafic and ultramafic rocks [10]. These observations suggest that massive phyllosilicates occupy a globally extensive layer of uncertain continuity, emplaced at the surface or shallow depths in the early Noachian period.

**Phyllosilicate-containing Intracrater Fans.** MRO observations of highland intra-crater fans [e.g. 11] have revealed that parts of several fans exhibit enhanced content of phyllosilicate (Fig. 3), most evident in Holden [12], Eberswalde [13], Terby [14], and Jezero [15]. Jezero is a type example because spectral contrast in the drainage basin provides a tracer for fluvial transport of sediment. The phyllosilicate is concentrated in lower, horizontally bedded parts of the fans whose morphology suggest a fine-grained texture and deposition in a lacustrine environment. These lower beds are overlain by coarser deposits interpreted as alluvial fans. Spectrally, the phyllosilicate is consistent with outcrops of massive or layered phyllosilicate in the drainage basin, suggesting that it was fluvially transported to a deltaic environment with minimal alteration [15].

**Glowing Terrain.** "Glowing terrain" was identified in THEMIS data based on thermal infrared properties indicating a significant content of minerals having an emissivity <<1.0. The geologically most reasonable candidate is chloride in excess of 25% mass fraction, consistent with the deposits' location typically in closed basins [16]. HiRISE images (Fig. 4) show distinct color properties, fine layering, and intense polygonal fracturing. CRISM data reveal a disinctive near-infrared signature characterized by a weak 3-μm $H_2O$ absorption and a red spectral slope, properties consistent with intermixture of a high-albedo anyhydrous component such as chloride. In addition this signature is sometimes located near the center of an irregular bulls-eye, surrounded by phyllosilicates that extend from flat areas containing the glowing terrain into surrounding highlands (Fig. 5).

**Hydrated Silica Deposits.** CRISM data have revealed the widespread occurrence of hydrated silica in light-toned layered deposits on the Hesperian-aged plains surrounding Valles Marineris (Fig. 6) [17]. The light-toned deposits are eroded in some places into yardangs, and in others display inverted channels suggesting eolian erosion of fluvial deposits. Discrete layers have a broad, shallow 2.2-μm absorption distinct

from that in phyllosilicates, but matching hydrated silica. The shape and center of the band, and strengths and positions of accompanying bands at 1.4 and 1.9 μm, indicate a variety of forms including altered glass, opal, and chalcedony. Other layers exhibit absorptions due to Fe sulfates. The relationship of the hydrated silica to high-Si deposits found by MER/Spirit [18] is unknown.

**Discussion.** The diversity and widespread occurrence of phyllosilicate and related phases suggests depositional environments that extend from the early Noachian (massive phyllosilicates) through early Hesperian (layered phyllosilicates and hydrated silica) periods. Key questions to develop a more compete understanding of formation of these materials include: (a) What were the genetic mechanisms of layered phyllosilicates, and how were they related to those of hydrated silica? (b) What are the spatial extent, lateral continuity, and mineralogic distributions of massive phyllosilicates? (c) Are the massive phyllosilicates equivalent to layered phyllosilicates that subsequently were buried and further altered into different phases, or did they form by distinct mechanisms such as hydrothermal alteration driven by radiogenic or impact heat? (d) What is the relationship of phyllosilicate-containing fans and glowing terrain with associated phyllosilicates? Do they represent a continuum of lacustrine environments with different proportions of evaporite and clastic sediments, or were they formed by distinct processes? As the MRO mission continues, the targeting strategy for new observations is incorporating the discoveries outlined above, to test these hypotheses with newly acquired data.

**References:** [1] F. Poulet et al., Nature, 438, 623, 2005. [2] J. Mustard et al., Nature, 454 , 305-309, 2008. [3] J. Bishop et al., Science, 321, 830-834, 2008. [4] E. Noe Dobrea et al., LPSC 39, 1077, 2008. [5] J. Wray et al., Geophys. Res. Lett., 10.1029/2008GL034385, 2008. [6] B. Ehlmann et al., 7th Mars Conf., 3270, 2007. [7] D. Loizeau et al., J. Geophys. Res., 112, doi:10.1029/2006JE002877, 2007. [8] B. Ehlmann et al. LPSC 39, 2326, 2008. [8] J. Mustard et al., this volume. [9] M. Malin and K. Edgett, Science, 290, 227, 2001. [10] D. Buczkowski et al., LPSC 39, 1030, 2008. [11] M. Malin and K. Edgett, Science, 302, 1931, 2003. [12] J. Grant et al., 7th Mars Conf., 3229, 2007. [13] R. Milliken et al., 7th Mars Conf., 3282, 2007. [14] M. Golombek et al., LPSC 39, 2181, 2008. [15] B. Ehlmann et al., Nature Geosciences, 1, 355-358, 2008. [16] M. Osterloo et al., 7th Mars Conf., 3269, 2007. [17] R. Milliken et al., Geology, in press, 2008. [18] S. Squyres et al., Science, 320, 1063-1067, 2008.

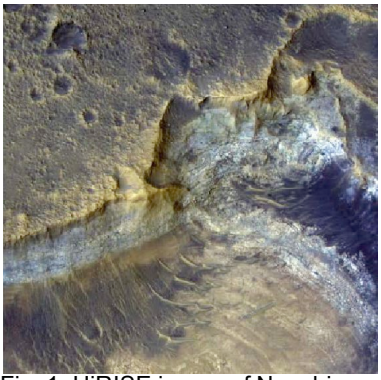

Fig. 1. HiRISE image of Noachian layered clays (type location, Mawrth Vallis). The light-colored materials are clay-bearing.

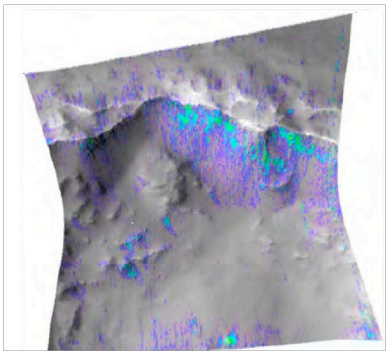

Fig. 2. CRISM image of massive phyllosilicate (in blue) excavated and exposed in a crater wall (type location, Tyrrehena Terra).

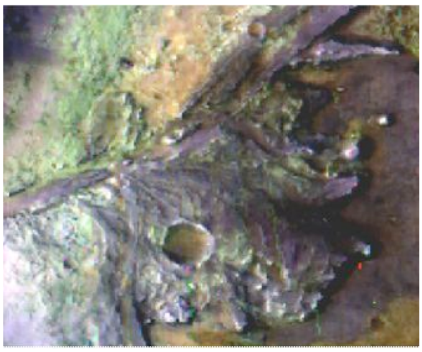

Fig. 3. CRISM IR false color image of intra-crater fan. Green material in the base of the fan is phyllosilicate-bearing (type location, Jezero crater).

Fig. 4. HiRISE image of the polygonally fractured surface of glowing terrain. Thermal IR properties are consistent with a high chloride content (type location, Terra Sirenum).

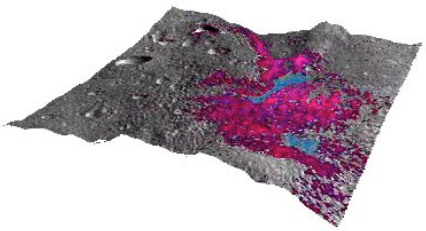

Fig. 5. CRISM spectral map of glowing terrain draped over MOLA topography with 5x vertical exaggeration. Blue areas are glowing terrain, and red areas contain Fe-Mg phyllosilicates.

Fig. 6. CRISM IR false color image of thin, light-toned layered deposits on the plateau around Valles Marineris. Discrete layers (having a bluish color) contain hydrated silica and jarosite (type location, Sinai Planum).

**GEOLOGIC ENVIRONMENTS OF PHYLLOSILICATE DEPOSITS FROM ORBIT** J. F. Mustard[1], S. L. Murchie[2], B. L. Ehlmann[1], R. E. Milliken[3], J-P. Bibring[4], F. Poulet[4], J. Bishop[5], E, Noe Dobrea[3], L. Roach[1] [1]Dept. of Geological Sciences, Box 1846, Brown University, Providence, RI 02912 John_Mustard@brown.edu, [2]JHU/Applied Physics Laboratory, Laurel, MD 20723, [3] JPL-CalTech, [4]IAS, University of Paris, Orsay, France. [5]SETI Institute/ NASA-ARC, Mountain View, CA, 94043, [6]University of Calif., Santa Cruz, CA, 95064.

**Introduction:** Phyllosilicate minerals were first definitively identified on Mars from orbit by the OMEGA (Observatoire pour la Mineralogie, L'Eau, les Glaces et l'Activitié) instrument on board Mars Express [1, 2]. Global mapping showed that sheet silicates are widespread but largely found in terrains of Noachian age. Phyllosilicate formation requires moderate to high pH and high water activity [3]. A major hypothesis presented by Bibring et al. [4] is that the conditions necessary for phyllosilicate formation were specific to the Noachian, the earliest era in Mars' history.

High spatial resolution, precision pointing, and nested observations by the Context Imager (CTX), Compact Reconnaissance Imaging Spectrometer for Mars (CRISM), and the High Resolution Imaging Science Experiment (HiRISE)) on the Mars Reconnaissance Orbiter (MRO) provide enhanced capabilities to analyze surface mineralogy across the planet and determine the nature and geologic setting of phyllosilicate deposits. Analysis of the diversity of phyllosilicates, associated hydrated minerals, and their geologic setting based on integrated OMEGA-CRISM-MRO analysis are described here.

**Mineralogy of Crustal Phyllosilicate Terrains:** Particular phyllosilicate minerals can be identified based on the cation-OH pairing, which can be distinguished using infrared spectroscopy though more work is needed to increase the fidelity of some identifications, particularly for Fe/Mg phyllosilicates [5]. Two principal classes of phyllosilicate minerals exist on the Mars surface: Al-phyllosilicates and, the more common and spatially dominant, Fe/Mg-phyllo-silicates. OMEGA identified the smectites nontronite (Fe-rich), saponite (Mg-rich), and montmorillonite (Al-rich), along with the Fe-rich chlorite chamosite [2]. The increased spatial and spectral resolution of CRISM has revealed an increased diversity of phyllosilicate minerals: kaolinite (Al-rich), illite or muscovite (K-rich), and Mg-rich chlorites.

CRISM data also show regions with phyllosilicate –bearing units typically have additional alteration minerals. Hydrated silicates such as opal, altered glass, and zeolite, specifically analcime, have also been mapped by CRISM associated with phyllosilicate bearing terrains [6]. Iron oxides are also present [7, 8]. Sulfates for the most part are absent though a few areas of alunite in association with Al-smectite clays have been found. Importantly, while prehnite has tentatively been observed in a few locations, minerals and assemblages indicative of metamorphism at elevated P/T conditions (T>300 C) such as pumpellyite, epidote, actinolite, and talc are not found.

A new class of hydrated silicate has been identified with CRISM data [9]. This is characterized by absorption near 2.2 μm and commonly has associated 1.4 and 1.9 μm bands. This 2.20-2.25 μm band is distinct from that observed with Al-OH phyllosilicates such as montmorillonite in that the absorption is broader and centered at longer wavelengths. These spectral characteristics are consistent with hydrated silica glasses such as opal or volcanic glass.

The lack of definitive high-temperature mineral assemblages is a highly significant finding and leads to three possible environments of formation: low temperature hydrothermal alteration in the crust; near-surface/shallow crustal alteration in connection with a hydrologic system; surface weathering in a pedogenic environment. A final possibility is that high-temperature assemblages may have been formed but have been altered to low temperature assemblages in the presence of water over the course of Mars history.

**Stratigraphic settings and Environment**: In the Murchie et al. [10] analysis of martian environments that host hydrated minerals there are three that focused on phyllosilicate-bearing systems: Massive deposits in crustal settings (e.g. Nili Fossae), layered terrains (e.g. Mawrth Valles), and intricate fan and fluvio-lacustrine units (e.g. Jezero Crater). We structure this abstract around these three.

CRISM has identified phyllosilicate and other hydrated silicates in the intracrater fan and fluvio-lacustrine layered deposits in Holden [11], Eberswalde, Jezero, and Gale craters. Some of these deposits are clearly fluvio-lacustrine in origin (e.g. Jezero [12] while others are less clear and may contain significant sequences of eolian sediments (e.g. Gale). These deposits often show phyllosilicates to be present in the source regions for the sediments, leading to the hypothesis that much, if not all, of the phyllosilicates in these deposits have been transported to the site of deposition. More observations and analyses are needed to resolve the origin and significance of the phyllosilicate in these regions.

The layered terrains in Mawrth Valles show spectacular deposits of Al and Fe/Mg phyllosilicates in distinct stratigraphic sequences (e.g. [13. 14. 15. 16]). The strong association of phyllosilicate mineralogy to specific layers over a large region (>$10^5$ $km^2$) indicates

regional alteration processes of deposition of sediments from source regions alternately rich in Al then Fe/Mg phyllosilicate. In Nili Fossae, laminated and layered phyllosilicate-bearing units are observed in exposures of Noachian basement [17, 18]. However, this region lacks the distinct Al-Fe/Mg phyllosilicate associations among stratigraphic units and coherent units are not as traceable over extensive regions. This suggests a complex evolution of the Noachian crust forming the layered units over an extended period.

Massive phyllosilicate deposits are observed in Noachian basement outcrops near Nili Fossae. They are in direct contact with Noachian-aged olivine-bearing units and establish unequivocal evidence for Noachian formation. Throughout the southern highlands, phyllosilicate-bearing outcrops are observed exposed by erosion and impact craters [18]. They are found in ejecta, walls, floors and central peaks of impact craters. If formed as a consequence of the impact process (e.g. [19]), the deposits would be expected in distinct settings such as along fractures or in floor deposits, and T/P conditions of these environments would results in specific mineralogy assemblages. The ubiquity and uniformity of mineralogy in all elements of the crater deposits argues for the alteration minerals to be present at the time of impact.

Phyllosilicate mineralogy is surprisingly uniform across Mars and apparently with depth [2, 18]. Central peaks in craters as large as 70 km and exposures of phyllosilicate-bearing outcrops near the base of Valles Marineris contain comparable mineral assemblages to those in Mawrth Valles and Nili Fossae [18]. Mineral assemblages expected for high temperature environments (e.g. prehnite, actinolite, talc) are not observed. This indicates that either the environment of phyllosilicate formation was uniform over the upper 5-10 km (e.g. [20]) of the crust, or mixing of basin ejecta incorporated minerals formed in the near surface to depth. More work is needed with the high-resolution CRISM observations to determine if there is a change in phyllosilicate mineralogy with depth.

While the phyllosilicate mineralogy is uniform on the broad scale, there are nevertheless distinct regional variations that may indicate specific processes or environments. The phyllosilicate-bearing outcrops surrounding the northern portions of the Argyre Basin [21] are uniformly chlorite-rich. In the highlands north of Syrtis Major there are three distinct phyllosilicate assemblages that define provinces [6]. Of note, the eastern province has Noachian basement rich in Fe/Mg smectite overlain by regionally extensive but thin and discontinuous kaolinite and carbonate-bearing units. The latter indicates a possible near-surface alteration environment fostered by Late Noachian to Early Hesperian hydrologic processes.

**Discussion:** Orbital data show a wide range of sheet silicates that occur in diverse geologic settings. However, there is an apparent lack of minerals formed in high temperature environments such as would be expected in some diagenetic, metamorphic, or hydrothermal settings expected on Mars. Exposure of phyllosilicate by impact craters and in the walls of Valles Marineris traverse a large range of apparent crustal depths (5-10 km), yet show a limited range of phyllosilicate variability. Does this indicate a limited range of temperature environments at the time of formation or processes that might have homogenized the mineral compositions with time?

The association of the phyllosilicate minerals with Noachian-aged terrains does not require Noachian age of formation and more work is needed to stratigraphically date these deposits. Specifically, the nature of the contact with overlying units (unconformable vs. gradational) and the stratigraphy of phyllosilicate-bearing units with respect to unaltered mafic units will be assessed using combined CRISM-CTX-HiRISE observations. In the regions where this has been investigated to date, however, there is little to no evidence for phyllosilicate alteration of Hesperian-aged units, though precipitates of hydrous silicates have been observed in Hesperian units [Milliken et al., 2008].

**References:** [1] Bibring J-P. et al, *Science* v307, 1576-1581 (2005). [2] Poulet F. et al., *Nature*, v438, 623-627 (2005). [3] Velde B. in Origin and Mineralogy of Clays (ed. B. Velde), Springer, Berlin (1995). [4] Bibring J-P. et al. *Science,* v312, 400-404 (2006). [5] Milliken, R. E., this meeting (2008). [6] Ehlmann B. et al. this meeting (2008). [7] Ehlmann, B. et al., LPSC 39, #2326 (2008). [8] Bishop, J. et al., LPSC 39, #2124 (2008). [9] Milliken, R. E., et al., Opaline Silica in (Geologically?) Young Deposits on Mars (in press) Geology (2008). [10] Murchie, S. L., et al., (this meeting) (2008). [11] Grant, J. A. et al., Geology 36, 195-198, (2008). [12] Ehlmann, B. L. et al., *Nature Geosci*. doi: 10.1038/ngeo207 (2008). [13] Loizeau D. et al., J. Geophys. Res. 112, E08S08, doi: 10.1029/2006JE002877 (2007). [14] Bishop, J. L. et al., Science 321, DOI: 10.1126/science.1159699 (2008). [15] Wray, J. et al., Geophys. Res. Lett., 35, L12202, doi:10.1029/2008GL034385 (2008). [16] Michalski, J. and E. Dobrea, Geology, 35(10), 951-954 (2006). [17] Mangold, N. et al. *J. Geophys. Res*. 112, E08S04, doi 10.1029/2006JE002835 (2007). [18] Mustard et al., Nature 454, 305-309 doi:10.1038/nature07097 (2008). [19] Newsom, H. E., Icarus 44, 207-216, 1980. [20] Parmentier E. M. et al., LPSC 39, #*1544* (2008). [21] Buczkowski, D. L., et al., LPSC 39, #1030 (2008).

**CLAY-BEARING UNITS IN WESTERN ARABIA TERRA: STRATIGRAPHY, EXTENT, AND POSSIBLE REGIONAL ALTERATION FRONTS**. E. Z. Noe Dobrea[1], J.L. Bishop[2], N.K. McKeown[3], R. Fu[1], C. Rossi[1], G. Swayze[4], J.R. Michalski[5], F. Poulet[5], J.-P. Bibring[5], J.F. Mustard[6]; R. Arvidson[7], R.V. Morris[8], S. Murchie[9], A.S. McEwen[10], E. Malaret[11], C. Hash[11], and the CRISM Team. [1] Calif. Inst. Tech./JPL, 4800 Oak Grove Drv, Mail Stop 183-501, Pasadena-CA-91109 (eldar@caltech.edu); [2] SETI Institute/NASA-ARC, Mountain View, CA; [3] UCSC, Santa Cruz, CA; [4] USGS, Denver, CO; [5] IAS, Univ. of Paris, Orsay, France; MD, [6] Brown University, Providence, RI; [7] Washington University, Saint Louis, MO 63130; [8] NASA-JSC, Houston, TX; [9] APL, Laurel, MD [10] U. of Arizona, Tucson, AZ; [11] ACT, Inc. Herndon, VA 20170

**Introduction:** The largest exposure of phyllosilicates on Mars occurs in the highland plains around Mawrth Vallis in western Arabia Terra. This exposure is known to extend discontinuously for about 300 km southward from the edge of the dichotomy boundary, covering an area greater than 200 x 300 km over an elevation range of ~2000 m (*e.g.* [1-5]). At least three different hydrated phyllosilicates, as well as examples of hydrated silica (*e.g.*, opal-A, hydrated glass), have been identified in OMEGA and CRISM data based on absorption bands near 2.3 and 2.2 μm (*e.g.*, [1],[5],[6]). Detailed studies of the light-toned layered units present evidence for a mineralogical stratigraphy: the Fe/Mg phyllosilicate-bearing units are overlayed by the Al-phyllosilicate and hydrated silica (Al/Si-OH)-bearing units, which are in turn overlain by a dark-toned, spectrally unremarkable capping unit (*e.g.*,[5],[6],[7]). Formation theories for these layered units include pyroclastic, sedimentary, and impact processes. Hypotheses addressing the formation of the phyllosilicates include direct precipitation, diagenesis [3,5,7,9].

Regional analysis of CRISM multi-spectral and targeted (FRT, 20 m/pixel) observations reveal hydrated minerals with absorptions at ~2.2 or 2.3 μm in locations up to 700 km away from the borders of the previously identified extent of clay-bearing units [8, 9], suggesting that the processes that formed the hydrated minerals at Mawrth Vallis may have been more ubiquitous and therefore more representative of the geologic state of ancient Mars than previously realized.

In this work, we are seek to constrain: 1) the extent of the clay-bearing units observed around Mawrth Vallis, 2) the geologic origin of the dark overlying mantle, and 3) the genesis of the hydrated minerals that are observed in association with the light-toned layered units. We have analyzed a selected set of FRTs covering western Arabia Terra (Fig. 1) and compared the mineralogy, morphology, and stratigraphy of the terrains that present spectral evidence for hydrated minerals.

**Results:**

*Morphology and stratigraphy:* Hydrated minerals have been identified in FRTs throughout western Arabia Terra (Fig. 1). Direct comparison between the observations of the hydrated units in the Mawrth Vallis region and hydrated units throughtout western Arabia show astounding mineralogical, morphological, and stratigraphic similarities among units scattered over an area greater than 1000x1000 km. We distinguish four different types of units based on morphology and texture at HiRISE resolution (25 cm/pixel), and diagnostic spectral features in CRISM data (Fig. 2):

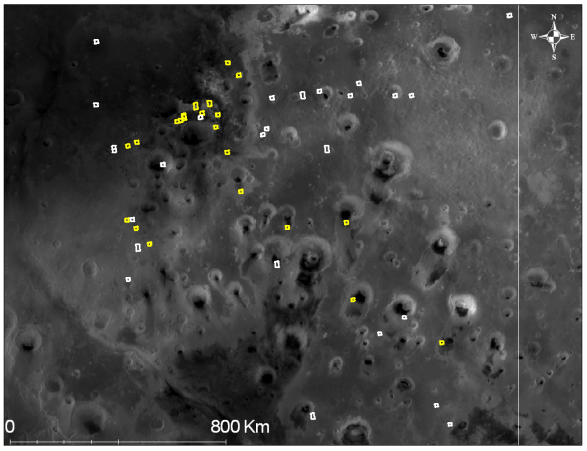


**Figure 1:** Footprints of FRTs used in this study. Yellow indicates locations where phyllosilicates were identified.

1) a dark, spectrally featureless, heavily cratered, capping unit, which appears to have been draped onto the underlying topography (Fig 2, upper unit). It sheds boulders and is massive in appearance at HiRISE resolution. Where possible, its thickness is measured from HiRISE stereo to be only a few meters in thickness. This unit is characterized by its resistance to erosion, which results in the erosional inversion of preexisting topography such as craters and valleys.

2) a light-toned, cliff-forming layered unit that presents spectra consistent with montmorillonite, kaolinite-group minerals, and hydrated silica (Fig 2., middle unit). This unit is ~20-50 m thick and it underlies the cap unit. This unit is not cratered, it does not shed boulders, and it is very finely layered at HiRISE resolutions. Incised in several locations of the unit are narrow meandering valleys which continue from broader ridges when the contact between this unit and the capping unit is crossed.

3) a light-toned, slope-forming layered unit that presents spectra consistent with Fe/Mg smectites plus a ferrous phase (Fig 2, lower unit). It underlies the Al/Si-OH unit. This unit does not to shed boulders, is not cratered, and apperas layered at HiRISE resolution.

4) a second dark, hummock-forming unit which embays units 1-3. This unit typically appears in the lowest-lying areas. Careful spectral, and morphological observations show that: a)the areas where the unit is thinner have the same polygonal fracturing as unit (3) at HiRISE scale, b) this unit embays unit (3) and sometimes unit (2); and c) the spectrum of this unit can be explained by a linear mixture of the spectra of units (1) and (3). These observations suggest that this unit is a spectrally neutral, unit which was deposited after the formation (and subsequent erosion) of units 1-3.

The morphology, stratigraphy, and surface texture of each of these units is similar to that of spectrally similar units throughout the region.

*Mineralogical constraints:* Analysis of the FRTs shows that the light-toned units have a 1.9 μm band, whereas the dark cap unit does not. FRT spectra of the dark cap unit have a negative slope in the 1-2.6 μm region, and are otherwise featureless. Spectra where a ~1.9 μm band is identified also show absorptions near 2.2 or 2.3 μm. The CRISM spectra with a band at 2.28-2.31 are consistent with the presence of Fe/Mg-bearing smectites. Spectra exhibiting a band near 2.21 μm are consistent with either montmorillonites (Al-OH), or with hydrated silica/glass or opal (Si-OH) in altered ash. Montmorillonites tend to have a band center at 2.21 μm, whereas hydrated silica and hydrated glass have a broader band in the range 2.18-2.26 μm [10,11]. Most of the spectra we observe here have band centers shortwards of 2.21 and widths similar to that of hydrated silica/glass. This component has also been observed in CRISM spectra from other regions [12,13,14]. A doublet near 2.17 and 2.20 μm, consistent with kaolinite, was identified in the spectra of several regions.

**Discussion:**

*Distribution and geologic setting of hydrate-bearing outcrops:* Units bearing absorptions 1.4, 1.9, and 2.x-μm, and which are therefore interpreted as hydrated, have been identified over a broad (>1000x1000 km) spatial extent in the western Arabia Terra Region. With no exception, these units are found in erosional windows. They are typically capped by a darker-toned unit which does not present a 1.4, 1.9, or 2.x-μm features, and is therefore interpreted not to be as hydrated as the underlying units. The erosional windows in which these hydrate-bearing unit are found often occur in association with wind streaks. In addition to exposing hydrate-bearing layered units, erosion of the dark-toned upper unit has resulted in the inversion of topographic features that are normally found in negative relief. These include features interpreted to be inverted craters and channels. Observations of channels cut into the phyllosilicate-bearing bedrock suggest that the region experienced an aqueous history where there was enough water to erode, and therefore transport and subsequently deposit sediments.

*Origin of the dark-toned capping unit:* The dark toned-capping unit appears to be pervasive throughout the region, and its removal via erosion results in stratigraphic windows in which the hydrate-bearing minerals are exposed. Perhaps the most striking characteristics of this unit are that it is indurated and that it mantles pre-existing topography, suggesting that rather than having been emplaced via flow processes, it was emplaced either as an air fall deposit or via subaqueous deposition. Possible methods for induration include cementation by evaporites, sintering or welding of molten rock from volcanic or impact processes, or cementation by burial.

*Origin of hydrated minerals:* Hypotheses for the formation of the Fe/Mg smectites and A/Si-OH bearing minerals are discussed in an accompanying abstract by Bishop *et al.* Here, we include (1) direct deposition of units in a lacustrine system, (2) diagenesis of primary minerals, (3) pedogenesis, and (4) hydrothermal alteration. Each of these hypotheses has its merits and will be further discussed at the workshop.

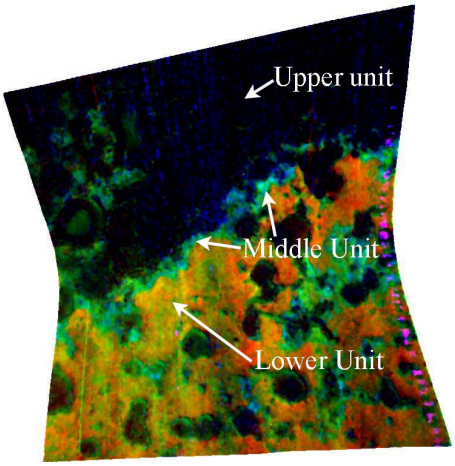


**Figure 3:** (B) Color composite of parameters maps for FRT8838, where R: D2300 (2.3 μm feature [7]), G: OLINDEX (ferrous index), B: BD2210 (2.21 μm feature).

**References**: [1] Poulet, F., *et al.* (2005) *Nature, 438*, 632-627. [2] Noe Dobrea, E.Z. and Michalski J.R. (2006) *AGU Fall 2006*, #P23D-0091. [3] Michalski, J.R. and Noe Dobrea, E.Z., (2007) *Geology,35*, pp. 951-954. [4] Loizeau D. *et al.* (2007) *JGR, 112* (E8). [5] Bishop *et al.*, 2008 *Science*, in press. [6] Louizeau *et al.*, 2008. *LPSC XXXIX* #1586 [7] Wray *et al.*, 2008, *GRL, in press.* [8] Noe Dobrea, E.Z. *et al.* (2007) *AGU Fall 2007,* #P13D-1560. [9] Noe Dobrea, E.Z., *et al.* (2008) *Lunar. Planet Sci. Conf. XXXIX* #1077. [10] Bishop J.L. *et al.* (2002) *Clay Minerals*, *37,* 617-628. [11] Bishop J.L. *et al.* (2007) *Clays and Clay Minerals, 55,* 1-17. [12] Mustard *et al.* (2008) *Nature (submited)*. [13] Milliken *et al.*, (2007) *AGU, Fall*, #P12A-02. [14] Swayze *et al.*, (2007) *7th Intl. Mars Conf. #3384.*

**DETERMINATION OF HYDRATION STATES IN SMECTITES USING LIBS.** A. M. Ollila[1,2], N. L. Lanza[1,2], S. M. Clegg[3], J. E. Barefield[3], H. Newsom[2], P. L. King[2], L. J. Crossey[1], R. C. Wiens[3], D. Vaniman[3]. [1]Department of Earth and Planetary Sciences, University of New Mexico, U.S.A. (MSC03 2050, 1 University of New Mexico, Albuquerque, NM 87131; aollila@unm.edu), [2]Institute of Meteoritics, University of New Mexico, Albuquerque, NM, U.S.A. [3]Los Alamos National Laboratory, Los Alamos, New Mexico, U.S.A.

**Introduction:** Smectite minerals may be present on Mars [e.g. 1] and the amount of water within their structures is a sensitive recorder of their environment [2]. In this study, we examine the capability of the Laser-Induced Breakdown Spectroscopy (LIBS) technique for detecting hydrogen [3] in smectites. This work is especially relevant given that a LIBS instrument will be onboard the upcoming Mars Science Laboratory (MSL) 2009 and ExoMars rover missions to Mars.

Smectites are capable of adsorbing water molecules on grain surfaces and in the interlayer between tetrahedral-octahedral-tetrahedral (TOT) sheets in addition to relatively fixed OH content within the TOT sheets. The amount of water adsorbed depends primarily on relative humidity (RH), interlayer cations, and layer charge [2], as well as temperature [4]. Experimental work and thermodynamic calculations [4] indicate that a Na-montmorillonite may adsorb up to two monolayers of water at low temperatures (-5°C) under high RH; additional water would be present as ice. When the RH is restricted to the average partial pressure of water in the Martian atmosphere ($1.5\times10^{-6}$ bar), Na-montmorillonites will likely hold less interlayer water [5].

The hydration state of smectites on Mars is likely to vary both seasonally and diurnally. Average RH values calculated for Mars by [6] reveal spatial variations as well. The number of water layers for a Ca-montmorillonite between 0 to 40% RH ranges from 0-2 (interstratified but increasing towards two layers as RH nears 40%) and up to three layers at RH greater than 90% [7].

Both MSL and ExoMars will be equipped with a LIBS instrument that is capable of detecting hydrogen. H peak heights can be used in a semi-quantitative fashion to determine relative water content (assuming OH is constant). It may also be possible to determine water content quantitatively. This experiment is currently in progress but initial proof-of-concept results have been obtained for a Ca-montmorillonite sample at four RH values.

**Sample Preparation:** For this pilot study, we used a Ca-montomorillonite #23 (Wards Sci. Est.) from Chambers, AZ. Small mineral chunks were crushed in a shatterbox for one minute and pressed to 20 tons to form pellets. Natural samples were used and thus may contain small amounts of impurities such as quartz. To compensate for any heterogeneity, multiple LIBS shots were taken and averaged over a line profile across the pellet (see LIBS Experimental Setup section).

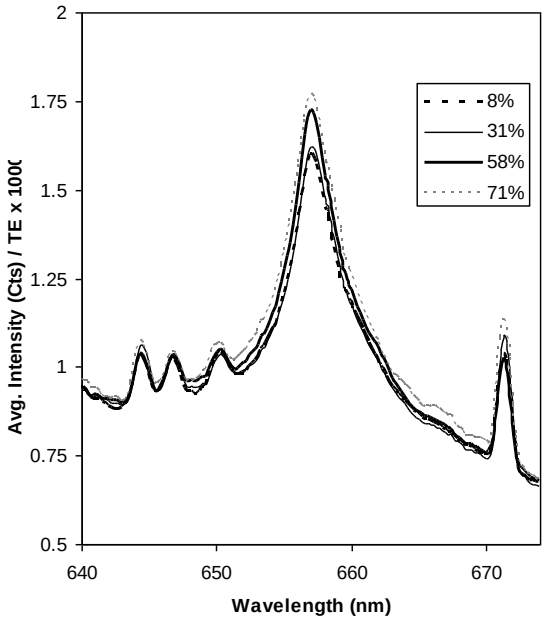


**Figure 1:** LIBS hydrogen peak heights (average intensity normalized to total emission (TE) x 1000) for Ca-montmorillonite samples prepared at different RH.

**Experimental Setup—***Relative Humidity Chambers:* Several small chambers were built to contain samples where the atmosphere was held constant at various relative humidities using saturated salt solutions. The following solutions and their corresponding RH values [8] were used in this experiment: NaOH (8%), KF (31%), NaBr (58%), and $SrCl_2$ (71%). Samples were in the chambers for 48 hours prior to being rapidly removed and placed in the LIBS chamber at room conditions.

*LIBS Setup:* Experiments were conducted at the Los Alamos National Laboratory LIBS laboratory. The LIBS technique uses a Nd:YAG pulsed laser at 1064 nm to ablate surfaces forming a plasma of excited atoms, ions, and molecules. When the excited species relax, light is emitted at wavelengths characteristic to these species. A portion of this light is collected by spectrometers that detect the spectrum from approximately 220-325 (UV), 380-470 (VIS), and 490-900 (VNIR) [9]. For this experiment we used a 25 mJ pulse at a 9 m stand-off distance. We took 10 shots per second with a one second exposure with five spectra per shot for a total of 50 shots per spot. The five spectra were normalized to the total emission to compen-

sate for variability in the LIBS procedure. The five normalized spectra were then averaged for each sample in order to control sample heterogeneity. This study was done under ambient terrestrial conditions; subsequent work will be conducted under Martian conditions.

**Results:** LIBS analyses indicate the presence of relatively high amounts of Ca, Mg, Si, H, and O with small amounts of K, Na, and Fe. This corresponds well with the chemical analysis of this particular clay given in [10]. Figure 1 shows the dominant H peaks at 656.27 and 656.29 nm (not individually resolvable). The relative H peak heights correlate with increasing RH.

**Discussion:** Figure 2 presents the normalized H peak heights for samples prepared at different relative humidities; error bars indicate the standard deviation between normalized spectra. The experiment demonstrates that the abundance of H in the sample does increase as the RH increases. Note that the RH was not measured independently in these syntheses nor was the amount of water in adsorbed into the sample. We also note that the 8 and 31% data points and the 58 and 71% data points are within error.

Based on work by [11] and [12], a linear increase in water content is not expected. Figure 3 shows a desorption isotherm for a homogenized Ca-montmorillonite from [11]. Measurements of water contents [e.g. 11,12] provide insight into the variability in water content based on interlayer cations and layer charge. This underscores the need to have samples processed to known conditions and water contents measured independently for calibration against LIBS observations. Future work will focus on calibrating H peak height with measured H content and maintaining controlled RH during LIBS analysis.

**Improvements for Future Experiments & Analyses:** Subsequent iterations of this experiment will examine the effects of equilibration time on the LIBS spectra of smectites by (a) preparing purified smectites for the experiments; (b) confining pellets to RH chambers and monitoring weight change to determine equilibration times; (c) obtaining LIBS spectra in stable RH conditions and (d) analyzing OH and $H_2O$ of a cross-section of the pellets using micro-infrared reflectance spectroscopy.

Because LIBS is a destructive sampling technique and analysis requires integration of multiple shots in the same spot, the hydration state recorded by a particular shot is likely affected by prior shots. We will investigate this hypothesis by examining spectra from individual shots of a depth profile through completely equilibrated pellets as determined by weight. Additional RH values will be investigated in an attempt to relate our results to adsorption/desorption isotherms given in the literature [e.g., 11,12]. Lastly, these experiments will be repeated in a Martian environment representative of both daytime and nighttime temperatures and $pH_2O$.

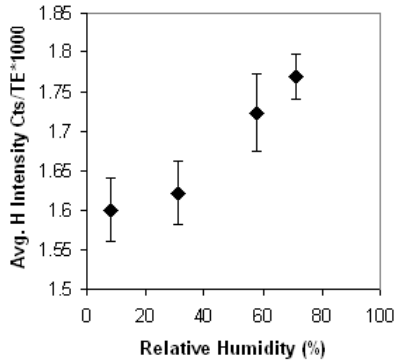


**Figure 2:** Hydrogen peak height (average intensity normalized to total emission (TE) x 1000) by % relative humidity.

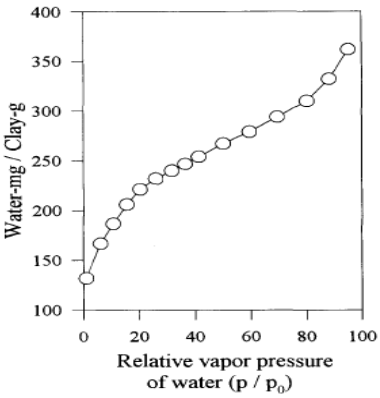


**Figure 3:** Example of a desorption isotherm for a pure Ca-montmorillonite from [11]. $p/p_o$ is equivalent to RH.

**Conclusions:** This proof-of-concept study has shown that LIBS is capable of detecting variations in the concentration of water in smectites based on hydrogen signature. In addition to improving the experimental parameters and analyses and running several more iterations using various smectites, future work will include determining elemental abundance from peak heights and constraining detection limits and uncertainties.

**References:** [1] Poulet, F. et al. (2005) *Nature*, *438*, 623-627. [2] Meunier, A. (2005) *Clays*, Springer-Berlin., p. 472. [3] Wiens, R. C. et al. (2007) *LPSC XXXVIII*, #1180. [4] Andersen, D.M. (1978) *Icarus*, *34*, 638-644. [5] Bish, D.L. et al. (2003) *Icarus*, *164*, 96-103. [6] Fialips C. I. et al. (2005) *Icarus*, *178*, 74-83. [7] Ferrage, E. et al. (2007) *Am. Miner.*, *92*, 1731-1743. [8] Greenspan, L. (1977) *J. Res. Nat. Bur. Stand.-A. Phys. Chem.*, *81A:1*, 89-96. [9] Clegg, S. M. et al. (2007) *7th Int. Conf. Mars*, #3216. [10] Anthony, J. W. et al. (eds.) (2001) *Handbook of Mineralogy V. II*, Miner. Soc. of Am. [11] Xu, W. et al. (2000) *Clays & Clay Mins.*, *48*, 120-131. [12] Dios Cancela, G. et al. (1997) *J. Coll. & Interface Sci.*, *185*, 343-354.

**Acknowledgements:** Thanks to Brendt Hyde for his assistance with the RH chambers

**LAB EXPERIMENTS TO SIMULATE COATINGS ON PHYLLOSILICATE ROCKS AND COMPARISON WITH CRISM DATA OF MARS.** Mario Parente[1,3], Janice L. Bishop[1,2], and Javier Cuadros[4], [1]Carl Sagan Center at the SETI Institute, [2]NASA Ames Research Center, [3]Stanford University, Dept. of Electrical Engineering, Stanford, CA, USA (Mario.Parente@stanford.edu), [3]Natural History Museum London, UK.

**Introduction:**. This study aims to test the spectral properties of potential Martian dust particles on phyllosilicate rocks in order to explain the visible and near-infrared (VNIR) spectral properties observed for the phyllosilicate-rich terrains in the Mawrth Vallis region of Mars. The Compact Reconnaissance Imaging Spectrometer for Mars (CRISM) [1] detected exposures of an Fe/Mg-smectite such as Mg-nontronite, hydrated silica, montmorillonite and kaolinite [2-4]. These studies have focused on the spectral features in the range 1.4-2.5 μm. In evaluating the extended visible region CRISM spectra where different clay minerals are observed, we found only subtle variations in spectral properties attributable to Fe electronic transitions in the different phyllosilicate units.

We performed experiments to test the spectral properties of dust on phyllosilicate rocks and the possibility that volcanic ash is only partially altered to phyllosilicates in the ancient rocks. One set of experiments evaluates the spectral effects of deposition of fine-grained ferrihydrate and altered basaltic ash particles on nontronite and montmorillonite rocks. A second experiment involves measuring the VNIR properties of chemical mixtures of partially altered volcanic tuff samples from a previous study [5]. Our results show promising similarities of CRISM spectra of Mawrth Vallis terrains with the laboratory spectra.

**Method:** Two phyllosilicate rocks were obtained from the Clay Minerals Society, Source Clays Repository: nontronite NG-1 from Hohen-Hagen, Germany, and the Ca-montmorillonite SAz-2 from Arizona. The dust particles used for these experiments include an altered volcanic basaltic ash is from Haleakala that was dry sieved to <45 μm for a previous study [7] and a ferrihydrite sample from Iceland [8].

We simulated dust deposition by sprinkling progressively increasing amounts of dust on top of the rocks using a spatula. We measured the spectra from 0.3 to 2.5 μm of the rock surfaces and the rocks with different amounts of both ferrihydrate and Haleakala ash on a black Teflon dish using an ASD spectrometer under ambient conditions. In order to qualitatively assess the amount of dust present on the rocks, we captured images of the samples with a microscope at multiple magnifications after dust deposition.

The volcanic tuff samples were primarily composed of rhyolitic glass and were exposed to hydrothermal alteration in the lab at temperatures ranging from 60 to 160 °C for up to a year [6]. VNIR and mid-IR reflectance spectra were measured at RELAB, Brown University. The alteration product is a random mixed-layer illite-smectite (I-S) with 75% smectite.

**Results:** VNIR reflectance spectra of the dust cover simulations are shown in Figs. 1-2.

*Montmorillonite rock:* The montmorillonite spectrum in Fig. 1 contains features due to Al-OH at 1.41 μm (OH stretch overtone) and 2.21 μm (OH bend+stretch combination band), interlayer and adsorbed $H_2O$ near 0.9, 1.2 1.4 and 1.9 μm. The altered volcanic ash sample from Haleakala includes related weak broad features near 1.93 μm due to $H_2O$ and near 2.2 μm due to non-crystalline Al/Si-OH species. The ferrihydrate spectrum includes broad water bands near 1.4 and 1.9 μm as well as a weak ferric minimum near 0.92 μm. The main effect of Haleakala ash deposition is the change in curvature in the montmorillonite visible spectrum near 0.6 μm and the loss of spectral contrast of vibrational bands in the NIR. The ferrihydrate deposition on the other hand primarily increases the spectral ratio of the montmorillonite from 0.4-0.7 μm

*Nontronite rock:* The spectrum of nontronite (Fig. 2) exhibits $H_2O$ bands near 1.4 and 1.9 μm. This sample and has bands due to Fe-OH at 1.42 μm (OH stretch overtone) and 2.29 μm (OH bend+stretch combination band). Another Fe-OH band is present near 2.41 μm, but is weaker. The Haleakala ash mutes the feature near 0.53 μm in the nontronite spectrum, while spectral contrast in the NIR is increased. The ferrihydrate dust experiment on nontronite behaviour seems consistent with the case of montmorillonite.

Spectra of selected altered glass samples are shown in Fig. 3 where the illite and Al-OH smectites exhibit an Al-OH stretching + bending band around 2.22 μm . The water band positions are typical of smectites. A magnified version of the visible part of the spectrum is also shown in Fig. 3. The main difference occurring in the spectra of the hydrothermally altered samples occur near 1 μm where the glass absorption band centered at 1.1 μm changes shape and shifts towards 1.0 μm for increasing smectite content.

**Discussion:** *Relation to CRISM spectra*. CRISM spectra from the Mawrth Vallis region on Mars (image ID FRT0000A2C2) were selected to compare with these lab data. The images were atmospherically and photometrically corrected using standard techniques by the CRISM team [9]. Residual artifact were removed using a destriping algorithm [10]. The short (S) and long (L) detector images were automatically spliced in order to obtain a complete spectrum of the pixels in the range of interest [11]. Removal of an instrument effect

around 1.2 μm was also performed. Fig. 4 represents a direct comparison of the CRISM spectra with the results of the two lab studies revealing that fine-grained dust is dominant at visible wavelengths in all spectra. Both altered glass and dust deposition seem to have an effect on the feature around 1 μm.

**Summary:** Our experiments indicate that only a few grains of ferrihydrate or altered volcanic ash coating a rock surface are sufficient to alter the spectral properties of the rock in the visible region . At the same time these coatings have only a minor effect on the glass bands from 1.9 to 2.5. Our experiments further show that partially unaltered glass mixed with phyllosilicates in rocks could account for the presence of the ~ 1 μm band in the clay units at Mawrth Vallis.

**References:** [1] Murchie, S. et al. (2007) *JGR,112*, E05S03. [2]Bishop, J. L., et al. (2008) *Science, 321*, 830-833. [3] McKeown, N. K., et al. (2008) *LPS XXXIX* Abstract #1400. [4]Noe Dobrea, E. Z., et al. (2008) *LPS XXXIX* Abstract #1077. [5] De La Fuente, S., et al. (2002), *Clays Clay Miner., 50-5*, 578-590. [6] De La Fuente, S., et al. (2000), *Clays Clay Miner., 48-2*, 299-303. [7] Bishop J. L. et al. (2007) *Clays Clay Miner., 55*, 1-17. [8] Bishop J. L. et al. (2002), *Geological Society special publ. 202*, 357-360. [9] Mustard J. F. et al. (2008) *Nature,454*, 305-309. [10] Parente (2008) *LPS XXIXX* Abstract # 2528. [11] Parente, M. et al. (2008*), to be submitted to JGR.*

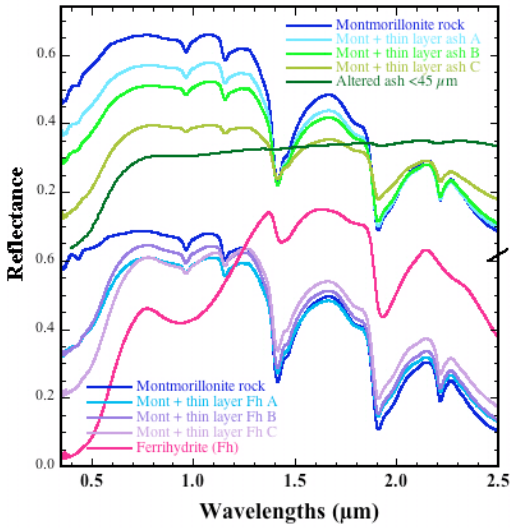


**Fig 1,2:** Spectra from the dust deposition experiment on a SAz-2 montmorillonite rock (left) and an NG-1 nontronite rock (top right) using altered volcanic ash and Ferrihydrate.

**Fig. 3**: (center right). Spectra of volcanic glass containing progressively larger smectite abundances

**Fig. 4:** (bottom right). Comparison of spectra from CRISM image A2C2 with lab spectra: altered glass 1 contains 8% smectite, while altered glass 2 contains more smectite. The montmorillonite and nontronite rock spectra have thin coatings of ferrihydrite (Fh) and altered volcanic ash from Haleakala (ash).

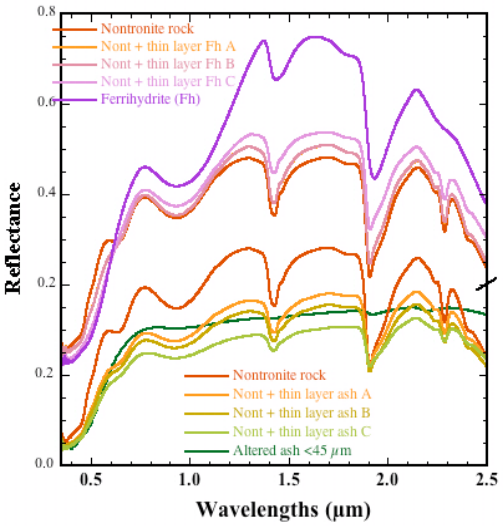


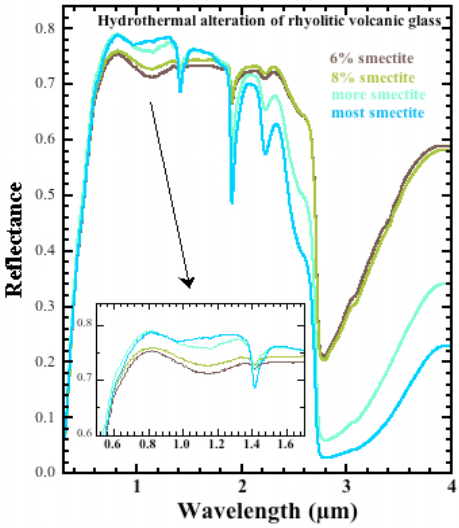


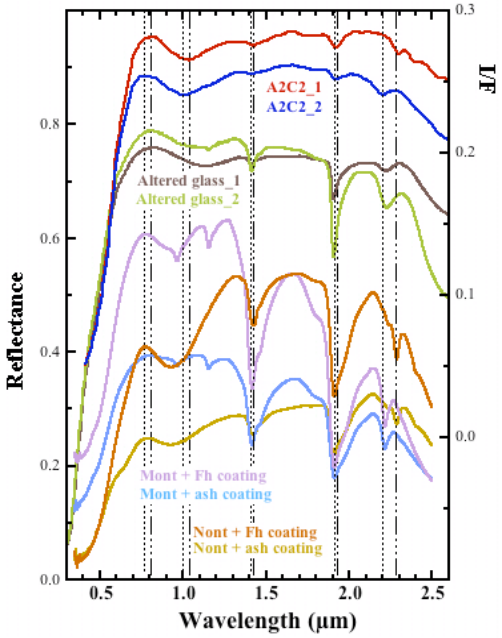

**IDENTIFICATION, MAPPING AND MINERALOGY OF PHYLLOSILICATES ON MARS AS SEEN BY MEx/OMEGA.** F. Poulet[1], J.-P. Bibring[1], J. Carter[1], Y. Langevin[1], N. Mangold[2], J. Mustard[3], D. Loizeau[2], B. Gondet[1]. [1]IAS, CNRS/Université Paris-Sud, 91405 Orsay, France, [2]IDES, CNRS/Université Paris-Sud, Orsay, France, [3]Brown University, Providence, USA. francois.poulet@ias.u-psud.fr

Global mapping by the visible and near-infrared imaging spectrometer on Mars Express has discovered unique deposits of phyllosilicates minerals widespread across the planet [1]. The presence of these minerals on Mars is of great exobiological relevance, because (1) the formation of these hydrous minerals requires moderate to high pH and high water activity, (2) some of phyllosilicates are potential prebiotic catalyst [2]. Here, we first reassess the detection of these minerals at the light of the analysis of new OMEGA data acquired since the publications of 2005 [1,3]. We emphasize the spectral diversity of each major class of phyllosilicates. While the Fe, Mg and Al-bearing smectites are the most common, kaolinite and chlorite are also potential spectral matches of some phyllosilicate-rich occurrences. New OMEGA observations consistently indicate the presence of phyllosilicates in deposits that are in place, rocky units (outcrops, scarps and crater ejecta) of ongoing erosion in Noachian terrains. A detailed analysis of each outcrop when high spatial resolution imagery is available confirms the major observation presented in [1]: phyllosilicate deposits are almost exclusively Noachian in age, indicating that the environments suitable for phyllosilicate formation were particular to the earliest era in Mars' history.

A few clay-rich deposits seem to differ from this statement. First, some phyllosilicates are associated with some sulfates in the etched terrains of Terra Meridiani, possibly indicating that the neutralization of the solutions that formed the sulfate-rich etched terrains could have occurred at least locally. Second, evidence of pumpellyite associated with clays is reported in the central peak of a few craters. This could suggest alteration resulting from metamorphism related to the impact that formed the crater, either by its pressure or heat or both. Alternatively, the impact central peak may have excavated materials from deep parts of the crust, where metamorphism forming pumpellyite could have occurred. Third, some low albedo terrains also exhibit signature of clays, but the origin of these deposits is still unclear.

Different alteration models of mafic rocks can be considered, but one of the most efficient processes of formation is alteration by leaching under ambient conditions. Such a process has been investigated by [5] in using calculations of the aqueous equilibria of phyllosilicates. The presence of $Fe^{3+}$-rich phyllosilicate nontronite indicates the following conditions: (1) a low aluminium activity, (2) a high oxidation level, (3) weakly acidic to alkaline conditions and (4) very low abundance of $SO_2$.

We then provide quantitative analysis of the surface spectra using nonlinear spectral mixing [6] in order to determine the modal mineralogy (mineral abundances) of some of the phyllosilicate-rich outcrops. This is done in using a nonlinear unmixing model based on the Shkuratov radiative transfer theory [7]. We focus our study on the two largest occurences where phyllosilicates were found on Mars: Mawrth Vallis and Nilo-Syrtis. Significant differences between these two regions in mineral abundances are found. The phyllosilicate-rich outcrops in Mawrth Vallis are best reproduced by ~60% of phyllosilicates (nontronite, montmorillonite) mixed with hydroxides (Ferrihydrite as a likely end-member) and some non-phyllosilicate materials (plagioclase and Martian dust). In the Nilo-Syrtis region, the total abundance of the phyllosilicate minerals is significantly smaller than in Mawrth Vallis and mafic materials such as pyroxene are always required in the mineral assemblage. This strongly suggests that the degree of alteration that formed the deposits in Mawrth Vallis was stronger than any other deposits on Mars.

**References:** [1] Poulet F. et al. (2005) *Nature 438.* [2] Ferris P. (2006) *Phil. Trans. R. Soc. B.361.* [3] Bibring J.-P. et al. (2005) *Science 307.* [4] Bibring et al. (2006) *Science 312.* [5] Chevrier V. et al. (2007) *Nature 448.* [6] Poulet F. and Erard S. (2004) *JGR 109.* [7] Poulet et al. (2008) *A&A, 487.*

**NEW HYDRATED SPECTRAL PHASE AND STRATIGRAPHY OF SMECTITE CLAYS, SULFATES AND OTHER HYDRATED MINERALS IN IUS CHASMA, VALLES MARINERIS.** L.H. Roach[1], J.F. Mustard[1], S. Murchie[2], R.E. Milliken[3], K. Lichtenberg[4], B.L. Ehlmann[1], J. Bishop[5], R.E. Arvidson[4], and the CRISM team. [1]Dept. of Geological Sciences, Box 1846, Brown University, Providence, RI 02912 Leah_Roach@brown.edu, [2]JHU/APL, Laurel, MD 20723, [3]JPL/Caltech, Pasadena, CA 91109, [4]Washington University in St. Louis, St. Louis, MO 63130, [5]SETI Institute, Mountain View, CA 94043.

**Introduction:** Ius Chasma is a long narrow trough in western Valles Marineris (VM) that shows strong tectonic control in its structure (Fig 1) [1]. CRISM (Compact Reconnaissance Imaging Spectrometer for Mars) data have revealed diverse hydrated mineralogy in Ius Chasma, in addition to the strong kieserite ($MgSO_4 \cdot H_2O$) and polyhydrated sulfate signatures identified by OMEGA (Observatoire pour la Mineralogie, l'Eau, les Glaces et l'Activité) [2]. We describe a new hydrated spectral type that is found in Ius Chasma and elsewhere in VM. Updated regional stratigraphy and geologic history brings new mineralogic mapping together with geomorphic and structural evidence.

**Datasets:** CRISM is a VNIR hyperspectral 2-D imager on the Mars Reconnaissance Orbiter (MRO) mission capable of multiple mapping modes [3]. It can acquire high-resolution targeted observations at 544 wavelengths from 0.362-3.92 μm and 15-19 m/pixel. Observations are photometrically corrected and provisionally atmospherically corrected, by an atmospheric transmission spectrum derived from CRISM data of Olympus Mons [4]. The atmospheric correction is similar to that used for OMEGA data [5]. Ratioing to a CRISM scene, rather than just a spectrum, is necessary to account for the spectral smile present in 2-D spectrometers. Additionally, some data is "destriped" to remove vertical striping caused by instrumental effects as in [6]. Spectra of interest are divided by a spectrally bland spectrum from the same column.

The HiRISE (High Resolution Imaging Science Experiment) camera aboard MRO is capable of acquiring co-aligned imagery with CRISM and can resolve details down to ~30 cm/pixel [7].

**Previous work:** Due to its impressive size and unique geomorphic features, the VM canyon system and its formation and erosion mechanisms have been well studied [e.g. 1,8-11]. Peulvast and Masson and coworkers have created a very thorough and sophisticated regional geologic history of central VM, especially Ius Chasma, using Viking imagery [1,11]. The established geologic history starts with Hesperian lava flows over Noachian basement and mega-regolith. VM forms by repeated tectonic extension in late Hesperian, forming horst and grabens in Ius Chasma. Geryon Montes, in the middle of Ius Chasma, are high-standing horsts. Louros Valles, along the south of Ius Chasma, formed by fluvial erosion. The morphology may be controlled by fractures related to VM formation or to older Noachian stresses. More recent tectonism cut across Louros Valles and possibly widened the connection between Ius and Melas Chasmata. Dry landslides and dust cover are the last events [12].

**Results:** We have identified a variety of hydrated minerals in Ius Chasma with CRISM data. Smectite clays, mono- and poly-hydrated sulfates, hydrated silica and an unknown hydrated material with a 2.2 and 2.28 μm doublet have all been identified (Fig 2). The unknown hydrated spectral type most closely matches gypsum or jarosite, of the hydrated minerals in the RELAB spectral library. Hydrated silica has a broad absorption in the 2.2x μm region, but the strong doublet feature in this spectral type argues for a more crystalline phase. In some places with Ius Chasma, it is difficult to distinguish between the unknown spectral unit and hydrated silica due to small outcrops and obscuring materials; it is possible the two materials are also intimately mixed. Another possible spectral match is an acid-leached Fe/Mg smectite**,** likely producing amorphous silica and poorly crystalline residual clays [13]. While this is mineralogically plausible, since the hydrated spectral type is often found with smectite clays, it is not a perfect spectral match because the hydrated spectral type also has a 2.4 μm absorption consistent with sulfates and not clay minerals.

The hydrated minerals are generally found at the lowest elevations within the chasma and are concentrated in light-toned layered deposits, landslides, and apparently draping units but are not seen in dunes or loose materials (e.g. layered materials in Fig 3). HiRISE image PSP_006718_1720 shows the hydrated spectral type or hydrated silica draping eroded layered smectite material in a regional depression (Fig 4, subset of Fig 5). Stratigraphic relationships allow placing these hydrated materials within the established geologic history and shed light on the role of water throughout the formation of Ius Chasma.

**Further work:** Further CRISM observations in Ius Chasma will help pin down contacts between sulfate and the unknown hydrated material, and reveal more about the regional mineralogic stratigraphy; many exposures of light-toned materials are visible in CTX and HiRISE data, but lack CRISM data to resolve mineralogy. The mineralogic identification of the unknown hydrated material with a 2.22 and 2.28 μm doublet is a significant outstanding issue.

**Acknowledgments:** We applaud the CTX, CRISM, and HiRISE science teams for all their dedication and hard work.

**References:** [1] Peulvast, J.P. and Ph.L Masson (1993) *Earth, Moon and Planets 61,* 191-217. [2] Gendrin, A. et al. (2005) *Science 307*, 1587-1591. [3] Murchie, S. et al. (2007) *JGR 112,* doi:10.1029/2006JE002682. [4] Mustard, J.F. et al., (2008) *Nature 454*, 305-309. [5] Langevin, Y. et al. (2005) *Science, 307*, 1584-1586. [6] Parente, M. (2008), *LPSC XXXIX*, Abst #2528. [7] McEwen, A. et al. (2007) *JGR, 109,* E06005. [8] Lucchitta, B.K. et al. (1992) 'The Canyon System on Mars.' Mars, UArizona Press, 453-492. [9] Lucchitta, B.K. et al. (1994) *JGR 99*, E2, 3783-3798. [10] Schultz, R.A. (1998) P*lanet. Space Sci. 46,* (6/7), 827-834. [11] Peuvlast, J.-P. et al. (2001) *Geomorphology 37*, 329-352. [12] Quantin, C. et al. (2004) *Icarus 172,* 555-572. [13] Tosca, N.J. et al. (2008), *LPSC XXXIX*, Abst #1745.

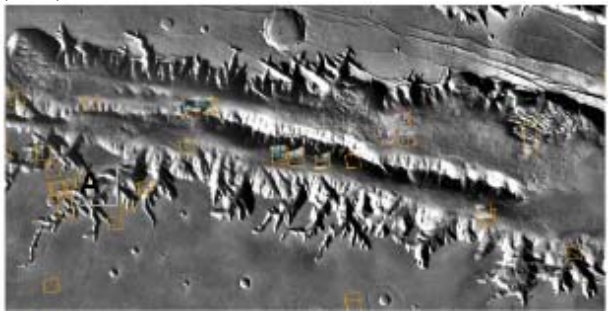


Fig 1. Map of central and eastern Ius Chasma with targeted CRISM observations in orange outlines.

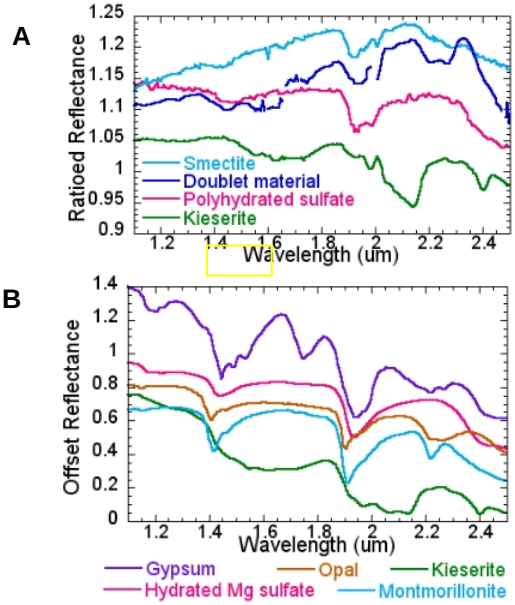


Fig 2. A. Representative CRISM spectra of kieserite, polyhydrated sulfate, smectite, hydrated silica, and an unidentified hydrated material distinguished by its 2.2-2.28 µm absorption doublet. Smectite from FRT00009B27; sulfates and unknown hydrated material from FRT0000A91C. B. RELAB library spectra are resampled to CRISM wavelengths. Gypsum offset by +0.5, kieserite by -0.1.

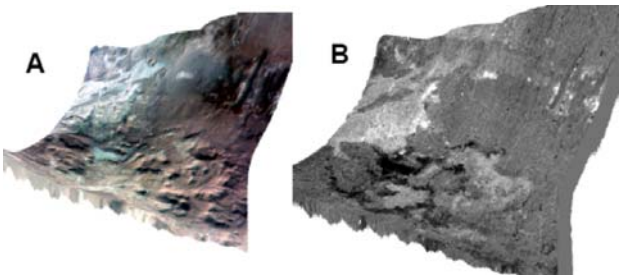


Fig 3. CRISM image FRT0000A91C draped on MOLA topography, 2x vertical exaggeration. A. False color RGB: 2.5, 1.5, 1.08 µm. B. 1.9 µm band depth parameter showing kieserite (in black), polyhydrated sulfate (white), and the unknown hydrated silica (light gray). Spectrally neutral, non-hydrated material is dark gray.

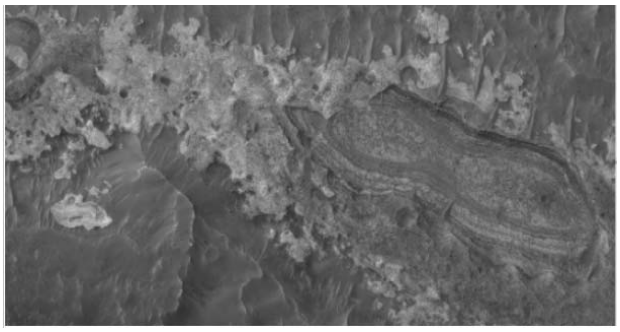

Fig 4. HiRISE image PSP_006718_1720 showing unknown hydrated spectral unit or hydrated silica unit draping previously eroded layered smectite unit. Dunes encroach both.

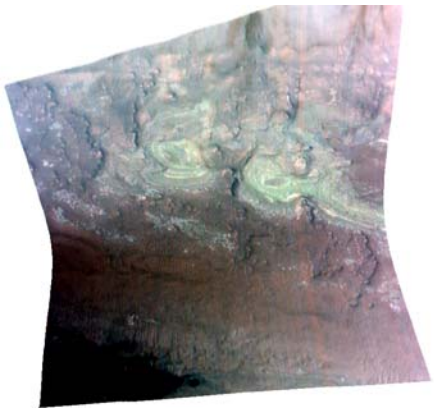

Fig 5. CRISM FRT000085A4. Smectite (green) and hydrated silica (light blue) in low-lying layered deposits south of Geryon Montes. Yellow box shows extent of Fig 4.

Fig 6. Schematic cross section showing superposition of hydrated materials. Colors same as Fig 2A.

**EMERGING CONNECTIONS BETWEEN TIR AND VNIR OBSERVATIONS OF MARTIAN PHYLLOSILICATES.** S. W. Ruff[1], [1]School of Earth and Space Exploration, Arizona State University, Tempe, AZ 85287-6305, steve.ruff@asu.edu

**Introduction:** With the advent of two visible/near infrared (VNIR) imaging spectrometers, the Mars Express OMEGA and Mars Reconnaissance Orbiter CRISM, spectral evidence for phyllosilicates on Mars appears definitive [e.g., 1, 2]. In contrast, thermal infrared (TIR) spectra from the orbiting TES instrument on the Mars Global Surveyor have not yielded such definitive evidence. Similarly, TIR spectra from the Mini-TES instrument on the two Mars Exploration Rovers (MER) have not shown unequivocal features of phyllosilicates, which is consistent with results from the Mössbauer (MB) spectrometer. Despite the sensitivity of TIR spectroscopy to even thin coatings (<10 microns), the lack of a clear identification of phyllosilicates has been enigmatic.

Laboratory TIR spectra of the dioctahedral smectites commonly observed with OMEGA and CRISM display two features in the low wavenumber range covered by TES and Mini-TES (~530 and ~465 $cm^{-1}$) that result from M-O-Si deformation and Si-O bending modes [e.g., 3]. The Si-O bending feature near 465 $cm^{-1}$ also is found in primary and secondary amorphous silicates and zeolites [4]. This feature has been identified in Mini-TES spectra of some rocks in the Columbia Hills of Gusev Crater that MB and APXS spectra indicate are highly altered [e.g., 5, 6]. A similar feature (the 465 index) has been mapped globally using TES spectra [7] and may serve as a proxy for some of the rocks encountered in the Columbia Hills. I have now discovered that many of the locations identified by OMEGA and CRISM as phyllosilicate-bearing display this feature in TES data, including parts of Mawrth Vallis, NE Tyrrhena Terra, and Nili Fossae. To date, I have observed the M-O-Si deformation feature near 530 $cm^{-1}$ along with the ~465 $cm^{-1}$ in one location near Nili Fossae. The full spectra from this location strongly resemble weathered basalt.

**Mawrth Vallis:** A map of the TES 465 index representing only the globally highest band depth values is shown in Fig. 1 along with an OMEGA phyllosilicate index map from [2]. The correlation between the two maps is notable along the west side of the valley. The presence of strong 465 index values in this location is especially notable given the relatively high albedo values (~0.2) of much of this terrain. Such albedo values elsewhere on the planet typically are associated with dusty surfaces that have no identifiable 465 feature.

Although there are areas with a positive correlation, other areas show a negative correlation. The dark-toned intracrater splotches display high 465 index values but no corresponding elevated phyllosilicate index. Because the 465 index is sensitive to a feature common to phyllosilicates and primary volcanic glass, the dark splotches probably contain minimally altered glass.

**NE Tyrrhena Terra:** Tyrrhena Terra is dominated by the spectral signature of TES type 1 basalt [8], yet displays isolated examples of strong 465 index values [7]. One such example in the northeast portion occurs in a crater that has been identified by [2] as having a strong phyllosilicate detection (Fig. 2). Although the CRISM data for this crater do not provide full coverage, there is a strong spatial correlation between the TES and CRISM indices. In this example, the full TES spectra are similar to the "Assemblee" type rocks measured by Mini-TES in the Columbia Hills, especially in the low wavenumber region. The type example was measured by MB and APXS. Although neither MB nor Mini-TES data provided clear evidence for phyllosilicates in this rock, the APXS data suggested a composition consistent with montmorillonite [6].

**Nili Fossae:** A crater at the transition between Syrtis Major and Nili Fossae shows a well-correlated TES 465 index and OMEGA phyllosilicate index [2] (Fig. 3). This is a rare example where the TES 530 index also is elevated. The combination of elevated 465 and 530 indicies is necessary but not sufficient for a robust TES detection of dioctahedral smectite. The full TES spectra from this crater clearly resolve a feature near 465 $cm^{-1}$ and a strong shoulder near 535 $cm^{-1}$. This spectral character is comparable to that shown by [9] in the spectra of smectite-bearing weathered Columbia River basalts.

**References:** [1] Poulet, F., et al., (2005) *Nature, 438*(623-627). [2] Mustard, J.F., et al., (2008) *Nature, 7097* 305-309. [3] Michalski, J.R., et al., (2006) *J. Geophys. Res., 111*(E03004) doi:10.1029/2005JE002438. [4] Ruff, S.W., (2004) *Icarus, 168*(131-143). [5] Ruff, S.W., et al., (2006) *J. Geophys. Res., 111*(E12S18) doi:10.1029/2006JE002747. [6] Clark, B.C., et al., (2007) *J. Geophys. Res., 112*(E06S01) doi:10.1029/2006JE002756,. [7] Ruff, S.W. and P.R. Christensen, (2007) *Geophys. Res. Lett., 34*(L10204) doi:10.1029/2007GL029602. [8] Bandfield, J.L., et al., (2000) *Science, 287* 1626-1630. [9] Michalski, J.R., et al., (2006) *Earth Planet. Sci. Lett., 248* 822-829.

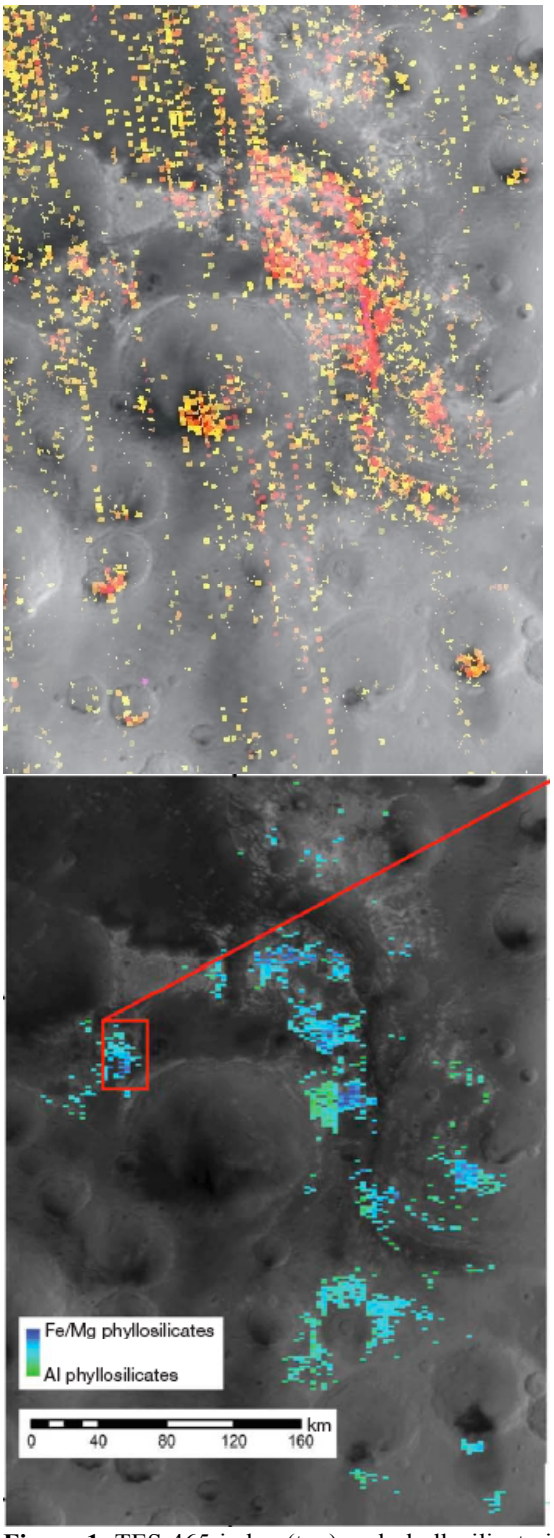


**Figure 1.** TES 465 index (top) and phyllosilicate indices from [2] for Mawrth Vallis.

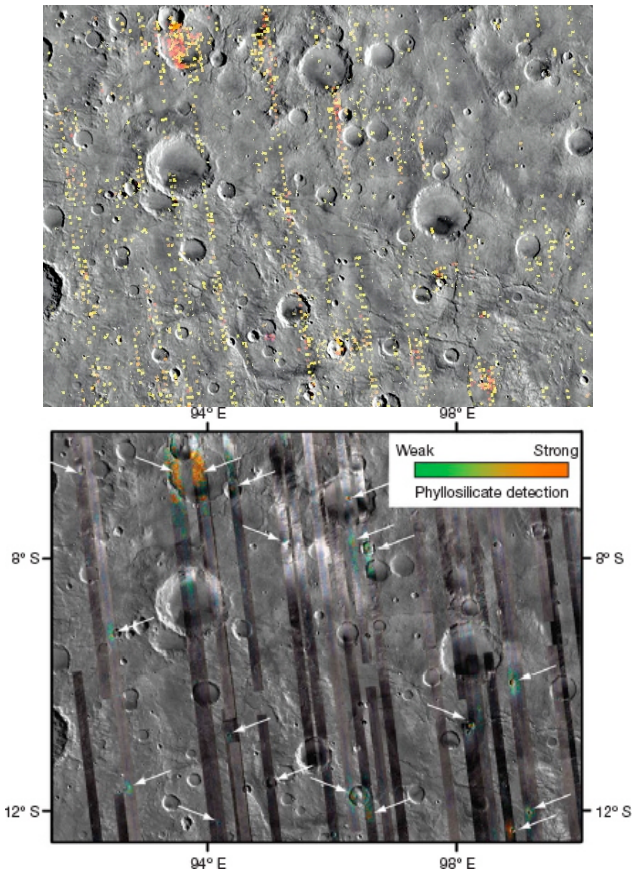


**Figure 2.** TES 465 index (top) and phyllosilicate index (bottom) from [2] for a portion of NE Tyrrhena Terra.

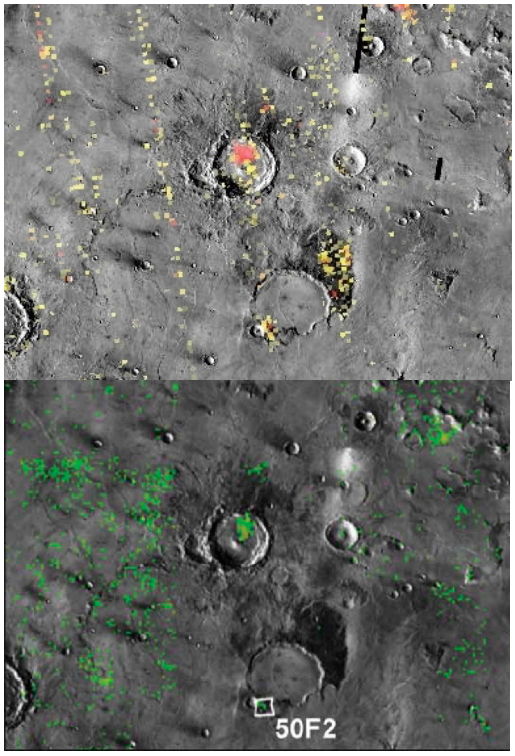


**Figure 3 (right).** TES 465 index (top) and phyllosilicate index (bottom) from [2] near Nili Fossae.

**PHYLLOSILICATES PRODUCED BY IMPACT-GENERATED HYDROTHERMAL SYSTEMS ON MARS.** Susanne. P. Schwenzer[1] and David. A. Kring[1], [1]Lunar and Planetary Institute, 3600 Bay Area Blvd., Houston, TX, 77058, USA; schwenzer@lpi.usra.edu, kring@lpi.usra.edu.

**Introduction:** Impact cratering is one of the dominant processes affecting planetary surfaces particularly early in their evolution. While on Earth that record is obliterated by subsequent geologic processes, the Moon and the ancient, Noachian, surfaces of Mars still reveal a detailed chronology of their early history. According to this record, the Moon and the terrestrial planets have been resurfaced by a cataclysmic event caused by main belt asteroids [1-3]. The cataclysm occurred at ~3.9 Ga and may have been as short as 10–150 My [1]. On Mars, impacts have long been recognized as cause for water related processes such as hydrothermal alteration of melt sheets [4] or as trigger for small outflow channels especially on old Noachian terrains [5]. And they are known to cause impact-generated hydrothermal systems whose lifetimes can be evaluated by the heat in central uplift material, the central melt sheets, and impact melt breccias [6]. Beyond the energy evaluation, the temperature distribution and water flow over the lifetime of an impact-generated hydrothermal system can be calculated. The HYDROTHERM approach by [7] provided first insights into the development of such systems over time. Our work on terrestrial [8,9] and Martian craters [10] extended this work to larger craters (thus longer lifetimes) and more sophisticated, realistic models, e. g. for the topography [10]. Therefore, temperature distribution and water flow of this important process over the entire lifetime of an impact-generated hydrothermal system are well understood. The next step is to determine how these systems affected mineral assemblages on Mars that can be detected by ongoing and future orbiter and lander missions. We will do this by evaluating information about hydrothermal alteration in large terrestrial impact structures and combining this knowledge with results from physico-chemical calculations considering Martian rocks and fluid conditions.

**Terrestrial craters:** As per 2005 more than 60 terrestrial impact structures showing hydrothermal alteration were counted [11]. There are, however, about the same number of structures in which hydrothermal mineral assemblages have not (yet) been detected [11]. To characterize the main features of impact-generated hydrothermal systems, Sudbury [12], Chicxulub [13,14] and three Russian craters Popigai, Kara and Puchezh-Katunki [11,15] serve as exemples. At Sudbury widespread hydrothermal alteration above and below the melt sheet is observed; and drilling activities revealed extensive alteration in the impactite units of Chicxulub crater. The main mass of alteration assemblages in both cases formed at moderate to low temperatures (i. e. below 300 °C). Comparable alteration temperatures are found in the Russian craters. Despite their large difference in target rock lithology and geological setting, all hydrothermal systems produced a variety of sheet silicates, including smectites.

**Modeling:** While the thermal evolution of impact-generated hydrothermal systems are controlled by the amount of heat produced by the impact [8–10], the chemical evolution of the system depends on host rock composition, oxygen fugacity, and other planet specific features. Therefore, physico-chemical modeling is a tool to transfer terrestrial observations to the Martian environment.

*CHILLER calculations.* We performed a series of calculations using the computer code CHILLER [16]. For details of assumptions and input data see [17,18].

*Whole rock:* Results obtained by calculations with whole rock chemistry were reported earlier and can be divided in three groups: 1) serpentine–chlorite–(amphibole–garnet) at low water to rock ratios (W/R), 2) nontronite–hematite at intermediate W/R and hematite dominating at very high W/R [17,18]. We will use the results presented in [17,18] in the discussion.

*Minerals:* To further evaluate the alteration processes we calculated alteration assemblages deduced from the individual minerals of the rock used in [17,18] at 150 °C and 550 bar. The mineral chemistry was taken from [19] and the fluid as in [17,18]. While the results of the pyroxene runs resulted in the same alteration phases – though in varying abundances – as the whole rock, results obtained with pure olivine and plagioclase chemistry were significantly different. Olivine forms hematite (at high W/R) and magnetite (at low W/R) with serpentine being the only silicate that exceeds 10 wt.-% of the precipitate at any W/R in the calculation. In contrast to this, plagioclase alteration is dominated by a mica–prehnite–zeolite–feldspar(–pumpelleyite–amphibole–garnet) assemblage at W/R of 1. Epidote is present over a small W/R range around W/R=10. Pyroxene is formed at the expense of the mica–...-assemblage at W/R > 10. Between W/R of 80 and 100 zeolite quickly fades out and is replaced by clay, which is the dominating phase until hematite (+diaspore) becomes prevalent (W/R ~8000). Note, that the plagioclase alteration took place in an Fe-Mg-Ca-rich fluid.

**Impact-generated hydrothermal alteration minerals in their geologic setting:** Resulting from our calculations [17,18, and this study] and by combining them with knowledge about crater formation [e. g. 20], fluid flow and temperature in time and space [8–10], and terrestrial observations [e.g. 12–15] the various alteration settings can be pictured as follows:

*Fractured basement:* According to modeling of fluid flow evolution [10], impact-generated convections reaches down several kilometers beneath the surface of a crater. It evolves around the hot rocks in the central uplift and merges inwards as they cool below ~350 °C [10]. The fractures are thereby expected to provide pathways for increased fluid flow. The minerals inferred in a Martian crater are hematite–clay-dominated assemblages where the flow is highest and chlorite and/or serpentine with or without amphibole and garnet as a more pervasive alteration assemblage. The occurrence is expected to differ between fractures, in which vein-type mineralizations may result, and the low W/R ratio setting, in which the overprint resembles a more disseminated, metamorphic-like setting. At the end of the system's lifetime, the latter may be pervasive and widespread throughout the whole rock volume under the crater. Despite the pervasiveness, a large volume of rock may be impermeable and thus persist alteration and remain fairly fresh, as can be observed in terrestrial hydrothermal systems.

*Crater rim and central peak:* The crater rim and the central peak are highly fractured parts of the structure. Upwelling fluid flow is observed here. Therefore, alteration assemblages reflecting intermediate to high W/R will occur. These may be found as hematite along fracture walls and hemtite–clay assemblages replacing the original mineralogy of the rock beyond the fracture wall. The highest degree of overprint is expected to occur in these two parts of the structure. Depending on fluid chemistry, temperature, and pervasiveness of the alteration, certain minerals will contribute to the alteration assemblage more than others. As shown by calculations with single minerals, especially prevalent olivine or plagioclase alteration will drastically change the resulting assemblage.

*Impactites:* From studies of terrestrial craters, the widespread presence of clay minerals in impact deposits can be expected. Thereby alteration of glass phases to clay minerals is prevailing in terrestrial settings [11–15]. For Mars this translates to the formation of nontronite, chlorite and other Fe-dominated clay minerals, which are expected to be especially prominent on crater floors where glass rich impactites are deposited.

*Surface:* Inside the crater, a lake may form [10]. It is fed by water venting the hydrothermal convection system beneath the crater and the mobilized ground water in its direct vicinity. Where fractures provide pathways for hot, hydrothermal fluids to vent, precipitation of dissolved species, such as $SiO_2$ is expected.

**Martian mineralogy:** Ongoing orbiter missions reveal a large variety of hydrous phases on Mars. The findings are restricted to the Noachian terrain and occur in outcrops, crater ejecta, and walls and central peaks of craters [21–23]. Thereby, the observation of hydrous phases and clay minerals in crater rims and central peaks is especially interesting [24,25] as the most prominent alteration is expected in these highly fractured and permeable parts of the structure. Clay minerals possibly result from the hydrothermal alteration caused by the upwelling fluids, while hydrous silica phases are likely deposited by the venting fluids. A possible explanation for the finding of pumpelleyite and epidote phases [24] can be found in the preferred alteration of plagioclase in an iron rich fluid.

**Conclusions:** During the early, Noachian history of Mars, impact cratering was an important geologic process [26]. Creating local hot spots impacts not only melt ice, but also establish temperature gradients along which fluid flow with subsequent mineral alteration will occur. Given a short time of extremely intense bombardment [1], after which many of the water related processes fade out or cease (e.g., rampart craters [27] and valley networks [28]), and the large volume of rock impacts affect, impact-generated hydrothermal systems have to be considered as a major if not the main source for phyllosilicates in Noachian strata.

**References:** [1] Strom R.G. et al. (2005) *Science, 309*, 1847–1849. [2] Bogard, D. D. (1995) *Meteoritics, 30*, 244–268. [3] Kring, D. A., Cohen, B. A. (2002) *JGR, 107,* 10.1029/2001JE001529. [4] Newsom H.E. (1980) *Icarus, 44,* 207–216. [5] Brakenridge G.R. et al. (1985) *Geology, 13*, 859–862. [6] Daubar, I., Kring D.A. (2001) *LPSC XXXII*, #1727. [7] Rathbun J.A., Squyres S.W. (2002) *Icarus, 157*: 362–372. [8] Abramov, O., Kring, D.A. (2004) *JGR, 109,* E10007, doi: 10.1029/2003JE002213. [9] Abramov, O., Kring, D.A. (2007) *MAPS, 42,* 93–112. [10] Abramov O., Kring D.A. (2005) *JGR, 110*: doi: 10.1029/2005JE002453. [11] Naumov, M.V. (2005) *Geofluids, 5*, 165–184. [12] Ames, D.E. et al. (2006) In: Cockell C. et al.: Biological Processes Associated with Impact Events, 55–100. [13] Zurcher L., Kring D.A. (2004) *MAPS, 39*: 1199–1221. [14] Zurcher L. et al. (2005) *Geo. Soc. America, Spec. Paper 384:* 223–238. [15] Naumov M.V. (2002) In: Plado J., Personen L.J.: Impacts in Precambrian Shields: 117–171. [16] Reed M.H., Spycher N.F. (2006) Users Guide for CHILLER. University of Oregon. [17] Schwenzer, S.P., Kring, D.A. (2008) *LPSC, XXXIX*, abstr. #1817. [18] Schwenzer, S.P., Kring, D.A. (2008) Workshop on the Early Solar System Bombardment: #3027. [19] Gleason, J.D. et al. (1997) *GCA, 61*: 4007–4014. [20] Grieve, R.A.F. (2006) Impact Structures in Canada. [21] Bibring, J.-P. et al. (2005) *Science, 307*, 1576–1581. [22] Poulet, F. et al. (2007) *JGR, 112*, : E08S02, doi: 10.1029/2006JE 002840. [23] Loizeau, D. et al. (2007) *JGR, 112*, E08S08, doi: 10.1029/2006JE2877. [24] Poulet, F. et al. (2008) Astronomy and Astrophysics, manuscript No. clayAAV2. [25] Mustard, J. F. et al. (2008) *Nature, 454*, 305–309. [26] Tanaka, K. L. et al. (1988) Proceedings of the 18th LPSC, G. Ryder (ed.), LPI & Cambridge University Press: 665–678. [27] Reiss, D. et al. (2006) *MAPS, 41*, 1437–1452. [28] Fassett, C. I., Head III, J. W. (2008) *Icarus, 195*, 61–89.

**INSIGHTS INTO THE PAST MINERALOGY & FLUVIAL ACITIVTY OF MARS WITH WATSEN**

T.Tomkinson[1], S.D.Wolters[1], A.Hagermann[1], A.F.Bohman[2], A.T.Sund[3], J.K.Hagene[2] and M.M.Grady[1&4], [1]PSSRI, The Open University, Walton Hall, Milton Keynes MK7 6AA, UK (t.o.r.tomkinson@open.ac.uk), [2]Norsk Elektro Optikk AS, Solheimveien 62 A, N-1473 Lørenskog, Norway, [3]NavSys AS, Fjellhamarveien 46, 1472 Fjellhamar, Norway, [4]Department of Mineralogy, The Natural History Museum, London, SW7 5BD, UK.

Mars is currently the main focus of extra-terrestrial planetary investigation in terms of the number of surface and orbital instruments deployed there. Although several missions have scratched into the surface (most recently Phoenix) there have not been deeper measurements of the martian subsurface. Phoenix has discovered the surrounding soil to be comparable to soils found in Antarctica's Dry Valleys [1]. It seems clear from the initial results that the soil is pH alkaline (8-9) and that water has been involved in the formation of the soil, detected in the form of subliming ice [2] (see figure 1). The presence of salts incorporating magnesium, sodium, chloride and potassium further suggests the presence of water interacting with soil at some point. Since conditions at the martian surface are unfavourable for the presence of water and potential organic signatures [3] it is necessary to look deeper into the subsurface.

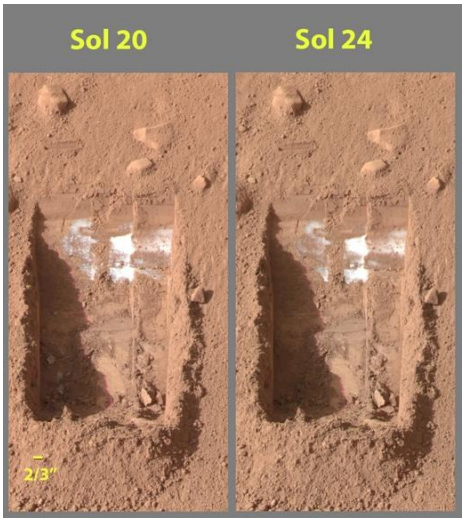


Figure 1 - Scoop marks from Phoenix arm exposing white ice that can be observed subliming between Sol 20 and 24 [2].

Recent classification of geological eras [4] (see figure 2) suggests an early warm and wet martian environment in which phyllosilicates formed [5], the Phyllosian era. Mawrth Vallis and Nili Fossae [6, 7] are two regions that the orbital VNIR and IR spectrometers OMEGA and CRISM [4, 8] have indentified which correspond mineralogically and through crater counts to this early Phyllosian era. These locations would be prime candidates for the detection of Mars' fluvial past, including the observation of carbonates (known to be abundant in the presence of water, $CO_2$ and an alkaline pH; all conditions hospitable for most terrestrial life).

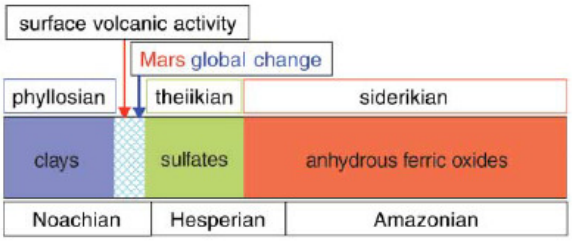


Figure 2 – Displays the main mineralogies thought to have formed (blue, green and red) and the two derived chronologies (geological chronology on top and crater count chronology at the bottom) along with major events in the martian history after J.-P. Bibring et al., 2006 [4].

So were those early conditions warm and wet and potentially favourable to life? Hopefully these questions will be answered by looking into the martian regolith with *WatSen*, a miniaturized instrument consisting of a combined Attenuated Total Reflectance (ATR) IR spectrometer, optical microscope and humidity sensor. *WatSen* is designed to be part of a suite of instruments onboard a mole on a planetary lander similar to ExoMars. A burrowing mole would allow *WatSen* to make multiple readings at intervals of depth providing an insight into mineral variation, humidity, water presence and perhaps biological activity. As part of a mole, *WatSen* could penetrate down to 5 m in depth. These would be the first measurements of the non-oxidised subsurface and may be below the zone of sublimation [9] (see figure 3).

The ATR sensor operates by measuring the changes that occur to the totally internally reflected infrared beam upon contact with the sample. Surface properties alter the spectral reflectance in a mineral grain, thus the ATR has a flat surface in intimate contact with the sampling surface [10]. The optical microscope will aid mineral identification with images of the grains in contact with the ATR being generated at each spectral location. The humidity sensor will continually detect any

water present in the bore hole during *WatSen*'s descent, whether it is in the form of vapour subliming or direct contact with liquid water. Detection of vapour or liquid is dependent on whether atmospheric or subsurface pressure is higher than expected, the mole penetrating below the zone of sublimination and the porosity of the regolith [9].

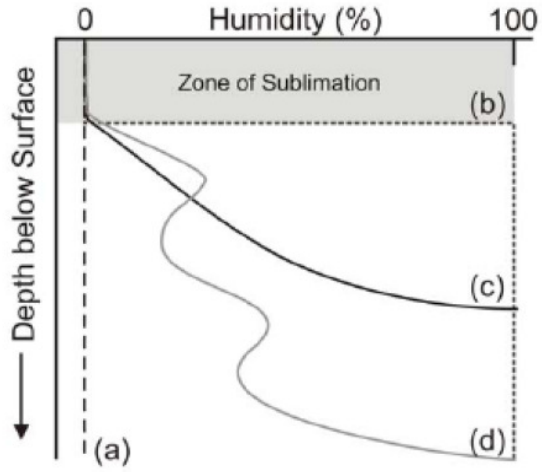


Figure 3 - Illustrating four possible variations in humidity with depth. a) represents no water in regolith; b) complete saturation beneath zone of sublimination; c) gradual increase in water content with depth; d) alternating saturation after Grady et al., 2006 [9].

Spectral studies show that soil components typical of Mars will be uniquely identifiable within the chosen wavelength range (5.5 - 10.8 µm, see figure 4). This wavelength range is a trade off between technical boundaries and the ideals wavelengths; $H_2O$ absorption is stronger at 3 µm, but strong and distinct absorption peaks for minerals occur in the mid infrared spectrum (5 - 11 µm). For example carbonate minerals, which have yet to be identified by direct surface analysis, display a unique spectral shape between 6.3 - 7.4 µm. Water IR spectral features are also displayed between 6 - 7 µm, but major features of anhydrous silicates occur at wavelengths greater than 9 µm. Furthermore, hydrated minerals such as clays display combined features of water and silicates. *WatSen*'s 0.015 $\Delta\lambda/\lambda$ resolution is sufficient to resolve distinct spectral features for water and minerals found on Mars.

An IR database of analog materials generated on the Open University's (OU) ATR spectrometer will be used to as a reference for the *WatSen* breadboard instrument. This autumn/winter tests will be carried out with various substrates, temperatures, pressures and water contents in the OU's Mars environment chamber. First we will test the functionality under ambient conditions compared with laboratory ATR instruments followed by martian environmental conditions. This will help identify any reliability and complexity issues with the instrument.

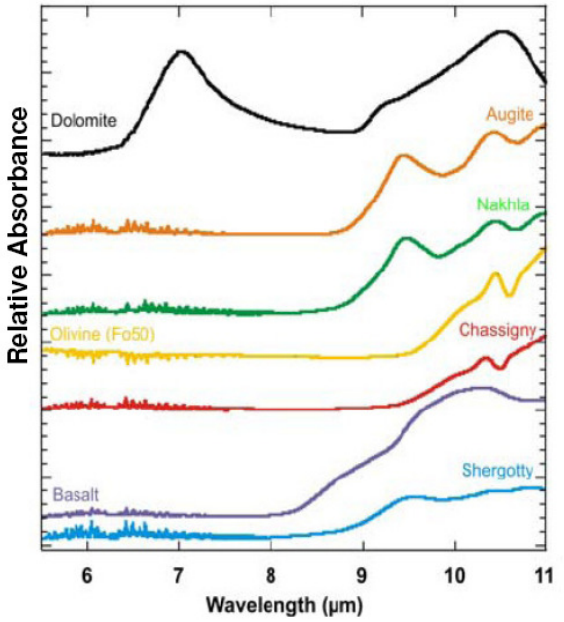


Figure 4 - IR spectra of powdered samples of Shergotty, Nakhla and Chassigny, along with a basalt, augite, olivine and dolomite. The spectra were acquired using an ATR at 295 K, and are offset for clarity [10].

As the surface of Mars is constantly weathered by the planet-wide dust storms that spread and mix the loose surface soil components it is the layered subsoil material that will reveal Mars' past history. In addition the surface oxidizing solar radiation makes conditions inhospitable for life, but beneath the surface in briny solutions this may not be the case. Rather than merely scratching the surface a penetrating mole would supersede its martian predecessors and with *WatSen*'s instruments would help characterize the past climate of Mars.

**References:** [1] Wentworth, S.J, et al., (2005) *Icarus*, *174*, 383-395. [2] http://www.nasa.gov/mission_pages/phoenix/news/phoenix/main/index.html [3] E.K. Gibson, et al., (2007) *LPI Contributions, 1353*, 3071. [4] J.-P. Bibring et al., (2006) *Science, 312*, 400. [5] F. Poulet et al., (2005) *Nature, 438*. [6] D. Loizeau et al., (2007) *JGR, 112,* E08S08. [7] J.F. Mustard et al., (2007) *JGR, 112*, E08S03. [8] S. L. Murchie et al., (2007) *JGR, 112,* E05S03. [9] M.M. Grady et al., (2006) *Int. J.Astrobiology*, 5, 211-219. [10] T. Tomkinson et al., (2008) *LPSC XXXIX*, Abs #2040.

**SMECTITE FORMATION ON EARLY MARS: EXPERIMENTAL CONSTRAINTS.** N. J. Tosca[1], R. E. Milliken[2], F.M. Michel[3] [1]Dept. of Organismic & Evolutionary Biology, Harvard University, Cambridge, MA 02138 (ntosca@fas.harvard.edu), [2]Jet Propulsion Laboratory, Pasadena, CA 91109 (Ralph.Milliken@jpl.nasa.gov), [3]Geological & Environmental Sciences, Stanford University, Stanford, CA 94305 (fmichel@stanford.edu).

**Introduction:** Noachian outcrops appear to be dominated by Fe- and Mg-bearing smectites [1], implying a distinct set of chemical conditions across much of the earliest martian surface. Smectites are stable over a wide range in temperature [2] and are sensitive to a variety of chemical parameters which may have controlled their formation on the ancient martian surface. Accordingly, it is a priority to constrain the limits and controls of smectite formation on Mars in a systematic way. Here, we describe a variety of experiments focused on identifying major controls on smectite formation. We have investigated the role of variable redox conditions, $Mg^{2+}$ concentration and pH using chemistries derived from chemical weathering of synthetic martian basalt [3]. With these experimental constraints in mind, smectite formation on Mars can be investigated in the framework of mineral weathering where the roles of structural inheritance and micro-fluid chemistry play crucial roles [4,5].

**Methods:** Smectite synthesis experiments were conducted using a fluid composition derived from the chemical weathering of synthetic martian basalt [3]. The fluids were synthesized by adding sulfate and chloride salts to control Mg, Fe, Ca, Al, Na and K. Aqueous silica was added using tetraethoxysilane (TEOS). Experiments were conducted at 25°C and 60°C for 2-5 weeks at both buffered and unbuffered initial pH values ranging from 4-9. For Fe-bearing anoxic experiments, reagents were added to $N_2$(g)-saturated deionized (DI) water and sealed after the addition of hydrazine (an $O_2$(aq) scavenger). Samples were collected and centrifuged/washed in $N_2$(g)-saturated DI and dried under vacuum. Both air-dried samples and oriented aggregates treated with ethylene glycol were analyzed by powder XRD to identify the precipitates and monitor crystallinity. Bulk samples were also analyzed by XRF and IR spectroscopy. For some samples, pair distribution function (PDF) analysis from high-energy total X-ray scattering data was performed at Argonne National Lab.

**The effect of variable redox conditions:** Products from oxic and anoxic $Fe^{2+}$-bearing experiments differed significantly; Fe-smectites were only formed under initially anoxic conditions. For oxic unbuffered pH experiments with initial pH ($pH_i$) from 4-9, Fe-oxidation and hydrolysis drove the pH to low values and formed jarosite ($pH_i$ = 4), jarosite + goethite ($pH_i$=5) and goethite ($pH_i$ = 6-7). At $pH_i$ = 8 and 9, the formation of a $Fe^{2+}$-smectite occurred before $Fe^{2+}$ was oxidized and so is an artifact of the experimental protocol (i.e., rapid addition of $Fe^{2+}$ and $SiO_2$(aq) at high pH). The main product present in $pH_i$ =5-7 experiments was a powder X-ray amorphous $Fe^{3+}$/$SiO_2$-bearing precipitate that, from total X-ray scattering, showed a high degree of crystallinity (coherent scattering domain >20Å) with Fe-O, Mg-O and Si-O features. In the vis/near-IR, this material displays several features that have been identified at the martian surface, including Si-OH and $Fe^{3+}$ features.

Anoxic unbuffered experiments produced $Fe^{2+}$/Mg-trioctahedral clay ($Fe^{2+}$ saponite) from pH 7-9. The clay exhibited a (001) peak (ethylene glycol saturation) at 18.06Å (Fig. 1) and an (060) peak at 1.52 Å. However, at pH 6 and 5, a green $SiO_2$(aq)-bearing precipitate formed with no identifiable peaks in powder XRD which may be indicative of a ferroan saponite "precursor". We are confirming whether oxidation of our $Fe^{2+}$-saponite clays leads to nontronite, as several previous studies report, via the half-cell reaction [6]:

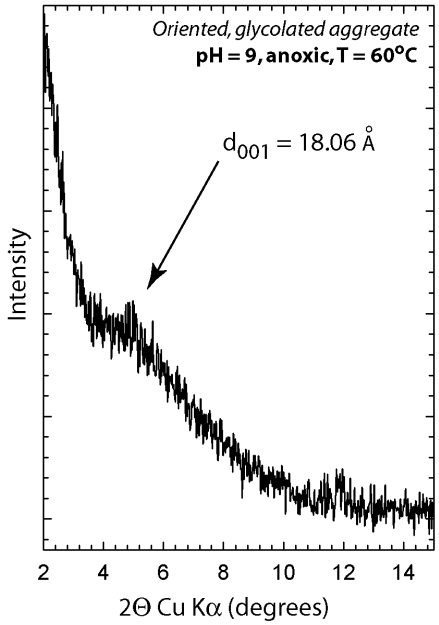


***Fig. 1 XRD pattern of a ferroan saponite produced under anoxic conditions at pH = 9.***

$$Si_4Fe_3^{2+}O_{10}(OH)_2 + 2H_2O \rightarrow$$
$$Si_4Fe_2^{3+}O_{10}(OH)_2 + FeOOH + 3H^+ + 3e^-$$

**The effect of [$Mg^{2+}$]:** Fe-free experiments were conducted under various $Mg^{2+}$ concentrations. For example, for buffered Fe-free experiments at [Mg] =

0.06 mol/kg and pH = 8, amorphous silica was the only product identified after 4 weeks (Fig 2).

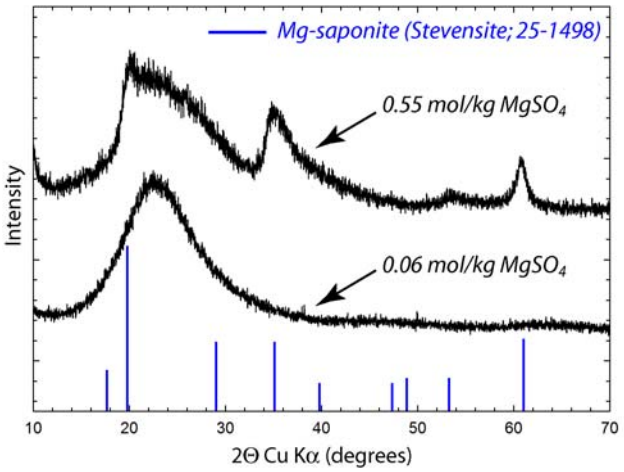


***Fig. 2 XRD patterns of amorphous $SiO_2$ and Mg-saponite formed at varying [Mg] (pH =8).***

However, in an identical experiment, but with a ten-fold increase in [Mg] to 0.5 mol/kg (added as $MgSO_4$), after 4 weeks a fully turbostratic Mg-saponite was identified (Fig. 2), exhibiting strong (001), (060) and *hkl* peaks in powder XRD. The effect of increases in [Mg] appears to expand the stability range of smectites to lower pH, with Mg-smectites appearing in pH 7-9 experiments at 0.5 mol/kg $Mg^{2+}$ compared to pH = 9 only in the [Mg] = 0.06 mol/kg experiments. This effect can be thermodynamically predicted, as Mg-saponite stability is a function of $SiO_2$(aq) and $Mg^{2+}$ activity in addition to pH [7]. Ongoing experiments are testing the limits of [Mg] on pH using $MgCl_2$ and likely late-stage martian brine compositions.

**The effect of pH:** Aside from the influence of elevated cation concentrations, there are significant differences in the range in pH that $Fe^{2+}$-saponites and Mg-saponites precipitate. For example, in anoxic $Fe^{2+}$ experiments, Fe-saponites were identified from pH 6-9 (with the possibility of precursors being formed at pH 5) whereas, under identical but Fe-free conditions, Mg-saponites formed only at pH 9 ([Mg] = 0.06 mol/kg). Although the mechanism of smectite formation in our experiments has yet to be identified, it has been suggested that under similar conditions smectite formation occurs through epitaxial precipitation [7]. This process first involves the formation of a double layer hydroxide material (e.g., brucite, $Fe(OH)_2$), subsequent $SiO_2$(aq) adsorption and finally crystallization [7]. The differences in pH stability of brucite and $Fe(OH)_2$ "templates" could explain the observed pH ranges over which $Fe^{2+}$- and Mg-smectites precipitate in our experiments. In addition, $SO_4$-green rust is an additional double layer hydroxide material that forms under a range of pH values (~4-7) in the presence of even trace amounts of $Fe^{3+}$ [8]. This material could also act as a template for Fe-saponite formation over a range of mildly acidic values in $SO_4$-bearing environments. Experiments conducted under elevated $Fe^{2+}$ (at pH = 5-6) have resulted in the formation of $SO_4$-green rust and could be indicative of such a mechanism.

**Applicability to the Noachian surface:** It is important to underscore that our experimental methods are designed to evaluate the macroscopic effects of chemical parameters on Fe- and Mg-smectite formation. However, the current challenge is to place these results in the context of mineral dissolution/weathering processes which occur at the micro- and nano-scales. The result of such complex processes is that the chemical conditions which lead to smectite formation are often not representative of the properties of the bulk solution [5]. For example, it is well known that smectite formation from the weathering of mafic minerals often proceeds by the inheritance of crystallographic elements, structural re-arrangement and transport of chemical species to and from reaction sites [4,5]; a mechanism which has not been accounted for in these experiments. The overall effect is that clay minerals are out of equilibrium with the bulk solution and surrounding environment.

Most importantly, our results suggest that initially anoxic conditions (either locally or globally) could be the only route by which to produce $Fe^{2+}$-saponites and nontronite on Mars. Fe-oxidation and hydrolysis results in a significant decrease in pH and the formation of $Fe^{3+}$-phases regardless of the presence of $SiO_2$(aq). It has been suggested that epitaxial smectite formation must proceed by a precursor with a double-layer hydroxide structure, which no $Fe^{3+}$-hydroxides possess [9]. These results are also consistent with previous investigations on anoxic and partially oxidizing routes of smectite synthesis [6]. Interestingly, even for topotactic Fe-smectite formation in terrestrial rocks, there are indications that the transport of Fe to reaction sites is required based on analyses of reaction stoichiometry [4]. This implies locally reducing conditions are required for $Fe^{2+}$ transport without oxidation or precipitation of Fe-(hydr)oxide phases.

**References:** [1] Mustard, J. et al. (2008) *Nature*, 454, 305. [2] Galan, E. (2006) in: *Handbook of Clay Science*, F. Bergaya, B. Teng, G. Lagaly Eds., Elsevier, pp. 1129-1162. [3] Tosca, N.J. et al. (2004) *JGR*, 109, E05003. [4] Velbel, M. & Barker W. (2008) *Clays & Clay Min.* 56, 112. [5] Banfield, J. & Barker, W. (1994) *Geochim. Cosmochim. Acta*, 58, 1419. [6] Decarreau, A. & Bonnin, D. (1986) *Clay Min.*, 21, 861. [7] Harder, H. (1972) *Chem. Geo.*, 10, 31. [8] Cornell, R. & Schwertmann, U. (2003) *The Iron Oxides*, Wiley, 664 p. [9] Harder, H. (1978) *Clays & Clay Min.*, 26, 65.

**QUANTITATIVE CHEMISTRY OF PHYLLOSILICATE MINERALS USING LASER-INDUCED BREAKDOWN SPECTROSCOPY.** J. M. Tucker[1], M. D. Dyar[2], S. M. Clegg[3], R. C. Wiens[3]. J. E. Barefield II[3], M. W. Schaefer[4], and J. L. Bishop[5], [1]Department of Astronomy, Amherst College, Amherst, MA 01002, jtucker09@amherst.edu, [2]Department of Astronomy, Mount Holyoke College, 50 College St., South Hadley, MA 01075, mdyar@mtholyoke.edu, [3]Los Alamos National Laboratory, P.O.Box 1663, Los Alamos, NM 87545, sclegg@lanl.gov, rwiens@lanl.gov, jbarefield@lan.gov, [4]Department of Geology and Geophysics, E235 Howe-Russell, Louisiana State University, Baton Rouge, LA 70803, mws@lsu.edu, [5]SETI Institute, 515 N. Whisman Rd., Mountain View, CA 94043, jbishop@seti.org.

**Introduction:** Laser-induced breakdown spectroscopy (LIBS) is a powerful analytical tool that will be employed by the ChemCam instrument on the Mars Science Laboratory (MSL) and a combined LIBS-Raman instrument on ExoMars. In LIBS, a short-duration laser pulse or multiple pulses are focused onto a sample which ablates the sample and produces a plasma of atomic, ionic, and simple molecular particles. Excited electrons in these species undergo quantized transitions, emitting photons with energy characteristic of the species. Spectroscopic analysis of collected photons sheds light on the physical and chemical properties of the plasma, and hence the original sample.

While LIBS is similar to other types of atomic emission spectroscopy such as ICP-AES, its advantages include minimal sample preparation (sample digestion is not needed), relatively low power requirements, the ability to perform remotely, and fast data acquisition. Despite its recent popularity and success in quantifying compositions of many different types of materials [1], LIBS is not easily employed on geological samples. Complex compositions and chemical and physical interactions tend to affect spectral intensities in unpredictable ways, giving rise to so-called chemical matrix effects.

This work explores the application of three different statistical techniques on a set of LIBS data obtained from 17 phyllosilicates. Because the samples are all of the same mineral group, the matrix effects ought to be consistent and predictable, unlike those in rocks. Additionally, phyllosilicate minerals have been detected on Mars in abundance [2,3] so LIBS characterization of them will be useful should the be encountered by MSL or ExoMars.

**Experimental methods:** The laboratory setup used in this study is constructed to mimic ChemCam and Mars conditions as closely as possible. Samples are placed in a vacuum chamber filled with 7 Torr carbon dioxide to simulate the Martian surface atmosphere, as LIBS plasmas are influenced by atmospheric conditions. The plasma is generated by a Spectra-Physics Indi Nd:YAG laser operating at 1064 nm and pulsing at a rate of 10 Hz with a 10 nanosecond pulse width. The laser energy is set to 17±1 mJ/pulse, similar to the ChemCam laser. The plasma emission is collected by a Questar Field Model 89 mm telescope (slightly smaller than ChemCam's 110 mm telescope) situated 9 meters from the sample. The light is transmitted via a fiber optic cable to one of three Ocean Optics HR2000 spectrometers covering the regions 223-326 nm (UV), 382-471 nm (VIS), and 495-927 nm (VNIR) with resolutions of 0.1 nm, 0.09 nm, and 0.42 nm, respectively. The exposure time is set to one second to record the cumulative emissions from ten laser shots. For each sample, five such exposures (50 laser shots total) were recorded in each spectral region, with the sample moved slightly between exposures to account for inhomogeneities in the sample.

**Samples:** The 17 samples selected for this study (Table 1) were obtained from the Source Clays Repository of the Clay Minerals Society (CMS), the Centre de Recherches Pétrographiques et Géochimiques (CRPG), the Czech Geological Survey (CGS), and the Harvard Mineralogical Museum (HMM).

**Table 1. Samples Studied**

| Sample | Mineral | Source | Form |
|---|---|---|---|
| Mica-Fe | biotite | CRPG | pellet |
| 119403 | glauconite | HHM | pellet |
| SHCa-1 | hectorite | CMS | pellet |
| IMt-1 | illite | CMS | pellet |
| IMt-2 | illite | CMS | pellet |
| KGa-1b | kaolinite | CMS | pellet |
| KGa-2 | kaolinite | CMS | pellet |
| SWy-2 | montmorillonite | CMS | pellet |
| STx-1b | montmorillonite | CMS | pellet |
| SAz-2 | montmorillonite | CMS | chip |
| NG-1 | nontronite | CMS | chip |
| NAu-1 | nontronite | CMS | pellet |
| NAu-2 | nontronite | CMS | chip |
| PFl-1 | palygorskite | CMS | pellet |
| Mica-Mg | phlogopite | CRPG | pellet |
| SepSp-1 | sepiolite | CMS | pellet |
| ZW-C | zinnwaldite | CGS | pellet |

**Analysis:** Example LIBS spectra are shown in Figure 1. The spectra are normalized to total emission intensity as described in [3]. Three chemometric techniques are employed to quantify the compositions of each sample:

**1) Univariate analysis:** For each element, the intensity of a peak caused by the element is taken to be proportional to the element's concentration. Thus a linear regression can correlate the elemental concentration and peak intensity. Although this technique is the most widely used method for interpreting LIBS data, it is the least useful for geologic samples because matrix effects cause spectral line intensities to deviate from proportionality with concentration.

**2) Partial Least Squares (PLS) analysis:** PLS is a statistical method that creates a correlation matrix **B** between a matrix of independent variables **X** and dependent variables **Y** yielding a calibration of the (very simplified) form **Y** = **XB**. In this case, the dependent variables are elemental concentrations and the independent variables are the LIBS spectra, more specifically the intensity at each wavelength channel. The correlation matrix can then be used to calculate elemental concentrations from the spectra of unknown samples. This method has been shown in previous work [4] to largely compensate for matrix effects, indicating that PLS is able to statistically identify changes in the spectra caused by varying matricies.

**3) Peak Area Step-wise Regression Analysis (PASRA):** In this treatment, peak areas are extracted using a fitting routine [5], and step-wise multiple regression analyses are run to search for correlations between peak areas and elemental concentrations [6]. For each element, a multiple regression equation of the form $Y = b_0 + b_1X_1 + b_2X_2 + b_nX_n$ (where Y is the elemental concentration, X is a peak area, and b is a partial regression coefficient) is calculated using a relatively small number of peaks. Whereas PLS uses intensities at every wavelength channel, PASRA only uses peak areas of the most statistically significant peaks.

**Discussion:** Because the chemical matrix of the phyllosilicates is consistent, all three methods give reasonable results for most elements. The conventional univariate analysis is the least effective in predicting chemical compositions accurately. Both PLS and PASRA appear to compensate for or exploit the chemical matrix effects, but the PASRA technique may be more instructive with regard to the physics contributing to the chemical matrix effects.

The approaches employed in this study relate to complementary studies of an analogous suite of samples analyzed under ambient conditions by [7]. Their approach, which relates patterns of LIBS spectra to specific phyllosilicate minerals, will also be a useful contribution to understanding Martian LIBS data but from a different perspective.

While PLS and PASRA were developed for calibration of rock samples, it is useful to apply them to this data set because these minerals share crystal structures and have similar chemical matricies. The results of this study will facilitate accurate future interpretation of Martian LIBS data and help to demystify the physical forces that convolute geologic LIBS spectra.

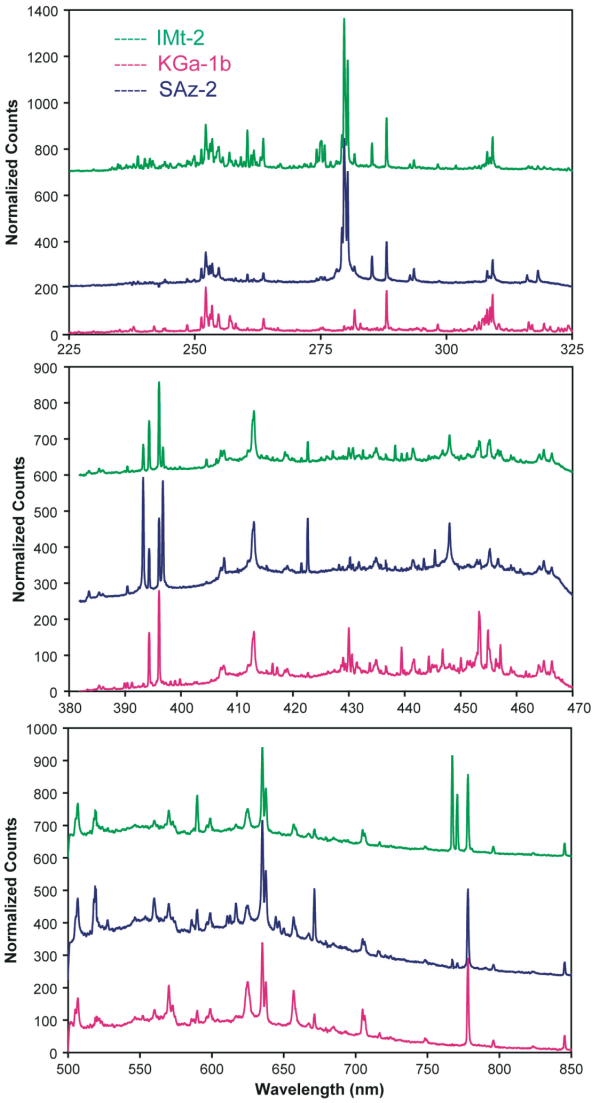


**Figure 1.** LIBS spectra of three phyllosilicates, offset for clarity

**References:** [1] Pasquini C. et al. (2007) *J. Braz. Chem. Soc.,* 18, 463-512. [2] Bishop J. L. et al. (2008) *Science*, 321, 830-833. [3] Mustard J. F. et al. (2008) *Nature*, 454, 305-309. [4] Clegg S. M. et al. *Spectrochim. Acta Part B* (accepted pending revision). [5] Schaefer M. W. et al. (2008) *LPSC XXXIX*, Abstract #2171. [6] Dyar M. D. et al. *GRL* (submitted). [7] Lentz, R. C. F. (2008) *LPSC XXXIX*, Abstract #2015.

**INTERPRETING MARTIAN PHYLLOSILICATES: TRANSFERABILITY OF AN INFERENTIAL FRAMEWORK FROM TERRESTRIAL EXPERIENCE TO MARS.** Michael A. Velbel, Department of Geological Sciences, 206 Natural Science Building, Michigan State University, East Lansing, MI 48824-1115, velbel@msu.edu.

**Introduction:** Orbiter and lander/rover studies of Mars' surface have identified and provided preliminary characterization of surficial materials including igneous and sedimentary rocks, possible volcaniclastic/pyroclastic rocks, and unconsolidated sediment. Some surfaces expose unaltered anhydrous silicates (militating against extensive interactions with water), but most results (including studies of Mars meteorites) indicate at least minor aqueous alteration of exposed surface materials. The extent of any chemical/mineralogical alteration, the relative importance of physical and chemical processes, the timing of any chemical alteration that may have occurred, and what information the surficial materials contain about the chemical history of Mars' surface and atmosphere are all matters of continuing research interest.

Clay minerals (phyllosilicates and other related alteration products) form by deuteric and hydrothermal alteration of igneous parent materials; weathering of any parent-rock type; and diagenesis of sediments (including volcaniclastics). This contribution reviews what can be inferred about mineral-environment interactions from the study of the clay-mineral products of mineral-water interactions, emphasizing low-temperature surface phenomena (weathering).

**Rock and mineral weathering**. During weathering, primary rock-forming minerals react with solutions and/or volatiles. Reactants (minerals and mobile species) are consumed through processes governed by interactions among structure, composition, surface properties, and solute composition (the latter itself influenced by the history of the solution, including its origin and other reactions the solution participated in prior to arriving at the current reaction site) [1-5]. Weathered regoliths produced by weathering reactions contain residual primary rock-forming minerals (remnant reactants) and secondary minerals (weathering products), and the composition of the solutions and/or volatiles are modified [1-5].

In many situations of interest, the solutions left the system long ago, and it is from the surviving solids that the former processes must be inferred [1-5]. Although reactant and product solutions and volatiles may no longer exist, considerable insight into their nature, abundance, and properties can be achieved by examining the reactant and product minerals. The compositional and textural relationships among reactants and products record mineral stability and elemental mobility, which in turn result from the thermodynamics and kinetics of the weathering reactions. Even on Earth, where high temperatures and abundant water facilitate relatively rapid kinetics (at least in comparison with present conditions on Mars), the mechanisms of weathering reactions often prevent the attainment of thermodynamic equilibrium. Most naturally weathered materials therefore represent various intermediate stages between unaltered parent materials and the ultimate weathering products [1-5].

**Formation of phyllosilicates as weathering products.** On Earth, clays formed by weathering vary with the interplay between (1) the dissolution mechanisms and kinetics of primary minerals and (2) the leaching intensity of the weathering environment. There are two grain-scale mechanisms by which primary silicate minerals in general, and chain silicates in particular, weather to secondary minerals; transformation and neoformation [1,6,7].

*Transformation.* In transformation, the bonds linking the apical oxygens of the silica tetrahedra in the chains of, for example, chain silicates are locally broken and remade, allowing single- and double-width chains to rearrange and reattach themselves laterally into extensive tetrahedral-octahedral-tetrahedral (T-O-T) sheets, the basic structural unit of 2:1 phyllosilicate minerals [3]. The earliest-formed products of transformation reactions retain large parts of the parent-mineral structure (e.g., mica to vermiculite or smectite; pyroxene to smectite [3]). Solution composition has only modest influence on the structure and composition of the alteration product, which at least initially consists dominantly of cations and structural units inherited from the parent mineral [3,8-11].

*Neoformation.* In neoformation, destruction of primary-mineral bonding is more complete [12], and secondary minerals are formed (often at some distance from the site of primary-mineral destruction) by crystal-growth of secondary minerals from solutes. Because secondary-mineral formation by precipitation does not require any specific structural relationship with the primary reactant-mineral surface (from which precipitation may be separated by considerable distance), there is no necessary crystallographic orientation relationship between primary (reactant) minerals and their neoformation products [12,13].

**Clay minerals and environmental conditions.** Secondary minerals vary among different geochemical

and leaching environments; terrestrial regolith geoscientists use a classification based on the major clay minerals formed [3]. At early stages of weathering (in the case of phyllosilicate formation by transformation) and/or under conditions of minimal leaching of dissolved products (in both transformation and neoformation), 2:1 clay-minerals form as weathering products; such weathering, forming products comprising two tetrahedral silicate sheets per octahedral sheet (e.g., smectite-group minerals), is termed *bisiallitic*. At intermediate degrees of weathering and/or leaching intensity, 1:1 clay-minerals form; such weathering, forming products comprising one tetrahedral silicate sheet per octahedral sheet, is termed *monosiallitic*. When weathering has been sufficiently extensive or intense that silica has been essentially completely leached from the weathering profile, hydroxides and oxyhydroxides of Fe and Al are the dominant weathering products; such weathering is termed *ferrallitic*.

With increased weathering, the influence of parent material on the structure and composition of weathering products diminishes, and the composition of the products is increasingly influenced by the compositions of the solutions driving the alteration. Solution composition during advanced weathering influences compositions of product minerals in terms of both the elements left behind in the products, and the elements transferred between the product-forming environment and other nearby weathering micro- and (if enough water is present) macro-environments. On Earth, leaching in wet climates removes those elements overabundant in parent minerals relative to products; in dry terrestrial environments such elements are retained in the local regolith [1-3,14]. On Mars such mobile products (esp. Si) appear not have moved far, suggesting that there was little water to carry them.

**What can clay minerals tell us about alteration conditions on Mars?** For most of Mars' natural history, Martian environments of aqueous alteration (surface and shallow subsurface environments like those sampled by Mars meteorites) were likely characterized by low fluid-rock ratios, negligible leaching, and highly reactive (mafic) parent materials. Rapid reaction rates of the mafic silicates and negligible leaching produce conditions more similar to closed-system conditions than in most other terrestrial weathering environments. Consequently, much analysis of Mars-surface mineralogy assumes that thermodynamic equilibrium adequately describes parent-product mineral relationships of weathered planetary surface materials [15-17]. However, metastability (not thermodynamic equilibrium) is common in low-temperature mineral-water systems, even for reactive primary minerals and soluble product minerals commonly assumed to easily attain equilibrium [18], so observations of kinetically controlled textures and mineral associations are more likely than thermodynamic modeling to detect evidence of processes and reaction paths [1-5, 14,18].

Smectites are widely distributed on the surface of Mars [19-22]. Smectites indicate either inheritance of structure and major elements from parent material with minimal modification by leaching (transformation) or precipitation from cation- and silica-rich solutions (neoformation). Optical-petrographic and electron-microscope-scale textural observations are required (from Mars meteorites or returned samples) to fully distinguish phyllosilicates formed by transformation from those formed by neoformation [8-13]. However, associations of phyllosilicates (especially smectite-group minerals) can be linked to categories of parent-material types from orbital imagery and spectroscopic data, so informed preliminary inferences about transformation or neoformation origins and their environmental significance are possible even in the absence of returned samples [19-22].

**References:** [1] Nahon D. B. (1991) *Introduction to the Petrology of Soils and Chemical Weathering,* 313 p. [2] Delvigne J. (1998) *Can. Mineral. Spec. Publ. 3*. [3] Taylor G. and Eggleton R. A. (2001) *Regolith Geology and Geomorphology*, 375 p. [4] Berner E. K. and Berner R. A. (1996) *Global Environment: Water, Air, and Geochemical Cycles*, 376 p. [5] Lasaga A. C. (1998) *Kinetic Theory in the Earth Sciences,* 811 p. [6] Duchaufour P. (1982) *Pedology*), 448 p. [7] Eslinger E. and Pevear D. (1988) *Clay Minerals for Petroleum Geologists and Engineers*: SEPM Short Course Notes 22, 422 pp. [8] Eggleton R. A. (1975) *Amer. Mineral., 60*, 1063-1068. [9] Eggleton R. A. and Boland J. N. (1982) *Clays & Clay Minerals, 30*, 11-20. [10] Banfield J. F. and Barker W. W. (1994) *GCA, 58*, 1419-1429. [11] Velbel M. A. and Barker W. W. (2008) *Clays & Clay Minerals 56*, 111-126. [12] Velbel M. A. (2007) *Developments in Sedimentology 58*, 113-150. [13] Velbel M. A. (1989) *Clays & Clay Minerals 37*, 515-524. [14] Wentworth S. J. et al. (2005) *Icarus, 174,* 382-395. [15] Gooding J. L. (1978) *Icarus, 33*, 483-513. [16] Gooding J. L. & al. (1992) in Kieffer H. H. et al. (eds.) *Mars*, p. 626-651. [17] Chevrier et al. (2007) *Nature, 448*, 60-63. [18] Velbel M. A. et al. (1991) *GCA, 55,* 67-76. [19] Bibring J.-P. et al. (2005) *Science, 307,* 1576. [20] Poulet F. et al. (2005) *Nature, 438*, 623. [21] Bibring J.-P. et al. (2006) *Science, 312*, 400. [22] Mustard J. F. et al. (2008) *Nature, 454*, 305.

**A THEMIS SPECTRAL INDEX FOR DETECTION OF PHYLLOSILICATES ON MARS.** C. E. Viviano[1], J. E. Moersch[1], and J. L. Piatek[2], [1]Department of Earth & Planetary Sciences, University of Tennessee, Knoxville, TN 37996; <cviviano@utk.edu>, [2]Physics & Earth Sciences Department, Central Connecticut State University.

**Introduction:** The Mars Express OMEGA and Mars Reconnaissance Orbiter CRISM experiments have discovered and mapped mineralogically diverse phyllosilicate deposits on Mars through hyperspectral detection in the near-infrared, e.g., [1], [2], [3], [4], [5]. Examples of these deposits have been reported in the Mawrth Vallis region (~24°N, 340°E), the Nili Fossae region (~22°N, 77°E), a Noachian-aged outcrop in Syrtis Major (~19.5°N, 73°E), and a dark deposit in Ismenius Lacus (~34°N, 17°E) [1], [2], [3], [4], [5]. OMEGA and CRISM spectra of these phyllosilicates are most similar to laboratory spectra of Fe/Mg and Al-rich varieties, e.g., [1], [3], [5], [6].

THEMIS, aboard the Mars Odyssey spacecraft, has acquired multispectral thermal infrared images of Mars at 100m/pixel spatial resolution with nearly global coverage. Observation of the primary silicate absorption feature in the thermal infrared may be used to constrain clay mineralogical identification [7]. Although it is recognized that THEMIS may detect spectral uniqueness in clay-rich areas [8], little has been done to utilize this feature, due to the lack of a definitive clay signal deconvolved from corresponding TES data.

Here, we have used THEMIS and OMEGA coverage of the Mawrth Vallis, Nili Fossae, Syrtis Major, and Ismenius Lacus to find a clay spectral signature in the thermal infrared. This signature was used to develop a spectral index that is sensitive to the spectral shape of clays. Application of this index to other THEMIS images will be used to identify clay-rich regions in areas of Mars not yet observed by OMEGA or CRISM.

**Methods:** THEMIS daytime infrared images of OMEGA-identified clay-rich regions were corrected for drift, rectified, "deplaided", radiance corrected, and map projected using the THEMIS image processing web interface (http://thmproc.mars.asu.edu). Initially, images with the highest average temperatures (a minimum of 240 K) were chosen to maximize signal-to-noise ratios in the scene. The ENVI 4.2 remote sensing software suite was used to run a custom TES-derived multiplicative atmospheric correction using techniques described in [9]. Mean spectra were extracted from regions of interest (ROIs) corresponding to the locations of OMEGA-identified phyllosilicate-rich deposits.

A spectral index was developed based on manual inspection of THEMIS spectral shapes within and outside the phyllosilicate areas mapped by OMEGA. This index was then refined through application to multiple THEMIS scenes of example areas on Mars where OMEGA has detected phyllosilicates.

***THEMIS Phyllosilicate Index =***
*3•(b7/b6)+(b8/b7)+(b7/b5)+(b8/b9)+2•(b8/b5)+2•(b3/b4)+(b6/b5)*
(Outputted values >11.2 correspond to OMEGA-identified clays)

Note that the spectral index above is refined from a preliminary version we have previously published [10], and will probably be further refined as we examine more clay-rich targets.

**Results and Discussion:** The results of applying our phyllosilicate spectral index to THEMIS data are shown in the left-hand panels of Figure 1 (below) for Mawrth Vallis, Syrtis Major, and Ismenius Lacus. THEMIS pixels with a phyllosilicate index greater than 11.2 correspond to OMEGA-identified, clay-rich regions (right-hand panels in Figure 1), though there are some slight discrepancies, particularly in a region NE of the clay deposit in Syrtis Major. We were unable to map clays in the Nili Fossae region using the same spectral index that worked in the other three locations. This lack of detection in Nili Fossae could be due to the physical nature of the clays in this region. It has been hypothesized that the region is comprised of >100μm olivine grains [11] within a possible matrix of clays produced by alteration [6]. If the clay grains in this matrix are sufficiently small (<~30μm), they would be more difficult to observe in the longer-wavelength thermal infrared wavelengths [12], [13], used by THEMIS than at the near-infrared wavelengths used by OMEGA. In contrast, the phyllosilicates observed in Mawrth Vallis are associated with layered rocks [1] part of a >100m thick geologic unit [3], which perhaps would be less affected by loss of spectral contrast associated with particle size effects. The output of the index also relies on the quality of the atmospheric correction of a region, which is dependent upon TES data quality, as well as signal-to-noise and atmospheric dust content in the THEMIS scene. THEMIS scenes with poor atmospheric corrections tend to give false-positive detections (index greater than 11.2) over the majority of the image. It was also determined that the THEMIS phyllosilicate index produces ambiguous results when used on clay-rich areas with brightness temperatures of greater than 255 K.

**Conclusions:** Our results suggest that the phyllosilicate-bearing outcrops in Mawrth Vallis, Syrtis Major, and Ismenius Lacus detected by OMEGA also have consistent THEMIS thermal infrared spectral properties that are distinct from surrounding terrain. These spectral properties can be quantified in a THEMIS spectral index. A reliable THEMIS spectral index for phyllosilicates would have tremendous utility in mapping the full distribution of these minerals because of the near-global coverage of the THEMIS dataset. THEMIS-based detections of new areas of phyllosilicates could be used to target future OMEGA and CRISM observations for confirmation.

**References:** [1] Poulet F. et al. (2005) *Nature*, *438*, 623-627. [2] Bibring J. –P. et al. (2005) *Science*, *307*, 1576-1581. [3] Mustard et al. (2008) *Nature*, *454*, 305-309. [4] Loizeau D. et al. (2007) *JGR*, *112*, E08S08. [5] Bishop J. L. (2008) *Science*, *321*, 830-833. [6] Mangold et al. (2007) *JGR*, *112*, E08S04. [7] Michalski, J. et al. (2005) *JGR*, *111*, E03004. [8] Michalski, J. et al. (2006) *LPSC XXXVII*, #1242. [9] Banfield J. L. et al. (2004) *JGR*, *109*, E10008. [10] Viviano et al. (2007) *LPSC XXXIX,* #2474. [11] Poulet et al. (2006) *EGU 3rd Gen. Assembly*, Apr. 2-7. [12] Moersch and Christensen (1995) *JGR*, *100*, 7465-7477. [13] Mustard and Hays (1997) *Icarus*, *125*, 145-163.

**Figure 1.** **A**, *left*: Mawrth Vallis phyllosilicate index image (see text) derived from THEMIS image I01199005. Red pixels correspond to index values greater than 11.2, which we consider a positive THEMIS detection of phyllosilicates. **A**, *right*: Subset of OMEGA-detected spectral indices of the 1.93μm, 2.20μm, and 2.3μm bands (blue, green, red, respectively) [3] for the same area as A, *left*. Both *right* and *left* centered at (~24°41'N, 340°48'E). **B**, *left*: Ismenius Lacus phyllosilicate index image derived from THEMIS image I03220002. **B**, *right*: Subset of OMEGA coverage of Ismenius Lacus (phyllosilicate in blue, pyroxene in green) [1]. Both *right* and *left* centered at (~34°10'N, 16°57'E). **C**, *left*: Syrtis Major phyllosilicate index image derived from THEMIS image I02469002. **C**, *right*: OMEGA coverage of Syrtis Major (phyllosilicate in blue) [1]. Both *right* and *left* centered at (~19°35'N, 73°1'E).
All OMEGA image panels are adapted from figures in [3] and [1].

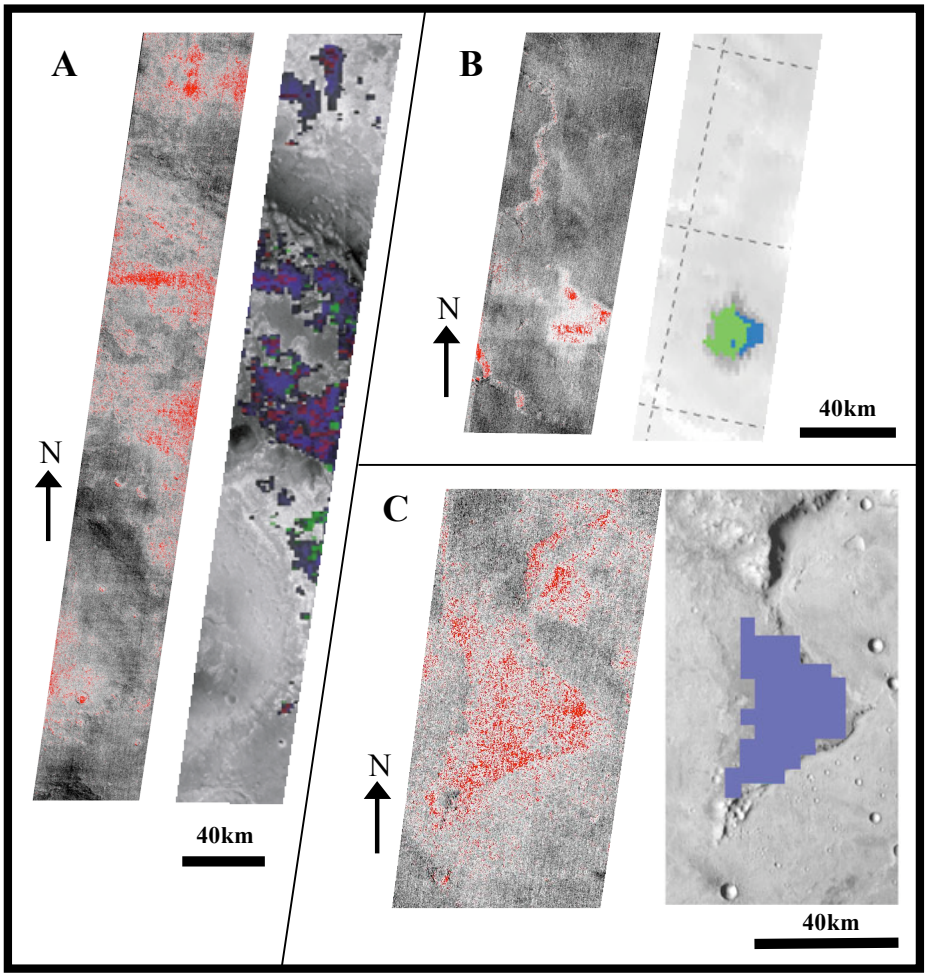

**STRATIGRAPHIC CONTEXT OF PHYLLOSILICATE DEPOSITS IN SINUS MERIDIANI, MARS.** S. M. Wiseman[1], R. E. Avidson[1], F. Poulet [2], R. V. Morris[3], S. Murchie[4], F. P. Seelos[4], J. C. Andrews-Hanna[5], and the CRISM Science Team. [1]Dept of Earth and Planetary Sciences, Washington University, St. Louis, MO (sandraw@levee.wustl.edu), [2]Institut d' Astrophysique Spatiale (IAS), Orsay, France, [3]NASA Johnson Space Center, Houston, TX, [4]Applied Physics Laboratory, Laurel, MD, [5]Dept of Geophysics, Colorado School of Mines, CO.

**Introduction:** Extensive sedimentary deposits [e.g., 1,2] previously mapped as etched (ET) terrain are exposed in the Sinus Meridiani region. The hematite-bearing plains unit (Ph) explored by the MER rover Opportunity covers portions of the ET (Fig. 1). Dissected cratered terrain (DCT) is exposed to the south of these deposits. Fe/Mg phyllosilicates and hydrated Mg sulfate deposits are detected in Meridiani using both Mars Express OMEGA [3] and MRO CRISM [4] near infrared spectral data [e.g., 5,6,7,8]. We are mapping the spatial distribution of both phyllosilciate and hydrated sulfate deposits within the Sinus Meridiani region using high resolution CRISM images. This work builds on previous studies [e.g., 6,9] and provides a stratigraphic context for the phyllosilicate deposits.

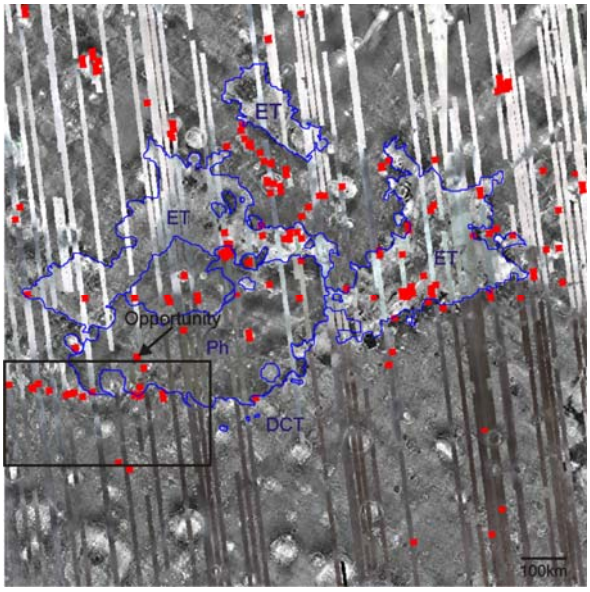


Figure 1. CRISM multipspectral survey coverage (R=2.5, G=1.5, B=1.1µm) overlain on a THEMIS nighttime IR mosaic. The context map extends from (10˚N, 10˚W) to (10˚S, 10˚E). CRISM high resolution targeted footprints are shown in red. Units similar to those mapped by [10] are indicated.

**Fe/Mg Phyllosilicates:** The DCT is a complex unit that contains fluvial features and buried and exhumed craters, some of which exhibit light toned layering [11]. Ph embays DCT along the southern boundary (Fig. 2). Phyllosilicate deposits are exposed within the DCT and occur in close proximity to the Ph unit in some areas. Detailed examination of these deposits revealed a stratigraphic relationship between the phyllosilciate-bearing deposits and Ph. In Miyamoto crater (Fig. 2), phyllosilicate-bearing deposits are located within ~30 km of the edge of Ph [11], which is presumably underlain by sulfate-rich deposits similar to those explored by the Opportunity rover. The deposits within Miyamoto crater are exposed only in areas where significant exhumation has occurred. The majority of the phyllosilicate exposures in the DCT (Fig. 2) exhibit spectral absorption features at 1.9, 2.3 and 2.4 µm, consistent with the presence of Fe/Mg phyllosilicates [9].

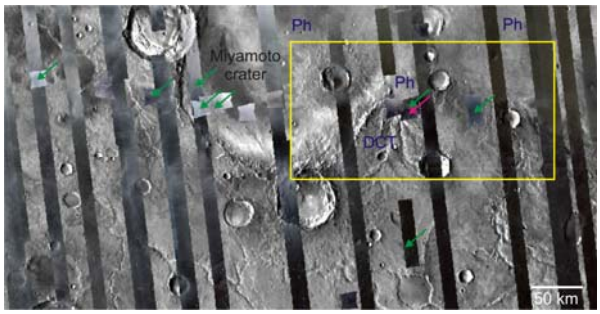


Figure 2. THEMIS daytime IR mosaic of the box shown in Fig. 1 with CRISM multispectral and high resolution coverage overlain (R=2.5, G=1.5, B=1.1µm). Areas that are indicated with green arrows exhibit CRISM spectra that are consistent with the presence of Fe/Mg phyllosilicates and the area indicated with a red arrow contains Al-rich phyllosilicates.

**Al-Rich Phyllosilicates:** We have identified Al-rich phyllosilicates, including montmorillonite and kaolinite (Figs. 5,6), for the first time in the Sinus Meridiani region. Fe/Mg smectites are also present in association with the Al-rich phyllosilicates. The phyllosilicate exposures occur within an in place bedrock unit that has been incised via fluvial erosion (Figs. 3,4). Similar phyllosilicate assemblages are found in exposures identified in Mawrth Vallis [e.g., 12]. These deposits occur within the DCT, close to the boundary with Ph (Fig 3). After formation, the phyllosilicate deposits were incised via fluvial erosion [Fig. 4]. Analysis of image and elevation data show that the younger Ph unit embays the phyllosilicate deposits [Fig. 4]. These exposures demonstrate that the pyllosilicate-bearing deposits predate the formation of Ph.

**ET Phyllosilicates:** Both hydrated sulfate and phyllosilciate exposures are identified in association with the ET [e.g., 6,7,8]. The geologic context of these deposits is difficult to decipher because the exposures represent erosional surfaces and are partially buried by mantling material in some areas. Within ET, the phyllosilicate and hydrated sulfate deposits occur in close proximity in some areas. Our current analyses focus on deciphering the stratigraphic relationship between these phyllosilicate and hydrated sulfate deposits.

**Discussion:** Detailed examination of the Al-rich and Mg/Fe phyllosilicate exposures within the DCT show that the phyllosilicate-bearing deposits predate the formation of the Ph unit explored by the Opportunity rover. The deposits record the transition from fluvial conditions which produced and/or preserved phyllosilicates deposits to a progressively acid sulfate dominated groundwater system in which large accumulations of sulfate-rich evaporites were deposited.

The stratigraphic relationship between the phyllosilciate and hydrated sulfate deposits is less clear within the ET. The geochemical conditions experienced by ET at various locations were driven by ground water recharge and evaporative loss rates [13]. Continued mapping of the distribution of phyllosilicate and hydrated sulfate deposits will help to elucidate the aqueous history of the Sinus Meridiani region.

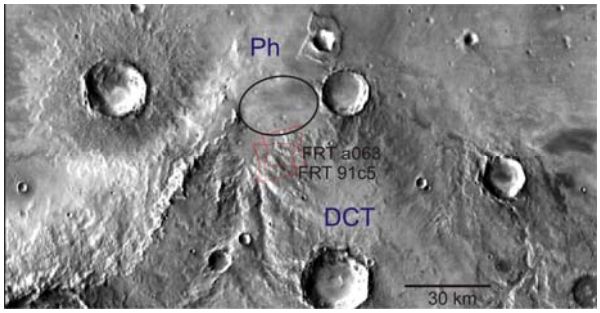


Figure 3. THEMIS daytime IR mosaic of the box shown in Fig. 2. The MSL candidate Southern Meridiani landing ellipse and CRISM FRT images of interest are indicated.

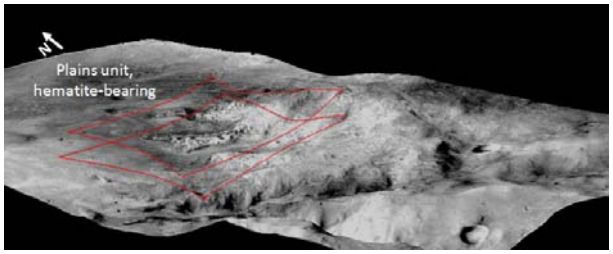


Figure 4. CTX P16_007348_1768 draped on MOLA topography, with a vertical exaggeration of 10. CRISM FRT footprints shown in Figure 3 are indicated in red.

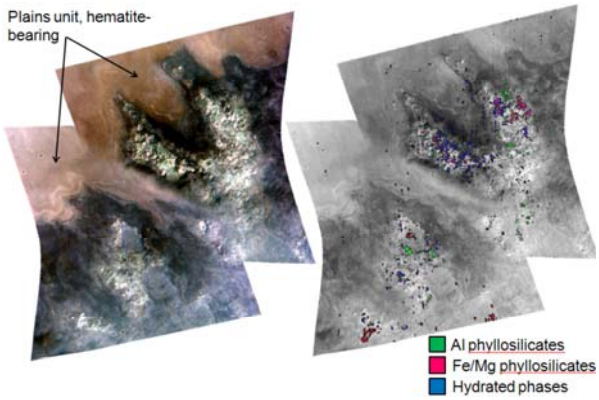


Figure 5. CRISM false color IR composite showing FRT 91c5 and FRT a063 (R=2.5, G=1.5, B=1.1μm) (*left*) and spectral index [14] composite (R=D2300, G=B2200, B=BD1900) (*right*).

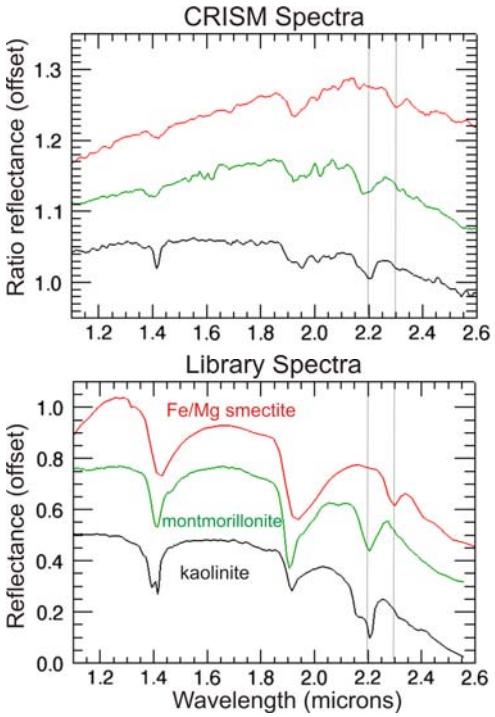


Figure 6. CRISM spectra extracted from areas indicated with arrows in Fig. 5 compared to library spectra.

**References:** [1] M. Malin and K. Edgett, (2000) *Science*, 288. [2] P.R. Christensen and S.W. Ruff (2004) *JGR*, 107. [3] J.-P. Bibring et al. (2004) *Mars Express: The Scientific Payload*, p37-49. [4] S. Murchie et al. (2007) *JGR*, 112. [5] F. Poulet et al. (2005) *Nature*, 438. [6] F. Poulet et al. (2008) *Icarus*, 195. [7] A. Gendrin et al. (2005) *Science*, 307. [8] S.M. Wiseman et al. (2007) *LPS XXXIX*, #1806. [9] S.M. Wiseman et al. (2008) *GRL*, submitted. [10] R.E. Arvidson et al. (2003) *JGR*, 108. [11] K.S. Edgett (2005) *Mars*, 1. [12] D. Loizeau (2007) *JGR*, 112. [13] J.C. Andrews-Hanna and M.T. Zuber (2008) *LPS XXXIX*, 1993. [14] S.M. Pelkey et al. (2007) *JGR*, 112.

**HYDRATED MINERAL EXPOSURES IN THE SOUTHERN HIGHLANDS.** James J. Wray[1], Frank P. Seelos[2], Scott L. Murchie[2], and Steven W. Squyres[1], [1]Department of Astronomy, Cornell University, Ithaca, NY 14853 (jwray@astro.cornell.edu), [2]JHU/Applied Physics Laboratory, Laurel, MD 20723.

**Introduction:** Orbital near-infrared spectroscopy has revolutionized our knowledge of the history of water on Mars. Sulfate minerals were first identified in Martian bedrock at Meridiani Planum by the Opportunity rover [1], but have since been found by OMEGA in numerous other light-toned layered deposits [2,3], where they are thought to reflect alteration by acidic solutions. Phyllosilicates, possibly indicative of more neutral-to-alkaline altering fluids [e.g., 4], have also been identified [2,5].

OMEGA global maps of hydrated minerals including phyllosilicates reveal that km-scale and larger surface exposures are scattered widely across low and mid-latitudes, but are relatively rare [6,7,8]. Sulfates at these latitudes are seen by OMEGA only in a narrow band surrounding the equator east of Tharsis [6], prompting the suggestion that they all may have formed via a single regional process [9]. But a more complex story is visible at higher spatial resolution. On the opposite side of Mars, ferric sulfates and opaline silica have been found in the Columbia Hills by the Spirit rover [10], while CRISM has found hundreds to thousands of Fe/Mg-clay exposures in the highlands of Terra Tyrrhena [11]. CRISM data now enable a reevaluation of the planetary-scale distribution of hydrated minerals.

**Methods:** We have undertaken a survey of publicly released CRISM observations in the Southern highlands. Using the online map of targeted observations (http://crism-map.jhuapl.edu/), we have examined the IR HYD and PHY browse products in search of spatially contiguous areas with absorptions characteristic of hydrated sulfate and phyllosilicate mineralogy. Promising observations are then processed using standard atmospheric and photometric corrections [11], and their spectra examined to confirm the presence of absorptions of interest. Regions currently under study by other investigators – including Terra Tyrrhena [11,12], Argyre basin [13], and Eridania basin [14] – have been omitted from our survey (Fig. 1).

We have focused initially on observations with the highest values of the summary parameters over many pixels. However, all web-released browse products were produced with a standard stretch, so future analysis of more subtle features on an image-by-image basis may reveal many additional hydrated mineral occurrences.

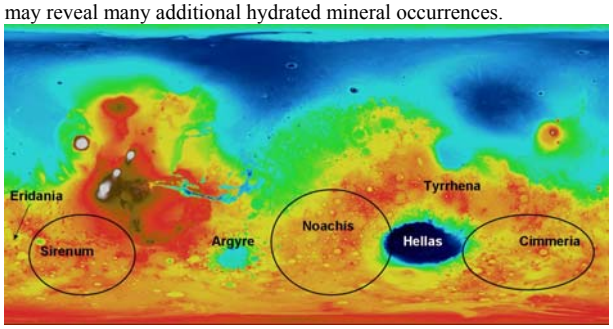


**Figure 1.** MOLA global topography with regions surveyed circled.

**Results:** Only a small subset of images exhibit strong hydrated mineral signatures. In Noachis, one image contains a broad exposure of a bright plains unit with a strong 2.3-μm band diagnostic of Fe/Mg-phyllosilicates, while a small impact crater in the same scene has bright ejecta with a 2.2-μm band indicative of Al-phyllosilicates. Two images south of Noachis contain strong evidence for hydrated sulfates. In one of these, at 63º S, polyhydrated sulfate is seen on top of a ~5-km wide hill; HiRISE images of this hilltop show a polygonally fractured surface with scattered ~10-m boulders.

In the Centauri Montes just East of Hellas, several spots on the hourglass-shaped glacier discussed by [15] exhibit absorptions at 1.5, 1.9, and 2.1 μm, consistent with lab spectra of water ice but possibly also consistent with the monohydrated sulfate kieserite (Fig. 2). If water ice, this material may be frost, but could also be exposed glacial ice as predicted by [16]. Seasonal monitoring should distinguish between these possibilities.

In Terra Sirenum, several images of the D~100 km Columbus crater reveal a complex mineral assemblage. Polyhydrated sulfate is the spatially dominant hydrated phase, but both Fe/Mg- and Al-phyllosilicates are also seen. The latter is much more common, and spectrally most consistent with a kaolin group mineral (e.g., halloysite) with a strong 1.9 μm band and doublet absorptions at 1.4 and 2.2 μm (Fig. 2). The polyhydrated sulfate occurs in a finely layered light-toned unit that overlies both types of phyllosilicate-bearing units (Fig. 3). This assemblage of sulfates, kaolinite, and other minor phyllosilicates occurring in sedimentary layers inside a closed (crater) basin is reminiscent of terrestrial acid-saline lake deposits [19].

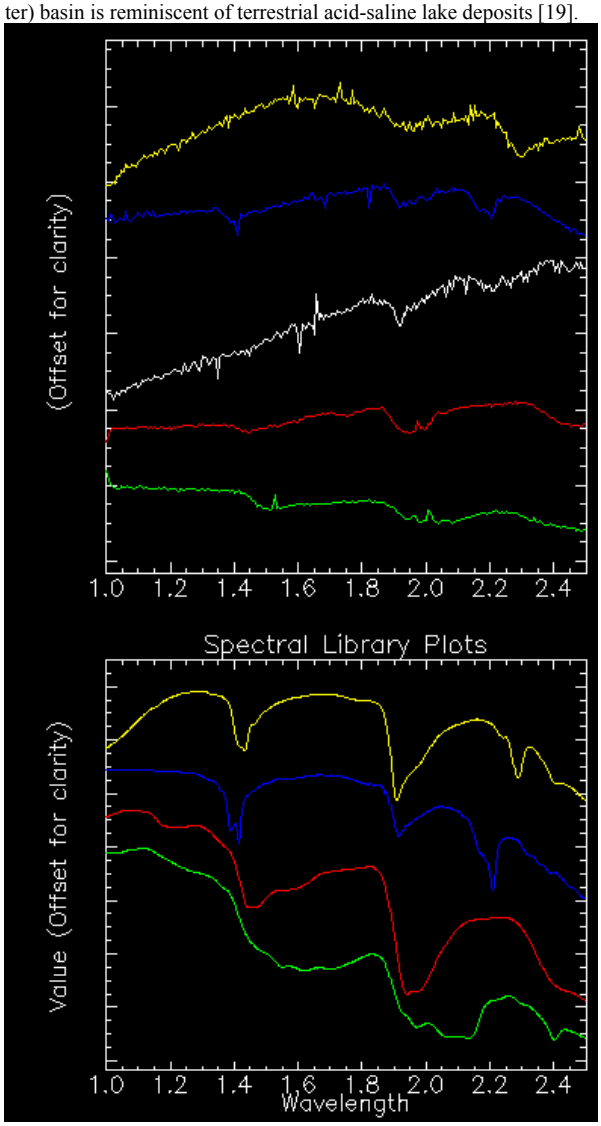


**Figure 2.** Top panel: CRISM ratio spectra (red, blue, and yellow from Columbus crater; green from Centauri Montes glacier; white from Icaria mound). Bottom panel: library spectra of nontronite (yellow), halloysite (blue), polyhydrated Mg-sulfate (red), and kieserite (green).

Elsewhere in Sirenum, several exposures of Fe/Mg-phyllosilicate occur immediately adjacent to exposures of the THEMIS "glowing" terrain interpreted to contain chloride salts [20]. In the three surveyed scenes containing both minerals, they occur in distinct light-toned units, with the glowing terrain relatively low-standing (either underlying or possibly embaying the clay-bearing unit). Farther East in Icaria Planum, a ~100 km-wide mound hosts an impact crater in which gullies have transported Fe/Mg-phyllosilicate downslope. Just outside the gully is a small exposure of material spectrally consistent with hydrated silica [e.g., 11], with a strong band at 1.9 μm and a broad, asymmetric band centered around 2.2 μm (Fig. 2).

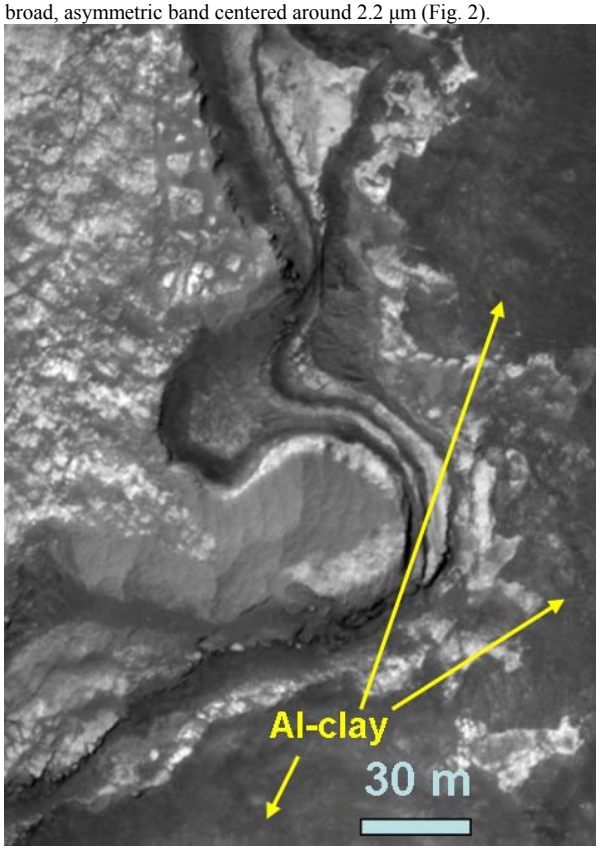


**Figure 3.** Portion of HiRISE PSP_005429_1510 in Columbus crater. Light-toned, layered unit contains polyhydrated sulfate, while underlying darker unit contains a kaolin group clay.

**Discussion:** One immediate conclusion from our survey is that sulfate minerals are more widespread than previously observed. OMEGA results have been used to infer a distinct period of sulfate formation during the early-to-mid Hesperian, coupled to Tharsis volcanic activity [6,9]. However, sulfates today are seen in locations far from Tharsis, and virtually all areas covered by our survey are mapped as Noachian in age (though the near-surface materials may be younger). Sulfate formation may have occurred locally or regionally at various times spanning a large fraction of Martian history.

We have observed hydrated silicates in a number of locations scattered throughout the Martian highlands. The various examples in Sirenum and Icaria do not occur near any of the large Martian impact basins, suggesting that phyllosilicate formation mechanisms related to hydrous basin impact melts [21] likely do not apply to these examples. Smaller impacts may have played a role, but we note that the phyllosilicates discussed above do not occur predominantly in association with impact craters as in Terra Tyrrhena [11,12].

Among the hydrated silicates observed, Fe/Mg-phyllosilicate appears to be most common overall, consistent with previous findings [5,11]. However, we note that the images we examined do not represent an unbiased sample of the highlands: while some images were targets of opportunity or ride-along observations with other MRO instruments, much of CRISM's targeting strategy is driven by previous discoveries of hydrated minerals at the lower resolution provided by OMEGA or CRISM multispectral data. Fig. 4 shows a small portion of Terra Sirenum in which multiple Fe/Mg-phyllosilicate exposures stand out in CRISM multispectral mapping strips. We are currently targeting these exposures for high-resolution CRISM and HiRISE observations.

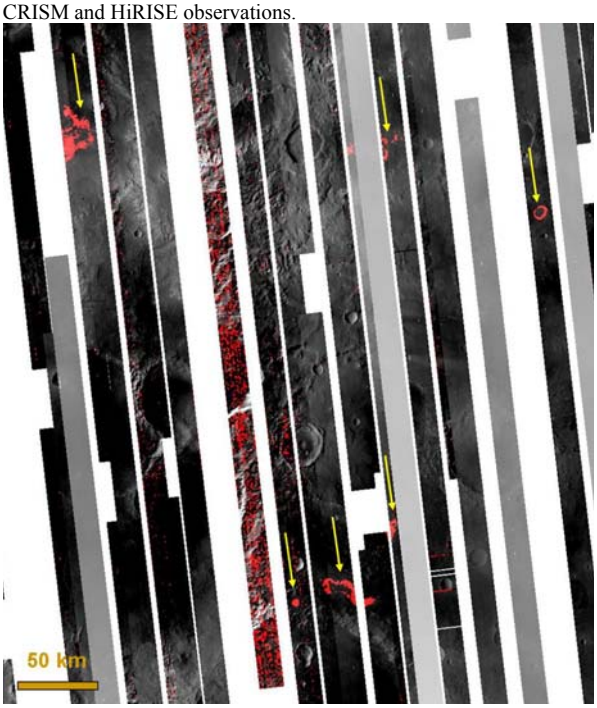


**Figure 4.** Mosaic of CRISM multispectral data in Terra Sirenum, (center ~30ºS, 185ºE). Background is IR albedo. The D2300 parameter, sensitive to Fe/Mg-OH absorption in phyllosilicates, is shown in red. Yellow arrows highlight exposures. Residual striping in some image strips is due to an uncorrected instrument artifact.

Our initial survey reveals the diversity of hydrated mineral occurrences in the ancient Southern highlands, and should precipitate several more focused studies of local areas of interest. Future work will also include analysis of high-resolution images to determine (where possible) the stratigraphic context of the hydrated mineral exposures, both relative to each other and to unaltered igneous units.

**Acknowledgements:** JJW thanks the Fannie & John Hertz Foundation and NSF Graduate Research Fellowship for support.

**References:** [1] Squyres S. W. et al. (2004) *Science* 306, 1709-1714. [2] Bibring J.-P. et al. (2005) *Science* 307, 1576-1581. [3] Gendrin A. et al. (2005) *Science* 307, 1587-1591. [4] Chevrier V. et al. (2007) *Nature* 448, 60-63. [5] Poulet F. et al. (2005) *Nature* 438, 623-627. [6] Bibring J.-P. et al. (2006) *Science* 312, 400-404. [7] Poulet F. et al. (2007) *Mars 7*, Abs. #3170. [8] Poulet F. et al. (2007) *JGR* 112, E08S02. [9] Bibring J.-P. et al. (2007) *Science* 317, 1206-1210. [10] Squyres S. W. et al. (2008) *Science* 320, 1063-1067. [11] Mustard J. F. et al. (2008) *Nature* 454, 305-309. [12] Pelkey S. M. et al. (2007) *LPS XXXVIII*, Abs. #1994. [13] Buczkowski D. L. et al. (2008) *LPS XXXIX*, Abs. #1030. [14] Noe E. (2007) *2nd MSL Landing Site Sel. Wkshp*, "Ariadnes Colles." [15] Head J. W. et al. (2005) *Nature* 434, 346-351. [16] Gillespie A. R. et al. (2005) *Nature* 438, E9. [17] Malin M. C. et al. (2006) *Science* 314, 1573-1577. [18] McEwen A. S. et al. (2007) *Science* 317, 1706-1709. [19] Benison K. C. & Bowen B. B. (2006) *Icarus* 183, 225-229. [20] Osterloo M. M. et al. (2008) *Science* 319, 1651-1654. [21] Tornabene et al. (2007) *Mars 7*, Abs. #3288.

**MINERALOGICAL COMPOSITION OF THE MARTIAN SURFACE ON THE BASIS OF INFRARED SPECTROSCOPY** Natalia Zalewska (Andrzejewska)[1], Paulina Wolkenberg[2] [1]Space Research Centre, Polish Academy of Science, ul. Bartycka 18a, 00-716 Warsaw, Poland, e-mail: natalia@cbk.waw.pl [2] Space Research Centre, Polish Academy of Science, ul. Bartycka 18a, 00-716 Warsaw, Poland, e-mail: paulina@cbk.waw.pl

**Introduction::** Mars is one of the most intensively studied planets in the solar system other than Earth. Space probes observing Mars are sending back a huge amount of data every day. They give us information about the probable mineral composition of Mars surface and atmosphere [1], [4], [8].

Infrared spectroscopy is applicable as a method of structural analysis to research the composition of rocks and minerals. We use two Martian infrared spectra from TES (Thermal Emission Spectrometer) instrument aboard the Mars Global Surveyor spacecraft with atmospheric contributions removed by the Radiative Transfer Algorithm method. The first spectrum is of a pure basalt surface which represents the Martian terrain -Cimmeria Terra and second an average dusty surface. We modeled these spectra by matching the infrared spectra of minerals from mineralogical library (in the wavenumber range 1700-200 $cm^{-1}$) using the Deconvolution Algorithm without contributions of the atmosphere.

The infrared radiation (5 – 50 μm or respectively in wavenumber 1700 – 200 $cm^{-1}$ ) is the best one to determine the mineral composition because the surface emits the radiation in this range of wavenumbers. Therefore we can obtain characteristic spectral features for different components of surface and atmosphere in this connection. The most important phenomena are absorption and emission by surface components as well as by atmosphere gases.

The major component of the Martian atmosphere is the carbon dioxide 95.3%, the other components are nitrogen -2.7%, argon -1.6% and trace admixtures as water vapour, carbon oxide, water ices, and dust. The largest seasonal and diurnal variation of abundance are observed for dust. During the changes of season there appear dust storms. Then the transparency of the atmosphere decreases [6], [11]. The knowledge of the variations of abundance of dust and the atmospheric gases helps to eliminate their influence on the infrared spectra of radiance emitted by the surface.

On the basis of TES measurements we find out Mars' geological dichotomy, determining that the northern hemisphere and some terrains on the southern hemisphere like Hellas [45 S; 70 E] or Daedalia Planum [18,4 S; 231,9 E] consist of lowlands and supposed remains of an ocean [5] composed of andesite or weathered basalt, whereas the southern hemisphere displays the features of alkali basalts [7]. This is confirmed by measurements of Viking 1 and 2 and Pathfinder, and Rovers: Spirit and Opportunity. Thanks to those measurements have been estimated the basic elements of Mars' surface composition [2], [3], [9]. Unfortunately, the full confirmation of these measurements was not possible, as in the present study we used the data from small part of Mars surface only, thus not reflecting the global petrologic structure of the whole planet. The research that was carried was devoted only to spectra from Cimmeria Terra. [37,8 S; 189,4 E] [4], (Fig.2) and the average dusty surface [1], (Fig.4).

**Methods:** First of all we would like to retrieve surface emissivity spectrum without contributions caused by atmospheric components. We present two methods that are used to separate the spectral features of atmospheric gases and surface. One of them (Deconvolution Algorithm) relies on fitting the linear combination of spectral features of each mineral and of atmospheric components to the measured spectrum simultaneously. This method uses the spectral mineral library to find the appropriate mixture of minerals.

The second algorithm uses the radiative transfer through the atmosphere (Radiative Transfer Algorithm). The radiances are calculated equation with assumptions regarding the amounts of dust, aerosols, water vapour. Then we can compare the calculated values with the measured ones to find successively the spectral shapes, first for atmospheric dust, then for water-ice aerosols and then, finally, for surface emissivity by least square fitting. Additionally we can assume the size of dust and water ice crystals and seek the best fit. [4], [10], [12].

**Results:** We modeled spectra by matching the infrared spectra of minerals. We added spectra of particular minerals from the mineralogical infrared library with size range 700-1000 μm for pure basalt and powder size for weathered basalt to receive spectrum similar to Martian spectrum from TES. We used the Deconvolution Algorithm method. The Martian atmospheric spectra used for comparison were removed by Radiative Transfer Algorithm.

Basalt spectrum is modeled with Decan basalt and weathered basalt spectrum is modeled with weathered basalt with clay minerals from the Krzeniów, Sudetes.

The Decan basalt contains labradorite 65%, augite 28%, forsterite 4% and hornblende 3% (Fig. 2). For the purpose of modeling augite was replaced by bronzite to smooth out the spectrum between 900 –1100 $cm^{-1}$. Then the fitting to Mars' spectrum is better. Bronzite is very common meteorite's component (Fig.1).

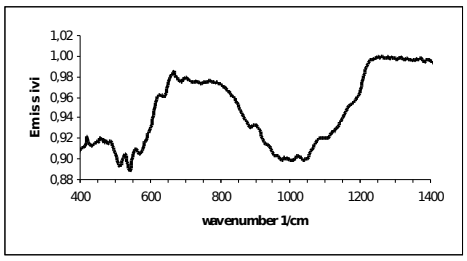


Fig.1 Basalt spectrum modeled with Decan basalt spectrum using the Deconvolution Algorithm

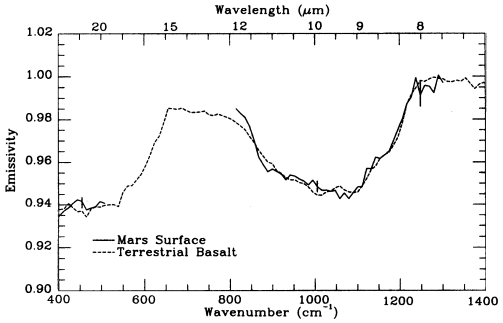


Fig.2 Comparison of the spectra of Cimmeria Terra and Decan basalt with atmosphere separated by the Radiative Transfer Algorithm [4]

The Martian surface is regarded as dusty when the albedo >0,18. Dust can be found on the surface and can be suspended in the atmosphere with particle sizes < 70 μm. We claim that a dust has in its composition weathered basalt with clay minerals-phyllosilicates.

The composition of a weathered basalt (waste) from Krzeniów contains 90-100% of smectite, 5-10% of kaolinite (clay minerals), magnetite and goethite. For the purpose of modeling we set up the composition: 90% of smectite, 7% of kaolinite and 3% of magnetite (Fig.3). We believe that water existed on Mars in the past and Mars' atmospheric pressure in some places allows water to remain in a liquid state**,** so clay minerals can appear on Martian surface.

This waste the best match to the dusty surface of Mars, but makes a problem with fitting minimum at 800-900 cm-1. This minimum is shifted toward shorter waves with components available from the used library.

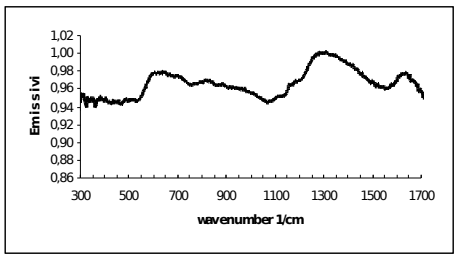


Fig.3 Weathered basalt spectrum modeled with the weathered basalt with clay minerals from the Krzeniów, Sudetes using the Deconvolution Algorithm.

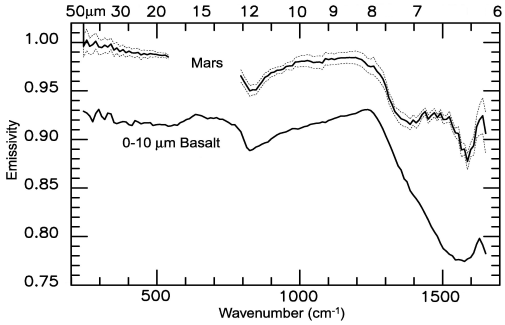


Fig.4 Comparison of the spectra of Mars surface dust and fine basalt with atmosphere separated by the Radiative Transfer Algorithm [1]

**Summary:** The spectrum of Cimmeria Terra surface (Fig.2) best matched by the spectrum of the Decan basalt where augite was replaced by bronzite. It is surface without dust (Fig.1). A dusty Mars' surface is compared to a spectrum of weathered basalt from Krzeniów Sudeten (Fig.3) but the fitting agrees roughly with the Mars' spectrum (Fig.4).

**References:** [1] Bandfield J. L. (2003) *Science* vol. 301 1084-1086. [2] Bell J. F., Mc Sween H. Y., (2000) *JGR*, vol. 105, no E1, 1721-1755. [3] Bridges N. T., Crisp J. A., (2001) *JGR* , vol. 106, no E7, 14,621-14,665. [4] Christensen P. R., (2000) *JGR*, vol.105, nr E4, 9609 – 9621. [5] Head J. W., Hiesinger H., (1999) *Science*, vol.286, 2134– 2137. [6] Martin L. J., (1993) *JGR*, vol. 98, No. E2, 3221. [7] Mittlefehldt D. W**.**, (2000) *Science* vol. 287, 1601. [8] Pearl J. C., (2001) *JGR*, vol. 106, No. E6. [9] Richard V., Morris D., (2000) *JGR*, vol. 105, no E1, 1757-1817. [10] Smith M. D., (2000a) *JGR*, vol. 105 nr E4. [11] Smith M. D**.,** (2000b) *JGR*, vol. 105 nr E4. [12] Wolff M. J., (2003) *JGR*, vol. 108, No. E9, 5097.

# NOTES

# NOTES